The physics of magnetic fusion reactors

John Sheffield

Oak Ridge National Laboratory, Oak Ridge, Tennessee 37831

During the past two decades there have been substantial advances in magnetic fusion research. On the experimental front, progress has been led by the mainline tokamaks, which have achieved reactor-level values of temperature and plasma pressure. Comparable progress, when allowance is made for their smaller programs, has been made in complementary configurations such as the stellarator, reversed-field pinch and field-reversed configuration. In this paper, the status of understanding of the physics of toroidal plasmas is reviewed. It is shown how the physics performance, constrained by technological and economic realities, determines the form of reference toroidal reactors. A comparative study of example reactors is not made, because the level of confidence in projections of their performance varies widely, reflecting the vastly different levels of support which each has received. Success with the tokamak has led to the initiation of the International Thermonuclear Experimental Reactor project. It is designed to produce 1500 MW of fusion power from a deuterium-tritium plasma for pulses of 1000 s or longer and to demonstrate the integration of the plasma and nuclear technologies needed for a demonstration reactor.

CONTENTS

 0034-6861/94/66(3)/1015(89)/$13.90

SYMBOLS AND UNITS

Subscripts: e =electron, i =ion, o =neutral, z =ion of charge z, b =beam, k =kilo, e.g., T_{ek} =electron temperature in keV, m =mega or maximum, a =plasma edge, w =wall, ϕ=toroidal, θ=poloidal, r =radial, v =vertical, z =axial, $\|$=parallel to magnetic field, $\perp$=perpendicular to magnetic field, T =temperature or tritium, D=deuterium, α=alpha particle, NC=neoclassical, n_{20}=density in units of 10^{20} m^{-3}, T_{10}=temperature in units of 10 keV

Superscripts: $\bar{x}$=average $\langle x \rangle$=volume average, $\hat{x}$=peak, or central value, $\tilde{x}$=fluctuating value.

a (m)	minor radius in the median plane
$\bar{a}$ (m)	average minor radius
A (m^2)	area
A_i	atomic mass number
b (m)	minor radius in z direction
B (T)	magnetic field
ΔB_{cs} (T)	magnetic-field swing in a solenoid
D (m^2 s^{-1})	diffusion coefficient
D_A (m^2 s^{-1})	ambipolar diffusion coefficient
$e=1.6\times10^{-19}$ (C)	charge on an electron
E (V m^{-1})	electric field
$E_{\rm crit}$ (eV)	energy at which rate of transfer to ions and electrons is equal
E_α, E_n (J)	fusion energy released in D-T fusion in alpha particle and neutron
E_b (MeV)	neutral-beam energy
f_α	fraction of alpha power lost by conduction
f_B	ratio of field in plasma to maximum field on a coil
$f_E=\phi/T_k$	normalized potential
f_{sb}	fraction of neutral-beam shine-through
F	field-reversal parameter in an RFP
g	troyon factor for beta $[a(\mathrm{m})\mathrm{B}_\phi(\mathrm{T})\langle\beta(\%)\rangle/I(\mathrm{MA})]$
I (A)	current
$I_{\rm bs}$ (A)	bootstrap current
j (A m^{-2})	current density
J (A m^{-2})	current density
$k=1.38\times10^{-23}$ (J K^{-1})	Boltzmann's constant
k (m^{-1})	wave number
K_0	total magnetic helicity
l, L (m)	length or gradient scale length
m (kg)	mass
m	poloidal mode number
$M_{\rm FI}$ (kg)	mass of the fusion island
n (m^{-3})	number density
$\bar{n}$ (m^{-3})	line-average density
n	toroidal mode number
p (W m^{-3})	power density
$p_{\rm br}$ (W m^{-3})	bremsstrahlung radiation power density
p_{cx} (W m^{-3})	charge-exchange power density
p_{ie} (W m^{-3})	ion-electron transfer power density
$p_{\rm LR}$ (W m^{-3})	line radiation power density
p_s (W m^{-3})	synchrotron radiation power density
p_α (W m^{-3})	alpha power density
p_Ω (W m^{-3})	ohmic power density
p_{wn} (W m^{-2})	neutron flux on first wall
$\bar{p}_{wn}$ (W m^{-2})	average neutron flux on first wall
P (W)	power
P_n (W)	neutron power

P_t (W)	total thermal power
P_α (W)	alpha power
P_a (W)	auxiliary power
q	safety factor
$q_{\psi 95}$	at 95% flux surface
q_ψ	on flux surface χ
Q	ratio of fusion power to power lost by plasma
Q_E	ratio of fusion power to total recirculated power
Q_e (J m^2 s^{-1})	energy flux
r (m)	minor radius of a torus
R (m)	major radius of a torus
R_{cs} (m)	solenoid radius
R_p (ohms)	plasma resistivty
$s=rq'/q$	magnetic shear
S	Lundquist number
S_z (m^{-3} s^{-1})	source rate of charge-Z ions
t (s)	time
t_F (s)	plasma current flat-top time
T (eV)	temperature
$\mathbf{u}$ (m s^{-1})	flow velocity
U_l (V)	loop voltage
v (m s^{-1})	speed
v_A (m s^{-1})	Alfvén speed
v_H (m s^{-1})	thermal speed
V (m s^{-1})	plasma flow speed
V_p (m^3)	plasma volume
W (J)	plasma energy
Z	ionic charge
$Z_{\text{eff}}=\dfrac{\sum_z Z^2 n_z}{n_e}$	
β	ratio of plasma pressure to magnetic pressure
$\langle\beta\rangle$	volume-average beta (generally given in %)
β_θ	poloidal beta
γ_R	neoclassical resistance anomaly
Γ (m^2 s^{-1})	flux
$\epsilon=r/R$	inverse aspect ratio
ϵ_ϕ, ϵ_h	toroidal and helical field ripple
η_a	efficiency of auxiliary plasma power
η_e	thermal-to-electrical conversion efficiency
η_r	fraction of power recirculated
$\eta_\parallel$ (ohm m)	parallel resistivity
η_r (ohm m)	resistivity
$\eta_i=L_n/L_T$	
θ	poloidal angle
Θ	pinch parameter
$\iota\equiv 1/q$	rotational transform
$\kappa=b/a$	ellipticity
λ (m)	mean free path or gradient scale length
$\ln\Lambda_e$	coulomb logarithm
$\mu_0=4\pi\times 10^{-7}$ (H m^{-1})	permeability of free space
ν_{ei} (s^{-1})	electron-ion collision frequency
ν^*	ratio of time to complete banana orbit to collision time
ρ (kg m^{-3})	density
ρ_e, ρ_i (m)	electron, ion gyroradius
ξ	plasma displacement
$\langle\sigma v\rangle_{\text{DT}}$ (m^3 s^{-1})	rate coefficient for D-T fusion
$\langle\sigma v\rangle_e$ (m^3 s^{-1})	rate coefficient for ionization
$\langle\sigma v\rangle_{cx}$ (m^3 s^{-1})	rate coefficient for charge exchange
τ_E (s)	energy confinement time
τ_s (s)	slowing down time for energetic ions
ϕ (V)	potential
χ (m^2 s^{-1})	thermal diffusivity
ψ	magnetic-flux function
ω (rad s^{-1})	angular frequency
ω_{ce}, ω_{ci} (rad s^{-1})	electron and ion cyclotron angular frequency
ω_{LH} (rad s^{-1})	lower hybrid angular frequency

I. INTRODUCTION

During the past two decades there have been substantial advances across the board in magnetic fusion research. In tokamaks, the main line of experimental research in the world program, reactor-level plasma conditions have been achieved (see Table I). Initial tests with deuterium-tritium fuel in the JET tokamak in 1991 led to the generation of 1.8 MW of fusion power (JET Team, 1992). More recently, the TFTR tokamak obtained over 6 MW of fusion power (TFTR Team, 1993). The characteristic time scale of plasma sustainment typical of the 1970s was 1 s. Tokamak and stellarator plasma parameters improved well above those attained in the 1970s have now been sustained for tens of seconds. The development of noninductive current drive (Yoshikawa and Yamato, 1966; Ohkawa, 1970; Fisch, 1980; Bevir and Gray, 1980) has opened the route to steady-state operation of the otherwise pulsed devices. The small superconducting tokamak TRIAM-1M (S. Itoh *et al.*, 1991) has been operated for one hour, at $\bar{n}=2\times 10^{18}$ m^{-3}, $T_e(0)=500$ eV.

Accompanying these advances in performance has been substantial progress in our understanding of the physics. The magnetohydrodynamics (MHD) behavior of plasmas is consistent with theoretical expectations, and sophisticated computer models are able to describe detailed MHD behavior. The theoretical predictions for the plasma-driven bootstrap current and noninductive current drive have been confirmed experimentally. While the transport area exhibits the greatest gulf between theory and experiment, neoclassical transport is observed in some circumstances, and progress has been made in relating theory and experiment in the plasma edge of tokamaks, stellarators, and reversed-field pinches

TABLE I. Key tokamak parameters: Achieved and required (Cordey *et al.*, 1992).

Parameter (not simultaneous)	1971	1981	1991	Steady-state *D-T* reactor
Central ion temperature T_{i0} (keV)	0.5	7	35	30
Central electron temperature T_{e0} (keV)	1.5	3.5	15	30
Energy confinement time τ_E (s)	0.007	0.05	1.4	3
Triple product $n_{i0}T_{i0}\tau_E$ (keV s m^{-3})	1.5×10^{17}	5.5×10^{18}	9×10^{20}	7×10^{21}
Plasma pressure $\beta=2\mu_0\Sigma nkT/B^2\times100$	0.1%	3%	11%	5%

(RFP's). The lack of a confirmed explanation of core transport is compensated by burgeoning experimental information in tokamaks, stellarators, RFP's, and compact tori, which has allowed empirical confinement scalings to be developed and some theoretical models to be tested.

Advances in technology supported many of the successes; see Table II. Multimegawatts of heating have been provided efficiently by neutral-hydrogen beams and by what is loosely called radio-frequency (rf) heating (frequencies from 1 MHz to 100+ GHz). Fueling by the injection of high-speed frozen pellets of hydrogen has led to improved plasma profiles and lower charge-exchange losses (Milora, 1989). The ability to handle effectively a large throughput of tritium has been demonstrated in the tritium systems test assembly (Anderson and Bartlitt, 1989). The use of high-field copper magnets, pioneered by MIT, has allowed high values of the plasma performance parameter—$nT\tau$—to be achieved in small facilities (Greenwald *et al.*, 1984), and leads to the possibility of compact deuterium-tritium (D-T)-burning, high-fusion-power (high-Q) tokamaks (Coppi, 1977; Cohn *et al.*, 1978). The ability to design for performance in large superconducting coil systems has been demonstrated in a number of facilities with coils at the 8-T level; see Table II. Improvements in superconducting materials and in manufacturing techniques permit 12-T coils to be considered for the next round of facilities, such as the International Tokamak Experimental Reactor (ITER); see ITER (Conceptual Design Team, 1991). Still higher-field coils are possible (Pourrahimi *et al.*, 1987).

Various materials, including graphite and beryllium, have been tested successfully as plasma facing components (Gauster, 1990; Thomas *et al.*, 1991). An increased understanding of the effects of 14-MeV neutron damage, using simulated neutron spectra in fission reactors, has led to the development of improved steels (Bloom, 1990). Tritium breeding tests in which small lithium blanket elements have been bombarded with neutrons are encouraging in showing a low retention for tritium, i.e., the reactor tritium inventory may be small (Johnson *et al.*, 1989). While remote handling for fusion is in its infancy, some successes have been achieved in applications on the JET tokamak (Jones *et al.*, 1991). These advances support the recent studies of magnetic fusion reactors and have allowed a refinement of the understanding of reactor physics needs.

In writing this review paper I have adopted the following strategy. First, I shall summarize briefly the fundamental building blocks that support the design of an effective reactor: power density (cost of electricity), power balance, transport equations and transport models, alpha-particle physics, MHD and beta limits, heating, fueling, and power and particle control. These areas are presented as generically as possible though inevitably the far greater amount of research done for the tokamak underpins much of our knowledge, and this work is presented to illustrate particular reactor problems.

Second, I shall discuss the physics of four toroidal reactor concepts: tokamak, stellarator, reversed-field Pinch (RFP), and a field-reversed theta-pinch configuration (FRC) as an example of a compact torus. The purpose is not to refer to all of the physics studies that have been done, but to refer to those studies that have a particular bearing on reactor design.

Third, an accurate description of the observed transport does not exist for any of the concepts. Reactor designers must make do with a mixture of empirical scaling, neoclassical transport, and, in some cases, theoreti-

TABLE II. Technology achievements.

Technology	Facility	Achievement
Neutral beams	TFTR	30 MW D° at 110 keV
RF	JET	22 MW ICH at 23 to 57 MHz
	JT-60	8 MW LHH at 1.7 to 2.2 GHz
	T-15	3 MW ECH at 75 and 81 GHz
S/C coils	LCTF	
	MFTF-B	$\lesssim$8-9 T
	Tore Supra	with both NbT_i and Nb_3Sn
	T-15	
Tritium handling	TSTA	1 kg per day

cally based models. In order to illustrate how the physics affects reactor scale and geometry, I have chosen to use for each concept a popular transport scaling with a multiplier. If readers feel that some other scaling is more appropriate, I hope they will find sufficient information in this paper to permit its use.

I have chosen not to make a comparative study of the four concepts, because they are not at the same stage of development. Since the early 1970s, the tokamak has been the major experimental vehicle for developing magnetic fusion. The other concepts lag the tokamak in demonstrated plasma performance, because the experiments have been smaller and comparable only with tokamaks of a decade or two ago. Nevertheless, in terms of relative performance, allowing for the difference in scale, a number of these concepts show sufficient promise to warrant their longer-term consideration (Sheffield, 1985). Success with the tokamak has led to the initiation of the engineering design phase of the International Thermonuclear Experimental Reactor (ITER) as a collaborative venture of the European Community, Japan, the Russian Federation, and the United States under the auspices of the International Atomic Energy Agency. ITER is designed to demonstrate controlled ignition and burn for 1000 seconds or longer in a deuterium-tritium plasma, and will provide a demonstration and integration test of reactor technologies (ITER Conceptual Design Team, 1991; Rebut, 1993). The present schedule calls for a construction start in 1998 and operation starting in 2005. ITER is a major element in the U.S. Magnetic Fusion Energy Program to develop a demonstration reactor by about 2025. A comparison of the parameters of ITER with those of present large tokamaks is given in Table III.

This review is built in great measure upon previous excellent reviews of reactors and related topics, and the reader is referred to them for a broader understanding of this interesting subject. The reviews include Rose, 1969; Post and Ribe, 1974; Furth, 1975; Miyamoto, 1978; Wesson, 1978; Rawls *et al.*, 1979; Proceedings of the IEEE 1981; Conn, 1981; Hagenson and Krakowski, 1981; Shohet, 1981; Stacy, 1984; Liewer, 1985; Bodin *et al.*, 1986; Freidberg, 1987; Tuszewski, 1988; Grieger *et al.*, 1989; Holdren *et al.*, 1989; Bodin, 1990; Nuclear Fusion Review, 1990; Krakowski *et al.*, 1991; and Post *et al.*, 1991.

The symbols and units (SI) are listed at the beginning of the article. In some places the units used differ because they are those used in the original paper. The original units are retained to allow easier comparison with the original paper.

II. GENERIC REACTOR CHARACTERISTICS

A. Representative reactor configuration

A cross section of a representative tokamak reactor is shown in Fig. 1. The magnetic field of about 4–8 T is produced, typically, by two sets of coils, a toroidal set producing a field B_ϕ and a poloidal set producing a field B_θ. The field lines twist around the toroidal plasma, forming nested flux surfaces; see Fig. 2. Generally, in a tokamak and stellarator $B_\phi \gg B_\theta$, in a very-low-aspect-ratio tokamak ($R/a \lesssim 1.5$) and a pinch device $B_\phi \gtrsim B_\theta$, whereas in a field-reversed configuration $B_\phi \ll B_\theta$. Linear systems such as the tandem mirror (Post, 1987, 1988; Hershkowitz *et al.*, 1990) no longer receive as much attention in the world program as reactor candidates, and will not be reviewed, though they are interesting as possible sources of 14-MeV neutrons for testing purposes. In a D-T-burning reactor, the average plasma temperature will be in the range 8–25 keV (100 000 000–300 000 000 K), at a density of 10^{20}–10^{22} m^{-3}.

The geometry of the flux surfaces is characterized by the major radius of the toroidal plasma (R), the minor radius (r), and the poloidal angle (θ). The flux surfaces may be elliptical; the minor radius of the edge of the plasma in the median plane is commonly denoted by (a), while the minor radius in the z (vertical) direction is denoted by (b). The ellipticity is denoted by $\kappa = b/a$ (this may vary with minor radius). In simplified treatments of this geometry, it is common practice to approximate the noncircular plasma by a circular plasma of equivalent minor radius $r(b/a)^{1/2}$, where r is the radius in the medi-

TABLE III. Parameters of modern large tokamaks and ITER.

Tokamak	TFTR	JET	JT-60	ITER
Major radius $R(m)$	2.45	3.10	3.40	7.75
Aspect ratio R/a	2.90	2.82	4.0	2.8
Ellipticity κ	1.0	1.8	1.6	1.55
Current I(MA)	3.0	6.0	6.0	25
Field B_ϕ (T)	5.12	3.4	4.2	6.0
Divertor	No	Yes	Yes	Yes
Coil type	Cu	Cu	Cu	SC
Fuel	H,D,T	H,D,T	H,D	D-T
Pulse length (s)	2	20+	20+	1000
Estimated fusion power (MW)[a]	~15	~50		~1500

[a]Projected fusion power. Obtained, JET 1992, 2 MW; TFTR 1993, 6 MW.

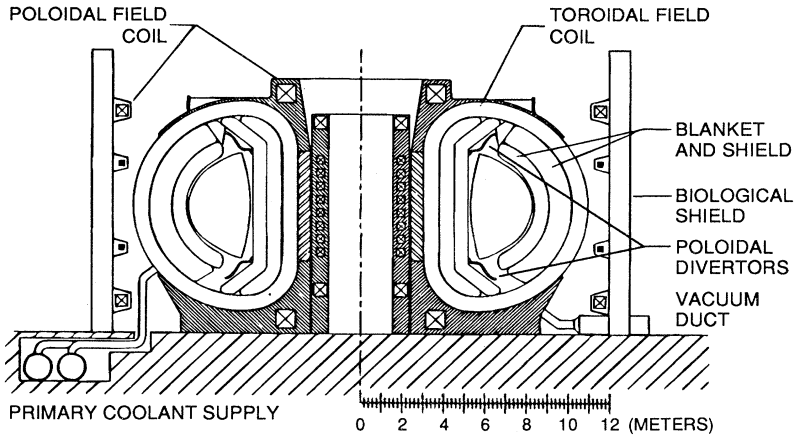

FIG. 1. Cross section of a representative tokamak reactor (Najmabadi *et al.*, 1991).

an plane. In this approximation, the average minor radius of the plasma edge is $(ab)^{1/2}$. In reality the flux surfaces may not be centered on the midpoint of the medium plane diameter, owing to the effects of finite plasma pressure, causing an outward shift of the plasma (see Sec. III B, Fig. 26). In addition, the shape is often more like a D, and such shapes may be characterized by an additional parameter, the triangularity (δ).

Parameters of importance in characterizing the fusion plasma are the energy confinement time (τ_E), which equals the stored energy in the plasma (W) divided by the heat (P) leaving the plasma (excluding the neutrons),

$$\tau_E = \frac{W}{P}(s) \tag{2.1}$$

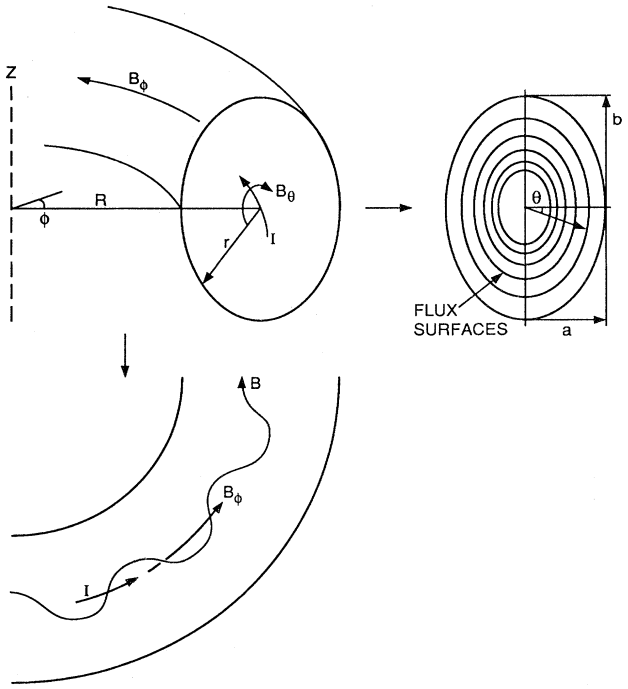

FIG. 2. Nested flux surfaces in a toroidal system.

and beta (β), which is the ratio of the kinetic pressure $(n_e kT_e + n_i kT_i + \Sigma n_z kT_z)$ of the plasma divided by the magnetic pressure,

$$\beta = \frac{(\text{pressure} \times 100)}{(B^2/2\mu_0)}\% \ . \tag{2.2}$$

The development of reactor levels of τ_E and β has dominated magnetic fusion research, and good progress has been made. However, much more is required for an attractive reactor than high τ_E and β. Equally critical are impurity minimization and control, low recirculating power for plasma production and control, the development of radiation-resistant, low-activation materials, and high reliability and maintainability.

The magnet coils are protected from the nuclear radiation by a moderator of the neutrons (usually called the blanket) and by a shield which absorbs neutrons and gamma rays. In the case of a D-T plasma, the blanket contains lithium to breed tritium to replace that burned in fusion reactions. In most configurations the outer magnetic flux surfaces are diverted onto targets, which absorb the heat, thus isolating most of the chamber wall from direct contact with the plasma. The first wall and the blanket and shield elements form a vacuum chamber. A coolant, liquid or gas, removes the heat deposited to the wall, blanket, shields, and divertor targets and transports it to heat exchangers and generators which produce electricity.

B. Nuclear fusion reactions and the fuel cycle

The nuclear fusion reactions of greatest relevance to magnetic fusion, because they occur at the lowest temperatures, are listed in Table IV. The charged-particle power per unit volume released is shown in Fig. 3. The final number is the equivalent electrical energy imparted to the nuclei (kWh) per gram mass of the reacting nuclei. For comparison, the chemical reaction $2H_2+O_2 \rightarrow H_2O+H_2O+0.000006$ MeV yields 0.0044 kWh/g. In the case of deuterium-tritium (D-T) fusion, because tritium does not occur naturally it is necessary to breed triti-

TABLE IV. Nuclear fusion reactions of greatest relevance to magnetic fusion. The final two quantities in each line refer to the total nuclear energy release in one reaction and to the energy release in the form of charged particles, respectively.

Reaction	Energy		
	Charged particle (MeV)	Total (MeV)	Total equivalent energy (kWh/g)
(1) $D+T\rightarrow{}^4He(3.52\ MeV)+n\ (14.06\ MeV)$	3.52	17.58	94,000
(2a) $D+D\rightarrow{}^3He(0.82\ MeV)+n\ (2.45\ MeV)$	0.82	3.27	22,000
(2b) $D+D\rightarrow T(1.01\ MeV)+p\ (3.03\ MeV)$	4.04	4.04	27,000
(3) $D+{}^3He\rightarrow{}^4He\ (3.67\ MeV)+p\ (14.67\ MeV)$	18.34	18.34	98,000

um by bombarding lithium with the fusion neutrons,

$$^6Li+n={}^4He+T+4.80\ MeV\ ,$$
$$^7Li+n={}^4He+T+n-2.47\ MeV\ . \qquad (2.3)$$

The D-T-Li fuel cycle is the most attractive, because a self-sustaining plasma may be realized at the lowest plasma temperatures $T\gtrsim 5$ keV (fusion power exceeds bremsstrahlung radiation losses), and it will be the basis of most of the discussion in this paper. The optimum temperature is about 15 keV.

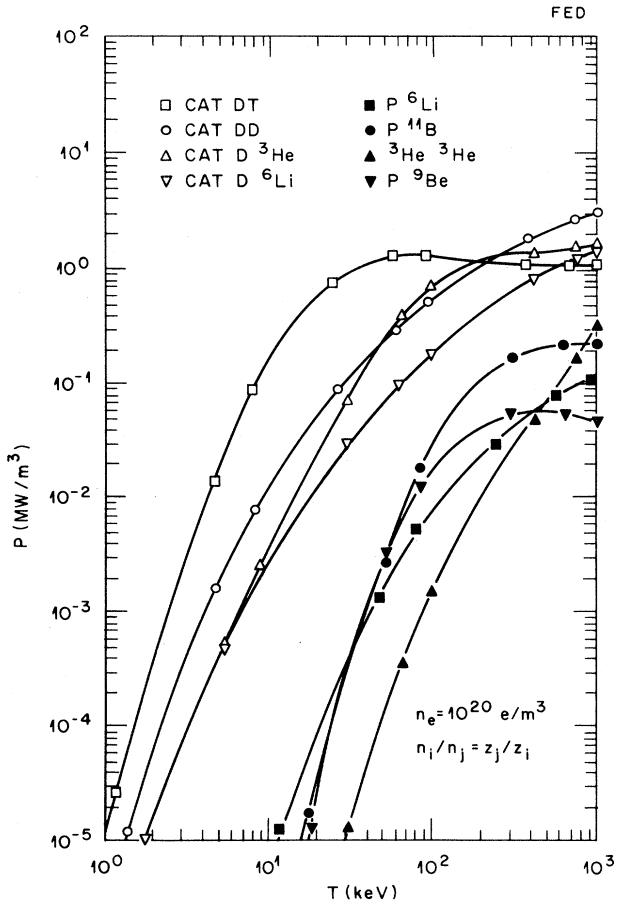

FIG. 3. Maximum charged-particle power density release vs temperature for the principal fusion fuels in thermalized plasmas at $n_e=10^{20}$ m^{-3} and $n_i/n_j=Z_j/Z_i$. Power output scales as the square of the electron density (McNally, 1982).

Deuterium is abundant in nature as about 1 part in 6500 in the hydrogen in water. It requires no fuel breeding; however, a plasma temperature $T\gtrsim 20$ keV is required by a self-sustaining deuterium plasma to overcome bremsstrahlung and synchrotron radiation. The optimum temperature is about 40 keV. It may be lowered to around 35 keV if the T and ^{3}He fusion products are recirculated, a scenario referred to as "catalyzed D-D." At first sight the lower fraction of neutron energy produced per reaction appears attractive for reducing neutron activation of the reactor structure. In fact, the number of neutrons per reaction, because of their lower energy, is not reduced enough to make a significant difference. The absence of a breeding blanket is an advantage.

The D-^{3}He reaction is attractive because it produces no neutrons. However, to take advantage of this, it is necessary to run with a lean mixture of deuterium to minimize D-D reactions. It also requires a high temperature, $T\gtrsim 30$ keV, for a self-sustaining plasma. A principal disadvantage is the lack of a source of ^{3}He on earth. Apparently it is abundant on the moon, and proposals have been made to mine the moon to support earth-based D-^{3}He fusion reactors (Kulcinski *et al.*, 1989).

The charged-particle power per unit volume produced by fusion reactions is given by the product of the densities of the reacting ions, the rate parameter $\langle\sigma v\rangle$, and the charged-particle power density released per reaction.

For a D-T plasma,

$$p_\alpha=n_D n_T\langle\sigma v\rangle_{DT}E_\alpha\ , \qquad (2.4)$$

where $\langle\sigma v\rangle$ is the product of the D-T reaction cross section σ and the relative velocity of the D and T nuclei, averaged over a Maxwellian velocity distribution. Cross sections and reaction rates are given in numerous reports (e.g., Glasstone and Lovberg, 1960; Bosch and Hale, 1992). Formulas have been developed to approximate the fusion power density for D-T plasmas in various temperature regions (Uckan *et al.*, 1990).

For model density and temperature profiles

$$n = n_0\left[1-\frac{r^2}{a^2}\right]^{\alpha_n},\quad T = T_0\left[1-\frac{r^2}{a^2}\right]^{\alpha_T}, \tag{2.5}$$

$$\langle p_\alpha\rangle \simeq 0.16 f(\alpha_n,\alpha_T)\left[\frac{n_{\rm DT}}{n_e}\right]^2 n_{20}^2 F_\alpha\left[\frac{T_{10}}{T_{10C}}\right]\ (\mathrm{MW\,m^{-3}}), \tag{2.6}$$

$$f(\alpha_n,\alpha_T) = (1+\alpha_n)^2(1+2\alpha_n+3\alpha_T)^2/(1+2\alpha_n+2\alpha_T)^3,$$

$$F_\alpha\left[\frac{T_{10}}{T_{10C}}\right] = \left[\frac{T_{10}}{T_{10C}}\right]^3,\quad T_{10} < T_{10C},$$

$$= \left[\frac{T_{10}}{T_{10C}}\right]^2,\quad T_{10C} < T_{10} < 2T_{10C},$$

$$= 4\left[\frac{T_{10}}{2T_{10C}}\right]^{1.5},\quad 2T_{10C} < T_{10} < 3T_{10C},$$

where

$$T_{10C} = [(1+\alpha_n)(1+2\alpha_n+3\alpha_T)]/[(1+\alpha_n+\alpha_T)(1+2\alpha_n+2\alpha_T)].$$

For reference profiles $\alpha_n = 0.5$ and $\alpha_T = 1.0$

$$\langle p_\alpha\rangle = 0.25\left[\frac{n_{\rm DT}}{n_e}\right]^2 (n_{20}T_{10})^2(\mathrm{MW\,m^{-3}})\ \text{ for } \langle T\rangle = 7.5 \text{ to } 15 \text{ keV}$$

$$= 0.25\left[\frac{n_{DT}}{n_e}\right]^2 (n_{20}T_{10}^2\left[\frac{1.5}{T_{10}}\right]^{0.5}(\mathrm{MW\,m^{-3}}) \text{ for } \langle T\rangle = 15 \text{ to } 22 \text{ keV}, \tag{2.7}$$

where $n_{20} = \langle n_e/10^{20}\ \mathrm{m^{-3}}\rangle$ and $T_{10} = \langle T/10\ \mathrm{keV}\rangle$, $n_{\rm DT}$ and n_e are the densities of deuterium plus tritium and electrons, respectively, and $\langle T\rangle$ is the density-weighted volume-averaged temperature. Note $n_{\rm DT} < n_e$ because of impurities n_z.

In practice, pressure profiles in tokamaks and stellarators are often more peaked, with $\alpha_n < 0.5$ and $\alpha_T \sim 2$, yielding somewhat higher fusion power for a given beta. In contrast, FRC profiles are somewhat flatter.

There are two other useful quantities for characterizing a reactor. The neutron flux leaving the plasma edge is

$$p_{wn} = \frac{P_{nm}}{A_w} = \frac{n_D n_T\langle\sigma v\rangle_{\rm DT} E_{nm} V_p}{A_w}\ (\mathrm{MW\,m^{-2}}), \tag{2.8}$$

where E_{nm} (measured in megajoules) is the neutron energy per reaction, $V_p = 2\pi^2 R a^2 \kappa$ is the plasma volume, κ is the plasma ellipticity, and A_w is the area of the chamber wall. The neutron fluence is the time integral of the neutron flux falling on the wall. For a reactor we may expect $p_{wn} \gtrsim 2\ \mathrm{MW\,m^{-2}}$, and we require a wall that can survive neutron bombardment for a number of years, i.e., survive a neutron fluence of, say, 15–25 MW yr m^{-2}.

C. Plasma power balance

The state of the plasma density and temperature is determined by the detailed balance of particle production and loss and power input and loss. In general, we shall be discussing hydrogen plasmas (H, D, T); however, the purity of such plasmas will vary owing to materials released from the chamber walls—impurities—and in the case of fusion plasmas owing to fusion products such as ^{3}He and ^{4}He. Quasineutrality will hold in the plasma. These impurities will be ionized and become multiply charged ($Z > 1$) so that in general $n_i < n_e = n_i + \sum_z Z n_z$, where Z is the charge state of each impurity ion. The subscripts i and e refer, respectively, to the hydrogen ions (combination of H, D, and T) and to electrons. A convenient measure of the impurity level is the parameter

$$Z_{\rm eff} = \frac{\sum_z Z^2 n_z + n_i}{n_e}. \tag{2.9}$$

The particle balance in a basically single-ion-species plasma, setting $n_i = n_e$, is given in a cylindrical (toroidal) system by

$$\frac{\partial n}{\partial t} = n n_n\langle\sigma v\rangle_e + \frac{1}{r}\frac{\partial}{\partial r}\left[rD_A\frac{\partial n}{\partial r} + rV_r n\right]\ (\mathrm{m^{-3}\,s^{-1}}), \tag{2.10}$$

where $\langle\sigma v\rangle_e$ is the ionization rate (Freeman and Jones, 1974) of the neutral particles that fuel the plasmas; see Sec. II.G, Fig. 17, where various rate coefficients are plotted. Note, different conventions are used for the sign of V_r; as used here a positive V_r denotes an inward convection of particles. Because the system acts to maintain

charge neutrality, the losses of electrons and ions are equal and proceed at the rate of the better confined species. The ambipolar diffusion coefficient D_A is used because the particle transport adjusts to maintain charge neutrality via the self-consistent electric field. In tokamak experiments it is observed that $D_A \sim (0.2-0.3)\chi_e$, where χ_e is the electron thermal diffusivity. The parameter V_r is a radial convective velocity.

The power balance may be written separately for each species. For the electrons, a simplified power balance is

$$\frac{\partial}{\partial t}\left[\frac{3}{2}neT_e\right]=\frac{1}{r}\frac{\partial}{\partial r}r\left[n_e\chi_e\frac{e\partial T_e}{\partial r}+\frac{3}{2}D_A eT_e\frac{\partial n}{\partial r}\right]+p_\Omega +p_{ie}-p_{LR}-p_{br}-p_S+p_r+p_{\alpha e} +p_{ae}\ (\mathrm{W\,m^{-3}})\ . \tag{2.11}$$

For the ions

$$\frac{\partial}{\partial t}\left[\frac{3}{2}n_i eT_i\right]=\frac{1}{r}\frac{\partial}{\partial r}r\left[n_i\chi_i\frac{e\partial T_i}{\partial t}+\frac{3}{2}D_A eT_i\frac{\partial n}{\partial r}\right] +p_{ei}-p_{cx}+p_{ai}+p_{\alpha i}+p_{ai}\ (\mathrm{W\,m^{-3}})\ . \tag{2.12}$$

Note that temperatures are given in electron volts. In addition there are similar equations for each impurity species. Generally, collisions between ion species maintain $T_z \sim T_i$. The transport of impurities is, however, more complex and, as discussed below, depends on details of the plasma gradients. Impurities may move radially, relative to the background plasma, either in or out. The parameters χ_e and χ_i ($\mathrm{m^2\,s^{-1}}$) are the electron and ion thermal diffusivities, and the p ($\mathrm{MW\,m^{-3}}$) are the power densities of the various mechanisms indicated. The overall power flow is illustrated in Fig. 4:

$$p_{ei}=-p_{ie}=3\nu_{ei}n_e\frac{m_e}{m_i}e(T_e-T_i)\ (\mathrm{W\,m^{-3}})\ , \tag{2.13}$$

where $\nu_{ei}=2.92\times10^{-12}Z_{\mathrm{eff}}nT_e^{-1.5}\ln\Lambda_e$ ($\mathrm{s^{-1}}$) and $\ln\Lambda_e = 30.9-\ln(n^{0.5}T_e^{-1})$ represent the collisional transfer of power from electrons to ions and vice versa, with n ($\mathrm{m^{-3}}$) and T_e (eV) (Braginskii, 1965).

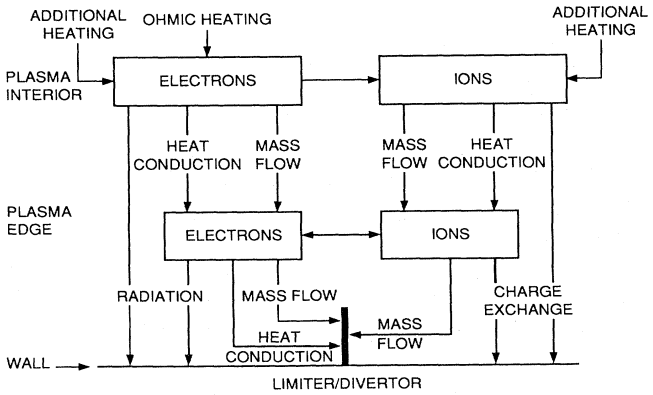

FIG. 4. Power flow in a typical toroidal plasma.

The line radiation is given by (Jensen *et al.*, 1977)

$$p_{\mathrm{LR}}=\sum_z n_e n_z f(z)(\mathrm{W\,m^{-3}})\ . \tag{2.14}$$

This is the dominant radiation term in present-day tokamaks (typically 20–40% of the power is radiated), and it is particularly important at the plasma edge. As shown in Fig. 5, $f(z)$ is a strongly increasing function of Z as the impurities become more massive. Consequently small amounts of heavy materials such as molybdenum and tungsten can have a disproportionately large effect. Recombination radiation (p_r) is generally less important than line radiation.

The bremsstrahlung power density (Rose and Clark, 1961, p. 232) for the range of $n(\mathrm{m^{-3}})$ and T_e (eV) values appropriate to D-T reactors is given approximately by

$$p_{\mathrm{br}}=1.7\times10^{-38}\zeta n_e^2 Z_{\mathrm{eff}}T_e^{0.5}(\mathrm{W\,m^{-3}})\ . \tag{2.15a}$$

This represents the total emission at all wavelengths of the continuum from the free-free energy transitions of the (optically thin) plasma electrons. The Gaunt factor ζ corrects for electron-electron collisions and relativistic effects. For 1 keV $< T_e <$ 100 keV, ζ varies from $1.2 < \zeta < 1.1$; see Ecker, 1972.

A formula for the average bremsstrahlung power density has been given by Uckan *et al.* (1990) for the model density and temperature profiles in Eq. (2.5),

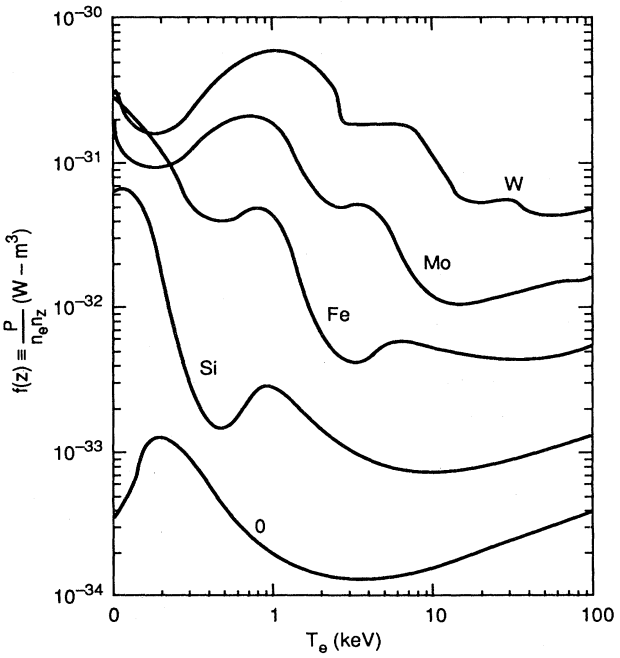

FIG. 5. Line radiation factor f (z) as a function of electron temperature for representative impurities (Jensen *et al.*, 1977).

$$\langle p_{\rm br}\rangle \simeq 1.6\times10^{4} Z_{\rm eff}\left\{\frac{(1+\alpha_n)^{3/2}(1+\alpha_n+\alpha_T)^{1/2}}{(1+2\alpha_n+0.52\alpha_T)}\right\} \times n_{20}^{2} T_{10}^{1/2}\ (\mathrm{W\,m^{-3}})\ . \tag{2.15b}$$

For reference profiles $\alpha_n=0.5$ and $\alpha_T=1.0$

$$\langle p_{\rm br}\rangle \simeq 1.86\times10^{4} Z_{\rm eff} n_{20}^{2} T_{10}^{1/2}\ (\mathrm{W\,m^{-3}})\ . \tag{2.15c}$$

It is informative to study the ratio

$$\frac{\langle P_{\rm br}\rangle}{\langle P_\alpha\rangle} \simeq 0.074 Z_{\rm eff} \Big/ \left\{\left[\frac{n_{\rm DT}}{ne}\right]^{2} T_{10}^{3/2}\right\}\ . \tag{2.15d}$$

Values of this ratio, for $\langle T\rangle=5.0$ to 15 keV, are given in Table V. For realistic impurity levels it is difficult to have a viable fusion reactor for an average temperature much less than 7.5 keV because the sum of bremsstrahlung, line radiation, and direct alpha-particle losses leaves too little power to sustain a reasonable-size plasma.

At low plasmas densities, low beta values, and high temperatures, the sychrotron radiation (Spitzer, 1962, p. 152) emitted by the electrons from their magnetic orbits is an important factor in the plasma power balance (Trubnikov, 1979),

$$p_s \simeq 1.3\times10^{-8} T_e^{2.5} B^{3}[1+X_{\rm syn}]^{0.5} \times(1-\mathcal{R})^{0.5}/a\ (\mathrm{W\,m^{-3}})\ , \tag{2.16}$$

where T_e (eV) and $X_{\rm syn}=5.7\times10^{2} a/RT_e^{0.5}$ is a correction factor for field inhomogeneity and Doppler broadening of the emission spectrum. $\mathcal{R}$ is the wall reflection coefficient.

The power input due to heating by a plasma current—ohmic heating—is given by

$$p_\Omega = 7.53\times10^{-5}\gamma_R Z_{\rm eff} j^{2} \ln\Lambda_e / T_e^{1/5} (\mathrm{W\,m^{-3}})\ , \tag{2.17}$$

where $\gamma_R \simeq (1-1.95\epsilon^{0.5}+0.95\epsilon)^{-1}$, $\epsilon=r/R$ is a neoclassical resistivity correction factor allowing for trapped-electron effects, and j is the local plasma current density.

The losses due to charge exchange of the plasma ions on the background neutral particles are given by

$$p_{cx} = nn_n \langle\sigma v\rangle_{cx} eT_i\ (\mathrm{W\,m^{-3}}) \tag{2.18}$$

when $\langle\sigma v\rangle_{cx}$ is the rate coefficient.

The additional (or auxiliary) heating, i.e., other than ohmic and alpha-particle heating, is represented for electrons and ions by p_{ae} and p_{ai}, respectively.

The average alpha-particle power density for a D-T plasma is given by Eq. (2.6). An approximate formula for the local value is

$$p_\alpha \simeq 6.2\times10^{-43} n_D n_T T_i^{2}\ (\mathrm{W\,m^{-3}}),\quad T<20\ \mathrm{keV}\ , \tag{2.19}$$

where T_i (eV) is the assumed common temperature of the deuterons and tritons.

The alpha particles are born with an energy of 3.5 MeV and initially slow down mainly by collisions with electrons. At a critical energy $E_{\rm crit}$, the rate of loss to the ions becomes equal to that to the electrons, and at lower energies the loss to the ions predominates (Stix, 1972):

$$E_{\rm crit} = 14.8 AT_e \left[\frac{1}{n_e \ln\Lambda_e}\left[\sum \frac{n_j Z_j^{2} \ln\Lambda_i}{A_j}\right]\right]^{2/3} (\mathrm{eV}) \simeq 0.1 AT_{10}\ (\mathrm{MeV})\ , \tag{2.20}$$

where A and A_j are the atomic weights of the slowing down particle and plasma ions, respectively, and Z_j is the charge number of the plasma ions. The average fraction G_i of the total energy given up to the thermal ions of the plasma is

$$G_i = \frac{E_{\rm crit}}{E}\int_0^{E/E_{\rm crit}} \frac{dy}{(1+y^{3/2})}\ . \tag{2.21}$$

For a pure fifty-fifty, D-T plasma at a temperature of 20 keV, $E_{\rm crit}=660$ keV and $G_i\simeq0.20$ for 10 keV, and $G_i\simeq0.33$ for 20 keV.

It is convenient to describe the energy losses in terms of an energy confinement time τ_E (s), which is equal to the plasma stored energy divided by the total power loss from the plasma in equilibrium (P).

For a toroidal plasma, major radius R, minor radius in the median plane a, and ellipticity κ,

$$\tau_E = \tfrac{3}{2} 2\pi^{2} Ra^{2}\kappa \frac{e\langle n_e T_e + n_i T_i\rangle}{P}\ (\mathrm{s})\ . \tag{2.22}$$

For a plasma sustained by the fusion alpha power, and $T_{10C}<T_{10}<2T_{10C}$, a parabolic temperature profile ($\alpha_T=1$) and square-root parabolic density profile ($\alpha_T=0.5$), from Eq. (2.7) we have $T_{10C}=0.75$ and

$$P_\alpha = 4.9\times10^{-42} \langle n_{DT} T_i^{2}\rangle^{2} Ra^{2}\kappa\ (\mathrm{W})\ , \tag{2.23}$$

where $n_{\rm DT}$ is the density of deuterium plus tritium ions. Substituting for P_α in Eq. (2.22), with $T_e=T_i=T$, leads to a requirement for a self-sustaining pure D-T plasma ($n_e=n_i$)

$$\langle n_{\rm DT} T_i\rangle \tau_E \simeq 1.93\times10^{24}\ (\mathrm{m^{-3}\ eV\,s})\ . \tag{2.24}$$

For example, if $\langle n_{\rm DT} T_i\rangle = 1.5\times10^{20}\ \mathrm{m^{-3}}\times10$ keV, we require $\tau_E=1.3$ s.

For a D-T plasma contaminated by impurities and helium we must allow for the depletion of D-T fuel by multiplying by $(n_e/n_{\rm DT})^{2}$.

It is useful to derive a relationship between the global energy confinement time and the thermal diffusivity χ. In steady state Eq. (2.11) may be rewritten as

$$\frac{1}{r}\frac{\partial}{\partial r} r\left[n_i e\chi_i \frac{\partial T_i}{\partial r} + n_e e\chi_e \frac{\partial T_e}{\partial r}\right] = f_\alpha p_\alpha\ , \tag{2.25}$$

TABLE V. Values of the ratio $\langle P_{\rm br}\rangle/\langle P_\alpha\rangle$ for $Z_{\rm eff}=1.8$ and $n_{\rm DT}/ne=0.8$.

$\langle T_{10}\rangle$	0.50	0.75	1.0	1.25	1.50
$\langle P_{\rm br}\rangle/\langle P_\alpha\rangle$	0.59	0.32	0.21	0.15	0.11

where all of the nonconduction losses and auxiliary heating sources have been wrapped up in the factor f_α. f_α is the product of two terms: $f_{\alpha 1}$ = the fraction of alpha power transferred to the plasma; $f_{\alpha 2}=1-f_r$ where f_r is the fraction of input power radiated. Sometimes quoted confinement times, derived experimentally, include radiation losses. In this case f_r should be set equal to zero unless the radiation losses are expected to be different in the reactor regime, e.g., if bremsstrahlung takes on a greater level of importance, when $f_1 \simeq \langle p_{\rm br}/\langle p_\alpha \rangle$ is large [see Eq. (21.5d)], or synchrotron radiation becomes large. If theoretical or experimentally based thermal diffusivities are used, then full account must be taken of line, bremsstrahlung, and synchrotron radiation. If auxiliary power is applied, for example for current drive, then there is a third factor $f_{\alpha 3} \simeq 1+f_a$, where $f_a = p_a/p_\alpha$. For example, in a tokamak reactor one might have $f_{\alpha 1} \simeq 0.95$, $f_{\alpha 2} \approx 0.85$, allowing for bremsstrahlung losses at $\langle T \rangle = 15$ keV and line radiation and, if auxiliary heating is applied with $f_{\alpha 3} \simeq 1.1$, in total we have $f_\alpha = 0.89$.

Integrating over the plasma volume yields

$$-4\pi^2 Rr \left[n_i e \chi_i \frac{\partial T_i}{\partial r} + n_e e \chi_e \frac{\partial T_e}{\partial r} \right] \Bigg|_{r=\bar{a}} = f_\alpha P_\alpha \ , \tag{2.26}$$

where for a noncircular plasma we have used the notation $\bar{a}=(ab)^{0.5}$ (see Sec. II. A). Assuming a parabolic temperature profile and roughly flat density profile, we find that $-rn(\partial T/\partial r)|_{r=\bar{a}} \simeq 4\langle nT \rangle$. Consequently when we equate Eqs. (2.26) and (2.22) with $P = f_\alpha P_\alpha$ we find that

$$\chi_E \simeq \frac{0.38ab}{\tau_E} \ \mathrm{m^2\,s^{-1}} \tag{2.27}$$

where τ_E represents the energy confinement in the face of conduction losses, and χ_E is a global value

$$\chi_E = \frac{\langle \chi_i n_i T_I + \chi_e n_e T_e \rangle}{\langle n_i T_i + n_e T_e \rangle} \ . \tag{2.28}$$

For example, if $a=1.5$ m, $b=3$, m, $\tau_E=1.5$ s, $\chi_E \simeq 1.14$ $\mathrm{m^2\,s^{-1}}$.

D. Generic reactor characteristics

In recent years numerous studies have been made of magnetic fusion reactors, including those of Badger, 1979; Hagenson *et al.*, 1979; Baker, 1980; Hagenson and Krakowski, 1981; Logan *et al.*, 1983; Miller *et al.*, 1983; Najmabadi *et al.*, 1990, 1991; Painter and Lyon, 1991; and Seki *et al.*, 1991. These studies, which involve estimates of the cost of the reactor and its operation, are used to show how fusion might be competitive with other energy sources, based on our present understanding of physics and technology capabilities. In using these studies we must be careful to decouple the limitations set by generic considerations from those deriving from our present understanding. On the one hand, advances can be expected in many areas, e.g., superconducting coils and better optimized beta. On the other hand, generic constraints such as classical (neoclassical) physics, neutron attenuation lengths in shield materials, and cross sections for tritium breeding and D-T fusion set ultimate limits. Fortunately, there is a great deal of commonality among the various reactor concepts (tokamak, RFP, stellarator, mirror). This fact has been used to generate the "generic toroidal reactor" (Shefield, 1986), which is a useful tool for identifying, in an approximate way, the combined physics requirements for an "attractive reactor," i.e., one that might be competitive with fission. The studies have been extended to include consideration of environmental and safety aspects (Holdren *et al.*, 1988, 1989). A recent review has been given by Holdren (1991).

The generic reactor is a steady-state toroidal system operating with D-T fuel, which includes all of the components common to the various types of fusion reactor—superconducting coils, a lithium breeding blanket, plasma heating and fueling systems, shielding, coil structure, power supplies, remote handling, buildings, generators, and cooling towers, as illustrated in Fig. 6. In a small-aspect-ratio version the generic reactor approximates a tokamak, at intermediate aspect ratios a stellarator, and at large aspect ratios a tandem mirror. It is a somewhat less accurate representation of systems such as the RFP and field-reversed configuration (FRC), in which the main field is produced by a plasma current. An example of coupled values of $\langle \beta \rangle$ and global thermal diffusivity χ_E is shown for reference 1200-Mw(e) reactors in which the aspect ratio is varied (see Fig. 7). in this example the neutron flux to the first wall (p_w) was in the range 5–6 $\mathrm{MW\,m^{-2}}$, and the maximum field on the toroidal coil (B_m) was in the range of 8–12 T. A different optimization was used in the recent ARIES-1 study (Najmabadi *et al.*, 1991), with $p_w \simeq 2.5$ $\mathrm{MW\,m^{-2}}$ and $B_m = 21$ T using more advanced superconducting technology. Under these conditions a lower value of $\langle \beta \rangle$ was permitted, $\simeq 2\%$ at $R/a=4.5$. Thus we see that the physics requirements for a magnetic fusion reactor are

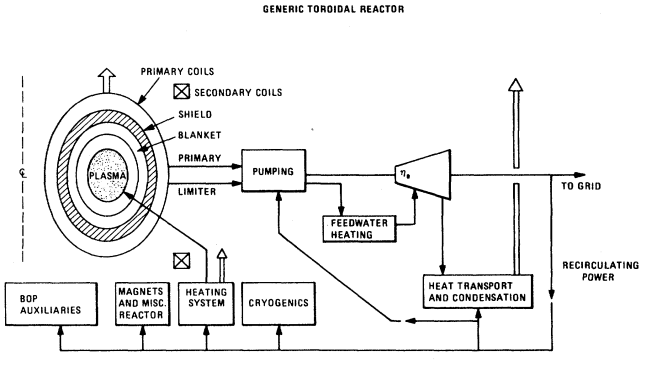

FIG. 6. Principal components of a generic D-T fusion reactor.

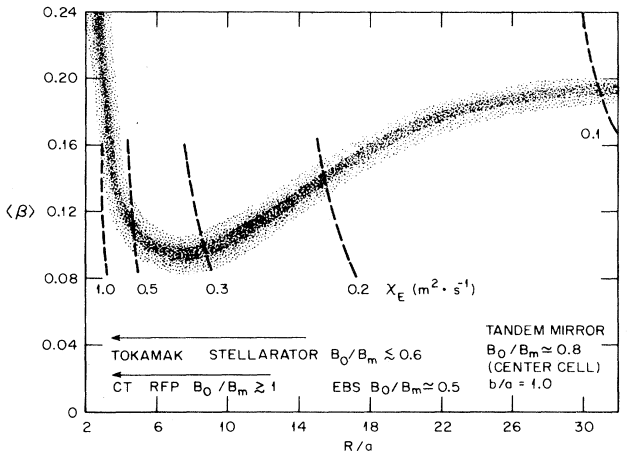

FIG. 7. Coupled values of $\langle\beta\rangle$ and χ_E required for a self-sustaining D-T toroidal plasma as a function of the aspect ratio, for $P_F=3500$ MW, $P_a=100$ M(e), $B_m=8$ to 12 T, and $b/a=1.0$ to 2.0 (Sheffield, 1986).

intimately bound up with the capabilities of the technology.

The cost of electricity (COE, 10 mills=1 cent) depends approximately linearly on the size (weight) of the reactor for a given power output, as illustrated in the generic reactor studies (Fig. 8). From both the individual reactor studies and the generic studies it is concluded that as a rough figure of merit an "attractive" magnetic fusion reactor should produce $\gtrsim 100$ kWe per tonne of the fusion island (coils, structure, blanket, and shield (Miller *et al.*, 1982; Conn and Gross, 1985; Sheffield, 1986). As can be seen in Fig. 8, the rate of change of COE with fusion island weight is slow because of the large fraction

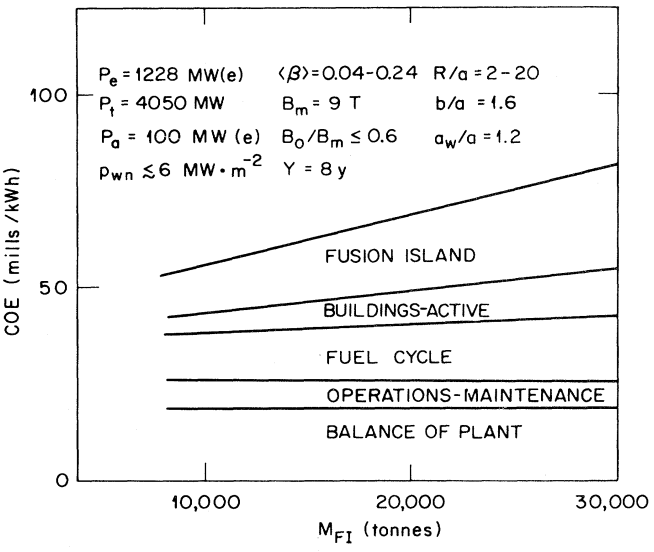

FIG. 8. The cost of electricity (COE) decreases linearly with decrease in the mass of the fusion island for a generic reactor (Sheffield, 1986).

of the costs fixed by the balance of plant and operations and maintenance. A change from 10 000 tonnes to 20 000 tonnes results is only a 30% penalty in COE. However, it should be noted that at 10 000 tonnes (1200 MWe) the estimated cost is on the high side of good fission reactor experience. The attractiveness of the fusion reactor lies in its potential for better environmental and safety characteristics than a fission reactor. Whether the reactor needs to weigh less than 10 000 tonnes or may weigh more depends on factors such as the ease of maintenance, complexity, level of power recirculated to the plasma, and the importance (costs benefit) assigned to environmental and safety features. The simple figure of merit is valuable because it allows us to understand the relative importance of the various physics and technology characteristics in a simple model, which relates the physics requirements, for a given magnetic configuration, to the technology capabilities and generic limitations (Spears and Wesson, 1980; Sheffield, 1985). This simplified model of a toroidal reactor fusion island is shown in Fig. 9. The weight of the fusion island is given by

$$M_{\rm FI}=2\pi^2 R[(a+b)t+t^2]\rho_{\rm FI}\ ({\rm kg})\ , \tag{2.29}$$

where the average density of materials in the fusion island, including the scrape-off layer (plasma-wall gap) and other gaps is $\rho_{\rm FI}\sim 5600\ {\rm kg\,m^{-3}}$; $t(m)$ represents the radial thickness of the scrape-off layer, blanket, maintenance gaps, shield, structure, and coils. The total thermal power for the reactor is given by

$$P_t=P_\alpha[1+4(1+g)]+P_a\ ({\rm W})\ , \tag{2.30}$$

where g is the blanket neutron gain. We shall use the value from the Starfire reactor study (Baker *et al.*, 1980), $g=0.14$. P_a is the auxiliary power injected into the plasma to sustain it. The net electric power is given by

$$P_e=\eta_e(1-\eta_r)[0.7+4.50]P_\alpha\ , \tag{2.31}$$

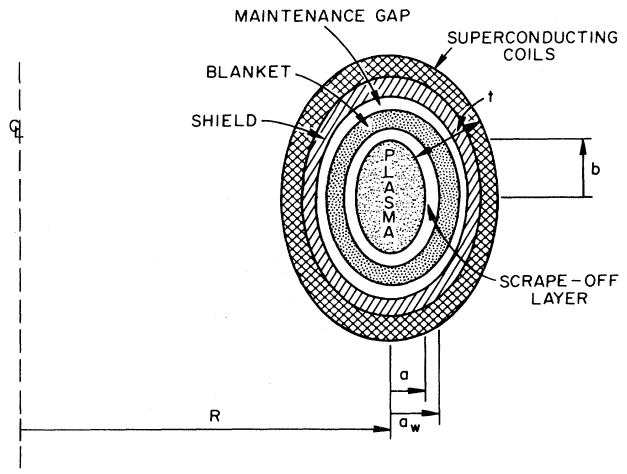

FIG. 9. Simplified model of the fusion island of a toroidal reactor.

where η_e is the thermal-to-electric conversion efficiency and we have approximated the useful thermal heat leaving the plasma ($P_\alpha+P_a$) by $0.7P_\alpha$ to allow for incomplete recovery of the heat. The fraction of power recirculated to the reactor is η_r.

A commonly used characteristic of a fusion reactor is Q, the ratio of the fusion power output P_F to the power injected in the plasma to maintain the plasma,

$$Q=\frac{P_F}{P_a} . \tag{2.32}$$

An engineering version, Q_E, takes that ratio of P_F to the total recirculated power $\eta_r P_t$

Defining η_{r0} as the fraction of power recirculated to the balance of plant and coils and setting $P_t \simeq 1.05P_F$,

$$\eta_r=\frac{0.95}{Q_E}=\eta_{r0}+\frac{P_\alpha}{\eta_a P_T}\alpha\eta_{r0}+\frac{0.95}{\eta_a\eta_E Q} , \tag{2.33}$$

where η_a is the efficiency of use of power recirculated to the plasma.

For a typical superconducting coil reactor producing ~ 1 GWe, $\eta_{r0}\simeq 0.07$, $\eta_a \simeq 0.3-0.7$, and η_e, related to the Carnot efficiency, ranges from 0.35–0.45 (at most ~ 0.6). For example, if $\eta_a=0.5$ and $\eta_e=0.4$, to obtain $\eta_r \leq 0.2$, $Q_E \gtrsim 5$ we require $Q \gtrsim 37$.

A simplified power-flow diagram for a reactor is shown in Fig. 10.

To make an "attractive" reactor we require (Sheffield, 1985)

$$\frac{4.8\times 10^{-5}\eta_e(1-\eta_r)P_\alpha}{R\,[(a+b)t+t^2]} \gtrsim 100 \text{ (kWe/tonne)} \tag{2.34}$$

where, allowing for impurities, Eq. (2.23) becomes

$$P_\alpha=4.9\times 10^{-42}\left[\frac{n_{\rm DT}}{n_e}\right]^2\langle n_e T_e\rangle^2 R a^2\kappa \text{ (W)} . \tag{2.35}$$

From Eq. (2.2), substituting the details of the plasma composition, we have

$$\langle\beta\rangle=\frac{4\times 10^{-23}\langle n_i T_i+n_e T_e+\sum_z n_z T_z+n_\alpha \bar{E}_\alpha\rangle}{B^2}\% . \tag{2.36}$$

In a fusion plasma, $n_i < n_e$ and the pressure of the energetic alpha particles ($n_\alpha \bar{E}_\alpha$) may be quite large. To allow for this effect and impurity depletion, we shall use

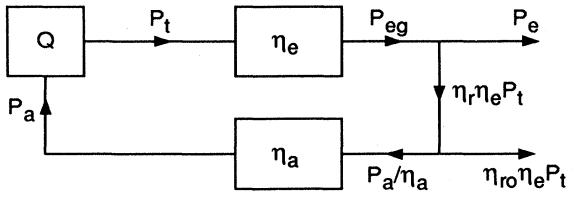

FIG. 10. Simplified power-flow diagram for a reactor.

the approximation

$$\langle\beta_i\rangle\equiv\frac{4\times 10^{-23}\langle n_i T_i\rangle}{B^2}\sim 0.35\langle\beta\rangle\% \tag{2.37}$$

and $\langle\beta_e\rangle\sim 0.46\langle\beta\rangle\%$. This is consistent with the impurity depletion numbers given in Sec. II.G, for $n_{HE}/n_e\sim 0.05$ to 0.10 and $\langle\beta_\alpha\rangle/\langle\beta\rangle$ approaching 0.2 at 20 keV; see Table VI. Using the factor f_α to allow for heat losses other than conduction and for auxiliary heating, and substituting in Eq. (2.36), Eqs. (2.22), and (2.27) yields

$$\chi_E\simeq\frac{3.6\times 10^{-6}f_\alpha P_\alpha}{R\langle\beta\rangle B^2} . \tag{2.38}$$

Equations (2.31) and (2.34)–(2.38) may now be solved for representative reactors to determine the coupled requirements for $\langle\beta\rangle B^2$ and χ_E. To indicate the typical demands placed on the physical performance, we shall consider the case in which $t=2.5$ m, $\eta_e=0.38$, $\eta_r=0.15$, $f_\alpha=0.73$, $n_{DT}/n_e=0.8$, $b/a=2$, there are parabolic temperature and square-root parabolic density profiles, and the figure of merit is 100 kWe/tonne. The results for four examples of net electric power (500, 1000, 1500, and 2000 MWe) are shown as a function of minor radius (a) and R/a in Figs. 11 and 12.

For this simple model, χ_E, $\langle\beta\rangle B^2$, $\bar{p}_{\omega n}$, and P_e/R vary with (a) independent of P_e. Not surprisingly, the smaller-minor-radius reactors require a higher $\langle\beta\rangle B^2$ and power density ($\bar{p}_{\omega n}$) with lower χ_E than the larger-minor-radius versions. The physics requirements are eased for larger reactors, i.e., lower $\langle\beta\rangle B^2$ and higher χ_E are permitted. Study of Fig. 12 shows that the lower-power-density devices are more readily achievable at low R/a, where the requirements for χ_E are also relatively less demanding. However, whether or not the lower-aspect-ratio regions are accessible depends on the mag-

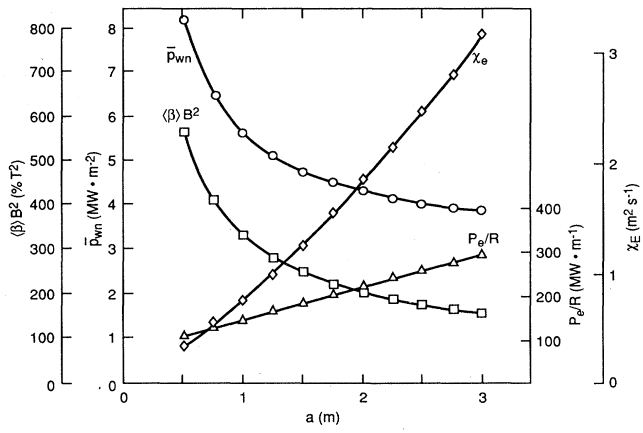

FIG. 11. Coupled values of $\langle\beta\rangle B^2$, average neutron flux to the first wall $\bar{p}_{wn}$, P_e/R, and χ_E, shown as a function of minor radius (a), for a self-sustaining D-T plasma in the simplified toroidal reactor model, operated at 100 kW(e) per tonne.

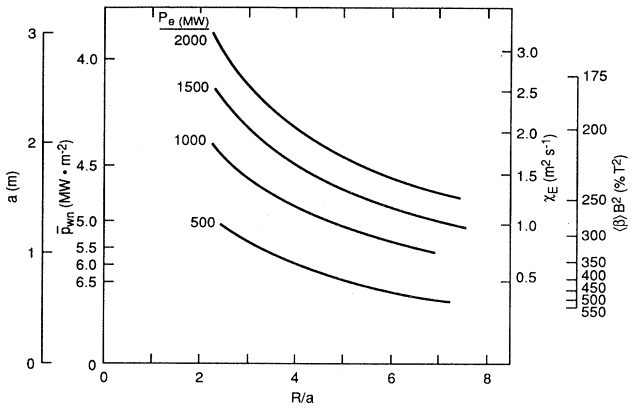

FIG. 12. Coupled values of minor radius (a), $\bar{p}_{wn}$, χ_E, and $\langle\beta\rangle B^2$ shown as a function of aspect ratio for four power levels, for the simplified toroidal reactor model, operated at 100 kW(e) per tonne.

netic configuration and magnetic field. Higher B lowers the requirement for $\langle\beta\rangle$ and lowers the experimental χ_E; classically or neoclassically $\chi_E \propto B^{-2}$, and for a variety of anomalous transport mechanisms $\chi_E \propto B^{-1}-B^{-2}$, though the multiplication factor is worse than the neoclassical value.

An important factor, therefore, is the field utilization factor f_B, which is the ratio of the magnetic field in the plasma (B) to the maximum magnetic field on the coils (B_m):

$$B = f_B B_m \ . \tag{2.39}$$

For a tokamak,

$$f_B = \left[1 - \left[\frac{a_w}{a} + \frac{\Delta}{a}\right]\frac{a}{R}\right] , \tag{2.40}$$

where a_ω/a is the ratio of the wall radius to the plasma radius, and Δ is the distance from the wall to the toroidal coil conductor on the median plane at the torus inside; Δ includes the first wall, blanket, shield, coil structure, and coil insulation.

Typical values are $a_\omega/a = 1.1$, $\Delta = 1.5$ m, e.g., for $a=2$ and $R/a=4$, $f_B = 0.54$.

Typical values for other configurations are

$$\begin{aligned} &\text{stellarator:} \quad \simeq 0.5 (R/a \gtrsim 7) \ , \\ &\text{RFP:} \quad \simeq 1.0-1.3 \text{(reactor)} \ , \\ &\text{FRC:} \quad \simeq 1.0 \ . \end{aligned} \tag{2.41}$$

It is difficult for devices such as the tokamak and stellarator, which require a strong, externally produced toroidal field, to access the smaller major radii (e.g., $\lesssim 4.0$ m), because their superconducting coils need a thick shield, and f_B becomes very small. Proposals have been made for small-net-electricity-generating tokamaks using water-cooled copper coils at conventional aspect ratios, but they suffer from high recirculating power or place extreme demands on the physics and technology (Wagner, 1981). One possible exception is the very-low-aspect-ratio ($R/a \lesssim 1.5$) tokamak with no blanket, a negligible shield in the bore, and a solid copper central toroidal conductor (Peng and Hicks, 1990). The RFP and FRC have, respectively, a weak toroidal field and no conductor down the torus axis, and both have fields primarily derived from plasma currents; theoretically, they can access the smallest region.

E. Beta and thermal diffusivity requirements

It is informative to display the physics requirement in the form of $\langle\beta\rangle/\chi_E$. First, we shall return to an important characteristic, the neutron flux falling on the first wall, Eq. (2.8). This may be approximated as

$$\bar{p}_{wn} \simeq \frac{0.8 P_F}{4\pi^2 (R/a)(a_w/a)(b/a)^{0.5} a^2} \ (\text{MW m}^{-2}) \ , \tag{2.42}$$

where P_F is the fusion power in MW ($P_n = 0.8\, P_F$).

Inherent safety arguments, involving an analysis of what could happen in a loss-of-blanket cooling accident, have been used by Logan (1988) to establish a maximum safe neutron flux for current blanket designs. His recommended maximum value is $(p_{\omega n})_{\max} \sim 10$ MW m^{-2}, and more realistically may be $\lesssim 6$ MW m^{-2}. Economic studies, (Sheffield, 1986) suggest that it is necessary for the first wall and blanket to withstand a neutron fluence of 15–25 MW m^{-2} before replacement. At an availability of 0.65, this requires surviving $\sim$4–7 years.

Consider now the plasma power balance for a self-sustained D-T plasma, Eq. (2.24). Allowing for impurities and losses other than conduction and some auxiliary heating (f_α), the equation becomes

$$\langle n_e T_e \rangle \tau_E \simeq \frac{1.7\times 10^{24}}{f_\alpha} \left[\frac{n_e}{n_{\rm DT}}\right]^2 (\text{m}^{-3}\ \text{eV s}) \ , \tag{2.43}$$

where an impurity depletion leading to $n_{\rm DT}/n_e = 0.73$ has been assumed; see Sec. II.G. Using Eq. (2.37) and Eqs. (2.27), (2.35), (2.39), and (2.42) with $\langle\beta_e\rangle \sim 0.46\,\langle\beta\rangle$ yields the relationship for a self-sustaining plasma

$$\frac{\langle\beta\rangle}{\chi_E}\simeq 1.9\times 10^4 \quad \underset{\text{geometry}}{\frac{R/a}{(b/a)^{0.5}}} \quad \underset{\substack{\text{scrape off}\\ \text{layer}}}{\frac{a_w/a}{f_B^2 B_m^2}} \quad \underset{\substack{\text{neutron}\\ \text{flux}}}{\frac{\bar{p}_{wn}}{f_\alpha P_F}} \quad \underset{\substack{\text{impurity}\\ \text{depletion}}}{\left[\frac{n_e}{n_{\rm DT}}\right]^2} \quad \%\,\mathrm{s\,m^{-2}}\ , \tag{2.44}$$

field utilization; maximum coil field; fraction of power to radial conduction; fusion power

where P_F is in MW and p_{wn} is in MW m^{-2}. Care must be exercised in using Eq. (2.44) because there are, separately, requirements on both $\langle\beta\rangle$ and χ_E. Using Eqs. (2.23) (with impurity depletion), (2.27), (2.43), and (2.44), we find for the reference profiles, where $\kappa=b/a$, that

$$\chi_E\simeq\frac{1.6\times 10^{-2}\kappa^{0.375}P_F^{0.75}f_\alpha}{(R/a)^{0.75}(a_w/a)^{0.25}(\bar{p}_{wn})^{0.25}}\left[\frac{n_{\rm DT}}{n_e}\right]\ (\mathrm{m^2\,s^{-1}})\ , \tag{2.45}$$

$$\langle\beta\rangle B^2 \simeq\frac{310(R/a)^{0.25}(a_w/a)^{0.75}(\bar{p}_{wn})^{0.75}}{(\kappa)^{0.125}P_F^{0.25}}\left[\frac{n_e}{n_{\rm DT}}\right]\ (\%\,\mathrm{T^2})\ . \tag{2.46}$$

As pointed out above in Sec. II.B, the fusion power varies with density and temperature profiles and with the temperature range, for the same beta. A ±20% change in the constant in Eq. (2.35) leads to a ±10% change in χ_e and a ∓10% change in the $\langle\beta\rangle B^2$ requirements. In the sections below we shall see how various configurations match up to these requirements.

F. Alpha physics

In a D-T fusion reactor, energetic (3.5-MeV) alpha particles produced by fusion reactions will provide the bulk of the plasma heating power. Modest auxiliary sources of power (P_a) may be used for control of the plasma, e.g., as drivers of plasma current. But for an economic reactor, we require, typically, that $P_a\lesssim 0.1P_\alpha$. Consequently it is important to understand what effects the alphas might have beyond providing beneficial heat to the plasma. This subject is discussed in numerous review articles, including those of Kolesnichenko (1980), Lisak and Wilhelmson (1987), Hively and Sigmar (1989), Sigmar (1989), Furth *et al.* (1990), and Bishop (1991).

First, we are concerned about confinement of the alphas as they slow down. The ratio of the gyroradius of a fusion alpha to the plasma minor radius (a) in a magnetic field (B) is given by

$$\frac{\rho_\alpha}{a}=2.89\times 10^{-4}\frac{(E_\alpha)^{0.5}}{aB}\ . \tag{2.47}$$

For a 3.5-MeV alpha, a field of 5 T, and a minor radius of 1 m, $\rho_\alpha/a=0.054$, showing that, to a close approximation, the majority of alpha particles should be confined well away from the walls of the vacuum chambers. In reality, in a toroidal system, incomplete cancellation of field gradient and curvature drifts between the top and bottom halves of the torus can lead to a greater radial excursion of the alphas (banana orbits). The requirement that $\rho_\alpha\lesssim a$, in order that alpha particles may be confined, may be used to establish a minimum current for a reactor when the radial excursion is normalized to the poloidal, rather than toroidal, magnetic field. The poloidal field $B_\theta=\mu_0 I/2\pi a$; substituting in Eq. (2.47), we find $I\gtrsim 2.7$ MA for $\rho_{\alpha\theta}\lesssim a$.

In addition, alphas trapped in the poloidally varying magnetic field, in externally produced field modulation (ripple), or in fields modulated by magnetohydrodynamic (MHD) instabilities, can walk out of the plasma rapidly; see Fig. 13. Such losses lead to local heating and, potentially, to damage of the first wall (Tani *et al.*, 1989). Ripple losses are discussed for the case of ITER in a review of Post *et al.* (1991; see also the discussion of ripple transport in Sec. III. C.7).

Second, the energetic alphas, while they are small in number compared to the background plasma, constitute a significant beta because of their high energy. The slowing down for alphas (Stix, 1972) is given by

$$\tau_{s\alpha}=\frac{2.09\times 10^{14}AT_e^{3/2}}{Z^2 n_e \ln\Lambda_e}\ln\left[1+\left[\frac{E}{E_{\rm crit}}\right]^{3/2}\right]\ , \tag{2.48}$$

where A and Z are the atomic weight and charge number of the slowing down ion, $E_{\rm crit}$ is given by Eq. (2.20), and Λ_e is defined by Eq. (2.13). Classical alpha showing down times are given in Table VI (Uckan *et al.*, 1988).

The relative density of alphas, where p_α is given by Eq. (2.19) or taken from a table of cross sections, is

$$\frac{n_\alpha}{n_e}=\frac{p_\alpha\tau_{s\alpha}}{E_\alpha n_e}\ . \tag{2.49}$$

The local beta of the energetic alphas, ignoring their radial excursions, is approximately

$$\beta_\alpha\simeq\frac{4n_\alpha\bar{E}_\alpha}{B^2}\ , \tag{2.50}$$

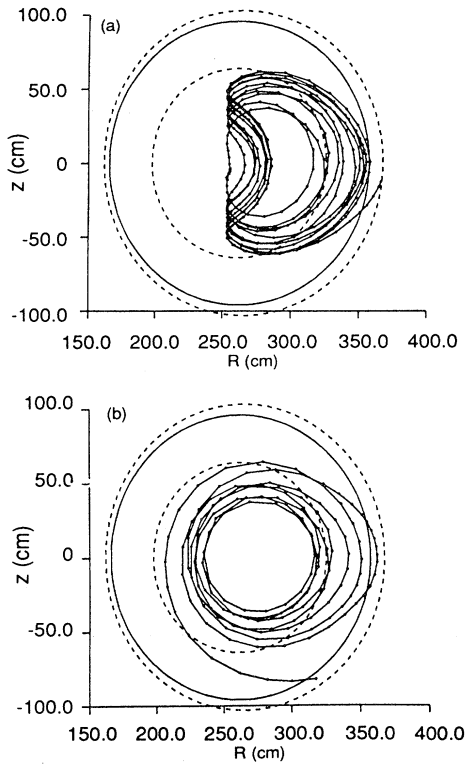

FIG. 13. Poloidal projection of (a) one trapped, and (b) one passing alpha orbit in TFTR, perturbed by a stationary ($m=2$; $n=1$) mode, having peak amplitude at the inner dashed circle. The wall is marked by the outer dashed circle, and the plasma edge by the solid circle (Mynick, 1992).

where for $T=10$–20 keV, the average energy during the slowing down to thermal energies is $\bar{E}_\alpha \simeq 1.4$ MeV. Values for $\langle \sigma v \rangle_{\rm DT}$, n_α/n_e, β_α/β, and $\bar{E}_\alpha/E_{a0}$ are given in Table VII, where β is the plasma beta (Uckan *et al.*, 1988).

Third, while the energetic alpha particles in a Maxwellian plasma are produced with an isotropic distribution function, they do not have a Maxwellian distribution; a discussion of the conditions for the velocity-space stability of the alpha-particle velocity distribution is given by Cordey *et al.* (1981). To prevent inversion of the distribution function, i.e., $\partial f_\alpha/\partial v > 0$, the source rate $S_\alpha(\mathrm{m}^{-3}\,\mathrm{s}^{-1})$ must not increase too rapidly as the plasma is heated, and the loss rate of alphas (τ_L) must be slow compared to the slowing down time [τ_s; see Eq. (2.48)]:

$$\frac{3}{\tau_s}-\frac{1}{\tau_L} > \frac{1}{S_a}\frac{\partial S_a}{\partial t}+\frac{1}{\tau_s}\frac{\partial \tau_s}{\partial t}-\frac{\partial (E_c^{1.5})}{\partial t}\Big/(E_\alpha^{1.5}+E_c^{1.5}) . \tag{2.51}$$

The presence of loss regions in velocity space can modify and destabilize the distribution function. Alphas are produced preferentially where the plasma is hottest ($\langle \sigma v \rangle_F \alpha T^2$) and can have strong radial, density, and pressure gradients. Their beta is finite, and their velocity v_α may exceed the local Alfvén speed [$v_A = 2.18\times 10^{16}\, B/(A_i n_i)^{0.5}\,(\mathrm{m\,s^{-1}})$]. For a D-T plasma,

$$\frac{v_\alpha}{v_A}=9.44\frac{n_{20}}{B}\left[\frac{n_{\rm DT}}{n_e}\right]^{0.5} . \tag{2.52}$$

All of these factors represent sources of free energy which may drive instabilities. On the negative side, these might lead to ejection of the alphas before they have transferred their heat to the plasma, and to increased losses. On the positive side, they might slow down the alphas more rapidly, reducing the alpha component of beta; they might enhance heat transfer to the plasma ions [see Eq. (2.21) for the normal state of affairs], and the large alpha orbits might stabilize some MHD modes. In addition, the rapidly lost alphas can generate radial electric fields in the plasma.

Fourth, the slowed down alphas—helium ash—are a ubiquitious and significant impurity in the plasma. Note that, in the absence of any other impurities, $n_{\rm DT}=n_e-2n_{\rm He}$! The density of helium is given by

$$n_{\rm He}\sim \tau_{\rm He} S_{\rm He}\ \mathrm{m}^{-3} ,$$

where $\tau_{\rm He}$ is the helium confinement time and the production rate of helium inside in the radius (r) is

$$S_{\rm He}=\frac{P_\alpha(r)}{2\pi^2 r^2 R\kappa 5 e E_{\alpha 0}}\ (\mathrm{m^{-3}\,s^{-1}}) . \tag{2.53}$$

Now

TABLE VI. Classical alpha slowing down time (local values).

T_e KeV	$\tau_{s\alpha}$ (s) $n/(10^{20}\ \mathrm{m}^{-3})$ 0.5	1.0	2.0	3.0	5.0	7.0	10.0
5	0.4	0.2	0.1	0.07	0.04	0.03	0.02
10	0.9	0.45	0.23	0.15	0.09	0.065	0.045
20	1.8	0.9	0.45	0.31	0.18	0.13	0.09
30	2.7	1.35	0.68	0.45	0.27	0.19	0.135
40	3.4	1.7	0.85	0.57	0.34	0.24	0.17
50	4.0	2.0	1.0	0.67	0.40	0.29	0.20

TABLE VII. Fast alpha density and beta (local values) (Uckan *et al.*, 1988).

T (keV)	$\langle\sigma v\rangle_{DT}$ (m^3/s)	n_α/n_e (%)	β_α/β (%)	$\bar{E}_\alpha/E_{\alpha 0}$
5	1.35×10^{-23}	0.01	0.73	0.30
10	1.13×10^{-22}	0.1	4.2	0.34
20	4.31×10^{-22}	0.8	19	0.39
30	6.65×10^{-22}	1.8	31	0.41
40	7.93×10^{-22}	2.7	34	0.41
50	8.54×10^{-22}	3.45	34	0.40

$$\tau_E(r)\simeq\frac{6\pi^2r^2R\kappa e n_e T}{P_\alpha(r)}\ (\mathrm{s})\ , \tag{2.54}$$

assuming only alpha heating. Consequently

$$\frac{n_{\mathrm{He}}}{n_e}\simeq 0.6\frac{T}{E_{\alpha 0}}\frac{\tau_{\mathrm{He}}}{\tau_E(r)}\ . \tag{2.55}$$

For example, for $T=25$ keV, if $\tau_{\mathrm{He}}\geq 12\tau_E(r)$ we find $n_{\mathrm{He}}/ne\geq 0.05$, i.e., a greater than 10% depletion of the D-T fuel.

Provided helium confinement is comparable with hydrogen confinement, $\tau_{\mathrm{He}}\simeq\tau_p\sim 3$–$5\tau_E$, there should not be a problem. Unfortunately, the convection term V_r in Eq. (2.10) can be inward. A relative inward motion of impurities is predicted for some conditions (Braginskii, 1965; Hinton and Hazeltine, 1976), and it has been observed in, for example, tokamaks (Stacey *et al.*, 1985). Helium transport and exhaust are reviewed by Hogan and Hillis (1991). A further problem is that energetic alpha particles bombard the wall and generate impurities, some of which will penetrate the scrape-off layer and enter the plasma.

The D-T fusion reaction rate increases strongly with temperature, as shown in Fig. 3 and Eq. (2.7), which have $p_\alpha\propto T^2$–$T^{1.5}$ for $\langle T\rangle\lesssim 22$ keV. Normally, ignition occurs as a balance between alpha power and loss mechanisms that have a weaker temperature dependence, such as bremsstrahlung ($T^{0.5}$) and conduction. Consequently, following ignition, the alpha power and temperature continue to rise until either (a) some other more strongly temperature-dependent mechanism, for example, synchrotron radiation, sets in and reestablishes a power balance or (b) the pressure (beta) limit is reached. In the latter case this thermal runaway may lead to gross instability of the plasma, as in the case of a tokamak disruption (see Sec. IV. E). An example of the density and temperature operating space for a tokamak, showing the ignition region and beta limit, is given in Fig. 49 of Sec. IV. A review of burn control possibilities for tokamaks has been presented by Haney *et al.* (1990).

While it is possible that the system may be self-regulating, its behavior might involve temperature oscillations leading to a time-varying heat load on the first wall and divertor and stress-fatigue problems. This is not a comfortable operating condition; therefore designers look for control methods, e.g., fuel density control and variable magnetic ripple, to remove alphas if a temperature excursion starts. Consider the case in which $\tau_E=C_1T^{-x}P^{-y}$ and $P=P_\alpha=C_2T^2$. The plasma power balance is given by

$$V\frac{\partial}{\partial t}(3nT)=-\frac{V3nTT^xC_2^{2y}T^{2y}}{C_1}+VC_2T^2-\mathrm{Radiation}\ . \tag{2.56}$$

If $(1+x)\geq 2(1-y)$, there will be no thermal runaway even if radiation losses are small (Engelmann, 1987). Empirical confinement scalings for tokamaks and stellarators often have $x=0$ and $y\sim 0.5$, so that the thermal runaway depends sensitively on details of the alpha power dependence on temperature, on radiation, and on profiles.

G. Impurities, limiters, and divertors

The control and minimization of impurities in a plasma is a major concern for a fusion reactor. As we have seen in the previous section, the helium ash created when the fusion alpha particles slow down and thermalize represents a minimum impurity constituent of the plasma. Wall-generated impurities are an additional problem. Unfortunately, there is a strong tendency for highly charged ions to diffuse from the wall region into the containment region (Taylor, 1974), and suppression of their generation and transfer to the plasma are important considerations for reactor design. Consider, for example, the reference ITER assumptions (Uckan *et al.*, 1990).

$$\text{helium } \frac{n_\alpha}{n_e}=5 \text{ and } 10\%,\quad Z_\alpha=2\ ,$$

$$\text{carbon } \frac{n_c}{n_e}=\left[0.9+0.6\left[\frac{0.7}{n_{20}}\right]^{2.6}\right]\%,\quad Z_C=6\ ,$$

$$\text{oxygen } \frac{n_0}{n_e}=0.1\%,\quad Z_0=8\ ,$$

$$\text{iron } \frac{n_{\mathrm{Fe}}}{n_e}=\left[0.05\left[\frac{0.7}{n_{20}}\right]^{2.3}+0.02\right]\%,\quad Z_{\mathrm{Fe}}=26\ .$$

For $\langle n_e\rangle=2\times10^{20}\ \mathrm{m}^{-3}$, we find

$$\text{for } \frac{n_\alpha}{n_e}=5\%,\quad \frac{n_{\rm DT}}{n_e}=0.83,\quad Z_{\rm eff}=1.59\ ,$$

$$\text{for } \frac{n_\alpha}{n_e}=10\%,\quad \frac{n_{\rm DT}}{n_e}=0.73,\quad Z_{\rm eff}=1.69\ .$$

The latter case has nearly a factor of two lower fusion output than a pure D-T plasma would have.

The impurities also radiate power from the plasma by increasing bremsstrahlung losses [Eq. (2.15)] and by line [Eq. (2.14)] and continuum radiation. High-Z impurities are the worst offenders because they do not become fully ionized, and minute quantities of, say, molybdenum and tungsten can radiate substantial amounts of power. Low-Z impurities become fully ionized in the bulk of the plasma and radiate predominantly from the colder outer regions. This has led to the suggestion of their controlled use to radiate heat from the plasma edge in a benign fashion to the walls, and to limit the conduction and convection load on limiters and divertors—the cold plasma mantle concept (Gibson, 1978; Watkins *et al.*, 1981). It is not clear whether this situation could be sustained (Samm, 1993).

A key issue is the transport of impurities in the plasma, both the helium ash and the wall-generated impurities that reach the plasma edge. Consider Eq. (2.10) for impurity transport with the source term turned off:

$$\frac{\partial n_z}{\partial t}=\frac{1}{r}\frac{\partial}{\partial r}\left[rD_z\frac{\partial n_z}{\partial r}+rn_zV_z\right]\ . \tag{2.57}$$

Let $n_z=n_{z1}\exp(-t/\tau_z)$; then if D_z and V_z are constant and aV_z/D_z is small,

$$\tau_z\sim\frac{a^2}{4(D_z-AV_z)}\ . \tag{2.58}$$

Neglecting the convection term, we require

$$\frac{S_{\rm DT}}{D_{\rm DT}}\gg\sum_z\frac{ZS_z}{D_z}$$

to prevent serious dilution of the D-T fuel. To ensure low $Z_{\rm eff}$ we need

$$\frac{S_{\rm DT}}{D_{\rm DT}}\gtrsim\sum_z Z^2\frac{S_z}{D_z}\ ,$$

where $S_{\rm DT}$ and $D_{\rm DT}$ are the source rate and diffusion coefficient for the D-T fuel.

However, if aV_z is large compared to D_z, and positive, and in the convention used here positive V_z means inward convection, τ_z can become negative and the impurities will accumulate (Braginskii, 1965; Hinton and Hazeltine, 1976; Hirshman and Sigmar, 1981). This phenomenon has been observed under some conditions in tokamaks; see the review by Stacy *et al.* (1985). Clearly, impurity accumulation regions must be avoided, and this fact places a restriction on operating regimes.

1. Plasma-wall interactions.

The complexity of the plasma-wall interactions is well illustrated by Fig. 14, which lists the wide range of elementary processes that can occur at the wall. There are numerous reviews of this topic, including those of McCracken and Stott (1979), Nygren *et al.* (1981), Langley *et al.* (1984), Post and Behrisch (1986), and Janev (1991). Sputtering is a major problem because after a lot of material is removed a component must be replaced. Low sputtering rates are essential to ensure a reasonably long time between maintenance and replacement. The extent of sputtering can exceed that due to knock-on processes, in which sputtered particles receive enough energy from collisions with the incident particles to overcome the surface binding energy, because of chemical interactions in which molecules are found. For example, commonly used wall, limiter, and target material—carbon—interacts with hydrogen to form CH_4. The sputtering yield for carbon bombarded by H, D, and He is given in Fig. 15, for varying carbon temperature. Radiation-enhanced sublimation increases the erosion rates for carbon-based materials (Nygren *et al.*, 1990). Carbon also suffers from the problem that it absorbs hydrogen, and in a D-T plasma this can lead to large trapped-tritium inventories. Beryllium, a lower-Z material, has been used successfully in JET (Thomas *et al.*, 1990). Redeposition can offset sputtering (Brooks, 1990), though it is not an advantage unless the redeposited materials retain the surface quality. Impurities, including the wall material itself, have higher sputtering yields than hydro-

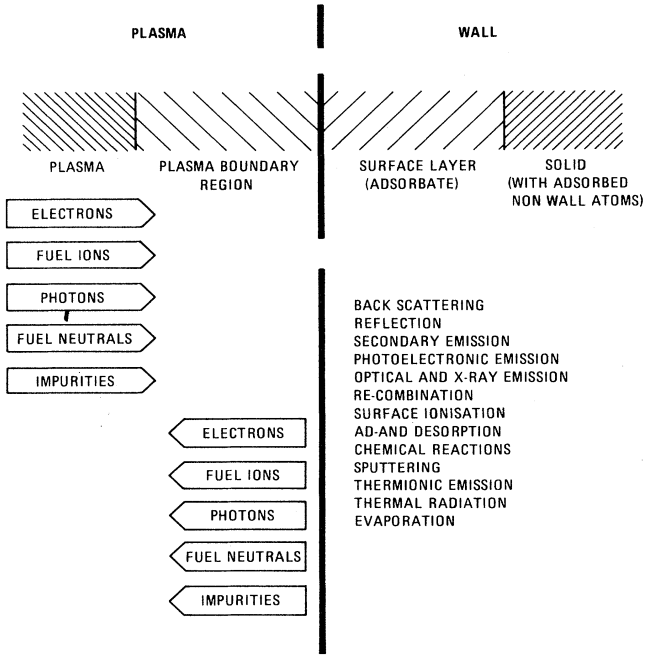

FIG. 14. Transition region (schematic) between plasma and solid and list of elementary process occurring at the wall (Bickerton, 1977).

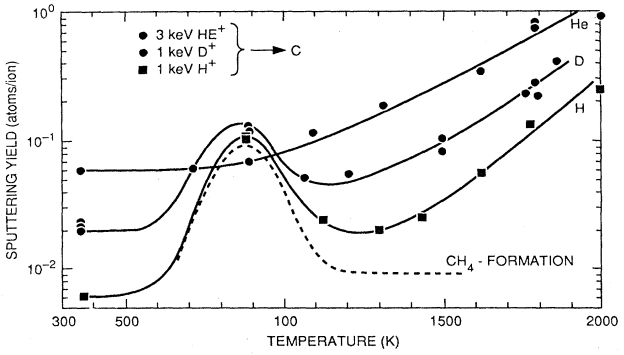

FIG. 15. Temperature dependence of the chemical sputtering yield of carbon with 1-keV H^+ and D^+, and 3-keV H_e^+ ions. Methane is formed at about 900 K, but above 1300 K no hydrocarbon could be found (Langley *et al.*, 1984).

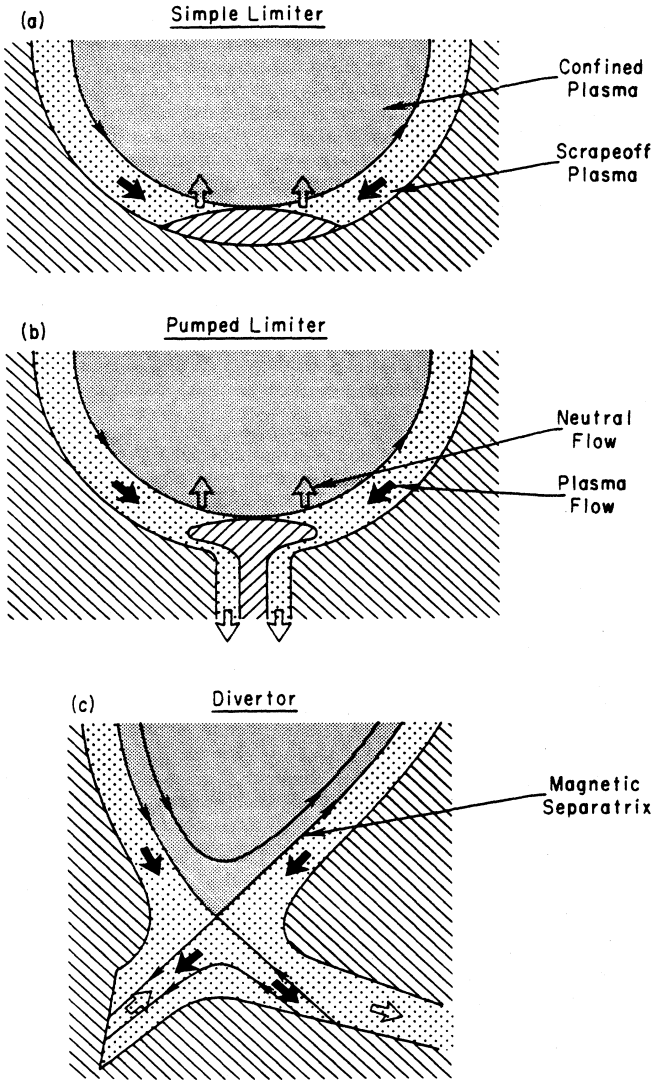

FIG. 16. Schematic illustration of power handling, particle exhaust, and impurity control options for a tokamak: (a) simple limiter; (b) pumped limiter; (c) poloidal divertor.

gen, and this is another reason to suppress them. In toroidal experiments, substantial reductions in the amount of gas, mainly oxygen, desorbed from the walls have been achieved by careful preparation of the surfaces, using a variety of cleaning techniques prior to operation of the full plasma (Oren and Taylor, 1977). Control of the plasma edge by a carefully contoured limiter or divertor is used to minimize impurity problems and remove particles (Komarek *et al.*, 1990). These options are illustrated in Fig. 16.

2. Limiters

Limiters have been used traditionally in toroidal devices to protect the vacuum chamber walls from plasma bombardment. In recent years they have been shaped so as to pump the gas formed by neutralization of the plasma—the pumped limiter [Kelley, 1973; Vershkov and Mirnov, 1974; Schivel, 1977; see Fig. 16(b)]. The plasma intercepts the limiter over a small radial distance—the scrape-off layer (SOL)—whose scale is determined by the ratio of the transport coefficients, radial and parallel to the magnetic field lines. The heat conducted and convected from the main body of the plasma streams along the field lines and is transferred by electrons and ions to the limiter. Most of the ions are neutralized at the limiter, either returning as dissociated molecules (energy ~ 5 eV) or reflecting as neutrals. A cloud of neutrals forms around the limiter. Because the charge-exchange rate for hydrogen is greater than the ionization rate (see Fig. 17), the neutrals migrate into the plasma for considerable distances beyond the limiter. Typically, they have the local ion temperature. The mean free path for this diffusion has been calculated by Podesta and Engelmann (1973) as

$$\lambda_0 \simeq \frac{1}{n(\langle \sigma v \rangle_{cx} + \langle \sigma v \rangle_e)} \left[\frac{\langle \sigma v \rangle_{cx}}{\langle \sigma v \rangle_e} \right]^{0.5} \left[\frac{eT_i}{m_i} \right]^{0.5} \text{(m)} \tag{2.59}$$

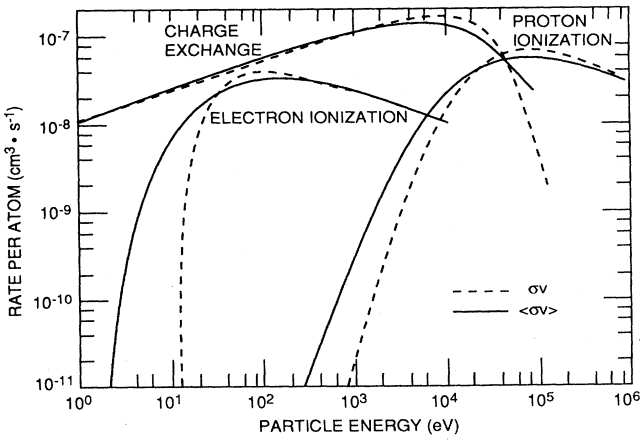

FIG. 17. Rate coefficient for atomic hydrogen (Freeman and Jones, 1974).

where, for $T_e \gtrsim 50$ eV, $n\langle\sigma v\rangle_{cx} \gtrsim 4\times10^5$ s^{-1} and $n\langle\sigma v\rangle_e \sim 3\times10^5$ s^{-1}. See also, Tendler and Ågren (1982).

For $T_e \lesssim 50$ eV, the charge-exchange rate is sufficiently greater than the ionization rate that most neutrals formed in the low-temperature region will march into the higher-temperature region. Assuming $T_i \sim T_e$, these $50+eV$ neutrals can cause substantial sputtering. For carbon, the peak sputtering rate is for hydrogen with energies in the range 50–1000 eV (see Langley *et al.*, 1984, p. 77).

A simple model for the SOL plasma density and temperature is given by a slab model in which y represents the radial direction and the subscript $\|$ denotes the magnetic-field direction (Howe, 1981):

$$\frac{\partial}{\partial y}\left[D\frac{\partial n}{\partial y}\right]=\frac{n}{\tau_\|}\ , \tag{2.60}$$

$$\frac{\partial}{\partial y}\left[n\chi\frac{\partial T}{\partial y}\right]+\frac{\partial}{\partial y}\left[3TD\frac{\partial n}{\partial y}\right]=\frac{2nT}{\tau_\|}(1+\gamma_e)\ . \tag{2.61}$$

Here D and $\chi=\chi_e+\chi_i$ are the diffusion and conduction coefficients, respectively; $n\equiv n_e=n_i$, $T\equiv T_e=T_i$, and $\gamma_e=1+0.25\ln(m_iT_e/m_eT_i)$ is the enhancement of the electron energy flux due to the surface sheath potential. The plasma particle $\Gamma_\|$ and energy fluxes $Q_\|$ are given by Emmert *et al.* (1980) as

$$\Gamma_\|=\tfrac{1}{2}n\tilde{V}_i(\mathrm{m^{-2}\,s^{-1}}) \text{ where } \tilde{V}_i=\left[\frac{8eT_i}{\pi m_i}\right]^{0.5}(\mathrm{m\,s^{-1}})\ ,$$

$$Q_{\|e}=2T_e\gamma_e\Gamma_\|\ , \tag{2.62}$$

$$Q_{\|i}=2T_i\Gamma_\|\ .$$

In a toroidal system the flux meets a toroidal limiter at an angle determined by the field-line pitch B_θ/B_ϕ where $q=aB_\phi/RB_\theta$. The particle flux incident on a segment of the toroidal limiter in the poloidal direction is given by

$$\Gamma_z=\Gamma_\|\left[\frac{B_\theta}{B_\phi}\right]=\Gamma_\|\frac{a}{R_q}\ .$$

For a slab of plasma between y and $y+dy$ this flux exactly balances the equivalent volume loss term in the density transport equation,

$$2\Gamma_z 2\pi R dy=\frac{n}{\tau_\|}2\pi a\,2\pi R\,dy\ , \tag{2.63}$$

where the factor 2 in front of Γ_z accounts for the two sides of the limiter:

$$\tau_\|=\frac{\pi an}{\Gamma_z}=\frac{2\pi R_q}{\tilde{V}_i}(s)\ . \tag{2.64}$$

For constant D and χ and ignoring the $T_i^{0.5}$ dependence of $\Gamma_\|$ the solutions are

$$n=n(0)\exp\left[\frac{-y}{\lambda_n}\right]\ (\mathrm{m^{-3}}),\quad T=T(0)\exp\left[\frac{-y}{\lambda_T}\right]\ (\mathrm{eV}) \tag{2.65}$$

where $\lambda_n=(D\tau_\|)^{0.5}$ m and

$$\eta=\frac{\lambda_n}{\lambda_T}=\frac{[(\alpha+3)^2+4\alpha(2\gamma-3)]^{0.5}-(\alpha+3)}{2\alpha} \tag{2.66}$$

where $\alpha=\chi/D$ and $\gamma=1+\chi_e$.

The density and temperature at the point of the limiter ($y=0$) are given by the requirement that all of the particles and power that leave the plasma by cross-field transport flow to the limiter:

$$\dot{N}_T=A\int_0^\infty\frac{n}{\tau_\|}\ \text{particle loss rate}\ (\mathrm{s^{-1}})=\frac{N_T}{\tau_p} \tag{2.67}$$

where N is the total number of particles in the plasma. $\tau_p^*=\tau_p/(1-R_r)$, where τ_p is the bulk-plasma particle confinement time and R_r is the recycling coefficient at the wall/limiter.

$$P_T=A\int_0^\infty\frac{2\gamma nT}{\tau_\|}dy\ \text{thermal power (W)} \tag{2.68}$$

where $A=4\pi^2Ra$.

Integration yields

$$n_0=\frac{\dot{N}_T\tau_\|}{A\lambda_n}\ \mathrm{m^{-3}}),\ \text{and}\ T_0=\frac{P_T}{2\gamma e\dot{N}_T}(1+\eta)\ (\mathrm{eV})\ . \tag{2.69}$$

The fall of the heat flux is given by

$$\frac{1}{\lambda_Q}=\frac{1}{\lambda_n}+\frac{1}{\lambda_T}\ . \tag{2.70}$$

Ergodization of the magnetic field at the plasma edge, using local coils, increases the radial heat decay length and can lower the average power density on a limiter (Samain *et al.*, 1984; DeGrassie *et al.*, 1989; Monier-Gorbet *et al.*, 1993).

Consider the following example for a pumped limiter: $R=6$ m, $a=2$ m, $q=3$, $\dot{N}_T=5\times10^{23}$ s^{-1}, $P_T=120$ MW, $\gamma=4$, $D=2$ m^2 s^{-1}, $\chi=D$, $\alpha=1$, and $\eta=1$, in a D-T plasma. $T_0=375$ eV; assume an average $T=T_0/2$, $\tilde{V}_i=1.4\times10^5$ (m s^{-1}), $\tau_\|=8.3\times10^{-4}$ s, $\lambda_n=0.04$ m$=\lambda_T$, $\lambda_Q=0.02$ m, $n_0=2.2\times10^{19}$ m^{-3}.

Let the radial extent of the limiter be 0.08 m; then the fraction of the heat intercepted on the front of the limiter $f_Q=1-\exp(-D_y/\lambda_Q)=0.98$. The fraction of the particle flow that gets behind the limiter to a pumping region is $q=(1-f_Q)^{\lambda_Q/\lambda_n}=0.14$.

The neutral mean free path, assuming the peak temperature and density in the SOL (if greater than ~50 eV), is given by Eq. (2.59) as $\lambda_0\simeq0.09$ m. If the poloidal extent of the limiter is about 1 m, then, allowing that most of the particle deposition will be towards the middle of

the limiters, one can see that ~10% of the neutrals may be in a cloud extending beyond the limiter, i.e., can cause sputtering of the wall. A computation of neutral density contours for the INTOR/FED pumped limiters is shown in Fig. 18.

Of the neutrals that leave the limiter, part will continue further into the plasma, eventually becoming ionized, and part, roughly a third, will return to the limiter and wall.

If we assume one-third must return to the limiter and the device is run for a year with a carbon wall, sputtering coefficient $S_s=0.1$, the total number of carbon atoms removed per year $=\frac{1}{3}\times5\times10^{23}\times0.1\times3600\times8760=5.3\times10^{29}$ C/yr, or 1.0×10^4 kg, or a volume of 4 m^3. The limiter area is 37.7 m^2, so the average depth of carbon removed is ~0.1 m. Redeposition of carbon might reduce the net erosion (Brooks, 1990).

The walls would be subject to a lower flux and less erosion. However, this example is operated at a much lower thermal power density than would be expected in a reactor (~0.25 MW/m^2 thermal flux at the plasma edge, compared to 0.5–1.0 MW/m^2 expected for an attractive reactor).

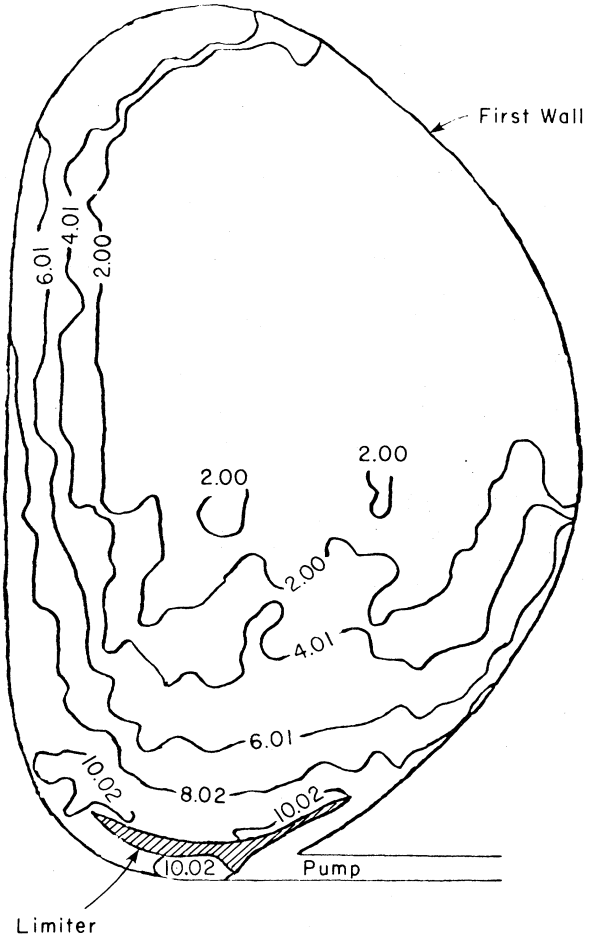

FIG. 18. Contour plot of the log of the density of the D° originating at the INTOR/FED pumped limiter at 6.6 s into the base discharge case, showing the D° population concentrated in the limiter region (Heifetz *et al.*, 1983).

3. Divertors

It is not clear whether a limiter can be used in a reactor plasma because of the problem of needing to remove particles while preventing unacceptable erosion due to the ions and neutrals. Certainly, if a cold plasma mantle could be formed this might alleviate some of the problems. Of course it would also alleviate problems for the alternative solution—the magnetic divertor.

Various designs of divertor have been proposed. They all consist of an arrangement of coils producing magnetic fields opposed to the confining fields, such that flux lines near the wall are diverted onto targets at a distance from the plasma much greater than the SOL thickness; see Fig. 19. For the tokamak, while a variety of approaches has been tried, only the poloidal divertor remains as a serious consideration. However, in other devices, toroidal and local divertors are still being considered. The use of magnetic islands to create divertor action has been proposed by Karger and Lackner (1977). The divertor serves a number of purposes (see Harbor, 1981):

(1) Act as a magnetic limiter, isolating the confined plasma from the wall. The fraction of particles that cross the separatrix and enter the divertor without first diffusing to the wall, the "unload efficiency," is

$$\eta_u=1-\exp\left[-\left[\frac{W}{\lambda_n}\right]\right], \tag{2.71}$$

where W is the width of the divertor throat. Again, if $W/\lambda_n\gtrsim4$ most of the particles go to the divertor region.

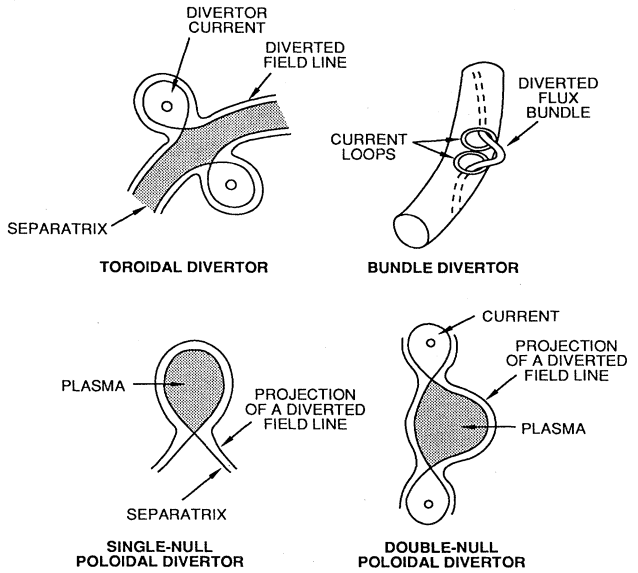

FIG. 19. Types of divertor incorporated in toroidal systems (Rawls *et al.*, 1979).

(2) Ionize incoming impurities from the wall in the SOL and sweep them into the divertor. The probability of ionization of an impurity in crossing the scrape-off layer is

$$\eta_i = 1 - \exp\left[-\frac{\langle \sigma v \rangle_e}{v_I}\right](n_s \lambda_n) , \tag{2.72}$$

where $\langle \sigma v \rangle_e$ is the ionization rate for the impurity and v_I is the impurity radial velocity. If $n_s \lambda_n > 4 v_I / \langle \sigma_i v_e \rangle$, $\eta_i \approx 1$, e.g., for oxygen at 1 eV, $v_I = 2.5 \times 10^3$ m s^{-1}, $\langle \sigma v \rangle_e \simeq 1 \times 10^{-13}$ m^2 s^{-1}. $n_s = 1 \times 10^{19}$ m^{-3}, $\Delta = 0.04$ m, the condition is met easily.

(3) Transport the heat to the divertor chambers rather than to the first wall.

(4) Minimize the neutral content of the SOL and the main body of the plasma.

(5) Be reliable and maintainable.

(6) Allow operation with a low T and high n at the target plate, even in some conditions in which there is a high T and low n at the edge of the main plasma.

Analyses of divertors have led to the identification of three regimes of operations (Post, Heifetz, and Petravic, 1982); a tokamak example is given in Table VIII.

In the first regime there is very little recycling, the temperatures are high, and the densities are low. The neutrals can easily escape down the pump or back to the main plasma without being ionized. The neutral pressure is low.

The second regime is characterized by a medium level of recycling. The neutral mean free path is shorter than the length of the divertor channel, but greater than the width of the channel, so that neutrals can escape to the pump but not to the main plasma. Radiation from hydrogen and charge exchange does not transfer much of the heat flux to the divertor walls before the plasma reaches the neutralizer plate. Sputtering yields are high in both regimes because ion energies exceed sputtering thresholds for realistic materials.

The third regime is characterized by large recycling rates. Each ion typically recycles 10 or more times before being pumped or reaching the main plasma. The neutral mean free paths are short compared to both the length and the width of the divertor. The electron temperature is $\lesssim 30$–40 eV and the density is high $\sim 10^{20}$ m^{-3}. The neutral pressure is high, $\gtrsim 10^{-3}$ Torr. Radiation and charge exchange can be important. Such operation was achieved first in the D-III expanded boundary divertor (Shimada *et al.*, 1981; Ohyabu *et al.*, 1982).

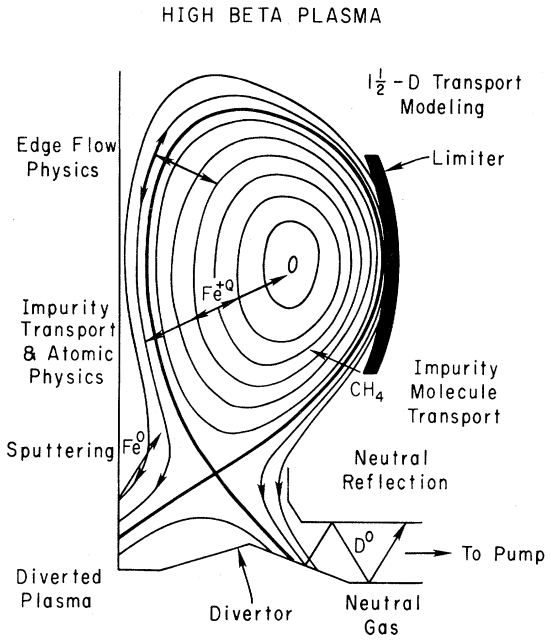

FIG. 20. Types of processes involved in a divertor for a high-beta plasma (Post *et al.*, 1982).

A representative divertor geometry is shown in Fig. 20, which also illustrates the large number of physical processes that must be taken into account.

It is necessary to treat ions and electrons flowing both across the magnetic field and along the field to a target plate, where they combine and reenter the SOL as neutrals. Neutrals atoms and molecules transport through the plasma, reflecting from the walls and undergoing charge exchange and ionizing collisions. Impurities are

TABLE VIII. Approximate operating regimes for a divertor of length L and width w, with INTOR level heat and particles fluxes (Post *et al.*, 1982).

Neutral recycling	Low	Medium	High
λ_0, neutral mean free path	$\lambda_0 > L, w$	$L > \lambda_0 > w$	$b, a > \lambda_0$
$R = \Gamma_{\text{plate}}/\Gamma_{\text{throat}}$	$R \sim 1$	$1 \le R \le 10$	$R \gtrsim 10$
T_e (eV)	200–1000	30–200	< 30
Edge plasma density	10^{17}–10^{18} m^{-3}	10^{19} m^{-3}	10^{20} m^{-3}
Importance of hydrogen radiation	Negligible	$\sim 10^{-8}$	10–90% estimate
Neutral pressure (Torr)	10^{-6}–10^{-7}	10^{-4}–10^{-2}	$> 10^{-2}$
T_e gradient	Small	$\sim 10\%$	Large

produced from the walls and targets by sputtering, arcing, vaporization, chemical erosion, desorption, etc. Zero-dimensional, one-dimensional, and two-dimensional models have been used. The last are necessary for an adequate description. The appropriate plasma equations for the base plasma, to be used in estimating the impurity generation and shielding and impurity removals are (Petravic *et al.*, 1985)

$$
\begin{aligned}
&\frac{\partial}{\partial x}(nv_{\parallel})=S_n+\frac{\partial}{\partial y}\left[D_{\perp}\frac{\partial n}{\partial y}\right],\\
&\frac{\partial}{\partial x}[n(mv_{\parallel}^2+T_i+T_e)]=S_p+\frac{\partial}{\partial y}\left[D_{\perp}\frac{\partial}{\partial y}nmv_{\parallel}\right],\\
&\frac{\partial}{\partial x}\left[\frac{5}{2}nv_{\parallel}T_i+\frac{1}{2}nmv_{\parallel}^2-\chi_{\parallel i}\frac{\partial T_i}{\partial x}\right]=-v_{\parallel}\frac{\partial(nTe)}{\partial x}+S_{Ei}+\frac{\partial}{\partial y}\left[D_{\perp}\left[\frac{5}{2}T_i+\frac{mv_{\parallel}^2}{2}\right]\frac{\partial n}{\partial y}+\chi_{\perp i}\frac{\partial T_i}{\partial y}\right]+Q_{ei},\\
&\frac{\partial}{\partial x}\left[\frac{5}{2}nv_{\parallel}T_e-\chi_{\parallel e}\frac{\partial T_e}{\partial x}\right]=v_{\parallel}\frac{\partial(nT_e)}{\partial x}+S_{Ee}+\frac{\partial}{\partial y}\left[D_{\perp}\frac{5}{2}T_e\frac{\partial n}{\partial y}+\chi_{\perp e}\frac{\partial T_e}{\partial y}\right]-Q_{ei},
\end{aligned}
\tag{2.73}
$$

where $n=n_e=n_i$, v is the ion parallel velocity and m is the ion mass. Q_{ei} is the electron-ion Coulomb energy-transfer term [see Eq. (2.13)] and S_n, S_p, S_{Ei}, S_{Ee} are the ionization (particle) source, momentum source, and ion and electron energy sources arising from the plasma interaction with neutrals. The use of a fluid model is justified for most useful conditions, since $L, w \gg \lambda_{ii}$, but not at the sheath in front of the divertor target, which is handled with boundary conditions. At the sheath the parallel velocity is estimated to be the sound speed, $v_{\parallel}^{\rm sh}=[(T_i+T_e)/m_i]^{0.5}$.

To obtain solutions it is customary to specify values for the flux $nv_{\perp}$ and the electron and ion heat fluxes at the upstream boundary $x=0$. Neutral source terms are computed using a separate neutral-particle transport code, for example, the Monte Carlo code DEGAS (Heifetz *et al.*, 1982), or with simple diffusion models. While simplified analytic expressions have been obtained for SOL and divertor parameters, it is necessary to calibrate their validity using a computer to solve the full set of equations. An example solution for the international thermonuclear experimental reactor (ITER) is given in Fig. 21.

Simplified expressions for the peak power per unit area on the divertor plate p_D and the adjacent plasma temperature T_D have been given for ITER by Harrison and Hotston (1990). The expressions are useful for indicating trends:

$$
\begin{aligned}
p_D &\propto \left[\frac{P^2}{n\chi_{\perp}}\right]^{7/9} Z_{\rm eff}^{-2/9} G_{\Lambda} G_m + \text{nonpertinent terms},\\
T_D &\propto \left[\frac{P^2}{\chi_{\perp}}\right]^{10/9} n_s^{-28/9} Z_{\rm eff}^{-8/9} G_{\Lambda}^2 + \text{nonpertinent terms}.
\end{aligned}
\tag{2.74}
$$

Here P is the alpha power and additional heating (current-drive) power flowing across the scrape-off layer, $\chi_{\perp}$ is the cross-field thermal diffusivity, n_s is the plasma density in the stagnation zone of the SOL, $G_{\Lambda}<1$ is a geometric parameter accounting for energy loss in the private flux region of the divertor (it decreases nonlinearly with increasing null-to-strike-point length Λ, measured in the poloidal plane). The geometric parameter $G_m=\sin\Omega(B_{\theta}/B_t)\ll 1$ allows for spreading of power over a toroidally symmetric divertor plate, inclined at an angle Ω relative to the magnetic flux surface.

The key points illustrated by these equations are (1) An increase in P causes a nonlinear increase in p_D and T_D. (2) T_D increases very strongly as n_s is reduced. (3) T_D can be reduced by increasing Λ.

While these results have been obtained for a tokamak, they have wider generic application. Two-dimensional simulations of the scrape-off-layer support the validity of the analytic expression, for temperature (Ueda *et al.*, 1989; Itoh and Itoh, 1990).

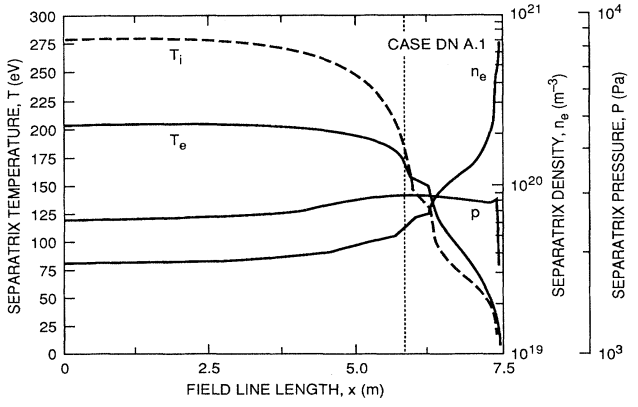

FIG. 21. Variation of the plasma parameters on the separatrix with position on the separatrix. The temperatures fall strongly and density rises as the field lines approach the divertor in such a way that the pressure remains nearly constant (Cohen *et al.*, 1990).

H. Auxiliary heating

The requirements for heating to ignition are obtained by solving the time-dependent power-balance equations (2.11) and (2.12). A computer code, for example, WHIST (Houlberg, 1982) or BALDUR (Singer *et al.*, 1986), is needed to account properly for the details of the radial dependences of ions, electrons, impurities, neutrals, and evolving magnetic field, let alone MHD effects. For the purpose of providing a simple solution, a rough answer may be obtained by integrating the equations over the plasma volume, using model profiles for the density and temperature (Sheffield, 1986; Uckan *et al.*, 1990). For startup conditions in a D-T reactor, the synchrotron radiation term is smaller than the bremsstrahlung term and may be dropped. The line radiation and charge-exchange terms are important at the plasma edge but play only a small role in the plasma center, for a clean dense plasma, and are dropped. Assuming $n=n_0$, $T_e=T_i=T_0(1-r^2/a^2)$, and taking the temperature gradient at $r/a=0.8$, leads to the following power-balance equation:

$$\frac{\partial}{\partial t}W \simeq \underbrace{-0.16Rn_{19}T_k(\chi_e+\chi_i)}_{\text{conduction losses}} \underbrace{-1.1\times10^{-3}RabZ_{\text{eff}}n_{19}^2T_k^{0.5}}_{\text{bremsstrahlung}} + \underbrace{\frac{0.08\gamma_R Z_{\text{eff}}RI_m^2}{abT_k^{1.5}}}_{\text{ohmic heating}} \underbrace{+1.9\times10^{-4}Rabn_{19}^2\left[\frac{n_{\text{DT}}}{n_e}\right]^2T_k^{2.5}}_{\text{alpha heating}} \underbrace{+P_a\ (\text{MW})}_{\text{auxiliary heating}} \tag{2.75}$$

where $n_{19}(10^{19}\ \text{m}^{-3})$, T_k (keV), I_m (MA), and average values have been used for $\xi\simeq1.1$, $\ln\Lambda\simeq19$. The alpha power formula ($p_\alpha\propto T_i^{2.5}$) is a best fit for a parabolic temperature profile for $2\lesssim T_{ik}\lesssim10$ keV. The factor $(n_{\text{DT}}/n_e)^2$ allows for fuel depletion owing to wall-generated impurities and helium ash. For most tokamak conditions the various terms have the form shown in Fig. 22; the conduction term is not shown. For neoclassical losses $\chi\propto T^{-0.5}$, and as we shall see in later discussion of various devices, theoretical mechanisms for anomalous transport have a wide variety of dependences on temperature. For configurations having moderate current densities, such as the tokamak with toroidal fields ~5 T, Ohmic heating is insufficient to raise the temperature to a level where alpha heating can take over. The Ohmic temperature (T_Ω) is obtained primarily by a balance of Ohmic heating and conduction losses. Setting $\chi_e+\chi_i=\chi_E'(T_k/10)^\delta$, we find

$$T_{\Omega k}\simeq\left[\frac{0.5(10)^\delta\gamma_R Z_{\text{eff}}I_m^2}{abn_{19}\chi_E'}\right]^{1/(2.5+\delta)}\ \text{keV}\ . \tag{2.76}$$

For example, let $\delta=0$, $\gamma_R=1.5$, $Z_{\text{eff}}=2$, $I_m=20$ MA, $a=2$, $b=4$, $n_{19}=10$, and $\chi_E'=2\ \text{m}^2\,\text{s}^{-1}$; then $T_k\simeq1.7$ keV.

A second temperature of interest is that at which the alpha power exceeds the bremsstrahlung losses,

$$T_{\alpha bk}\simeq2.4(Z_{\text{eff}})^{0.5}\left[\frac{n_e}{n_{\text{DT}}}\right]\ \text{keV}\ .$$

For $Z_{\text{eff}}=2$, $n_{\text{DT}}/n_e=0.73$, $T_{\alpha bk}\simeq4.6$ keV. This value is less than the value for a flat temperature profile because of gain in alpha power from the higher central temperatures.

The addition of conduction losses raises the temperature at which the alpha power takes over (ignition). The gap from the Ohmic temperature must be bridged with auxiliary power. In a stellarator with no Ohmic heating, the auxiliary power must also be used to produce the initial plasma.

For very high current-density configurations, high-field tokamaks, the RFP's, it is theoretically possible for the Ohmic power to provide all the heating and lead to ignition, the dashed line in Fig. 22. Assuming that $\partial W/\partial t=$constant, the maximum auxiliary power occurs where $\partial P_a/\partial T=0$. This is given, approximately, by balancing the rate of change of alpha heating against the

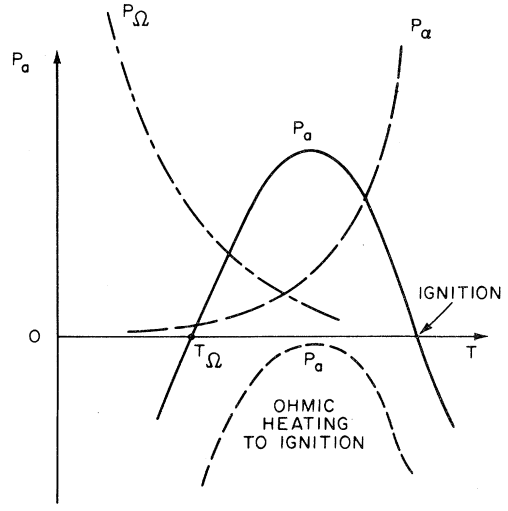

FIG. 22. Auxiliary power requirements for tokamaks, showing a characteristic variation with plasma temperature owing to the temperature dependences of ohmic, bremsstrahlung, and alpha power.

rate of change of conduction losses, provided $\delta \leq 1$,

$$T_{m\kappa} \simeq \left[\frac{340(1+\delta)\chi'_e}{(10)^{\delta} a b n_{19}} \left[\frac{n_e}{n_{DT}} \right]^2 \right]^{1/(1.5-\delta)} \text{(keV)} . \quad (2.77)$$

For example, if $\delta=0$, $\chi'_E=1$, $n_{\rm ND}/n_e=0.73$, $a=2$, $b=4$, $n_{19}=10$, $T_{mk} \simeq 3.2$ keV. The minimum value of P_{am} occurs when $\partial W/\partial t=0$. For the above example and $\gamma_R=1.5$, $Z_{\rm eff}=2$, $I_m=20$, $R=7$,

$$P_{am} = \underset{\text{conduction}}{72} + \underset{\text{bremsstrahlung}}{22} - \underset{\text{Ohmic}}{15} - \underset{\text{alpha}}{21} = 58 \text{ (MW)} .$$

Ignition occurs at about 7 keV.

To raise the plasma to ignition in a finite length of time requires additional heating. Assuming a rise time of 30 s to 7.5 keV for the example above requires $\partial W/\partial t \simeq 2.5$ MW. So the total auxiliary power needs to be about 80 MW. For Ohmic ignition the minimum heating power occurs at $T_{a\Omega}$, where $P_\alpha = P_\Omega$, and this represents the highest hurdle to cross, assuming conduction losses, like bremsstrahlung losses, vary slowly with temperature:

$$T_{a\Omega} \simeq 4.5 \gamma_R^{0.25} Z_{\rm eff}^{0.25} \left[\frac{I_m}{a b n_{19}} \right]^{0.5} \text{keV} . \quad (2.78)$$

The ignition requirement is that

$$\frac{0.16 \gamma_R Z_{\rm eff} I_m^2}{a b T_{a\Omega}^{1.5}} > 0.16 R n_{19} \chi'_E T_{a\Omega}^{1+\delta} + 1.1 \times 10^{-3} R a b Z_{\rm eff} n_{19}^2 T_{a\Omega}^{0.5} .$$

A variety of methods have been used successfully to heat toroidal plasmas (see Fig. 23)—neutral-beam injection (Menon, 1981), radio-frequency heating (Hwang and Wilson, 1981; Bornatici *et al.*, 1983; Colestock, 1984; Cairns, 1991; Stix, 1992), and adiabatic compression (Bol *et al.*, 1975).

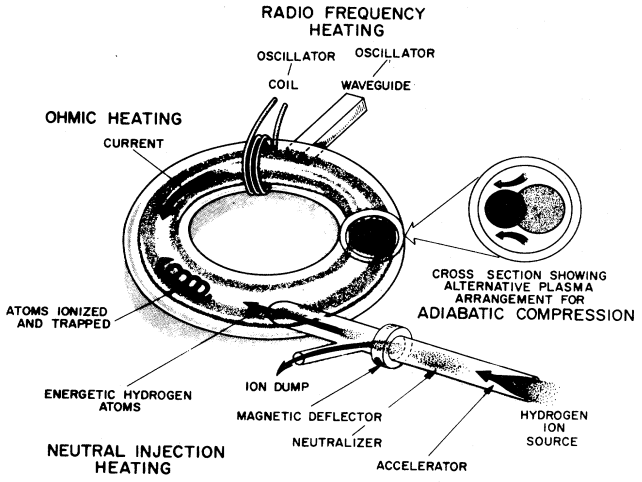

FIG. 23. An illustration of the main heating systems that have been used on tokamaks.

1. Neutral-beam injection

This heating technique involves injecting an intense beam of energetic atoms, generally hydrogen or deuterium, into the plasma. To date, energies up to 150 keV have been used. At such energies it is possible to form the beams by neutralization of energetic positive ions. For the higher energies envisaged for ITER and rectors ($\gtrsim 1$ MeV), positive-ion neutralization is inefficient and negative ions must be used. Because the atoms are neutral, they can cross the outer regions of the confining magnetic field and reach the plasma. The atoms penetrate the plasma until they are either ionized or charge exchange on plasma ions. In most applications a small percentage of the beam passes through the plasma. (Avoidance of damage to the chamber wall sets a limit on the maximum beam energy.) The energetic ions produced are trapped by the magnetic field and orbit within the plasma, slowing down by collisions that heat the plasma. Some energetic ions may suffer collisions that transfer them into uncontained orbits as they slow down. In practice, for most practical conditions losses are $\lesssim 10\%$.

The fraction of beam shine-through (Uckan *et al.*, 1990), for hydrogen-beam energies of ~ 0.5 MeV/amu, is

$$f_{sb} \simeq \exp[-(\bar{n}_{20} d_b)(0.795/E_b)^{0.78}] . \quad (2.79)$$

Here E_b (MEV) is the beam energy, $\bar{n}_{20}$ (10^{20} m^{-3}) is the average density along the beam path, and $d_b \simeq 2R_0[(1+a/R_0)^2-(R_{\rm tang}/R_0)^2]^{1/2}$, where $R_{\rm tang}/R_0$ is the cosine of the angle between the beam ions and the toroidal field at R_0.

The energetic ions slow down initially on the electrons and, after they reach a critical energy (E_c), on the ions. The formulas for the critical energy and for the fraction of energy transferred to the ions are in Eqs. (2.20) and (2.21). The first demonstration of substantial ion heating in a toroidal device was on PLT (Stodiek *et al.*, 1981), where the central ion temperature was raised to 7.5 keV (the electron temperature to 3.5 keV) with 3 MW of power. Since that time the ion temperature has reached over 30 keV in TFTR (Bell *et al.*, 1989), and the electron temperature 13 keV in JET (Keilhacker *et al.*, 1991), with up to 25 MW of power. For deuterium injection into a D-T plasma, the energetic ions can fuse, thereby enhancing the alpha power in the plasma (Jassby, 1976). While the gain is too small to make an economic power reactor, it is of interest in making volume neutron sources for fusion nuclear testing. Neutral-beam injection may also be used to drive a plasma current; see Sec. IV.B.

2. Radio-frequency (RF) heating

This technique involves driving oscillating currents in the plasma at frequencies for which the plasma impedance is high. In fusion, the term RF heating is used loosely for systems operating in the range from 25 kKz to 250 GHz. Each system consists of a high-power oscillator with feed cables or waveguides going to a launching structure made of coils or waveguides which are close to the plasma.

a. Absorption

For good absorption, by Landau damping or transit-time magnetic pumping, it is necessary for the phase velocity of the propagating wave to match the velocity (v_q) of either the electrons ($q=e$) or the ions ($q=i$). For cyclotron resonant interactions the requirement is $(w-mw_{cq})/k \rightarrow v_q$ where m is an integer and w_{cq} is the cyclotron frequency. The thermalization of power by the particles resonant with the wave may be by collisions, Landau damping, or cyclotron damping or, at very high power densities, by nonlinear interactions resulting from turbulence generated by the incident wave.

The attractions of RF heating are that, in principle, the power may be preferentially deposited in the resonant region, which may be selected; either electrons or ions may be heated; and, as discussed in Sec. IV.B, momentum may be transferred to the plasma in a way that drives a plasma current.

b. Efficient coupling

Efficient coupling of the power requires that the incident wave penetrate the plasma and be absorbed. The behavior of the waves will depend upon the radial profiles for the plasma density and magnetic field, and to a lesser extent on the temperature. At very high frequencies [$\omega \gg \omega_{pe}$ (electron plasma frequency) and ω_{ce} (electron cyclotron frequency)], the waves are transmitted with only a minute amount of power being scattered by the plasma. At lower frequencies ($\omega \lesssim \omega_{pe}$ and ω_{ce}) the waves may be reflected or absorbed, depending on the plasma profiles and launcher geometry. In an unmagnetized plasma, the waves will propagate to the point at which the density has risen to a level where $\omega_{pe}=(n_e^2/m_e t_0)^{1/2}=w$. At this point, called a "cutoff", the waves will be reflected. The situation is more complicated in a plasma containing a magnetic field.

c. Electron cyclotron frequency range

In a magnetized plasma, the behavior is modified and cutoff may occur where $\omega_{pe}=\omega$ or where $(\omega_{pe}^2-\omega^2)^2=\omega_{ce}^2\omega^2$, depending upon the mode of the waves. Propagation occurs provided the density remains below a value corresponding to cutoff,

$$n_{\max}=1.24\times10^{18}(\mathrm{m}^{-3})\left[\frac{w}{10\ \mathrm{GHz}}\right]^2\times\begin{cases}1+\dfrac{1}{m} & \text{extraordinary mode } (E_w\sim B)\ ,\\ 1 & \text{ordinary mode } (E_w\| B)\ ,\end{cases} \tag{2.80}$$

where w and $\kappa=2\pi/\lambda$ are the incident-wave frequency and wave number, respectively, and m is the cyclotron harmonic number. Power is coupled to harmonics of the electron cyclotron frequency, generally to the first or second harmonic. Because these are high frequencies, $w_{ce}=7-14\times10^{11}$ (rad s^{-1}) (110–120 GHz) and $\lambda \ll a$, it is necessary to satisfy the cutoff condition. The development of the gyrotron in Russia opened the way for the deployment of high power ($\sim$MWs). A program in *T*-10 (Parail and Alikaev, 1984; Alikaev and Parail, 1991) demonstrated both heating—the ability to modify MHD activity with up to 2.2 MW of power at 86 GHz—and current drive (Lohr *et al.*, 1991). Significant heating has been obtained in DIII-D (Luce *et al.*, 1991), with 1.4 MW at 60 GHz. An excellent review has been given by Bornatici *et al.* (1993).

d. Lower hybrid frequency range

The lower hybrid frequency is w_{LH} where

$$\frac{1}{w_{\mathrm{LH}}^2}=\frac{1}{(w_{ci}^2+w_{pi}^2)}+\frac{1}{w_{ci}w_{ce}}\ . \tag{2.81}$$

The frequency is sufficiently high that waveguides may be used for launching it, e.g., $n\simeq10^{19}-10^{20}$ m^{-3}, $B\sim4-10$ T, in a deuterium plasma. The launching structure must be placed close enough to the plasma that the plasma density near the launcher is above the cutoff level for the waves. The wave is then evanescent to the cutoff region and propagates beyond it. For a simple launching geometry (e.g., single waveguide), the wave would be reflected. Access to the resonance zone then requires the incident wave to have a finite wave number parallel to the magnetic field. This may be provided by using a set of waveguides with the wave phase alternated (Brambilla, 1976). Experiments show that the coupling varies as a function of phase angle, in agreement with the Brambilla theory. Substantial heating and efficient current drive have been demonstrated on JT-60 with 4.5 MW of power (Nagami *et al.*, 1991).

e. Ion cyclotron frequency range

Two modes of the wave are possible: a "slow wave," which behaves in a manner similar to the lower hybrid case and requires a complex launcher structure to avoid

reflection; and a "fast wave," which is evanescent between the launcher and a cutoff region in the plasma, but can propagate beyond the cutoff without attenuation. Decay of the curves in the evanescent region has the form $\exp(-2\kappa_{\|}\Delta r)$, where Δr is the launcher-to-cutoff region separation. Provided the scale of the launcher is large enough ($\gtrsim 4\pi\ \Delta r$), most of the wave power will propagate into the plasma.

The ion cyclotron frequency is $\omega_{ci}=eB/m_i$ (rad s^{-1}). For a deuterium plasma and a field in the range 4 to 8 T, $\omega_{ci}=1.9-3.8\times10^8$ (rad s^{-1}). There are a variety of resonances to which power may be coupled: (1) the harmonics of the ion cyclotron frequency, and (2) when two ion species are present, the hybrid frequency.

Most of the applications to date have been directed at heating a minority H or ^{3}He component in a deuterium plasma. The region of power deposition depends upon the fraction $\eta=n_H/n_D$ or $n_{^3He}/n_D$. For $\eta\sim0.05$ the power is absorbed at the minority cyclotron frequency, providing a very energetic minority component; this component then slows down in a manner similar to the energetic ions in neutral injection, heating both electrons and ions. For large η ($\gtrsim0.1$), near the ion hybrid resonant layer, there is a competition between cyclotron damping on the minority species and conversion to Bernstein waves, which are absorbed subsequently by Landau damping, again leading to both electron and ion heating. Power has also been successfully coupled at the second harmonic frequency. While experiments to data have used loop antennae, a recent development, the folded waveguide, makes the waveguide approach possible for larger or higher-field devices (Owens, 1986). Ion cyclotron heating has been applied successfully to a wide number of experiments. For example, ion and electron temperatures of 10 keV or more have been obtained in JET (Tubbing *et al.*, 1991).

f. Adiabatic compression

Major radius adiabatic compression was first demonstrated on ATC (Bol, 1975), and has been explored further on TFTR (Tait *et al.*, 1985). It is not favored in tokamak reactors because of the constraints it imposes on the coils. However, it is of interest to FRCs; see Sec. VII.E.

I. Fueling

In the earliest experiments, the plasma chamber was evacuated and then filled with the working gas to a density somewhat less than that required for the plasma. Ionization of the gas fill plus gas evolved from the walls led to the final plasma density. The plasma density varied in time as the plasma came into equilibrium with the walls. Today, to control the density, a gas input with feedback from the line density is used. As discussed in Sec. II.G, charge exchange of the gas on the plasma ions can lead to wall bombardment by energetic neutrals and to wall erosion. In addition, the sources at the plasma edge generates a relatively flat density profile unless the particle pinch term is large.

1. Pellet injection fueling

The injection of high-speed frozen pellets of hydrogen isotopes has been used to overcome these problems (Milora, 1981, 1989; Combs, 1993). The model of pellet ablation which best matches the experimental measurement of pellet penetration is the neutral-gas shielding mode (Parks, Turnbull, and Foster, 1977). In this model, the plasma heat flux ablates molecular hydrogen from the pellet surface. The cloud of hydrogen gas shields the pellet from the hot plasma and in effect increases the energy required to remove a molecular from the surface from the sublimation energy of 0.01 to $\sim$2 eV. The pellet suffers little charge exchange, alleviating the wall bombardment problem. The rate of reduction of the pellet radius (r_p) is

$$\frac{dr}{dt}=\frac{3.1\times10^6}{n_s^0}n_e^{1/3}T_e^{1.64}r_p^{-2/3}\ \mathrm{m}^{-1/3}\ , \tag{2.82}$$

where n_e (m^{-3}) and T_e (eV) are the local plasma parameters, $n_s^0=3.1\times10^{28}$ m^{-3} is the molecular number density of solid deuterium, and m is the molecular mass. For $T_e=T_e(0)(1-r/a)$ and $n_e=n_e(0)(1-r/a)$ the pellet lifetime, for penetration to the plasma axis, is

$$\tau=5.8\times10^{-7}n_s^0n_{e(0)}^{-1/3}T_{e(0)}^{-1.64}r_p^{5/3}\ \mathrm{m}^{1/3}\ (\mathrm{s})\ . \tag{2.83}$$

The speed required to reach the axis is τ/a. The response of the plasma density to the injection of a pellet in the JET tokamak is shown in Fig. 48.

For use in a reactor, the pellet size should be small enough not to overperturb the plasma, e.g., $\sim$10% of the plasma particle content. For example, if $R=7$ m, $a=2$ m, $b=4$ m, $n=2\times10^{20}$ m^{-3}, $N=4.4\times10^{-23}$ atoms. A pellet radius of about 5.5 mm would yield a 10% density increase. The time to penetrate to the center assuming $T_e(0)=20$ keV, $n_e(0)=3\times10^{20}$ m^{-3} would be 61 μs, requiring a pellet speed of 33 km/s. The present maximum speed is 3 km/s without a sabot to protect the pellet during acceleration. Speeds of 5–10+km/s are expected for systems using sabots. It seems unlikely that speeds capable of reaching the axis of large reactors will be developed. Nevertheless this technique can certainly lead to penetration to one-third to half of the radius (50 to 75 % of the plasma volume) and in any circumstances to much reduced charge-exchange problems.

2. Compact toroid plasma injection

An alternative approach to fueling using the injection of compact toroid plasmas has been proposed (Perkins *et al.*, 1987). Both plasma guns (Jarboe *et al.*, 1980), and field-reversed pinch devices (Hoffmann, 1992) have been

suggested for the production of dense, high-beta plasmoids. Calculations of the energetics (Gouge *et al.*, 1988; Hoffman, 1992), suggest that the higher-beta, FRC approach may be favored.

III. TAXONOMY OF TOROIDAL SYSTEMS

A. Introduction

The majority of work in magnetic fusion, directed towards power reactor development, is concentrated on the relatively small number of closed magnetic configurations shown in Fig. 24. Work on open systems, such as the linear pinch and mirror, has declined because of the difficulty of blocking the end losses efficiently. Closed magnetic systems avoid the end losses by bending the field back on itself to form a torus, with average toroidal field B_ϕ. However, the curvature of the field, introduced by the bending, leads to a new rapid loss of plasma because charged particles of opposite sign drift apart parallel to the axis of symmetry. The ensuing electric field drives the plasma outward radially, and there is no equilibrium. There are a number of ways of overcoming this problem.

1. Axisymmetric systems

The addition of a current, driven along the toroidal field, causes the total field to twist owing to the poloidal field (B_θ) of the current (see Fig. 27 below), and the charged particles tend to follow the helical field lines. Consequently a particle that starts drifting up will soon follow the helical field line down, and vice versa, thus preventing the charges from separating. However, the net result of these motions is a displacement of the particle orbit from a flux surface, and some complicated orbits which affect transport. An additional vertical field is required to counteract the tendency of the plasma and plasma current to expand in major radius and provide an equilibrium. Such a current and vertical field preserve the axisymmetry of the simple torus. The field lines circle the torus in such a way that their intersections on a poloidal plane form a set of nested magnetic surfaces, $\psi = \oint \mathbf{ds}\cdot\mathbf{B}_\theta = \text{constant}$, as illustrated in Fig. 2. The number of times a field line circles the torus in the toroidal direction for one transit in the poloidal direction is called the safety factor q. The safety factor may be written in terms of an integral over the projection of the surfaces on a poloidal plane, where the major radius coordinate is denoted by R:

$$q_\psi \equiv \left.\frac{d\zeta}{d\theta}\right|_\psi = \frac{RB_\phi}{2\pi}\oint \frac{dl}{B_\theta R^2} \ . \tag{3.1}$$

Here ζ and θ are the angular variables the long and short way around the torus. For a large-aspect-ratio circular plasma,

$$q \simeq \frac{rB_\phi}{RB_\theta} \ . \tag{3.2}$$

Note that situations in which a field line closes on itself after an integer number of toroidal (n) and poloidal (m) transits ($q = n/m$) can be unstable to perturbations. The Kruskal-Shafranov stability limit addresses the case in which $q_a = 1$ at the plasma edge, for which case violent instability can occur.

A variety of systems use a plasma current to provide equilibrium. They are distinguished by the range of q_a in which they operate to avoid crippling instabilities:

Tokamak

$$q_a \gtrsim 3 \text{ typically, } B_\theta \sim \frac{aB_\phi}{Rq_a} \ll B_\phi \ ,$$

except low $R/a < 2$, and high noncircularity $\kappa = b/a \gtrsim 2$.

Reversed-Field Pinch (RFP)

$$q_a \simeq 0.5 \ ,$$

since typically $R/a \sim 6$, $B_\theta \lesssim B_\phi$.

Field-Reserved Configuration (FRC)

$$\frac{R}{a} \sim 1, \frac{b}{a} \text{ large (e.g., } \sim 6) \ ,$$

$B_\theta \gg B_\phi$ for reactor candidates. Typical radial profiles of B_ϕ and B_θ for representative configurations are shown in Fig. 25.

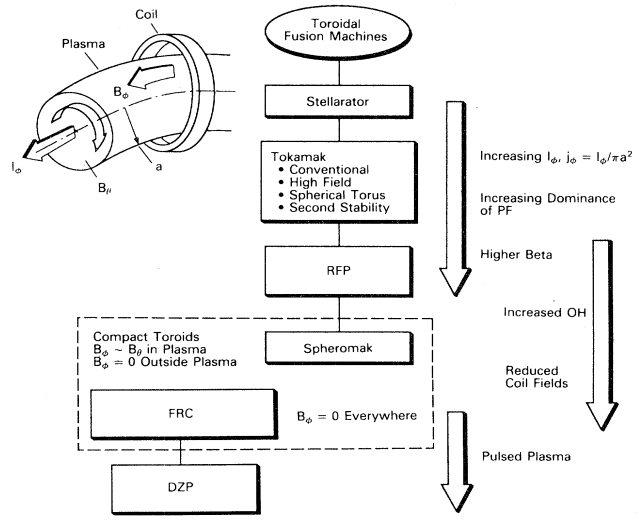

FIG. 24. Representative toroidal systems with nested flux surfaces; stellarator, tokamak, reversed-field pinch, spheromak, field-reversed configuration, and dense Z pinch.

2. Nonaxisymmetric systems

An alterative approach is to produce the twist in the field lines by twisting the external coils—the stellarator. Such systems also have magnetic-flux surfaces, but introduce a nonaxisymmetry into the field which modifies the particle orbits and increases the role of the electric field in transport.

In stellarators it is commonplace to use the rotational transform (ι) rather than q to characterize the flux surfaces,

$$\iota \equiv \frac{1}{q} . \tag{3.3}$$

As shown in Sec. V (Fig. 50), stellarators inhabit a wider range of ι-space than do tokamaks, because of their greater ability to vary the form of their poloidal field. In general, the radial dependence of the safety factor is opposite to that in a tokamak [which rises center to edge, $q(0) < q(a)$]. Stellarators can also be created with a helical axis. Representative configurations include

stellarator $l = 2,3$ alternate pairs of coils carry opposing currents ,

torsatron-heliotron $l = 2$, 2 coils carry currents in the same direction ,

heliac $l = 1$, helical axis.

In all cases the helical coils, vertical-field coils, and poloidal-field coils can be modularized as nonplanar toroidal coils.

3. Strength and weaknesses

The strength of the axisymmetric systems lies in the use of a plasma current which provides relatively good coupled values of confinement and beta. The mainline tokamak has exhibited the best confinement, with low thermal diffusivities and, in large devices such as JET, energy confinement times of more than 1 s. The current is also a weakness because it is a source of free energy, which, in certain conditions, can lead to rapid plasma ejection—disruption—notably at the highest plasma pressures and densities. In addition, a mechanism must be found to sustain it or the plasma will be pulsed. These two problems constrain the optimization of plasma performance.

The strength of the stellarators is their external control of the magnetic field. It allows planned optimization of the plasma performance, in which the inherent steady-state nature of the field does not constrain the optimization. However, in the present configurations the coil geometry is more complex than that of the axisymmetric systems. Also, while thermal diffusivities in the present modest-scale facilities are comparable with those in similar-scale tokamaks, there is the concern that at lower collisionality the non-axisymmetric effect will degrade confinement.

An appealing concept, which has not yet received significant attention in reactor design, because of the lack of an experimental and theoretical basis, is to combine stellarator and axisymmetric current-carrying features in a single hybrid. One potential advantage is the suppression of disruptions in tokamaks by the application of an externally applied helium transform, as has been demonstrated experimentally (Fussman *et al.*, 1979; Robinson, 1980).

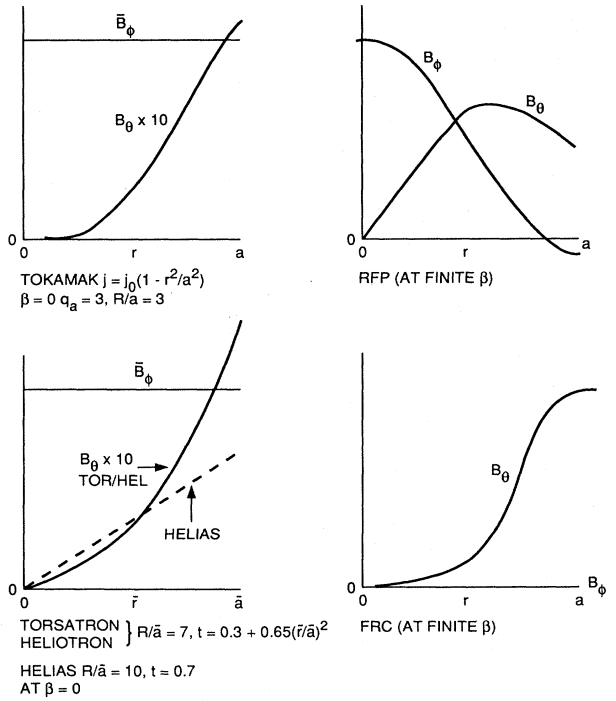

FIG. 25. Typical radial profiles of B_ϕ (average $\bar{B}_\phi$) and B_θ for representative toroidal systems.

B. Magneto-hydrodynamics

On the macroscopic scale, the toroidal plasma may be treated as a conducting fluid; the behavior of this fluid and of the confining magnetic fields is described by the magnetohydrodynamic (MHD) equations:

$$\frac{\partial \rho}{\partial t} + \nabla \cdot \rho \mathbf{v} = 0, \quad \rho = \sum mn , \tag{3.4}$$

conservation of mass ,

$$\left[\frac{\partial}{\partial t} + \mathbf{v} \cdot \nabla \right] p \rho^{-\gamma} = 0, \text{ adiabatic law} , \tag{3.5}$$

$$\rho\left[\frac{\partial \mathbf{v}}{\partial t}+\mathbf{v}\cdot\nabla\mathbf{v}\right]=-\nabla p+\mathbf{j}\times\mathbf{B}\ , \tag{3.6}$$

conservation of momentum ,

$$E+\mathbf{v}\times\mathbf{B}=\eta\mathbf{j},\ \text{Ohm's law}\ , \tag{3.7}$$

$$\nabla\times\mathbf{E}=\frac{-\partial B}{\partial t}\ , \tag{3.8a}$$

$$\nabla\cdot\mathbf{B}=0\ , \tag{3.8b}$$

$$\nabla\times\mathbf{B}=\mu_0\mathbf{j},\ \text{Maxwell's equations}\ . \tag{3.8c}$$

In "ideal MHD," the plasma is assumed to be perfectly conducting and the resistivity (η) in Eq. (3.7) is set to zero; the magnetic field is frozen into the plasma. In resistive MHD, the resistivity allows field lines to reorganize.

1. Plasma equilibrium

In a stationary system with no plasma flow, Eqs. (3.6) and (3.8) may be combined to give

$$\nabla\left[p+\frac{B^2}{2\mu_0}\right]=\frac{1}{\mu_0}(\mathbf{B}\cdot\nabla)\mathbf{B}\ . \tag{3.9}$$

In the large-aspect-ratio approximation $r/R\ll 1$, analytic solutions may be obtained for the equilibria (Shafranov, 1966). The flux surfaces, assumed to be circles, have their centers displaced (Δ) from the magnetic axis ($r=0$); see Fig. 26. Analytical equilibria for elliptical surfaces have been calculated by Freidberg (1982). If the poloidal flux is due entirely to a plasma current, the poloidal field at the plasma boundary ($r=a$) is

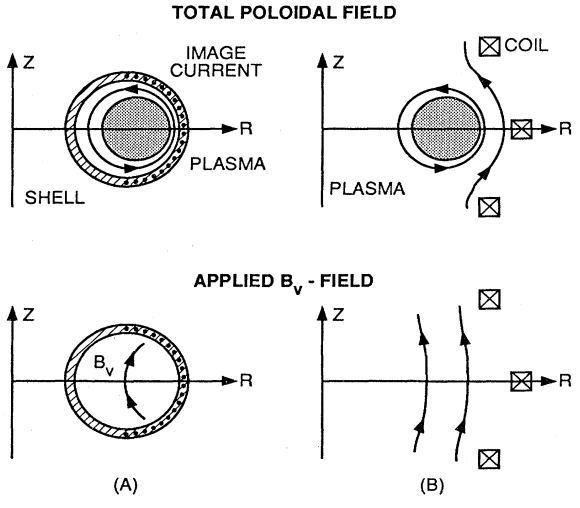

FIG. 26. Plasma equilibrium may be provided by a conducting shell (a), or by external coils only (b). In either case, the required inward force (along R) is due to the Lorentz force from plasma currents flowing across the vertical field B_v.

$$B_\theta(a,\theta)=\frac{\mu_0 I}{2\pi a}\left[1-\frac{a}{R}\left[\ln\frac{8R}{a}-\frac{1}{2}\right]\cos\theta\right]\ . \tag{3.10}$$

The plasma pressure is constant on a flux surface; however, the magnetic pressure is nonuniform, being stronger on the inside ($\theta=\pi$) than on the outside ($\theta=0$). Consequently a vertical field B_v must be provided to establish an equilibrium. In early tokamaks this was provided by image currents in a conducting shell; nowadays it is provided by coils. Shafranov (1966) showed that the required field is

$$B_v=\frac{\mu_0 I}{4\pi R}\left[\ln\left[\frac{8R}{a}\right]-\frac{3}{2}+\beta_\theta+\frac{l_i}{2}\right]\ , \tag{3.11}$$

where l_i is the internal inductance per unit length of the plasma, typically $l_i\lesssim 1$.

The poloidal beta is the ratio of the plasma pressure to the poloidal magnetic pressure,

$$\beta_\theta=\frac{2\mu_0\int p\,dV}{V\langle B_\theta^2\rangle_{\text{flux}}}\ , \tag{3.12}$$

where $\langle B_\theta^2\rangle_{\text{flux}}$ is the flux-surface average of the poloidal field at the plasma edge.

The equilibrium in an RFP is also provided by a conducting shell and, on long time scales, by fields produced by external coils. The equilibrium in an FRC is provided by a conducting shell.

There is no exact, simple solution to the equilibrium of the toroidal stellarator, unlike the case for axisymmetric systems. Approximate solutions may be found analytically by expansion of the magnetic-field properties about the magnetic axis. More exact numerical solutions may be found by looking for an energy minimum of the system when the plasma profile is perturbed. Such solutions must be found at the required beta because the configuration evolves owing to plasma-driven currents, as the pressure is raised. The Pfirsch-Schlüter current is given by

$$j_\phi\simeq\frac{2}{\ell}\frac{1}{B_0}\frac{\partial p}{\partial r}\cos\theta\ . \tag{3.13}$$

It yields a vertical field B_v, which causes an outward shift of the magnetic axis (Δ), given by

$$\frac{\Delta}{R}=-\frac{B_v}{\ell(\Delta)B_0}\ . \tag{3.14}$$

An approximate equilibrium limit to beta in a stellarator may be defined by requiring the shift to be less than the minor radius (typically $\Delta\simeq a/2$ is used),

$$\beta\le\frac{a}{R}(\ell)^2\times 100\%\ . \tag{3.15}$$

In fact, higher beta can be achieved than this simple model by careful adjustment of the configuration to reduce the current (Carreras *et al.*, 1983; Nuhrenberg

and Zille, 1986). Since the equilibrium in a stellarator is established by the constant external fields, feedback stabilization is not required. Changes in the external fields, e.g., vertical field or quadrupole field, may be used to optimize the configuration for equilibrium, stability, and transport as the beta is raised (Carreras *et al.*, 1984).

2. Plasma stability

The previous section discussed conditions for a toroidal plasma to be in equilibrium. An important question is whether this equilibrium is stable, for the plasma and plasma currents represent significant sources of free energy. Good reviews of this topic have been given by Bateman (1978), Wesson (1978), Schmidt (1979), and Freidberg (1982, 1987).

The energy principle may be used to determine which ideal MHD modes are linearly unstable (Bernstein *et al.*, 1958). A perturbation ξ is applied to the plasma equilibrium and an equation is derived for the change in energy of the plasma and magnetic field, $\delta W = \delta W_{\text{plasma}} + \delta W_{\text{surface}} + \delta W_{\text{vacuum}}$. The major instabilities may be discussed in terms of

$$\delta W_{\text{plasma}} = \frac{1}{2}\int d^3x \left\{ \frac{|\mathbf{B}_{1\perp}|^2}{\mu_0} + \mu_0 \left| \frac{B_{1\parallel}}{\mu_0} - \mathbf{B}_0 \frac{\boldsymbol{\xi}\cdot\nabla p_0}{B_0^2} \right|^2 + \gamma p_0 |\nabla\cdot\boldsymbol{\xi}|^2 \right.$$

Slow, shear Alfvén wave; fast, magnetoacoustic compressional wave; acoustic wave

stabilizing terms

$$\left. + \frac{\mathbf{J}_0\cdot\mathbf{B}_0}{B_0^2}\mathbf{B}_0\times\boldsymbol{\xi}\cdot\mathbf{B}_1 - 2(\boldsymbol{\xi}\cdot\nabla p_0)(\boldsymbol{\xi}\cdot\mathbf{K}) \right\} \tag{3.16}$$

Kink free energy; interchange or ballooning free energy

destabilizing terms

with $\mathbf{B}_1 = \nabla\times(\boldsymbol{\xi}\times\mathbf{B}_0)$ and where $\mathbf{K} = \mathbf{b}\cdot\nabla\mathbf{b}$ is the curvature vector of the equilibrium field and $\mathbf{b} = \mathbf{B}_0/B_0$. The subscripts 0 and 1 refer to the equilibrium and perturbed fields. An equilibrium is stable only if $\delta W \geq 0$ for all allowed displacements (ξ). The first term represents the energy required to bend the magnetic-field lines. The second term corresponds to the energy needed to compress the magnetic field, while the third term represents the energy needed to compress the plasma. The latter two terms are sometimes referred to as current-driven and pressure-driven destabilizing terms (Freidberg, 1982).

3. Resistive modes

Combining Ohm's law, Eq. (3.7), and Maxwell's equations, Eq. (3.8), leads to an equation for the evolution of magnetic perturbations,

$$\frac{\partial \mathbf{B}}{\partial t} = \nabla\times(\mathbf{v}\times\mathbf{B}) + \frac{\eta}{\mu_0}\nabla_\perp^2 B \tag{3.17}$$

motion of the plasma fluid with the magnetic field; slippage of the magnetic field relative to the plasma

The magnetic field and plasma fluid are no longer tied together, and the magnetic field can diffuse out of the system. There is less restriction on plasma collective motions, particularly near rational surfaces, and this leads to a modification of the ideal MHD instabilities. In addition the field lines can, in effect, break and rejoin to form a lower-energy state (Furth, Killeen, and Rosenbluth, 1963). The reconnected fields form islands, which extend radially and lead to enhanced transport.

C. Transport

Broadly speaking there are three ways in which the charged particles that constitute a plasma can cross a magnetic field: (a) by virtue of collisions causing them to diffuse across the field; (b) because of drift motion arising from gradients and curvature of the magnetic field; and (c) because of electric fields. Such transport is termed *classical.* When it includes the more complicated orbits to be found in a toroidal configuration such as the tokamak or stellarator, it is called *neoclassical.* Owing to instabilities within the plasma, the transport may be increased above the classical or neoclassical level. In either the microscopic or the macroscopic domain, this may

occur because nonthermal fluctuating electric fields are set up or because currents are set up that locally reconnect magnetic-field lines—the so-called island formation—allowing charges to move radially with ease. Such enhanced transport is termed "anomalous."

1. Diffusion

The characteristic diffusion flux is given by $nv_x = -D/(\partial n/\partial x)$. The diffusion coefficient $D \sim \Delta x^2 \nu$, where Δx is the step size of the particle. In this case Δx is the radial displacement of a particle from a field line and ν is the collision frequency. For a uniform and straight magnetic field $\Delta x \sim \rho$, the gyroradius of the charge orbit is

$$\rho = \frac{v_{th} m}{ZeB}, \text{ where } v_{th} = \left[\frac{2eT}{m}\right]^{0.5}. \tag{3.18}$$

For electron-ion collisions ν is given by Eq. (2.13).

2. Drift

In nonuniform magnetic fields, the orbit of a charged particle consists not only of the basic helical motion around a field line but also of drifts arising from gradients and curvature of the magnetic field. For toroidal systems, the net result is to add to the helical motion about the field lines a vertical drift owing to the toroidal field gradient and a drift in and out in major radius. If the particle is moving almost parallel to the field, its orbit projected on the R-Z plane is a displaced circle. Particles with a greater perpendicular motion may be reflected by the higher magnetic field on the inner side of the toroidal plasma—the "mirror effect." This latter class of particles has the characteristic banana-shaped orbit shown in Fig. 27. The characteristic radial excursion of a banana

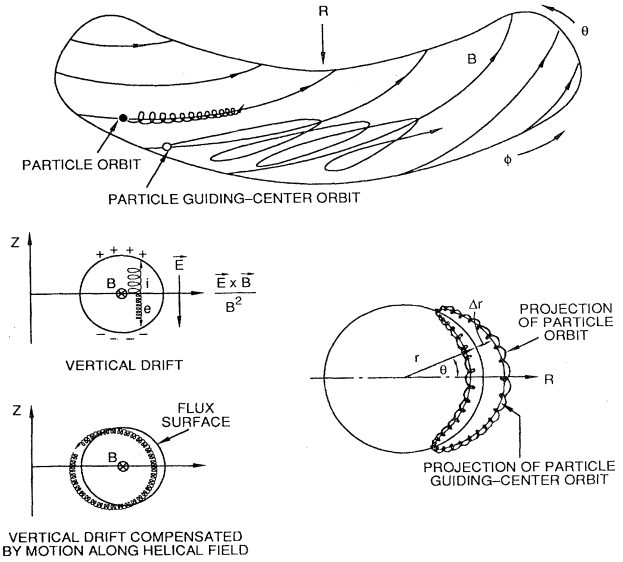

FIG. 27. Trapped-particle orbits in a tokamak.

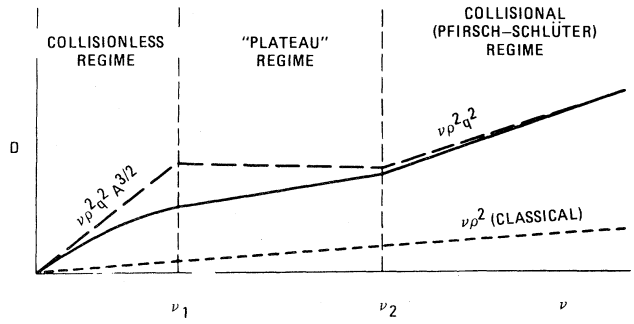

FIG. 28. Schematic illustration of the dependence of the neoclassical diffusion coefficient D on collision frequency ν, the transitions between the different regimes occurring at $\nu_1 = (a/R)^{3/2}$, v_{th}/qR, and $\nu_2 = v_{th}/qR$.

orbit exceeds the gyroradius and is $\Delta r \sim (r/R)^{0.5}\rho_\theta$, where the gyroradius in the poloidal field (B_θ) is $\rho_\theta = (v_{th} m/ZeB_\theta)$.

The fraction of charged particles executing banana orbits is of order $(2r/R)^{0.5}$. The banana diffusion coefficient $D_B \sim (2r/R)^{0.5}\rho_\theta^2 \nu$ exceeds the simple classical diffusion. However, for this term to be important the collision frequency must be low enough to permit the charges to complete banana orbits. Thus one may characterize the diffusion in terms of the parameter

$$\nu^* = \left[\frac{R}{r}\right]^{3/2} q\frac{R}{v_{th}}\nu, \tag{3.19}$$

which is the ratio of the time to complete a banana orbit divided by the collision time. It is conventional to define three diffusion regions: (1) $\nu^* > (R/r)^{1.5}$, the collisional or Pfirsch-Schluter regime, where banana effects are unimportant as particles do not ever complete an orbit around the torus; (2) $\nu^* \ll 1$, the collisionless or banana regime; and (3) $\nu^* \gtrsim 1$, the so-called plateau regime, where banana effects play a weak role. A schematic illustration of the form of the diffusion coefficient is given in Fig. 28.

3. Thermal conductivity

The preceding discussion was centered on particle diffusion; this is one mechanism for transporting heat across the magnetic field. In addition, heat is conducted by collisions. In the same manner as for diffusion, one may view heat conduction in terms of the collision frequency and the radial distance over which a particle can transfer its energy, that is, the heat flow $Q = n_e \chi \partial T/\partial x$. The detailed calculation of the transport neoclassical coefficients given by Hinton and Hazeltine (1976) has been updated by Hirshman and Sigmar (1981) and Chang and Hinton (1982, 1986) with regard to impurity and aspect-ratio effects. For a tokamak with $T_e = T_i$ and profiles such that, approximately, $nT \propto T^{3/2}$, a simple

formula for the radially averaged thermal diffusivity may be derived for a reactor-grade D-T plasma (Sheffield, 1985),

$$\bar{\chi}_{iNc} \sim 0.04 \left[\frac{R}{\bar{a}} \right]^{3/2} \bar{q}^{\,2} \frac{\langle \beta \rangle}{\langle T_k \rangle^{3/2}} \ (\mathrm{m^2\,s^{-1}}) , \qquad (3.20)$$

where $\bar{a} = \kappa^{1/2} a$ and T_κ is the temperature in kilovolts. Equating Eqs. (3.20) and (2.44) yields an expression for the minimum fusion power that can be sustained against neoclassical ion losses, assuming that electron losses are similar:

$$P_F \gtrsim 1.3 \times 10^3 \frac{(R/a)^{5/2} (a_w/a) \bar{p}_{wn}}{(b/a)^{5/3} f_B^2 B_m^2 f_\alpha} \times \left[\frac{n_e}{n_{\mathrm{DT}}} \right]^2 \frac{\bar{q}^{\,2}}{\langle T_k \rangle^{3/2}} \ (\mathrm{MW}) . \qquad (3.21)$$

For example, for $R/a = 4$, $b/a = 2$, $a_w/a = 1.1$, $f_B = 0.5$, $B_m = 12$ T, $\bar{p}_{wn} = 4$ MW m^{-2}, $f_\alpha = 0.8$, $n_{\mathrm{DT}}/n_e = 0.8$, $\bar{q} = 2$, $\langle T_k \rangle = 15$ keV, we find $P_F \gtrsim 450$ MW. Raising T_k while reducing the density provides more margin; however, a balance must be struck with the need to meet other objectives, such as achieving low impurity levels. A cross check against MHD limits is needed to obtain consistent values of T, n, and β.

4. RFP thermal conductivity

Neoclassical transport in a RFP is similar to that in a tokamak. However, the higher value of B_θ/B_0 (much lower $q_a \sim 0.2$, compared to $\gtrsim 3$ in a tokamak) leads to improved orbits, which reduce χ_{iNc} (Boozer, 1983).

5. FRC thermal conductivity

For this device, the classical thermal diffusivity is similar to that of a cylindrical system and

$$\bar{\chi}_i \simeq 0.02 \frac{\langle \beta \rangle}{\langle T_k \rangle^{3/2}} \ (\mathrm{m^2\,s^{-1}}) . \qquad (3.22)$$

6. Stellarator thermal conductivity

As in a tokamak, there are toroidally circulating particles and particles trapped in the magnetic mirrors of the high-field region on the inside of the torus. In addition, there are particles trapped in the helical field, which are reflected from its local mirror regions. In contrast to axisymmetric systems, there is an increasing particle transport as collisionality decreases (see Fig. 51 of Sec. V). The large level of transport would make it very difficult to design an economic reactor were it not for the ability to tailor the magnetic geometry (Nuhrenberg and Zille, 1986, 1988; Mynick, Chu, and Boozer, 1982). Alternatively, large radial electric fields may induce rotation, improve the particle orbits, and reduce transport as shown in Fig. 51 below.

The modifications to the ion thermal transport have been calculated by Shaing (1984) for a torsatron and/or heliotron. The average $\bar{\chi}_{iNc}$ compared to a tokamak is given by

$$\bar{\chi}_{iNC} \simeq (\bar{\chi}_{iNC})_{\mathrm{tok}} \left[0.6 + \frac{3.2 \times 10^3}{\langle T_k \rangle (R/a)^2 f_E^2} \right] \mathrm{m^2\,s^{-1}} , \qquad (3.23)$$

where $f_E = \phi / T_k$ and ϕ is the radial potential. For a carefully tailored magnetic field, such as in a helias configuration, the transport is similar to that with $f_E \simeq 2$–3 (see Fig. 51 of Sec. V). For example, if $\langle T_k \rangle = 15$ keV, $R/a = 7$–10, and $f_E = 2$–3, we find

$$\frac{(\chi_{iNC})_{\mathrm{stell}}}{(\chi_{iNC})_{\mathrm{tok}}} \simeq 0.84\text{–}1.7 .$$

7. Ripple transport

Even in nominally axisymmetric systems there can be inhomogeneities owing to the use of discrete coils. In a tokamak, the toroidal field ripple, resulting from the use of a finite number of toroidal coils, can lead to local trapping of a small fraction of particles, proportional to the square root of the modulation. An excellent review of the subject has been given by Kovrizhnykh (1984).

Increased losses of particles and heat occur both due to the ripple trapped-particle diffusion and due to asymmetry induced in the reflection points of toroidally trapped particles, owing to the toroidal field ripple's causing incomplete compensation of the vertical drift.

For large ripple, the losses can be severe, and tokamaks are generally designed to have a toroidal field ripple $\epsilon_\phi = (B_{\max} - B_{\min})/(B_{\max} + B_{\min}) \leq 1$ or 2% at the plasma edge and $\leq 0.1\%$ on axis, to avoid problems.

A simple empirical formula has been derived to relate the major radius in the median plane to the ripple (δ_ϕ), number of toroidal coils (N_c), and major and minor radii of the circular coil set, R_c and a_c, respectively (Core, 1974; Sheffield and Gibson, 1975):

$$R_{\delta_\phi} = (R_c + a_c) \left[1 - \ln \left[\frac{2.6 \sin\lambda}{2\epsilon_\phi A_r \sin\lambda_0} \right] \Big/ 1.1 N_c \right] , \qquad (3.24)$$

where $\lambda_0 = \pi[(R_c - a_c)/(R_c + a_c)]$, $\lambda = \lambda_0 \ A_r$, and A_r is the ratio of the coil cross section on the outside of the torus to the cross section in the bore of the toroidal assembly. There are some limited experimental data that support the theoretical models of heat and particle loss (Scott *et al.*, 1985). One unpleasant effect of the ripple can be to concentrate an energetic particle flux on the walls, causing damage.

Direct loss of energetic alpha particles and alpha power is a concern for devices such as ITER and reac-

tors, both because of the loss of heating and because of the potential for damage to the walls, as discussed in Sec. II.F. Recent studies of energetic-ion losses have been made in TFTR (Boivin *et al.*, 1990; Zweben *et al.*, 1983), and in JT-60U (Nishitani *et al.*, 1993). In comparing theory and experiment for energetic-particle losses in JT-60U it was necessary to allow for electric-field effects (Itoh and Sanuki, 1991). Alpha-particle losses in ITER are discussed by Post *et al.* (1991). For representative plasma profiles a variety of computations indicate a power loss of $\lesssim 1\%$ for full-current operation in ITER. The results are sensitive to the profile.

8. Anomalous transport

Unfortunately, the observed transport in all of the devices described above is anomalously higher, particularly for the electrons, to the extent that, instead of the expected $\chi_e \ll \chi_i$ in the axisymmetric systems, $\chi_e \gtrsim \chi_i$ and $\chi_i \sim (1-10)\times\chi_{iNc}$. Therefore ion neoclassical losses (tokamak case) and electron neoclassical losses (stellarator case) can be used only as lower limits to set a minimum reactor size for a given power and field. Anomalously high transport in plasmas results from instabilities that are driven by sources of free energy in the plasma, e.g., pressure, density, temperature, resistivity, etc. gradients, which are inherent to the plasma configuration. Various reviews of plasma instabilities have been given, including those of Kadomtsev and Pogutse (1970, 1971), Mikhailovskii (1974), Wesson (1978), Tang (1978), Rosenbluth and Rutherford (1981), Liewer (1985), Ross (1987), Romanelli (1989), Callen (1991), and Carreras (1992). While much of this discussion has been in relation to tokamaks, nevertheless, the underlying mechanisms have wider application to toroidal systems. There has been only limited success in identifying particular mechanisms as being credible candidates to explain transport in certain regions of toroidal devices. I am including a brief review of this subject in the hope that, during the useful life of this paper, greater progress will be made and it will be helpful to the reader.

In a turbulent plasma the particle flux given in Eq. (2.10), $\overline{\Gamma}=D_A \partial n/\partial r + V_r n$, must now be modified to include additional terms resulting from correlations of the various fluctuations. For example, when $n=\langle n(r,t)\rangle + \tilde{n}$, where $\langle\ \rangle$ denotes a time average and $\phi=\langle\phi\rangle+\tilde{\phi}$, there is an additional term involving $\langle \tilde{n}(r,t)\tilde{\phi}(r',t')\rangle$. Allowing also for magnetic fluctuations, we find

$$\overline{\Gamma}=\frac{\langle \tilde{E}_\theta \tilde{n}\rangle}{B_\phi}-\frac{\langle \tilde{j}_\parallel \tilde{b}_r\rangle}{eB_\phi}\ , \tag{3.25}$$

where B_ϕ is the toroidal field, and $\tilde{j}_\parallel$ and $\tilde{b}_r$ are, respectively, the fluctuating parallel current and radial magnetic fields.

Additional fluxes in the power balances are

$$\frac{3}{2}n\kappa\frac{\langle \tilde{E}_\theta \tilde{T}\rangle}{B_0}+\frac{3}{2}kT\frac{\langle \tilde{E}_\theta \tilde{n}\rangle}{B_0}+\pi R v_e\left[\frac{\tilde{b}_r}{B_0}\right]^2, \tag{3.26}$$

where the latter term is a quasilinear expression valid for collisionless plasmas (Wooton, 1991).

9. Weak turbulence

In weak-turbulence theory it is assumed that the decorrelation time of fluctuations is short enough that they do not affect each other directly. In quasilinear theory, contributions are truncated at first order, $f=f_0+\epsilon f_1$, and a modification to the background comes from terms $\langle f_1\phi_1\rangle$. Saturation of the fluctuations occurs when the background equilibrium is modified sufficiently to limit the fluctuation level, e.g., flattening of a gradient. Dimensional analysis and/or mixing-length theory leads to a diffusion coefficient

$$D=\Delta^2\tau^{-1}\ , \tag{3.27}$$

where Δ is the mixing length and τ is the decorrelation time. It is common practice to take $\Delta\sim 1/k_\perp$, the width of the mode, and $\tau\sim 1/\gamma$, where γ is the linear growth rate of the mode. There are very few models solved analytically. In the case of resistive pressure-gradient-driven turbulence it was found analytically that $D=\Lambda^2\gamma/k_\perp^2$, where the multiplier Λ depends logarithmically on the collisional dissipation. At the next level of theory, nonlinear wave-particle and wave-wave interactions are included, as discussed by Tsytovich (1970).

10. Strong turbulence

In strong turbulence the various modes are strongly interacting, and the level of each mode depends directly on interactions with the other modes, rather than on a modification of the background conditions or weak intermode interactions. Solutions require either the use of a computer or the incorporation of strong, averaged effects of the modes on each other—renormalization theory (see for example, Kadomtsev, 1965).

Substantial efforts are underway to relate theory and experiment (Ross, 1987; Callen, 1990,1991), but it is a difficult task because of the plethora of terms in the transport equations. There is even debate on the correct form for the transport equations to be used (Ross, 1990). In practice, in predicting reactor performance it is commonplace to use empirical values for D, V, and χ, based upon experimental data, in combination with the neoclassical values. On occasion it is possible to replace or supplement the empirical models with theoretical models for anomalous transport.

Some progress has been made in characterizing the turbulence in the edge of the plasma by comparing fluctuations in tokamaks, stellarators, and RFP's with various theories (Wootton, 1991). It has been shown that the fluctuations in $\tilde{n}$, $\tilde{\phi}$, and $\tilde{T}$ are sufficient to account for the anomalous edge transport in tokamaks and stellarators at moderate temperatures (~ 100 eV), while $\tilde{b}$ enters

into the losses for RFP's.

As for our understanding of turbulence in the core plasma, there has been less progress, owing to the greater difficulty of making fluctuation and correlation measurements. A wide range of instabilities remain candidates to explain the anomalous losses. Various models are classified in Table IX (Liewer, 1985).

In resistive MHD, magnetic-field lines reconnect to form a lower-energy state (Furth, Killeen, and Rosenbluth, 1963). The reconnected fields form islands in the magnetic field, as seen in a field-line plot in a poloidal plane; the islands extend the radial distance which electrons can transverse without a collision ($\tilde{v}_r = v_\parallel \tilde{B}_r / B$). The instabilities start on rational surfaces at different radii, forming islands as indicated in Fig. 29. If the islands grow large enough, they may overlap, leading eventually to an ergodization of the field. This ergodization may be seen in the fuzziness of the field lines at intermediate radii in Figs. 29(c) and 29(d). Mode overlap is also shown in Fig. 42 of Sec. IV. As tangling of the field lines increases, the electron radial transport is enhanced. It is generally assumed that, unless tangling is extreme, the ions, with their greater natural excursions, are less affected. The average squared radial displacement Δr in moving along a field line a distance s is given by $\langle (\Delta r)^2 \rangle = 2sD_m$, where

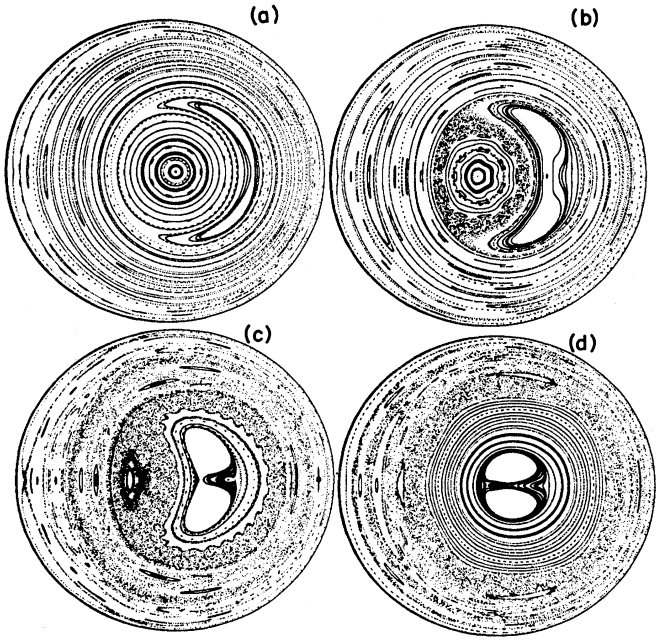

FIG. 29. Field-line plots during a crash (simple sawtooth). Note the development and healing of stochastic regions (Aydemir *et al.*, 1989).

TABLE IX. Classification of some modes of turbulent transport, Liewer (1985).

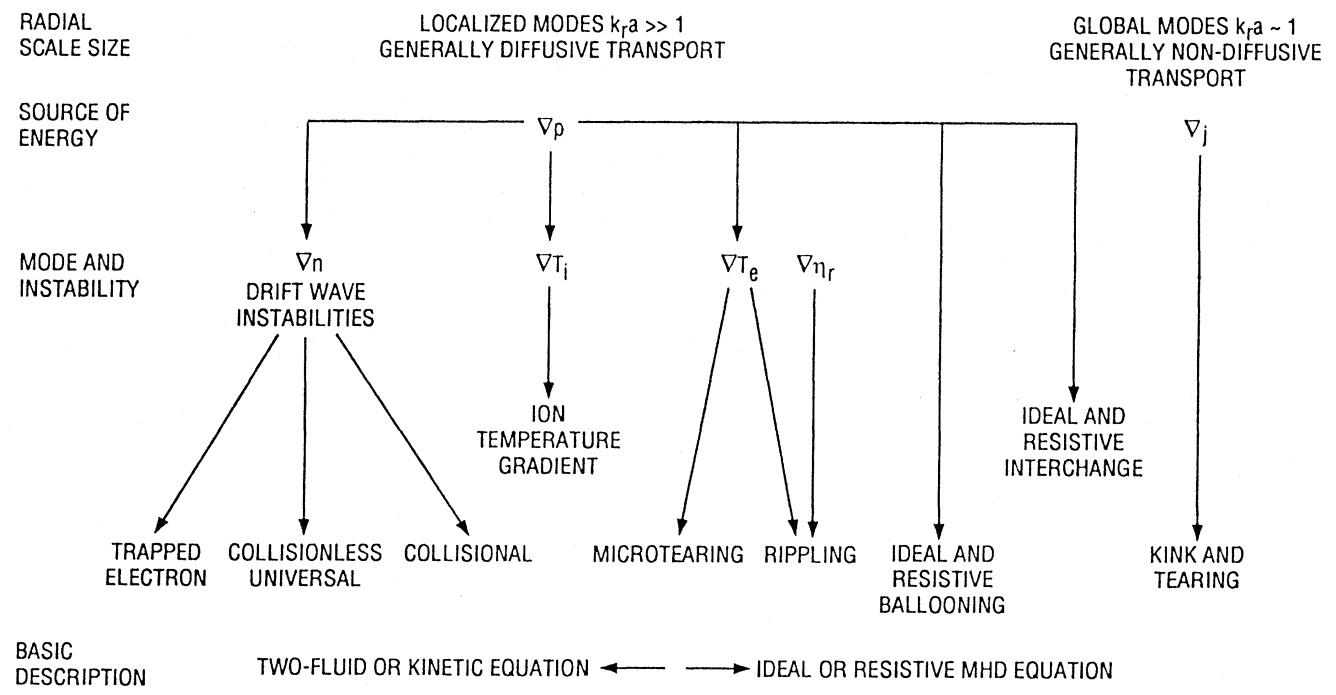

$$D_m = \int_0^\infty dz \langle b_r(0) b_r(z) \rangle = L_0 b_0^2 \ . \tag{3.28}$$

Here $b_r = \tilde{B}_r / B_0$, $b_0 = \langle |b_r(0)|^2 \rangle$, and L_0 is the parallel autocorrelation length of the radial magnetic fluctuations. In the collisionless regime, $\lambda_e \gg L_k$,

$$\chi_e^c = v_e D_m \ . \tag{3.29}$$

In the collisional regime, $\lambda_e \ll L_k$, where L_k is the characteristic length over which two neighboring field lines diverge, Rechester and Rosenbluth (1978) found

$$\chi_e^{RR} = v_e D_m \frac{\lambda_e}{L_k} \ . \tag{3.30}$$

A simple formula for the enhanced losses has been given by Callen *et al.* (1979),

$$\tau_{Ee} \rightarrow \tau_{Ee} \left[1 - 4 \sum_s \frac{r_s^3 \delta_s}{a^4} \right] , \tag{3.31}$$

where r_s and δ_s are the radial position and width of each island.

Islands may also be caused by field errors, stemming from an inadequately designed coil system, e.g., in current leads. In stellarators, it is possible to measure the islands directly using electron beams and detecting screens. An example of calculated flux surfaces for the ATF stellarator in the presence of field errors, in good agreement with experimental measurements, is shown in Fig. 30. Increased transport in the outer plasma region was observed, leading to peaked profiles, when the field errors were uncompensated.

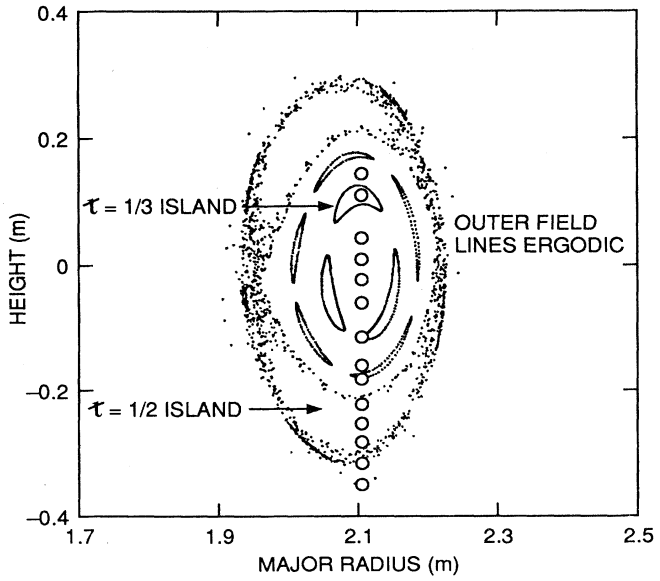

FIG. 30. Calculated flux surface islands formed when a perturbation of $\tilde{B}_z \simeq 68$ G on axis is applied [6 kA in the perturbation coil for a 1 T helical field (Colchin *et al.*, 1992)].

11. Low-frequency microscopic modes

These modes have a frequency $\omega \ll \omega_{ci}$ ($\omega_{ci} \simeq 2 \times 10^8$ rads s^{-1} in a D-T plasma at 5 T). In one type of mode, drift instabilities, plasma inhomogeneity leads to amplification of ion sound waves into two branches related to the drifts of electrons and ions, respectively. In the case of drift modes, the density gradient provides the drift that produces the wave part of the instability. However, some other phenomenon is needed to break the adiabaticity and lead to transport. For example, trapped electrons can provide this function and introduce a drive through the electron temperature gradient. These modes are electrostatic at low β, in that no involvement of the magnetic field is required. As β is raised (e.g., $\beta > 1\%$), the fluctuation of the pressure causes magnetic-field fluctuations, which can enhance transport.

For $\beta > m_e / m_i$, the shear Alfvén mode can be driven unstable, leading to microtearing, kinetic ballooning, and drift-tearing modes. These modes are intrinsically electromagnetic.

12. Electron drift-wave instability

For these modes, $k_\perp \sim \rho_s \equiv c_s / \omega_{ci}$ where the sound speed $c_s = (eT_e / m_i)^{1/2}$. The most unstable modes have $k_\parallel \ll k_\perp$. The phase velocity satisfies the relationship $v_i \ll \omega / k_\parallel \lesssim v_e$, where $\omega \simeq \omega_{*e} = k_\theta T_e / eBL_n$, where the density-gradient scale length is $L_n = -n / (dn/dr)$. The modes are electrostatic provided $\omega \ll k_\perp V_A$, where V_A is the Alfvén speed, $V_A = B / (\mu_0 n m_i)^{1/2}$. The potential fluctuation is $e\tilde{\phi} / T_e \simeq \tilde{n} / n$. There are three classes of instability, dependent on electron collisionality:

(a) Collisional or dissipative drift instabilities, $\nu_{ei}(qR/v_e) > 1$, temperature-gradient driven.

(b) Collisionless instabilities, $(r/R)^{1.5} < \nu_{ei}(qR/v_e) < 1$, curvature driven. When a polarization drift is included, the universal drift wave is obtained.

(c) Trapped-electron modes for $\nu_{*c} = (r/R)^{1.5} \nu_e (qR / v_e) < 1$.

13. Ion drift waves

These modes propagate in the ion diamagnetic direction; their phase velocity is $\omega / k_\parallel \sim v_i \ll v_e$. The ion temperature-gradient mode is unstable when $\eta_i = L_n / L_{Ti} \gtrsim 1$. This mode can also give rise to electron thermal and particle transport.

14. Trapped ion modes

These occur when both electrons and ions are trapped.

15. Electromagnetic drift-Alfvén modes

These occur when $\beta > m_e / m_i$. Their poloidal mode number is large ($m \gg 1$).

16. Rippling modes and their relatives

These are electron drift waves that are obtained when the resistivity (η_r) is large (typically at the edge). Similar modes may also be driven by impurity and ionization gradients.

17. MHD modes

There are two types of MHD mode with generally low poloidal model number and $\omega/k_\parallel \gg v_e$, which can lead to transport.

Kink modes are driven by the free energy in the poloidal magnetic field of the plasma current.

Interchange modes are driven by unfavorable curvature in the magnetic field, $\nabla B \nabla p > 0$. The modes are stabilized by favorable curvature and by magnetic shear $dq/dr \neq 0$.

D. Dimensionless plasma scaling

Because of the limited progress in relating plasma theory to experiment, it is a common practice to use empirical confinement scalings based upon the wealth of experimental confinement data. A concern with the empirical approach is the lack of a theoretical basis for the prediction; what if some new physical mechanism should intercede between the limits of present operation and the region of projected operation? While reliance on existing data can never, short of a full theoretical model, guarantee performance in a new regime (i.e., different dimensionless parameters), there is a complementary approach that can at least establish the performance of the new plasma under some conditions. This approach, described by Buckingham (1914) and Bridgeman (1937), uses dimensionless analysis to scale from one experiment to another. Its use in scaling plasma and fluid data was proposed by Bickerton and London (1958, for pinch experiments), Beiser and Raab (1962), Kadomtsev (1975), and Bickerton (1989). It has been applied in one form or another to the tokamak, stellarator, and RFP.

The set of equations that describe a physical system—in fusion, a reasonable picture is given by Maxwell's equations, the Fokker-Planck equation, and the multifluid equations (Braginskii, 1965)—may be written in terms of dimensionless parameters. A set of scaling laws may be established in which the dimensionless combinations of the physical parameters remain constant when the quantities are changed in scale. A corollary to this approach is the use of dimensionless scaling to validate empirical formulas (Connor and Taylor, 1977). An extension of the use of invariance properties to determine formulas for plasma transport was made by Connor and Taylor (1984). They determined confinement scalings for transport governed by the "reduced" resistive MHD equations for tokamaks and RFP's.

The dimensionless parameters for a fusion plasma are R/a, κ, δ, q, ν_*, ρ/a, β, A_i, $Z_{\rm eff}$, n_e/n_i, T_e/T_i, ϕ/T, V/v_{th}, v_{th}/c, N_D, and λ_n/a To make an analysis correct, the source terms for particles, momentum, and power must scale appropriately to maintain similar solutions for the governing equations (Sheffield, 1990).

The particle source term scales as $nT^{1/2}/a$. If pellet injection is used, and a divertor suppresses neutral gas fueling, λ_n/a may be neglected. The penetration distance for a pellet λ_p is given by Eq. (2.82) and the pellet speed (v_p). To keep λ_p/a constant and have the same source term requires $v_p \propto B^{1.71}$, the pellet radius $r_p \propto B^{0.233}$, and the pellet repetition rate $f_p \propto B$, when we compare to plasmas at constant ν_*, β, and ρ/a. The momentum source term $R_{\rm ext}$ scales as nT/a.

The power density source (p) scales as ηj^2 (the Ohmic power density). In order to maintain the same local values for T_e/T_i, it is necessary to maintain the same scaled power separately, for electrons and ions:

$$\frac{p_e}{\eta j^2} = \frac{[(p_{\rm ext})_e + \eta j^2 - p_{\rm rad}]}{\eta j^2} = \text{const.}\ ,$$
$$\frac{p_i}{\eta j^2} = \frac{[(p_{\rm ext})_i - p_{cx}]}{\eta j^2} = \text{const.} \tag{3.32}$$

In practice, as pointed out by Kadomtsev, not all of the dimensionless parameters need be held constant. The number of particles in a Debye sphere N_D is not important unless, for example, V/v_{th} is very large or we are concerned about the divertor sheath. The potential function ϕ/T is related to other dimensionless parameters if $\nabla \cdot \mathbf{E} = 0$ and the displacement current is negligible, i.e., phenomena such as lower hybrid or c/w_{pe} modes are unimportant. The normalized flow velocity V/v_{th}, n_e/n_i, and T_e/T_i are also invariant if the other parameters are invariant and the source terms are scaled appropriately. Relativistic effects may normally be ignored. The change in the distribution functions when alpha heating is involved may lead to differences; Bickerton (1989) showed that to achieve similarity among a family of burning plasma devices we should adjust the isotopic mix. Assuming that alpha power may be treated like another power source, the key dimensionless parameters for fixed R/a, κ, δ, q, A_i, and $Z_{\rm eff}$ are

$$\text{the collisionality } \nu \propto \frac{qRn}{T^2}\ ,$$
$$\text{the normalized gyroradius } \frac{\rho}{a} \propto \frac{A_i^{1/2} T^{1/2}}{aB}\ ,$$
$$\text{the beta } \beta \propto \frac{nT}{B^2}\ , \tag{3.33}$$

and the normalized power density $\frac{p}{\eta j^2} \propto \frac{T^{3/2}P}{B^2R}$.

Combining these parameters, we find in comparing two devices that similar conditions will hold if

$$\frac{a_2}{a_1}=\left[\frac{B_1}{B_2}\right]^{0.8}, \quad \frac{T_2}{T_1}=\left[\frac{B_2}{B_1}\right]^{0.4}, \quad \frac{n_e}{n_1}=\left[\frac{B_2}{B_1}\right]^{1.6}, \quad \frac{P_2}{P_1}=\left[\frac{B_2}{B_1}\right]^{0.6},$$
$$\frac{\tau_2}{\tau_1}=\frac{B_1}{B_2}, \quad \frac{(nT\tau)_2}{(nT\tau)_1}=\frac{B_2}{B_1}, \quad \frac{I_2}{I_1}=\left[\frac{B_2}{B_1}\right]^{0.2}, \quad \frac{N_{D2}}{N_{D1}}=\left[\frac{B_1}{B_2}\right]^{0.2}. \tag{3.34}$$

The thermal diffusivity may be written in the general form $\chi \sim D_B(\rho/a)^{\alpha}$. $F(\nu,\beta,R/a,q,\ldots)$, where $D_B \sim T/B$ is the Bohm diffusion coefficient, which is characteristic of processes having large scale lengths. For $\alpha=0$, the losses have a Bohm-like scaling. For $\alpha=1$, the characteristic scale of the loss processes is a gyroradius, and the losses have a so-called gyro-Bohm scaling.

IV. TOKAMAK REACTORS

A. Introduction

Numerous design studies have been made of tokamak reactors, including those of Badger *et al.* (1979), Baker *et al.* (1980), Hancox *et al.* (1981), Cooke *et al.* (1989), Najmabadi *et al.* (1991), and Seki *et al.* (1991). The parameters are listed in Table X. These studies and those of other configurations have been useful in refining our understanding of what is needed to make an "attractive reactor." Based on present achievements, with a margin allowed to ensure divertor and wall survival for a reasonable time, an economical reactor will be at least 1 GW(e) in output and more likely ~2 GW(e) (Rebut *et al.*, 1990). This large size may be the best route, not just for tokamaks, because of the potential need to operate at moderate power density ($\lesssim 4$ MW m^{-2} neutron flux) in order not to overstress the system. The alternative route—higher power density, smaller size, $\lesssim 1$ GW(e)—requires either very high coil fields (15–20 T) or much better physics performance, that is, higher $(\langle\beta\rangle)/\chi_E$ coupled with optimum divertor conditions and low recirculating power.

ITER is planned to provide a demonstration of a controlled, burning D-T plasma for times of 1000 s or more, at a reactor level of fusion power (~1500 MW) (Rebut, 1993). ITER will also demonstrate and integrate fusion reactor technologies. Reference parameters are given in Table X. The Tokamak Physics Experiment (TPX; Schmidt *et al.*, 1993; and Thomassen *et al.*, 1993) is being designed in the U.S. program to help optimize a tokamak reactor by studying steady-state, advanced (improved-transport, higher-beta, lower-recirculating-power) modes of operation. TPX parameters are given in Table XI.

TABLE X. Parameters of recent tokamak reactor designs.

Reactor reference	Reactor 1 Cooke *et al.*, 1989	ARIES 1 Najmabadi *et al.*, 1991	SSTR Seki *et al.*, 1991	ARIES II Najmabadi *et al.*, 1992
Major radius R (m)	7.07	6.52	7.00	5.5
Aspect ratio R/a	3.49	4.5	4.0	4.0
Ellipticity κ	2.0	1.6	1.8	1.4
Current I (MA)	22.4	12.0	12.0	5.5
Field B_ϕ (T)	6.44	13.0	9.0	7.5
Field on coil B_m (T)	13.5	21.0	16.5	$\lesssim 16$
Confinement factor C_H	$\lesssim 2$	$\lesssim 2$	~2	~3
Troyon factor g(% Tm/MA)	3.0	3.2	3.0	6.7
Current drive	Neutral beam	Fast wave	Neutral beam	ICRF
Bootstrap fraction	0.3	0.53	0.75	0.95
Burn time (s)	10^6	∞	∞	∞
$\bar{p}_{wn}$ (MW m^{-3})	3.1	2.8	5.0 (peak)	3.5
Divertor	Double null	Double null	Single null	Single null
Total thermal power MW (th)	4920	~2800	3710	
Net electric power MW (e)	1200	1000	1080	1000

TABLE XI. Representative modern tokamak parameters.

Tokamak	DIII-D	TFTR	JET	Tore Supra	Asdex U	T-15	JT-60U	Triam U	TPX
Major radius R (m)	1.65	2.45	3.10	2.25	1.65	2.43	3.40	0.80	2.25
Aspect ratio R/a	2.75	2.90	2.82	3.75	3.3	3.5	4.0	5.0	4.5
Ellipticity κ	~2.0	1.0	1.8	1.0	1.6	1.0	1.6	1.5	2.0
Current I (MA)	2.0	3.0	6.0	2.0	2.0	1.4(2.0)	6.0	0.1→0.5	2.0
Field B_ϕ (T)	2.0	5.2	3.4	4.5	4.0	3.5(5.0)	4.2	8.0	4.0
Pulse length (s)	10+	2	20+	≲600	10+	1.5+	20+	∞	100→∞
Divertor	Yes	No	Yes	No	Yes	No	Yes	Yes	Yes
Coil type[a]	Cu	Cu	Cu	S/C	Cu	S/C	Cu	S/C	S/C

[a]Cu=copper; S/C=superconducting.

B. Tokamak characteristics

There are numerous reviews of tokamak research, for example, those of Artsimovich (1972), Furth (1975), Rawls *et al.* (1979), Sheffield (1981), Kadomtsev *et al.* (1990), and Post *et al.* (1991). The parameters of some representative modern tokamaks are listed in Table XI. Success in the tokamak area is well illustrated by the plot of progress in achieving good confinement $N_i\tau_E T_i$ vs T_i in Fig. 31. The drawing of the ARIES-1 tokamak reactor in Fig. 32 illustrates the basic features of a modern tokamak. The plasma is produced in a toroidal vacuum chamber (torus) of elliptical cross section, which, in a reactor, will be made of a low-activation material.

While tests are being made of a pumped limiter, recent engineering test reactors and reactor design use a poloidal divertor to remove helium ash and limit wall-generated impurities from entering the plasma (see Sec. II.G). The torus walls, blanket, and shield must have sufficient electrical resistance to avoid drawing large currents during plasma current initiation, but must also act as a metal shell to provide image currents, which will stabilize some MHD modes.

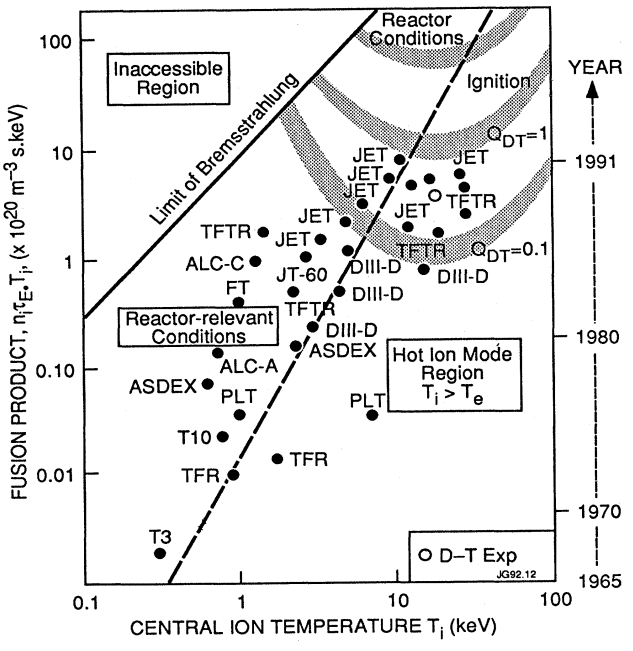

FIG. 31. Performance of tokamaks, JET Team, 1992.

1. Coils

To date, most tokamaks have used water-cooled or liquid-nitrogen-cooled copper coils, though a few superconducting coil tokamaks are operating, namely, Tore Supra, T-15, and TRIAM (Komarek *et al.*, 1990). According to present knowledge of the physics capabilities, superconducting coils seem to be essential for tokamak reactors with $R/a \gtrsim 3$, to provide an acceptably low recirculating power. As a consequence, the blanket shield thickness on the inner bore of the plasma must be $\Delta \sim 1-1.5$ m thick to limit radiation damage to the coil insulation and conductor and overheating of the coils. Since the dominant field in a tokamak is provided by the toroidal field, this sets a limit on the field ratio, Eq. (2.40),

$$f_B = \left[1 - \left[\frac{a_w}{a} + \frac{\Delta}{a}\right]\frac{a}{R}\right] .$$

For example, let $(a_w/a)=1.1$, P_F+3500 MW, $\bar{p}_{wm}=4$ MW m^{-2}, $b/a=2$; then $a=3.38\ (R/a)^{-0.5}$ m, and we find for $\Delta=1.5$ m:

$$R/a \quad 2.5,\ 3,\ 3.5,\ 4,\ 4.5,\ 5 ,$$

$$f_B \quad 0.28,\ 0.38,\ 0.45,\ 0.50,\ 0.55,\ 0.58 .$$

The decrease in useful field affects the gains in beta of going to a lower aspect ratio, and drives tokamak reactor designers to higher aspect ratios than those used in most experiments, which do not need a shield.

An alternative solution (Peng and Hicks, 1990) is to dispense with the blanket and shield in the torus bore, and use a solid copper central toroidal conductor and an aspect ratio $R/a \lesssim 1.5$. This approach has the potential to achieve a high-mass power density, but at the expense of a higher recirculating power and regular replacement

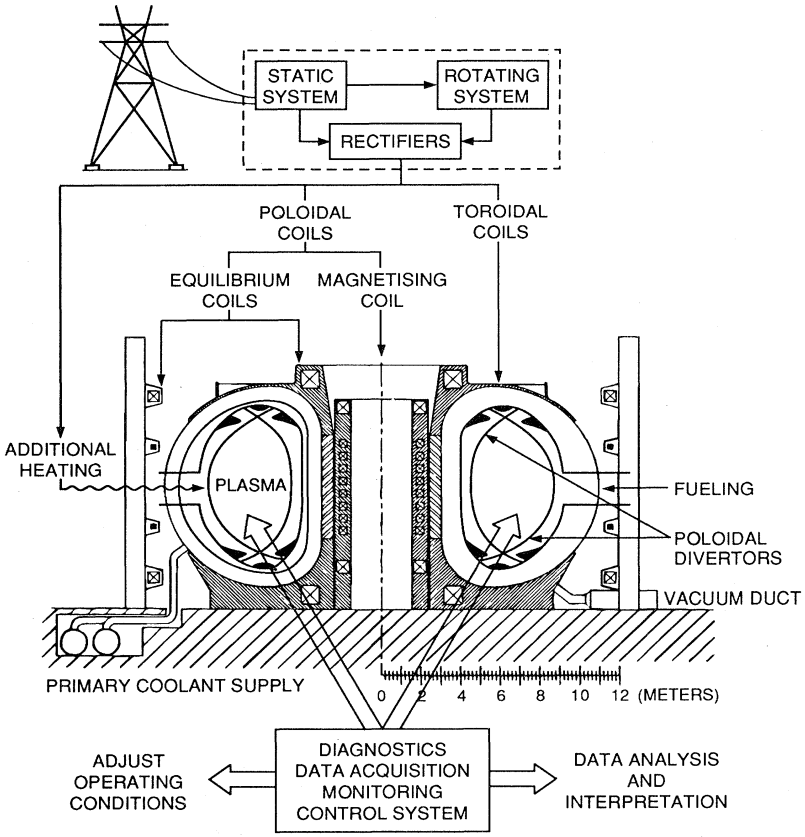

FIG. 32. Drawing of representative tokamak showing the principal features.

of the central coil limb.

The magnetic field has, in essence, three components: a strong toroidal field, poloidal fields produced by the plasma current, and a set of poloidal coils.

The poloidal coils perform four functions: (1) a solenoid on the inner bore of the plasma produces the plasma current by transformer action; (2) a second set of coils provides a (mainly) vertical field B_v, which provides some volt-seconds for driving the plasma current, interacts with the plasma current, and balances the outward expansion of the plasma and plasma current (see Sec. III.B). In addition (3) the coils shape the plasma and provide stability against a bulk vertical shift of the plasma by curving the field lines. They may also be used (4) to produce a field opposing the poloidal field of the plasma current, forming a separatrix and diverting flux to a divertor region. In practice, in optimized designs, the smallest number of coils is used to provide all of the above functions in a time-dependent way, by careful programming of the current in each coil.

The fields of the plasma current and coil set produce a set of nested flux surfaces. As the plasma pressure is raised, the poloidal beta [(β_θ), Eq. (3.12)] increases and the plasma attempts to shift outward in major radius. An increase of the vertical field is used to hold the position of the outer flux surface, but the center of the plasma moves out, as shown in Fig. 26. In computer models of the plasma it is common practice to work in flux coordinates in order to accommodate the effects of the changing flux geometry.

An approximate formula for β_θ is

$$\beta_\theta \simeq \frac{0.375a^2[1+\kappa^2(1+2\delta^2-1.2\delta^3)]\langle n_{20}(T_{ek}+T_{ik})\rangle}{[I(\mathrm{MA})]^2}, \tag{4.1}$$

where $\kappa = b/a$ is the plasma ellipticity and δ is a measure of the triangularity of the plasma flux surfaces.

With allowance for plasma shaping and toroidal effects, the safety factor at the 95% flux surface is

$$q_{\psi 95} = \frac{2.5a^2B[1+\kappa^2(1+2\delta^2-1.2\delta^3)](1.17-0.65\epsilon)}{IR(1-\epsilon^2)^2}, \tag{4.2}$$

where $\epsilon = a/R$, a, R, (m), B (T), and I (MA).

For a system with a poloidal divertor, $q_{\psi a} \to \infty$, and to define plasma characteristics it is normal practice to use q_{95}, the safety factor at the flux surface, which includes 95% of the toroidal flux in the plasma.

2. Startup

The first step is to evacuate the torus to $\sim 10^{-7}$ torr. To ensure a low residual impurity gas level, the wall ma-

terials will be run at elevated temperatures, e.g., 300–500 °C. The torus is then prefilled to $\sim 10^{-4}$ torr with D-T fuel, which will lead to an initial density of $\lesssim 10^{19}$ m^{-3} of D-T plasma. The toroidal field is already established. A voltage (U_l) is then induced around the torus by transformer action, leading to breakdown. Preionization by electron cyclotron heating, and auxiliary heating in general, may be used to lower the loop voltage and reduce the usage of transfer volt-seconds in raising the plasma current (Gilgenbach *et al.*, 1980; Lloyd, 1991). The breakdown voltage depends on the electron loss channels, toroidal drift, transverse diffusion, recombination and attachment, and poloidal stray magnetic fields ($B_\perp$). If the stray magnetic field dominates ($B_\perp > 10^{-4} B_\phi$), the requirement on loop voltage is

$$U_l \gtrsim 1.3\times 10^4 2\pi R p / \ln\left[530 p a \frac{B_\phi}{B_\perp}\right] \text{ (V)} , \tag{4.3}$$

where p is measured in torr, and R and a are measured in meters. With electron cyclotron heating assistance, a toroidal electric field $E_\phi \simeq 0.3$ V/m is sufficient to initiate breakdown and start the plasma current.

Care must be exercised during current ramp-up to allow current penetration into the conducting plasma; otherwise a hollow current profile may develop, which is unstable to the double tearing-mode instability (Furth, Rutherford, and Selberg, 1973). In a reactor the main concerns are waste of volt-seconds (for a pulsed reactor), wall bombardment during instability, leading to damage and impurity generation, and the need to establish a route to the desired current profile to support an optimized plasma.

3. Plasma duration

If transformer volt-seconds were the only source of current drive, the pulse length of the tokamak would be limited. Denoting by t_R the time to raise the current, and by t_F the maximum duration of the plasma at peak current, we find that the flux (volt-seconds) required to support the current is given by

$$\int_0^{t_R+t_F} U_l dt = \phi_m = L_p I + \int_0^{t_r} R_p I dt + R_p I t_F \text{ (V s)} , \tag{4.4}$$

where $L_p \simeq \mu_0 R[\ln(\bar{a}_c/\bar{a}) + 0.25]$ (H) is the plasma inductance and R_p (Ω) its resistance, while $\bar{a}_c$ and $\bar{a}$ are the average radii of the poloidal coils and plasma, respectively. In tokamaks with unassisted startup, the second term is typically $\sim 0.5\, L_p I$, which is the flux used up in overcoming losses during startup. In assisted startup, some of this flux may be saved (Lloyd, 1991).

The available flux (volt-seconds) is typically 1.3 times that given by the central solenoid ($\phi_{cs} = \pi R_{cs}^2 \Delta B_{cs}$), where R_{cs} is the radius of the solenoid and ΔB_{cs} (T) is the full swing in the solenoid. The extra 30% comes from other poloidal coils, whose flux links the plasma.

The plasma resistivity is a result of collisions between the electrons and ions in the plasma. The resistivity parallel to the magnetic field is given by Book (1990, p. 37) as

$$\eta_\parallel = \frac{5.2\times 10^{-5} \gamma_R Z_{\text{eff}} \ln\Lambda_e}{T_e^{3/2}} \text{ ohm m} , \tag{4.5}$$

where $\gamma_R = (1 - 1.95\sqrt{r/R} + 0.95 r/R)^{-1}$ is an increase in resistivity owing to the effects of electrons trapped by the increasing field on the inner side of the torus. Λ_e is given by Eq. (2.13) and Z_{eff} by Eq. (2.9). We can calculate the plasma resistance for a given electron temperature profile. Assuming constant Z_{eff} and $\ln\Lambda_e$ and an average $\bar{\gamma}_R$ [(say, at $r = a/2$); for $R/a \sim 2.5$–4 an empirical fit is $\bar{\gamma}_R \simeq 4.3 - 0.6 R/a$ (Uckan *et al.*, 1988)], we find

$$R_p \simeq \frac{2.6\times 10^{-4} R \bar{\gamma}_R \overline{Z_{\text{eff}}}\, \overline{\ln\Lambda_e}}{a^2 \kappa T_{e0}^{3/2}} \text{ (Ohms)} \tag{4.6}$$

for a parabolic temperature profile and a noncircular plasma, $\kappa = b/a$. Combining Eqs. (4.6) and (2.8) yields the maximum flat-top current duration,

$$t_F \lesssim \frac{[1.3\phi_{cs} - (\sim 1.5 L_p I)] a^2 \kappa T_{e0}^{3/2}}{2.6\times 10^{-4} R \bar{\gamma}_R \overline{Z_{\text{eff}}}\, \overline{\ln\Lambda_e} I} \text{ (s)} . \tag{4.7}$$

For present-day experiments this time is relatively short ($\lesssim 60$ s). However, for a large reactor operating at high temperature, e.g., $T_{e0} = 20$ keV, it can be ~ 1 hour. Consider the following case: $R = 8$ m, $a = 2.0$ m, $\kappa = 2$ m, $R_{cs} \simeq 3.4$ m, $\bar{\gamma}_R = 1.9$, $\overline{Z}_{\text{eff}} = 1.8$ m, $\ln\overline{\Lambda}_e \simeq 17$, $I = 17$ MA ($q_{95} = 3.3$) $\bar{a}_c/\bar{a} \simeq 3$, $B_0 = 6.5$ T, $B_{cs} = 20$ T, $1.3\phi_{cs} \simeq 950$ V s., $1.5 L_p I \simeq 350$, we find $t_F \simeq 6\,600$ (s).

Optimization to a higher aspect ratio would allow even more room for the solenoid. Pulsed operation is not desirable, because of thermal stresses caused by the cycling and the need for heat reservoirs to maintain the blanket and wall temperature, as well as electricity output. Nevertheless, it is a tradeoff issue to be balanced against the cost and complexity of providing steady-state operation with noninductive current drive. One natural feature of the tokamak can help to alleviate this problem—the bootstrap current.

4. Bootstrap current

This current appears in the neoclassical theory of transport through the equation for conservation of momentum (Galeev and Sagdeev, 1968; Bickerton *et al.*, 1971; Galeev, 1971). It is driven by the radial pressure gradient and depends on details of the particle orbits, notably the fraction of trapped particles [$f_t \propto (R/R)^{0.5}$]. A "seed" current must still be driven on axis where there is no pressure gradient. A theory applicable for all collisionality regimes has been given by Hirshman and Sigmar (1981), showing the detailed dependence of the

current on the temperature and density gradients. The existence of the current has been inferred in tokamaks by analysis of contributions to the loop voltage at high poloidal beta (Zarnstorff *et al.*, 1988; Challis *et al.*, 1989; Kikuchi *et al.*, 1990; Navratil *et al.*, 1991), but for times less than a skin time. Studies for ITER (Fujisawa, 1990a, 1990b) show that the bootstrap current depends on the current profile, owing to changes in the areas of the various flux surfaces. A simple empirical formula valid for $1.0 < q_\psi(95)/q_\psi(0) < 5.0$, which may be used to give a rough global estimate of the fraction of bootstrap current, is

$$\frac{I_{\rm bs}}{I} \simeq C_{\rm bs}\left[\left[\frac{a}{R}\right]^{0.5}\beta_\theta\right]^{1.3} \tag{4.8}$$

where

$$C_{\rm bs} = 1.32 - 0.235\left[\frac{q_\psi(95)}{q_\psi(0)}\right] + 0.0185\left[\frac{q_\psi(95)}{q_\psi(0)}\right]^2,$$

and β_θ may be represented by Eq. (4.1).

For cases with high bootstrap current, where the detailed distribution of current can affect MHD stability, it is necessary to use the complete description given by Hirshman and Sigmar (1981) to properly account for the effects of the temperature and density gradients.

The recent results from TFTR (Navratil *et al.*, 1991) support the idea that a valuable mode of operation for a reactor might be at relatively high $q_\psi(95)$, e.g., q in the range of 5–10, i.e., lower current than normal, to obtain high β_θ. In addition this would facilitate operating with $q_\psi(0) \gtrsim 2$ (Ramos, 1991), which has been predicted to allow access to a second region of stability and higher beta (Coppi *et al.*, 1979; Mercier, 1979). Recent results from D-III D, which show relatively improved transport as q_ψ is raised (Jackson *et al.*, 1991) are encouraging for this mode of operation. The question is what self-consistent optimized level of beta, transport, and bootstrap current can be achieved (without impurity problems). Examples of model profiles for pressure and current, which lead to very high bootstrap current (>90%) in the second stable region, have been developed by Ramos (1991), but without a self-consistent transport model. An example of the required profiles is given in Fig. 33. Note the zero bootstrap current on axis ($r/R \to 0$), which means that some sort of noninductive current drive will be required to complete and control a desirable profile. In Fig. 34, values of $\epsilon\beta_\theta$ are given for stable operation as a function of q (0). Advanced modes of operation, such as those described above, are being studied in present-day, moderate-pulse-length tokamaks and will be tested in steady-state operation in TPX (Schmidt *et al.*, 1993; Thomassen *et al.*, 1993).

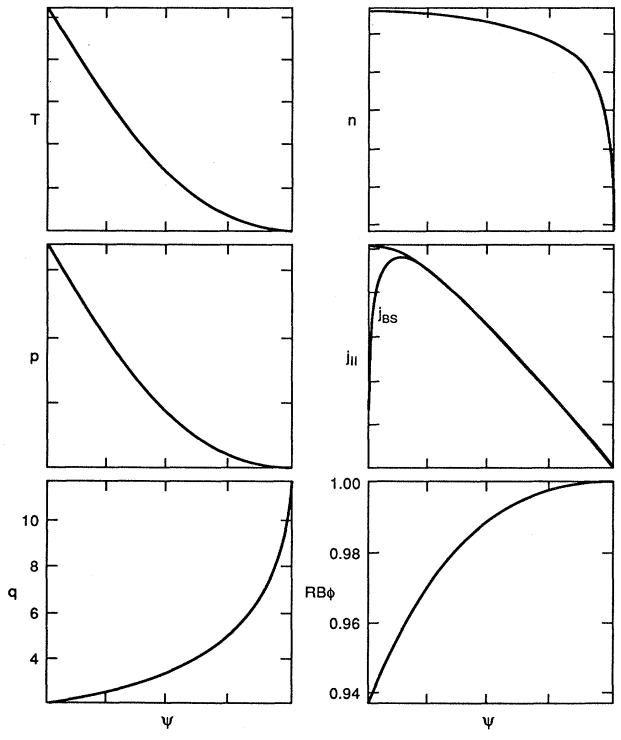

FIG. 33. Reference plasma parameter profiles, in flux coordinates, for high-bootstrap-current operation (Ramos, 1991).

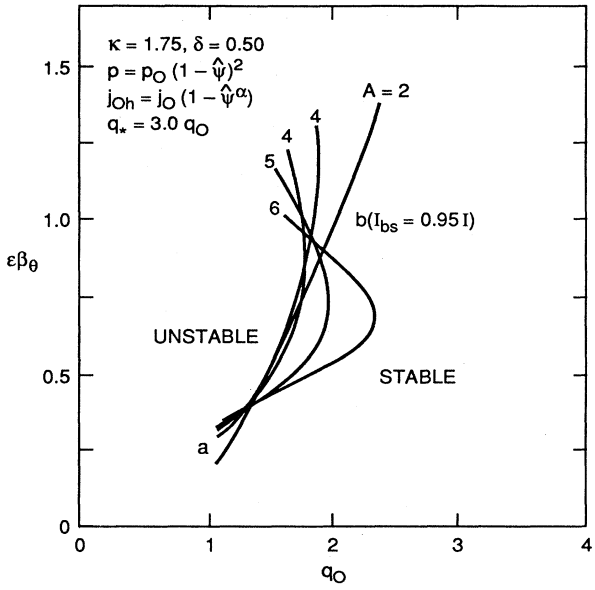

FIG. 34. Values of $\epsilon\beta_p$ and q_0 required for stable operation at high bootstrap current, for representative aspect ratio (Ramos, 1991).

C. Noninductive current drive

Numerous techniques have been proposed and tested for driving a plasma current noninductively; for recent reviews see Uckan (1985), Fisch (1987), Post *et al.* (1991), and Moreau *et al.* (1991). These techniques rely on

transferring axial momentum to one of the charge species in the plasma in a way that leads to a net drift asymmetry in the parallel velocity distribution function, without producing a compensating effect on the other charge species. A current-drive figure of merit is commonly used to characterize the various techniques,

$$\gamma_{\rm CD}(10^{20}\ {\rm A/m^2\,W}) = n_{e20} I_{\rm CD} R / P_{\rm CD} \ . \tag{4.9}$$

In *neutral-beam drive,* the ions formed when a neutral beam is ionized by the plasma constitute a current. In a uniform, pure hydrogen plasma, this current is exactly compensated by an electron shielding current, created as electrons gain momentum from the beam ions and themselves slow down on the background plasma. In a tokamak, the presence of trapped electrons and impurities affects the momentum transfer, and complete compensation no longer occurs (Ohkawa, 1970; Cordey, Jones *et al.*, 1979; Hirshman, 1980):

$$J_{\rm CD} = J_b \left\{ 1 - \frac{Z_b}{Z_{\rm eff}} [1 - G(Z_{\rm eff}, \epsilon)] \right\} \ ({\rm A\,m^{-2}}) \tag{4.10}$$

where the subscript b refers to beam ions, and $\epsilon = r/R$.

A model for neutral-beam current drive incorporating approximate corrections $\sim(r/R)$ to the trapped-electron contribution has been developed by Mikkelsen and Singer (1983) for a tokamak plasma, taking into account profile effects:

$$\begin{aligned} I_{\rm CD} = I_b \Big\{ & 1 - \frac{Z_b}{Z_{\rm eff}} [1 - (1.55 + 0.85/Z_{\rm eff}) \bar{\epsilon}^{1/2} \\ & + (0.22 + 1.55 Z_{\rm eff}) \bar{\epsilon}] \Big\} (A) \\ \equiv & I_b Z_b F(Z_{\rm eff}, Z_b, \bar{\epsilon}) \ , \end{aligned} \tag{4.11}$$

which is a reasonable approximation in the banana regime of collisionality for $\bar{\epsilon} \le 0.2$ and $1.0 < Z_{\rm eff} < 3.0$.

For deuteron beam energies ~ 1 MeV, the efficiency for neutral-beam drive is given approximately by

$$\begin{aligned} \gamma_{\rm ND} \approx & (5 A_{bd} T_{10})(1 - f_{\rm sb}) \left[\frac{R_{\rm tang}}{R} \right] \\ & \times [5 J(x,y)] F(Z_{\rm eff}, Z_b \cdot \bar{\epsilon}) \ , \end{aligned} \tag{4.12}$$

where the following notations are used:

$\bar{\epsilon} \approx a/2R_0$.

$J(x,y) \simeq x^2/[4 + 3y + x^2(x + 1.39 + 0.61 y^{0.7})]$; $x = (E_b/B_{bd}E_c)^{0.5}$, $y = Z_2/3$, and E_c is given by Eq. (2.20).

$R_{\rm tang}/R_0$ is the pitch angle (cosine of the angle of the beam ions to the B field).

$f_{\rm sb} \simeq \exp\{-(\bar{n}_{20} d_b)[0.775/E_b\ ({\rm MeV})]^{0.78}\}$ is the fraction of the beam that penetrates the plasma and reaches the far wall, for deuteron beams at energies ~ 1 MeV.

$Z_2 = [\sum_j (\ln\Lambda_j n_j z_j^2/A_b]/[\sum_j \Lambda_j n_j Z_j^2/A_j] \simeq 12 Z_{\rm eff}/5A_b$ when $n_{\rm DT}/n_e \ge 0.9$.

$A_{bd} \simeq 0.08$ and $B_{bd} \simeq 1.0$ are fitting factors.

$d_b \simeq 2R_0[(1 + a/R_0)^2 - (R_{\rm tang}/R_0)^2]^{0.5}$ is the distance along the beam path in the plasma. $\bar{n}_{20}$ is the line average density,

$$\ln\Lambda_j \simeq 23.7 + \ln\left\{ \left[\frac{A_j}{(A_j + A_b)} \right] \left[A_b E_b \left[\frac{T_{10}}{n_{20}} \right] \right]^{0.5} \right\} .$$

To obtain adequate penetration for reactor plasmas, i.e., to provide current drive on axis, requires MeV-level neutral beams. In ITER, $a = 2$ m, $\bar{n} \sim 10^{20}$ m^{-3}, 1.3-MeV deuterium beams are optimum to provide an on-axis current drive, but have only a small percentage of shine-through on the far wall, $f_{\rm sb} \le 0.05$.

Radio-frequency (rf) power may be injected so as to transfer axial momentum to one of the charge species. One scheme, that of Fisch (1980), relies on the Landau damping of high-phase-velocity waves launched in one direction parallel to the magnetic field. There are three main approaches to current drive:

(i) High-speed waves with phase velocities that are several times the electron thermal speed.

(ii) Low-speed waves with subthermal phase speeds, which have the most momentum per unit energy—for example, the fast wave [i.e., compressional Alfvén wave (CAW)] at low frequencies and the magnetosonic wave above the ion cyclotron frequency.

(iii) Selective heating, which creates an anisotropic particle distribution and indirectly drives current. Examples are ion and electron cyclotron heating.

A normalized efficiency factor $\hat{J}/\hat{p}$ may be used to compare current-drive schemes, as shown in Fig. 35 (Uckan, 1985),

$$\mathbf{J} = ne\mathbf{V}_{\rm rel}\ ({\rm A\,m^{-2}}) \ , \tag{4.13}$$

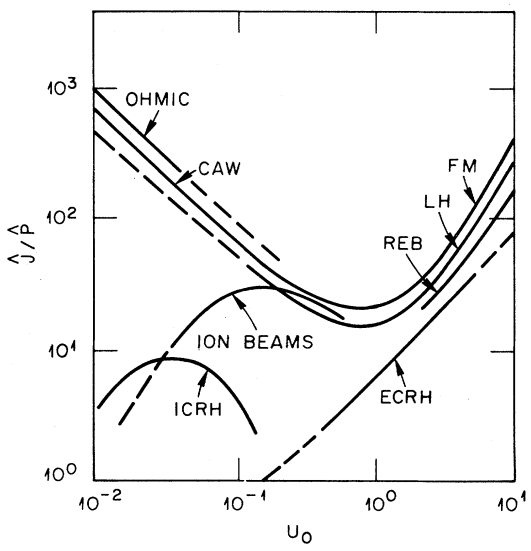

FIG. 35. Normalized current-drive efficiency factor vs $U_0 = (\omega - l\omega_c)/k_\parallel v_e$ with ω_c, the cyclotron frequency for waves, and $U_0 = V_b/v_e$, for particle injection at V_b (Uckan, 1985).

where $\mathbf{V}_{\rm rel}$ is the relative velocity of the ion and electron species.

The power to maintain the current is

$$P = mn\nu \mathbf{V}_{\rm rel}^2 \ (\mathrm{W\,m^{-3}}) \ .$$

The normalized values are

$$\hat{J} = \frac{|\mathbf{J}|}{nev_e}, \quad \hat{P} = \frac{P}{m_e n v_e^2 \nu_0} \ , \qquad \frac{\hat{J}}{\hat{P}} = \frac{m_e \nu_0}{m\nu} \frac{1}{U_0} \ , \tag{4.14}$$

where v_e is the electron thermal speed, $\nu_0 = ne^4 \ln\Lambda_e / (2\pi\epsilon_0^2 m_e^2 v_e^3)$, ν is the collision frequency, $U_0 = \mathbf{V}_{\rm rel}/v_e$ and ν_0/ν is a function of U_0. Various rf heating schemes are discussed in Sec. II.G.

For *lower hybrid current drive* the figure of merit is given by Ehst and Karney (1990),

$$\gamma_{\rm LH} \equiv \gamma_0 F(x, Z_{\rm eff}) G(\epsilon, x) \ , \tag{4.15}$$

where γ_0 is the "Fisch-Boozer" efficiency, $F \simeq 1.5-1.9$ is a temperature correction term, and $G \sim 0.7$ is a correction to allow for trapped electrons:

$$\gamma_0 = \left[\left[\frac{2m_e \epsilon_0^2 c^2}{e^3 \ln\Lambda_e} \right] \right] \left[\frac{1}{\langle N_\parallel \rangle^2} \right] \left[\frac{4}{(5+Z_{\rm eff})} \right] \ ,$$

$$\frac{1}{\langle N_\parallel \rangle^2} = \left[\frac{1}{N_{\parallel \rm min}^2} - \frac{1}{N_{\parallel \rm max}^2} \right] \Big/ \ln \left[\frac{N_{\parallel \rm max}^2}{N_{\parallel \rm min}^2} \right] \ ,$$

where $N_{\parallel \rm min}$ and $N_{\parallel \rm max}$ are minimum- and maximum-wave parallel refractive indices in the local lower-hybrid-wave spectrum. The minimum value is set by the accessibility limit,

$$N_{\parallel, \rm acc} = \frac{w_{pe}}{w_{ce}} + \left[1 + \frac{w_{pe}^2}{w_{ce}^2} - \sum_j \frac{w_{pi}^2}{w^2} \right]^{0.4} \ ,$$

a function mainly of n/B^2. The maximum penetration value is set by Landau damping, which limits penetration,

$$N_{\parallel, \rm max}^2 T_{e, \rm max} = \text{constant}$$

(for ITER conditions 60–90 keV). The two restrictions lead in effect to be a beta limit for lower hybrid penetration. To obtain maximum penetration requires a narrow spectrum, e.g., $\Delta N_\parallel / N_{\parallel, \rm min} \lesssim 0.1$. Assuming a reactor has conditions similar to or more restrictive than ITER, this limits lower-hybrid-wave current drive to low-density startup and in the full-density plasma to heating and current drive in the outer part of the plasma, $r/a \gtrsim 0.6$.

Ion cyclotron waves can drive current by damping fast waves on either electrons or ions and at a variety of temperatures, at low frequency (below the tritium ion cyclotron resonance), between the second harmonics of tritium and deuterium, and above the third deuterium harmonic. The optimum scenario is calculated to be low-frequency fast-wave current drive on the electrons. It has the advantage of higher efficiency and avoids ion cyclotron resonances within the plasma. It concentrates current drive near the plasma center, neatly complementing the bootstrap current. Optimized computer figures of merit have

$$\gamma_{\rm FWCD} \simeq 0.5 \left[\left[\frac{\langle Te \rangle}{10 \ \mathrm{keV}} \right] \Big/ (2+Z_{\rm eff}) \right] \left[10^{20} \frac{A}{\mathrm{m^2\,W}} \right] \ , \tag{4.16}$$

depending on the sophistication of the calculation, with a multiplier $\gtrsim 0.5$ or the ITER conceptual design (Batchelor *et al.*, 1990). Further refinements are needed to include, more fully, toroidal effects and relativistic effects, which can limit efficiency.

Electron cyclotron current drive is mainly considered for plasma initiation and for detailed profile control to stabilize MHD modes. The drive relies on creating an asymmetric plasma resistivity by preferentially heating the electrons that are moving in one direction along the magnetic field so that they collide with the ions less than those moving the other way (Fisch and Boozer, 1980; Cohen, 1987). The efficiency may be comparable with that of other techniques (see Fig. 35), but the generally higher cost of electron cyclotron systems compared to radio-frequency systems has restricted their consideration to that of meeting high leverage needs such as detailed profile control.

Oscillating-field current drive involves applying audio-frequency oscillating voltages to the toroidal and poloidal circuits in the appropriate phase ($\delta = \pi/2$) to drive a dc toroidal current in the plasma (Bevir and Gray, 1980). This technique has been considered primarily in relation to RFPs and is discussed in Sec. VI.E.

D. Tokamak transport

An excellent review of tokamak and stellarator transport has been given by Wagner and Stroh (1993). The neoclassical theory of tokamak transport is mentioned in Sec. III.C. A complete calculation of the neoclassical transport coefficients given by Hinton and Hazeltine (1976) has been updated by Hirshman and Sigmar (1981) and Change and Hinton (1982,1986) with regard to impurity and aspect-ratio effects:

$$\chi_{iNc} = k_2 \left[\frac{R}{r} \right]^{3/2} q^2 \rho_s^2 \nu_{ei} \left[\frac{2T_e m_e}{T_i m_i} \right]^{0.5} \ (\mathrm{m^2\,s^{-1}}) \ , \tag{4.17}$$

where $\rho_s = 1.02 \times 10^{-4} \ (T_e A_i)^{0.5}/B$ (m), ν_{ei} is given by Eq. (2.13), A_i is the atomic mass, and

$$k_2=\{[0.66(1+2.54\alpha_{nc})+(1.88\epsilon^{1/2}-1.54\epsilon)(1+2.29\alpha_{nc})]/[1+1.03\mu_i^{*1/2}+0.31\mu_i^*)]\}\frac{\alpha_{nc}}{Z_{\rm eff}}$$
$$+\{1.17[1+4.38\alpha_{nc}(1+0.3\alpha_{nc})/(1+1.17\alpha_{nc})]\mu_i^*\epsilon^3/[1+0.74\mu_i^*\epsilon^{3/2}]\}\frac{\alpha_{nc}}{Z_{\rm eff}} .$$

Here $\epsilon=r/R$, $\alpha_{nc}=n_i/n_e$, and

$$\mu_i^*=[1+2.54\alpha_{nc}]\nu_{ei}qR(T_e/T_i)^2/(\sqrt{2}\epsilon^{3/2}v_e) .$$

The second term in k_2 is the Pfirsch-Schlüter contribution. For reactor conditions, the first term dominates except, possibly, in the scrape-off layer ($T_e\sim 0.1$ keV). Theoretically, the neoclassical electron losses are much less [$(m_e/m_i)^{1/2}$ less]. As pointed out in Sec. III.C, neoclassical ion losses are usually small, but they should not be neglected at large (R/a), large $\langle\beta\rangle$, and low temperature; see Eq. (3.20).

If neoclassical losses represented the only mechanism, then, provided impurity levels were low, it would be straightforward to provide tokamak reactor-grade plasmas at modest fusion power levels, i.e., a few hundred megawatts. Unfortunately, transport is much higher, owing to instabilities that generate fluctuating electric and magnetic fields. Anomalous transport mechanisms are also discussed in Sec. III.C. The transport in tokamaks is often discussed in terms of three radial regions—the edge, where atomic processes are important; the center, $q\lesssim 1$, where sawtooth MHD activity dominates; and the high-gradient region in between, which provides most of the confinement. This is illustrated in Fig. 36.

To date, while some progress has been made in characterizing edge transport (Wootton, 1991), there is no clear connection between theory and experiment that would allow the accurate projection of reactor plasma parameters. As a consequence, reliance is placed on empirical models of transport obtained by regression analysis of data from a wide range of experiments (Reidel, 1990). Early empirical formulas were derived for Ohmically heated plasmas (Cohn *et al.*, 1976; Pfeiffer and Waltz, 1979). The most striking dependences of the formulas are (a) a strong dependence on density, (b) no explicit dependence on field (though the maximum density attainable increases with field), and (c) a greater than quadratic dependence on the plasma scale. The so-called neo-Alcator formula (Parker *et al.*, 1985) is commonly used:

$$\tau_{\rm OH}\simeq 0.07\bar{n}_{20}R^2aq_a \ ({\rm s}) . \tag{4.18}$$

Variants of this formula add dependences on A_i and κ. It is interesting that this formula is very similar to what would be expected if the dissipative trapped-electron (DTE) mode dominated the plasma (Perkins, 1984). Allowing that electron losses dominate in an Ohmically heated plasma,

$$\chi_\epsilon^{\rm DTE}=1\times 10^{22}\left[\frac{r}{R}\right]^{3/2}T_e^{7/2}/[B^2L_n^2n_e\ln(\Lambda_e)Z_{\rm eff}] . \tag{4.19}$$

This may be combined with Eq. (2.27), the power-balance equation (2.22), and Ohmic power $P_\Omega=R_pI^2$, Eq. (4.6), to eliminate T_e, yielding an approximate formula for τ_E (assuming $T_i/T_e=$constant, and ignoring additional terms)

$$\tau_E\propto\bar{n}R^{2.4}a^{0.2}q^{1.2}B^{-0.3} . \tag{4.20}$$

While the agreement is tantalizingly good, the experimental evidence remains equivocal as to the cause of core transport (Callen, 1991; Wooton, 1991). Nevertheless, the analysis shows that even diffusive transport does not have to scale as a^2, and the explicit dependence on field may be weak, even though $\chi_E\propto B^{-2}$.

Following the application of substantial auxiliary heating ($P_a\gg P_\Omega$), it was discovered on ISX-B (Swain, 1981) that confinement degraded with increasing power but increased with current, $\tau_E\propto(I^{2/3}/P^{2/3})$. Again, there is a similarity to the collisionless trapped-electron

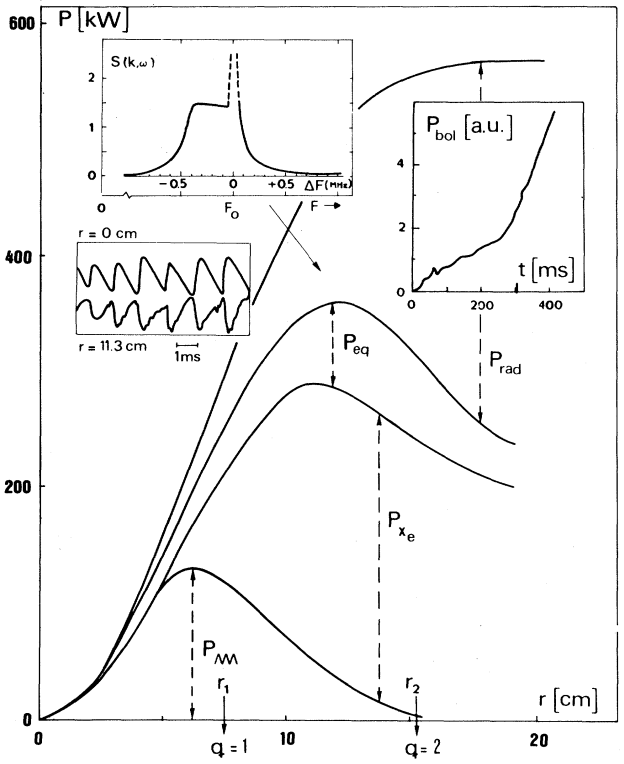

FIG. 36. Power balance for a TFR-600 plasma. In the inserts are shown the experimental results for the dominant physical mechanism in each of the three plasma regions: sawtooth activity, microturbulence, and spectral radiation (Equipe TFR, 1980).

mode scaling (Perkins, 1984), which yields $\tau_E \propto a^{1.8}R^{0.8}n^{0.6}B^{0.8}/P^{0.6}$. Subsequently, as data became available from other experiments, formulas involving the plasma size were developed (Goldston, 1984; Kaye and Goldston, 1985; Rebut *et al.*, 1987; Odajima and Shimomura, 1988). A model based upon the role of a critical electron temperature gradient has been developed by Rebut, Lallia, and Watkins (1989; see also Rebut *et al.*, 1991). More recently the ITER group has developed formulas (Yushmanov *et al.*, 1990). There are two types of ITER formulas for operation in the so-called low (L) mode of tokamak operation ($C_H=1$): first, a power series,

$$\tau_e^{\text{ITER-P}}=0.048C_H I^{0.85}R^{1.2}a^{0.3}\bar{n}_{20}^{0.1} \times\kappa^{0.5}B^{0.2}A_i^{0.5}/P^{0.5}\ (\text{s}), \tag{4.21}$$

and second, an offset-linear type of scaling, which reflects the view that there is an Ohmic scaling plus an incremental auxiliary heating scaling:

$$\tau_e^{\text{ITER-OL}}=0.064C_H I^{0.8}R^{1.6}a^{0.6}\bar{n}_{20}^{0.6}\kappa^{0.2}B^{0.35}A_i^{0.2}/P +0.04C_H I^{0.5}R^{0.3}a^{0.8}\kappa^{0.6}A_i^{0.5}\ (\text{s}) \tag{4.22}$$

where the units are I (MA), a, R (m), $\bar{n}_{20}(10^{20}\ \text{m}^{-3}$, line-average density), B (T), P (MW) and A_i is the atomic mass number. These formulas are valid for $q_{95}\gtrsim 3$. For lower safety factors the confinement is usually worse, owing to MHD activity.

Interestingly, for very low aspect ratio, the confinement in the Ohmic regime is better than neo-Alcator scaling would predict and closer to the more favorable Rebut-Lallia-Watkins scaling (Hender, 1993).

1. The H mode

As discovered in the ASDEX tokamak (Wagner *et al.*, 1982; Asdex Team, 1989), the confinement can be improved in tokamaks with a divertor—the high or H mode. A typical value for the H-mode factor (C_H) is $C_H\simeq 2$ for $q_{\psi a}\gtrsim 3$. Similar confinement improvements have been obtained in plasmas with a limiter, e.g., "supershots" on TFTR, $C_H\simeq 3$, when careful conditioning is used to reduce deuterium recycling from the limiter (Hawryluk, 1987). Recently a very high (VH) mode has been seen in diverted discharges in DIII-D, when wall conditioning with boron was used, $C_H\simeq 3.5$ at $q_{\psi a}\simeq 4$ (Jackson *et al.*, 1991).

A possible explanation for the LH transition lies in the effect of a radially varying poloidal rotation on the turbulence, which causes anomalous transport. It is postulated that a bifurcated solution for transport exists with two different, coupled levels of rotation and turbulence. Itoh and Itoh (1988, 1989, 1990, 1991) and Shaing *et al.* (1988, 1989, 1990; Shaing, 1991) proposed that a change in ion orbit losses at the edge leads to a radial current and a $\mathbf{j}_r\times\mathbf{B}_\phi$ force, which changes the poloidal rotation and allows a jump to a different solution for transport. The effect of changing the radial current has been seen (Taylor, 1989; Weynants and Taylor, 1990), in experiments in which an electrode inserted in the plasma was used to induce a current (Fig. 37). Various models have been developed to show how turbulence may be reduced by gradients and curvature in the poloidal rotation (Biglari, Diamond, and Terry, 1990; Leboeuf *et al.*, 1991); and how a shear can be generated by turbulence (Carreras, Garcia, and Lynch, 1991; Diamond and Kim, 1991). Flow generation and turbulence reduction are closely interrelated. As L-to-H transition model, integrating self-consistently both effects, has been presented by Diamond *et al.* (1991). Detailed examinations of the edge parameter which have been made in DIII-D (Groebner *et al.*, 1990; Burrell *et al.*, 1991) and in JFT-2M (Ida *et al.*, 1990) support some of the postulates of these models.

In most experiments the transition from L to H mode leads to a substantial increase in the plasma edge density and to a relatively flat density profile. The temperature of the edge also rises, but the temperature retains its normally peaked profile. These features are well represented by the model profiles, $T=T_0(1-r^2/a^2)^2$ and $n=n_0(1-r^2/a^2)^{\alpha_n}$, $\alpha_n=0$–0.5.

A condition must be set for the LH transition to occur. Empirical formulas for the condition have been given (Ryter, 1993; Kardaun, 1993),

$$P_{\text{tot}}\gtrsim(0.04-0.07)\bar{n}_{20}B(T)A_p\ (\text{MW}), \tag{4.23}$$

where A_p (m^2) is the surface area of the plasma.

Empirical scalings for H-mode operation are at an earlier stage of development (Christiansen *et al.*, 1991). The quality of confinement depends upon the level of activity of edge localized modes (ELMs), in which the H mode crashes on a transient basis (Wagner *et al.*, 1982). For

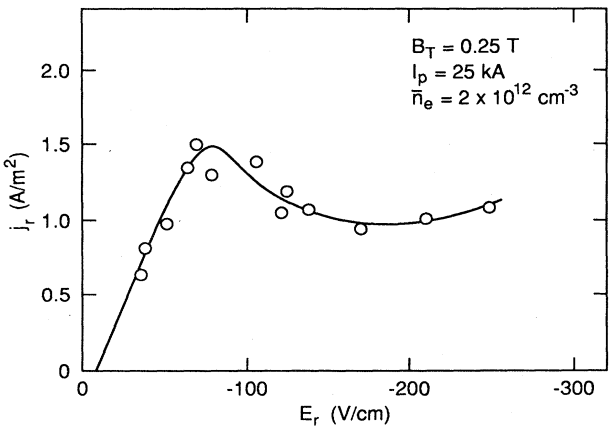

FIG. 37. The radial particle current in CCT varies as a function of the applied electric field (poloidal rotation). The current is related to the poloidal damping force. This "runaway"-like damping can support bifurcation in the poloidal rotation and in the corresponding radial electric field (Taylor *et al.*, 1989).

ELM-free data an empirical fit is given by Post *et al.* (1991),

$$\tau_E(\text{ELM-free}) = 0.064 I^{0.87} R^{1.82} a^{0.12} \bar{n}_{20}^{0.09} \times \kappa^{0.35} B^{0.15} A_i^{0.5} / P^{0.5} \text{ (s)} . \quad (4.24)$$

When ELM activity is high, $\tau_e \simeq 0.75\tau_e$ (ELM-free).

Most theoretical work has concentrated on explaining the anomalous transport in terms of drift-wave-type instabilities, with frequencies below the ion cyclotron frequencies and $k_\perp \rho_s \gtrsim 0.5$, i.e., short wavelengths. However, recent experimental data, e.g., those of Efthimion *et al.*, 1991, show the largest fluctuations occurring at lower values, $k_\theta \rho_s \lesssim 0.4$. Also, the frequencies (<50 kHz), when allowance is made for the Doppler shift coming from plasmas flows, are much less than those expected from drift waves. Possible candidates for these low-frequency, long-radial-correlation-length modes are instabilities such as the trapped-ion modes and neoclassical MHD tearing modes (Callen, 1991). Ion temperature-gradient modes, which are important when $L_n / L_{Ti} \gtrsim 1$, were believed to be an important contributor to such phenomena as the saturation of confinement at high densities in Ohmically heated plasmas and L-mode confinement degradation. However, recent calculations, which incorporate more realistic kinetic effects, predict a lower level of transport and suggest they may have importance only in the plasma center (Callen, 1991).

2. Dimensionless plasma scaling

The scaling relations derived in Sec. III.D may now be applied to the empirical formulas to see if they satisfy $\tau_E \propto B^{-1}$. We find for Eq. (4.18) $\tau_{OH} \propto B^{-0.8}$, suggesting that a slightly weaker dependence on density $n^{0.9}$ might be appropriate. For Eq. (4.21), $\tau_E^{\text{ITER-P}} \propto B^{-0.97}$; for Eq. (4.24), $\tau_E^{\text{ITER-OL}} \propto B^{-1.11} + B^{-0.78}$; and for Eq. (4.24), τ_E (ELM-free) $\propto B^{1.09}$, in fair agreement with the requirements. In the Connor and Taylor (1977) analysis, the exponents of the parameters are related for particular plasma models.

Evidence is growing that tokamak transport is Bohm-like in character rather than gyro-Bohm-like (Deboo *et al.*, 1991; Christiansen *et al.*, 1992; Waltz *et al.*, 1990; Scott *et al.*, 1993). In fact, when ITER-P scaling is expressed in terms of a diffusivity,

$$\chi^{\text{ITER-P}} = \text{constant} T_e / B (\beta^2 \nu^*)^{1/4} \quad (4.25)$$

(Scott *et al.*, 1993).

A plot of experimental $\tau_E B$ is given in Fig. 38 for the ITER, L-mode scaling (Goldston, *et al.*, 1992). JET data can be used as benchmarks for both an ignition experiment and ITER; at reduced operating parameters correspond to equal dimensionless parameters (Sheffield, 1990). It is expected that a power reactor will not be much larger than ITER; therefore benchmarking, in ITER, of the empirical scalings should give confidence in the ability to predict reactor performance.

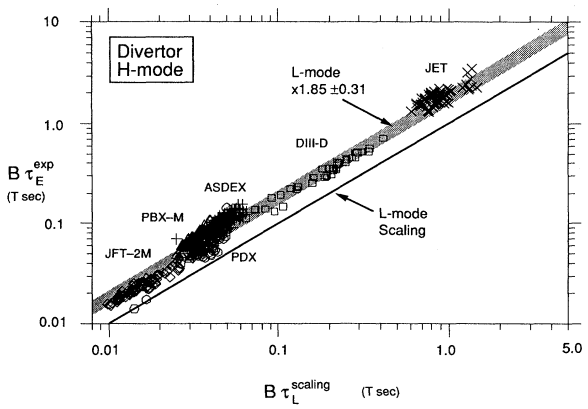

FIG. 38. Plot of $B\tau_E^{\text{exp}}$ vs an empirical scaling law for a variety of tokamaks operating in the H mode, showing a reproducible and systematic enhancement of confinement over L-mode operation (Goldston *et al.*, 1992).

E. MHD limits

Good reviews of this topic have been given by Bateman (1978), Wesson (1978), Schmidt (1979), and Freidberg (1982,1987; see also Sec. III.B). The dominant modes in a tokamak are (a) kink instabilities, (b) ballooning instabilities in which a pressure-gradient drive causes interchange of plasma and field in the region of poor magnetic-field curvature localized on the outside of the plasma (Fig. 39); and (c) low-order resistive kink instabilities, which lead to magnetic island formation.

Whether the equilibria are stable can be checked by

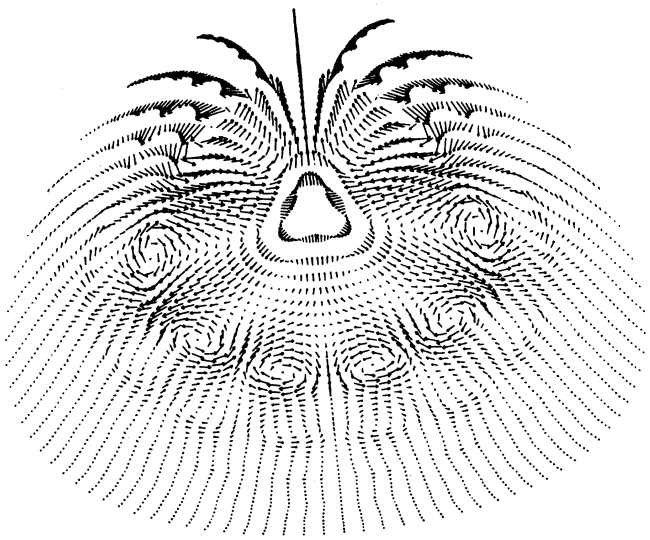

FIG. 39. Projection of the displacement vector of the $n=3$ fixed boundary ($b/a=1$) mode for a $\beta=9\%$ case with $R/a=3.5$ and $1<q<3.0$ (Todd, 1979).

linearizing Eqs. (3.4)–(3.8) and then subjecting the fluid elements to small perturbations of the form

$$\xi_r = \xi(r)\exp[i(m\theta + n\phi - \omega t)] , \tag{4.26}$$

where m and n are integers (0,1,2,3,...). Modes for which the imaginary part of $\omega = \omega + i\gamma$ is positive will grow; these modes are linearly unstable. They may be stabilized by nonlinear effects when the plasma and field reach a new but time- or space-varying equilibrium. Various modes are observed in toroidal plasma, even when, on a long time scale, the system is in a stationary state. When modes are not stabilized, the plasma can move into the wall—the "major disruption"—or can suffer relaxation oscillations with periodic enhancements of transport—tokamak "sawtooth" oscillations. A stability diagram for modes having a variety of toroidal (n) and poloidal (m) mode numbers and different current distributions is shown in Fig. 40. In the ideal MHD calculations with a vacuum region surrounding the plasma, these bulk modes would appear as perturbations to the plasma surface. When finite resistivity is included in the calculation, the sharp plasma-vacuum boundary becomes blurred and other instabilities can be found inside the plasma, for instance, the resistive kink modes termed "tearing modes" (Furth, Killeen, and Rosenbluth, 1963), which dominate the low-β MHD activity in the plasma. In tokamaks, the ($m=1$, $n=1$) mode occurs when $q<1$ inside the plasma and induces sawtooth oscillations; see Fig. 29.

Large m-number modes are localized near the resonant surface, $q = m/n$, while small m numbers may have a greater radial extent. The stability criterion for radially localized modes was derived by Mercier (1960). For a large-aspect-ratio tokamak (Shafranov and Yurchenko, 1968),

$$-p'(q^2-1) + \frac{rB_\psi^2}{8\mu_0}\left[\frac{q'}{q}\right]^2 > 0 . \tag{4.27}$$

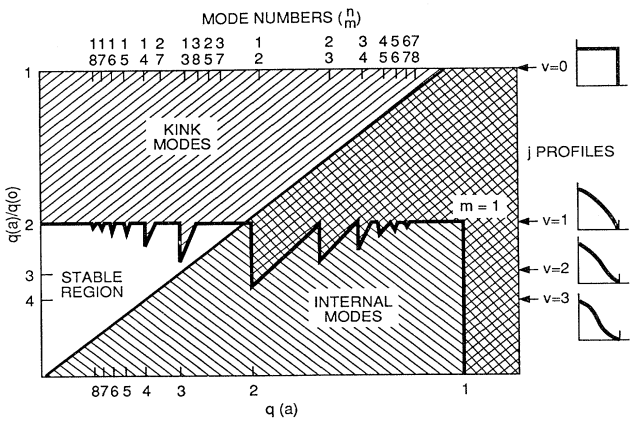

FIG. 40. Stability diagram for ideal kink and internal modes. Stability to internal modes requires $q(0)>1$; to $m=1$ kinks requires $q(a)>1$; and to $m>1$ kink modes requires a minimum peaking of the current profile (Wesson, 1978).

The prime denotes differentiation with respect to ψ. For the normal case of $p'<0$, both terms are stabilizing if $q>1$.

The addition of resistivity modifies the ideal criterion because, in a narrow region around the resonant surfaces, it allows the field lines to break and rejoin. The modified criterion is

$$-p'\left[(q^2-1) + \left[\frac{q}{r}\right]^3 q' \int_0^r \left[\frac{r^3}{q^2} + \frac{2R^2r^2}{B_\phi^2}(-p')\right] dr\right] > 0 . \tag{4.28}$$

The resistivity has removed the large shear stabilizing term. Nevertheless, stability is still achieved for $q'>0$ if $q>1$.

Some modes are localized in the parallel direction with a finite wavelength on the outside of the toroidal plasma, where the magnetic curvature is unfavorable—these are the so-called "ballooning modes." Analytic expressions for stability against ideal ballooning modes have been given by Pogutse and Yurchenko for circular (1979) and noncircular (Pogutse, Chudin, and Yurchenko, 1980) plasmas,

$$\frac{1}{2}s^2 + \frac{2r\mu_0}{B^2}p'\left\{1 - q^2\left[1 - \frac{7}{4\epsilon}\left[1 - \frac{5}{6}s^2\right]\exp\left[\frac{-1}{|s|}\right]\right]\right\}$$

Shear magnetic well or hill

$$-3s\left[\frac{r\mu_0 p'}{B^2}\right]^2 \frac{q^4}{\epsilon^2} > 0 \tag{4.29}$$

ballooning drive

where

$$s = \frac{r}{q}q' , \quad \epsilon = \frac{r}{R} .$$

This formula illustrates the stabilizing influence of magnetic shear (the first term) and of a magnetic well (the second term). The third term shows the stabilizing effects of negative shear ($s<0$).

1. Resistive ballooning modes

Resistivity modifies the stability properties of ballooning modes (shear is ineffective) and lowers the stability threshold. These modes can be important at high beta and low temperatures ($\lesssim 1$ keV) where the resistivity is higher. They may be important in the edge region of tokamaks and stellarator reactors, where they can enhance transport.

2. Beta limit

For optimized pressure and $q(r)$ profiles, which just avoid ideal ballooning and kink instabilities, the maximum value average beta is (Bernard *et al.*, 1983; Sykes *et al.*, 1983; Troyen *et al.*, 1984)

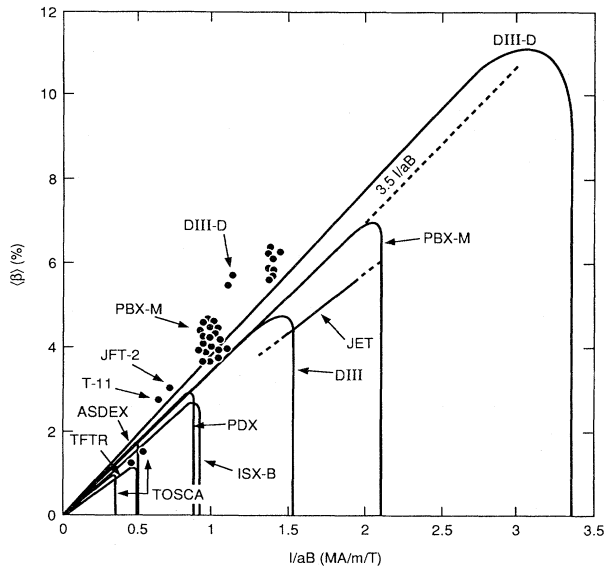

FIG. 41. The stable operating space for each indicated tokamak lies below the corresponding curve. A pressure-driven limit, often accompanied by ballooning-type modes with low mode numbers, is encountered at about $\beta_T=3.5$ in all these high-beta experiments. The vertical line to the right in each is approximately I/aB, the "kink" limit at $q_a=2$ for that device (Callen *et al.*, 1992).

$$\langle\beta_c\rangle = g\frac{I}{aB_{\phi 0}}\%, \quad g\simeq 2.8 \text{ to } 4.4\ , \tag{4.30}$$

where I (MA), a (m), B (T), and $\langle\beta_c\rangle = 2\mu_0$ (pressure$\times 100)/B_t^2\%$, B_t is the total field, and $B_{\phi 0}$ is the vacuum toroidal field. The coefficient g is a weak function of δ and κ. A plot of performance in a number of tokamaks, Fig. 41, shows that $g=3.5$ is typical of the beta level achieved. Generally, the limit is set by a combination of ballooning and kink modes.

At low aspect ratio ($R/a \lesssim 2$), paramagnetic effects become important and the toroidal field becomes larger than the vacuum value. In addition, the poloidal field may be large ($\beta_\theta \lesssim B_\phi$) as R/a drops to $\lesssim 1.5$. The total field $B_t=(B_\theta^2+B_\phi^2)^{1/2}\sim 2B_\phi$ at $R/a\sim 1.2$. Calculations of MHD stability show similar values of the Troyon coefficient to values calculated for conventional aspect ratios (Bespoludennov *et al.*, 1986; Hender, 1993).

3. Second stable operation

For high enough pressure the distortion of the magnetic geometry by the plasma moves the low (absolute) shear regions to places with more favorable curvature and permits higher values of beta. This self-stabilization effect was first calculated for ballooning modes in tokamaks by Mercier (1979) and Coppi *et al.* (1979). Subsequently the effect was also seen in calculation of interchange (Mercier) modes in stellarators (Carreras *et al.*, 1983; Shafranov, 1983). The region in which some mode is calculated to self-stabilize is often referred to as a second stable region. Use of such terminology does not necessarily imply that the whole plasma is stable nor that some other mode is stable in some other part of the plasma. For example, in a tokamak, modification of the magnetic field in the outer region might lead to self-stabilization of ballooning modes there, while the sawtooth mode was still active in the plasma interior. Direct access to the region is theoretically possible for highly D shaped or even indented "kidney bean" tokamak plasma cross sections, as in the PBX-M tokamak, or by raising $q_\psi(0)$ to ~ 2. Kink modes, however, are an obstable to self-stabilization. Calculations with optimized profiles predict g up to 5.5, stable to both classes of modes (Ramos, 1991).

Operation in the second stable region at high bootstrap current fractions is an interesting mode for reactors; see Fig. 34.

Ideal modes can be driven unstable by non-Maxwellian particle distribution functions, as in the "fishbone" instability driven by perpendicular neutral-beam injection (Chen *et al.*, 1984) or in the case of the predicted alpha-particle instabilities (Spong *et al.*, 1985, 1987).

4. Resistive modes

The high electrical conductivity of tokamak reactor plasmas ($T_e \gtrsim 10$ keV) leads to a high Lundquist number $S \equiv$ magnetic diffusion time/poloidal Alfvén time $\equiv(\mu_0 r^2/\eta)/(R_0 q/v_{A\theta}) \gtrsim 10^7$, where $v_{A\theta}=2.18\times 10^{16} B_\theta/(A_i^{1/2} n_i^{3/2})$ (m s^{-1}). As a consequence, the modes in a tokamak are generally constrained to a narrow region around the mode rational surface ($q=m/n$). The modes grow relatively slowly ($\sim 10^{-4}$–10^{-2} seconds) compared to ideal modes, and saturate when all of the accessible free energy has been accommodated in rearranging the local magnetic field, creating an island. Only the low mode numbers are unstable, i.e., $m/n=1/1$, 3/2, 2/1, 3/1, ... These modes account for the macroscopic MHD phenomena observed in tokamaks. The 1/1 mode leads to a relaxation oscillation and the characteristic sawtooth behavior of the plasma center when $q_0 \lesssim 1$ (see Fig. 36). This mode flattens the central temperature profile, reducing the potential for fusion reactions at fixed beta. The mode also decreases confinement below the normal empirical value if the $q=1$ surface becomes large, generally a problem when $q_{\psi a}<3$. It may be stabilized by careful control of the current profile to hold $q(0)>1$, for example by using ICRH (see Phillips *et al.*, 1992).

The other modes are normally present and lead to island formation with some modest degradation of confinement [see Eq. (3.18)].

5. Disruptions

Rapid loss of energy and plasma current can occur in a tokamak as a result of MHD instabilities, usually involv-

ing the M=2, N=1 mode. A computation showing growth and overlap of the 2/1 and 3/2 modes leading to instability is shown in Fig. 42. Conditions that are vulnerable to disruptions, because they can have unstable profiles, include (a) plasmas cooled at the edge by impurities near the density limit; (b) low-q operation, i.e., $\lesssim 2$; (c) operation near the beta limit; and (d) transient conditions—startup, current ramp-down, strong sawtooth activity, strong ELM activity, changes in configurations, and termination of additional heating. A review of disruptions is given by Post *et al.* (1991). A slow rise in radiation or in MHD activity (e.g., the 2/1 mode) can be a precursor to a disruption. The disruption then leads to an energy quench, in which the plasma loses from 50% to 80% of its energy directly to plasma facing components or by radiation, in a time typically in the range of several hundred microseconds to a few milliseconds. The decrease in pressure causes the plasma to move inward in major radius. Following this phase the current usually flattens and rises, owing to the lower inductance. The current then quenches in a time as fast as 5 to 15 milliseconds. Most of the magnetic energy (over 75%) is lost by radiation. The plasma usually moves inward and may also suffer a vertical displacement. Large currents can appear in plasma facing components, and very energetic electrons ($\gtrsim 50$ MeV) may be generated.

In present-day experiments, a few percent of disruptions cannot be attributed to an identified cause (Post *et al.*, 1991). Disruptions remain an obstacle to the development of an acceptable tokamak reactor.

Reactor designs are often restricted to less than the Troyon limit to ensure minimal disruption. Two approaches to disruption prevention are being considered: (a) Using current drive to control the current profile and suppress mode growth, and (b) using an externally applied transform ($\iota \gtrsim 0.15$), which has been shown to prevent disruptions in Pulsator (Fussman *et al.*, 1979) and in TOSCA (Robinson, 1980).

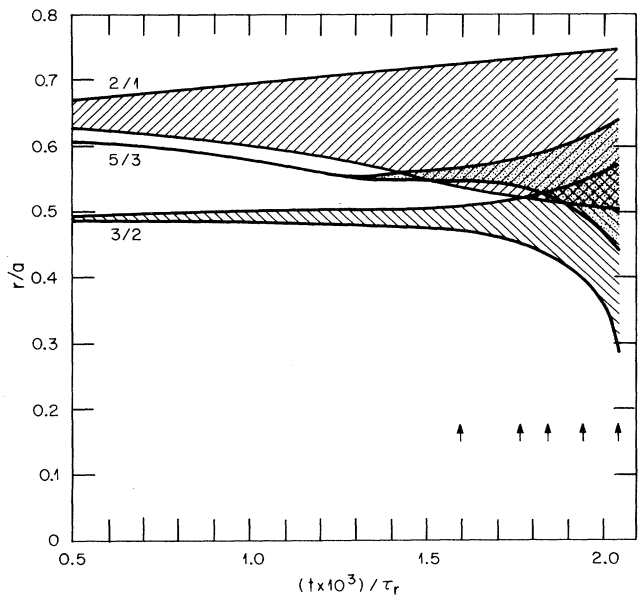

FIG. 42. Time evolution of the magnetic island width for the ($m=2$; $n=1$) and ($m=5$; $n=3$) modes in a multiple-helicity calculation, leading to a disruptive condition (Carreras *et al.*, 1980).

In summary, the limits set by MHD activity, in terms of the Troyon factor g, are estimated to be roughly (a) $g \lesssim 2.5$ if profiles are not controlled, in order to minimize disruptions; (b) $g \simeq 3.5$ in the first stable region if there is some profile control; (c) $g \lesssim 5.5$ when on-axis $q(0)$ is raised to ~ 2, and with higher $q_\psi(a)$ to retain sufficient magnetic shear and put some of the plasma in a second stable region.

F. Density limit

There is a maximum density at which the plasma becomes disruptive. With increasing density the plasma edge cools, leading to a shrinking of the inductively driven current channel. In turn the $m/n=2/1$ tearing mode is destabilized when $q_\psi=2$ is reached. A formula for the density limit was given first by Murakami (1976) for Ohmically heated plasmas,

$$\bar{n}_m \leq 1.5\frac{B}{Rq_{\rm cyl}}(10^{20}\ {\rm m}^{-3}) ,$$

where

$$q_{\rm cyl}=\frac{2.5a^2B}{RI}(1+\kappa^2) .$$

For auxiliary heated plasma the multiplier was found to be ~ 2.5. Subsequently, Greenwald *et al.* (1988) showed that for noncircular plasmas the limit was higher than given by the Murakami formula, and

$$\bar{n}_m \simeq \frac{I({\rm MA})}{\pi[a(m)]^2}(10^{20}\ {\rm m}^{-3}) . \tag{4.31}$$

A second limit may occur owing to loss of thermal equilibrium in front of the divertor plate (Borrass, 1989). An analytic model provides a relationship between the separatrix density and the divertor temperature, in terms of the heat flux across the separatrix, the connection length, and the impurity radiation loss in the scrape-off layer.

G. Alpha-particle effects

The general effects of alpha particles in fusion plasmas are discussed in Sec. II.F; see also Furth *et al.* (1990) and Sigmar (1989). There are also specific collective effects which may be important in tokamak reactors when the parallel velocity $v_{\alpha\|}$ approaches the Alfvén speed. A summary of collective alpha instabilities is given in Table XII.

TABLE XII. Collective alpha instabilities. Frequencies evaluated for TFTR (Zweben 1988). Symbols: $\omega_{d\alpha}$=alpha precession frequency; ω_A=Alfvén frequency; $\omega_{c\alpha}$=alpha cyclotron frequency; $\omega_{*\alpha}$=alpha diamagnetic frequency; S_α=alpha source rate.

Instability	Frequency (kHz)	Physical mechanism(s)	Important parameters	Possible effects	Possible diagnostic(s)
Alpha-driven sawteeth	<0.1	Central electron heating by alphas—sawtooth crash	$\frac{P_\alpha(0)}{P_{\text{heat}}(0)}$	Modification of $q(r)$ profile; expulsion of alphas from center	Gyrotron alpha scattering, soft x-ray emission
Alpha-driven fishbones	$\sim 10^{-1}$–10^2	Resonance of alpha precession and internal $m=1$ mode	$\beta_\alpha(0)$ β_{th} $\omega_{d\alpha}/\omega_A$	Expulsion of trapped alphas from center	Escaping alpha detectors, soft x-ray emission
Alpha-driven drift wave or ballooning	~ 10–10^3	Resonance of alphas with $m \gg 1$ modes	Gradients of β_α and n_α/n_e	Reduction of beta limit; change of plasma transport	Microwave scattering escaping alpha detectors
Alpha-driven Alfvén waves (e.g., TAE mode)	$\sim 10^3$–10^4	Passing alphas with $v_\alpha > V_A$ excite Alfvén modes	v_α/V_A $\omega_{*\alpha}/\omega_A$ $\nabla\beta_\alpha$	Anomalous loss of passing alphas; electron heating	Microwave scattering external $\tilde{B}$
Alpha loss-cone-driven Alfvén waves	$\sim 10^4$–10^5	Velocity space instability near trapped/passing boundary	TF ripple n_α/n_e $\omega_{c\alpha}$	Anomalous loss of trapped alphas; ion heating	Ion cyclotron emission escaping alpha detectors
Alpha population-inversion-driven Alfvén wave	$\geq 10^5$–10^6	Bump-on-tail instability due to fast alpha turn-on	$\frac{1}{S_\alpha}\frac{\partial}{\partial t}(S_\alpha \tau_\alpha)$	Anomalous alpha slowing down; ion heating	Ion cyclotron emission escaping alpha detectors

1. Destabilization of Alfvén waves

A variety of shear Alfvén waves may be destablized by alpha populations. The radially localized kinetic Alfvén waves (KAW) can be excited both by trapped energetic particles (Mikhailovskii, 1975) and by passing particles, through inverse Landau damping with $\omega \approx k_\parallel v_{\parallel\alpha}$ (Rosenbluth and Rutherford, 1975). The global Alfvén eigenmode (GAE) is a radially extended, low-n, low-m mode occurring below the continuum $[\omega^2 < (k_\parallel v_A)^2_{\min}]$; it has been shown to be destabilized by alphas (Li, Mahajan, and Ross, 1987). The global Alfvén eigenmode has recently been excited with neutral beams in the Wendelstein 7-AS stellarator (Jaenicke *et al.*, 1993) and may be an issue in the low-shear central regions of tokamaks, where the alpha pressure gradients are large. When toroidal geometry is included, spectral gaps occur in the shear Alfvén continuum, leading to the existence of the toroidal Alfvén eigenmodes (TAE) (Kieras and Tataronis 1982; Cheng *et al.*, 1984; Fu and Van Dam, 1989). The conditions for the instability to occur are $v_\alpha \leq v_A$ and $mv_\alpha\rho_\alpha/rL_\alpha > 0.5v_A/R_0q$, evaluated at the radial location of the gap, where L_α is the radial scale length of $n_\alpha(r)$. In addition, the toroidal Alfvén eigenmode has a β_α threshold caused by balancing the alpha pressure-gradient drive against a variety of damping mechanism. The existence of toroidal Alfvén modes has been demonstrated on TFTR (Wong *et al.*, 1991) and DIII-D (Heidbrink *et al.*, 1991) by using neutral beams at low magnetic fields. The fact that the observed β_α thresholds generally exceed those of the simple analytic theory by an order of magnitude has focused attention on various damping mechanisms for the toroidal Alfvén eigenmode, such as continuum damping (Rosenbluth *et al.*, 1992), ion Landau damping (Betti and Freidberg, 1992), Landau damping on trapped collisional electrons (Gorelenkov and Sharapov, 1992), and finite-orbit effects (Berk *et al.*, 1992).

Assessing the potential importance of these modes will require (a) a better understanding of linear stability boundaries (including all relevant damping effects) and (b) nonlinear studies to determine the saturated amplitudes and their impact on the α particles. Some of the approaches being used to address these questions are gyrofluid models (Spong *et al.*, 1992), hybrid fluid-particle models (Gang *et al.*, 1992; Park *et al.*, 1992), and Monte Carlo following of alpha-particle orbits in an externally imposed toroidal Alfvén eigenmode structure (Hsu and Sigmar, 1992).

2. Destabilization of ballooning modes

Ballooning modes may be destabilized by trapped and circulating alpha particles, with mode frequencies either in the toroidal Alfvén eigenmode range ($\omega \cong v_A/2qR$; Spong *et al.*, 1990; Rewoldt, 1988) or in the ion diamagnetic frequency range ($\omega \cong \omega_{*\text{ion}}/2$; Spong *et al.*, 1985, 1987; Biglari and Chen, 1991. The underlying destabilization mechanism is inverse Landau damping through transit, drift, or bounce resonances, which then couple either with a toroidal Alfvén eigenmode (TAE) or a kinetic ballooning mode (KBM). The calculated effect is to lower the background plasma beta limit (see Fig. 43; Spong *et al.*, 1990) and increase the radial diffusion of the alpha particles (Rewoldt, 1988). An important question of future devices will be which mode (TAE or KBM) is dominant in the operational regime of interest. The toroidal Alfvén eigenmode growth rate is expected to be lowered (due to enhanced continuum damping) near the Troyon beta limit, while the kinetic ballooning mode persists in this regime (Biglari, Zonca, and Chen, 1992).

3. Fishbone oscillations

Trapped alphas with drift frequencies resonant with the $m=n=1$ internal kink mode ($\omega \cong \omega_{\text{dh}}$) will lower the beta threshold for this instability, leading to "fishbone" oscillations (Coppi *et al.*, 1990; White *et al.*, 1990). This instability leads to ejection of fast particles in bursts. Nonresonant alphas ($\omega \ll \omega_{d\alpha}$) can be stabilizing if $\omega_{*\alpha}/\omega_{d\alpha} > 0$ or destabilizing in the opposite case. The former limit was apparently achieved using anisotropic minority ICRF tails in JET, where sawtooth stabilization was demonstrated (Campbell *et al.*, 1988). However, in the case of isotropic alphas, both signs of $\omega_{d\alpha}$ will be contained in the pitch-angle distribution, and it is not expected to be possible to maintain either the stabilizing ($\omega_{*\alpha}/\omega_{d\alpha} > 0$) or purely nonresonant limits ($\omega \ll \omega_{d\alpha}$) over the entire tokamak radius (Cheng, 1990).

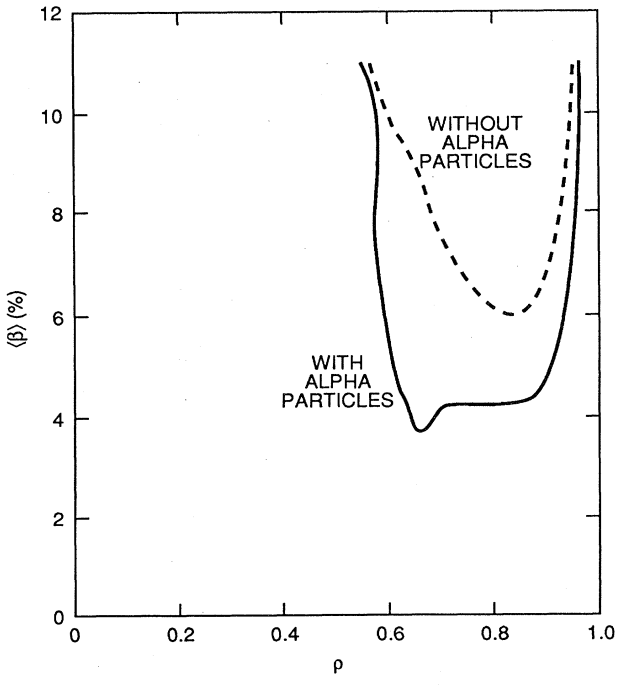

FIG. 43. ITER stability contours (at $y=0.02\omega_A$) for an elongation of $b/a=2.0$ (Spong *et al.*, 1990).

Some experimental data on the alpha-induced modes should come from TFTR and JET. However, ITER will probably be the first device to have a fully reactor-grade plasma in which alpha heating dominates.

H. Power and particle control

The generic issues and solutions for power and particle control are discussed in Sec. II.G. For a tokamak it seems that a poloidal divertor (Figs. 19 and 20), with high recycling of the neutrals (Table VI) is the best solution for handling the heat leaving the plasma edge, for blocking wall-generated impurities, for pumping, and for minimizing divertor plate erosion. The operation of the divertor may be improved by radiating power in the divertor region, provided this is controllable. The most extensive studies of tokamak reactor-relevant divertor configurations have been made for ITER (Post *et al.*, 1991). Tests in existing facilities, their upgrades, some new steady-state facilities, and ultimately ITER will be required to validate predictions, optimize divertor designs, and determine the best reactor plasma operating conditions.

External sources of power and particles are important for establishing plasma profiles and thereby controlling the plasma behavior. In a reactor, for example, producing 3500 MeV of fusion power [$\sim$GW(e)], the alpha power is 700 MW. It is not likely that affordable external sources of heating can have impact on the temperature profile. However, power may be used to control the current profile with noninductive current drive and to affect low-order MHD activity (Zakharov, 1989).

Fueling is discussed in Sec. II.I. While pellet injection to the axis of a tokamak reactor may be difficult to achieve, penetration well into the plasma may be used to affect the edge density profile.

I. Modeling of tokamak plasmas

The system of equations that describes the tokamak core, edge, divertor region, and walls is far too complex to solve, even with a computer, except by splitting up the problem and simplifying the calculations for each region. Nevertheless very good progress has been made on modeling experiments, and there is some ability to predict performance (McNamara, 1981; Killeen, 1992). Numerous programs exist which model the plasma in circular and noncircular geometries and follow its time his-

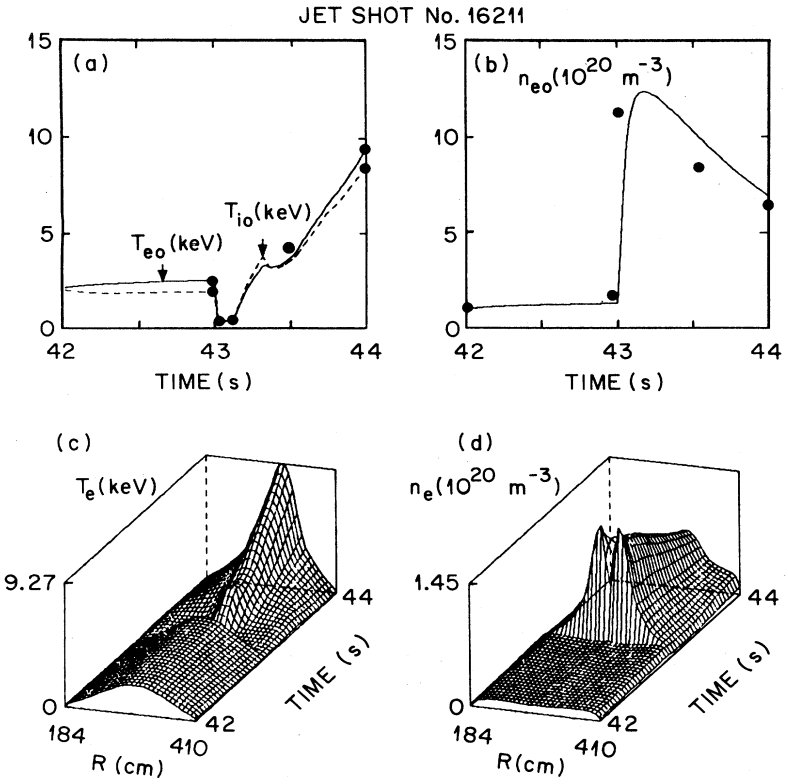

FIG. 44. A comparison of computed and experimental data for pellet injection in JET, showing (a) the central electron and ion temperatures; (b) the central electron density; (c) the evolving electron temperature profile, and (d) the evolving density profile (Houlberg, 1990).

tory (Houlberg, 1982; Pfeiffer *et al.*, 1980; Singer *et al.*, 1986). These codes solve the multifluid equations, allowing for the evolution of the flux surfaces with changing pressure and current profiles, and include subroutines that (a) model neutral injection; (b) include fusion reactions and fusion product heating; (c) follow the evolution of a fast-ion distribution; (d) model rf heating; (e) model gas and pellet fueling; (f) track neutral hydrogen as it charge exchanges multiply in the plasma; (g) calculate the production of impurities by sputtering; (h) track multiply charged impurities that penetrate the plasma; allow for the absorption and emission of hydrogen from the wall; (i) include the effects of divertor action and model the effects of MHD modes. An example calculation for pellet injection in JET is shown in Fig. 44. The codes may be used to map the power contours for operation over T, n space as illustrated in Fig. 45. Other codes can model features of the scrape-off layer and divertor (Heifetz *et al.*, 1982; Petravic *et al.*, 1985; Braams, 1987).

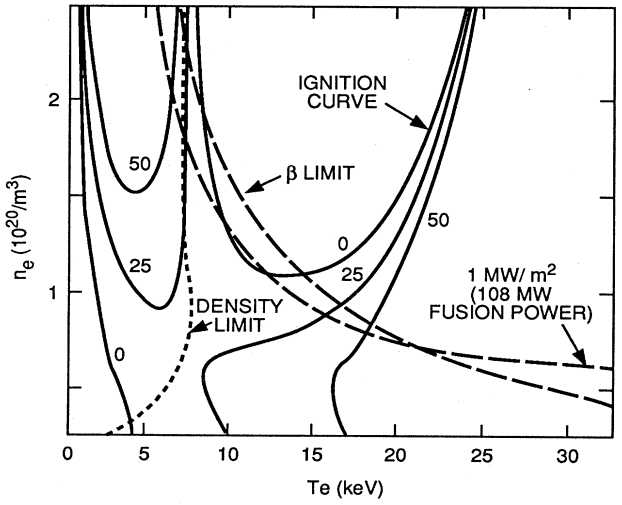

FIG. 45. ITER plasma operating contours (POPCONS) in n-T space for ITER H-mode scaling (H=2.0). Contours denote auxiliary neutral-beam power required to maintain an equilibrium power balance. P_{NB}=0 is the true ignition boundary. Operation constraints of the beta limit, density limit, and required neutron flux are shown (Post *et al.*, 1991).

J. Tokamak reactor options

Numerous studies have been made of tokamak reactors, for example, those of Badger *et al.* (1979), Baker and Quinn (1980), Cooke *et al.* (1989), Najmabadi *et al.* (1991), and Seki *et al.* (1991). Only recently, however, have the authors had available a good basis for a transport model; see Sec. IV.D. A systematic study of principal options is now being undertaken in the Advanced Reactor Innovation and Evaluation Study (ARIES). The ARIES-1 design uses the present best physics base, with advanced technology and engineering. The design criteria lead to a requirement for a 21-T toroidal coil. A slightly different approach taken in the Japanese SSTR design (Seki *et al.*, 1991) has a 16-T coil. The ARIES-II

design relieves the pressure on the technology and engineering by utilizing the potential benefits of advances in tokamak physics, such as may be achieved with better current profile control—that is, second stable operation (higher g)—and better edge control and enhanced confinement (higher C_H).

In Sec. II.E a simple model was used to define the requirements for χ_E and $\langle B \rangle$ for an ignited plasma [Eqs. (2.45) and (2.46)]. These requirements are now equated to the empirical formulas for τ_E, Eq. (4.21), and $\langle \beta \rangle$, Eq. (4.30). Using Eq. (2.42) for the average neutron flux at the wall and Eq. (4.2) for the plasma current, we find the requirements for fusion power P_F, toroidal magnetic field (B), and minor radius (a) of a tokamak reactor:

$$P_F \simeq \frac{1.16\times 10^4 (a_w/a)^{0.106} (\bar{p}_{wn})^{0.106} \kappa^{0.947} q_{\psi a}^{1.11} (1-a^2/R^2)^{2.21} g^{1.79}}{\bar{n}_{20}^{0.34} A_i^{1.7} f_\alpha^{1.7} (n_{\rm DT}/n_e)^{1.62} (R_a)^{0.277} [1+\kappa^2(1+2\delta^2-1.2\delta^2)]^{1.11} \left[1.17-0.65\frac{a}{R}\right]^{1.11} C_H^{3.4}} \ (\mathrm{MW}) , \tag{4.32}$$

$$B = \frac{3.46 (a_w/a)^{0.36} (\bar{p}_{wn})^{0.36} q_{\psi a}^{0.36} A_i^{0.21} f_\alpha^{0.21} (R/a)^{0.66} (1-a^2/R^2)^{0.72} C_H^{0.426}}{(n_{\rm DT}/n_e)^{0.30} \kappa^{0.18} [1+\kappa^2(1+2\delta^2-1.2\delta^3)]^{0.36} (1.17-0.65a/R)^{0.36} g^{0.723}} \ (\mathrm{T}) , \tag{4.33}$$

$$a = \frac{0.142 P_F^{0.5}}{(R/a)^{0.5} (a_w/a)^{0.5} \kappa^{0.25} (\bar{p}_{wn})^{0.5}} \ (\mathrm{m}) . \tag{4.34}$$

The examples below illustrate how these formulas may be used to define various reactor options.

(1) ITER-like plasma parameters for an Engineering Reactor (ITER). $a_w/a=1.1$, $\bar{p}_{wn}=1.0$ (MW m^{-2}), $\kappa=1.6$, $q_{\psi a}=3.0$, $R/a=2.8$, $g=2.0$, $\bar{n}_{20}=1.2$, $A_i=2.5$, $f_\alpha=0.9$, $n_{\rm DT}/n_e=0.55$, $\delta=0.4$, $C_H=2$. These values yield $R=7.91$ m, $a=2.83$ m, $B=6.2$ T, $P_F\simeq 1540$ MW. The tradeoff issues for the ITER design are discussed by Post and Uckan (1992), who show the high leverage of using higher ellipticity.

(2) Aries-1-like reactor (see Table X). $a_w/a=1.1$, $\bar{p}_{wn}=2.6$ MW m^{-2}, $\kappa=1.8$, $q_{\psi a}=4.5$, $R/a=4.5$, $g=3.2$, $\bar{n}_{20}=1.5$, $A_i=2.5$, $f_\alpha=0.8$, $n_{\rm DT}/n_e=0.73$, $\delta=0.4$, $C_H=2.8$.

The higher values of C_H and $q_{\psi a}$ are consistent with the very high mode of confinement seen in the DIII-D tokamak (Jackson *et al.*, 1991). These values yield $P_F\simeq 1900$ MW, $B\simeq 9.2$ T, $a\simeq 1.51$ m, $R=6.78$ m, $I=9.8$ MA, $\langle n_{20}T_{10}\rangle\simeq 2.3$, $\langle\beta\rangle\simeq 2.2\%$.

An advantage of this mode of operation is the high bootstrap current fraction. Assuming $q(0)=1.5$, $I_{\rm BS}/I\simeq 0.67$ from Eq. (4.8) assuming the fast alpha pressure does not contribute to the bootstrap current. A problem for this mode is the requirement of a large field on the toroidal coil. Assuming the inner blanket, shield, and Dewar have a thickness $\Delta=1.5$, the field ratio, Eq. (2.40) is $f_B\simeq 0.535$ and the field on the coil is $B_{\max}\simeq 17.2$ T for this model.

(3) Higher-beta reactor. Second stable operation is projected for higher q_ψ operation. For example, let $g=5.0$ for $q_{\psi a}=6.0$, $q_\psi(0)=1.5$, $\kappa=2$ with the same parameters as case 2. The reactor parameters for $\Delta=1.5$ are $g=5.0$, $P_F\simeq 3440$ MW, $B\simeq 7.2$ T, $f_B=0.59$, $B_{\max}=12.3$ T. The higher beta factor allows the use of a lower field coil, but at the price of a bigger unit power. The bootstrap current is about 100% of the total current. Whether such parameters are possible depends on whether the actual transport leads to stable profiles and whether impurity accumulation is avoided.

Note that the average neoclassical ion thermal diffusivity, Eq. (3.20), is about half of the permitted level.

(4) Better-confinement reactor. The better the confinement, the lower the unit power is allowed to be, Eq. (4.32). However, everything else being equal, the field will be higher for improved confinement as can be seen in Eq. (4.33). Improved confinement is still advantageous in providing a margin that allows more power to be radiated: less power is required to support conduction losses, and f_α may be smaller. Note that the product $f_\alpha^{0.5} C_H$ appears in both Eqs. (4.32) and (4.33). For example, if $C_H=4.2$ rather than 2.8, we may drop f_α from 0.8 to 0.4, i.e., halve the power leaving the plasma by conduction, and alleviate the divertor problem.

The aspect ratio dependence of Eq. (4.32) is very weak, $(1-a^2/R^2)^{2.21}/[(R/a)^{0.277}\cdot(1.17-0.65a/R)^{1.11}]\simeq 0.59$ for $R/a=2.5-5.0$. For $\kappa=1.5\rightarrow 2.0$, the κ-dependent terms are given by $0.3\pm 12\%$. Assuming $a_w/a=1.1$, $\bar{p}_{wn}=2.6$ (very weak dependence), $\bar{n}_{20}=1.5$ (weak dependence), $A_i=2.5$, $f_\alpha=0.8$, $n_{\rm DT}/n_e=0.73$ we find

$$P_F \simeq \frac{1030 q_{\psi a}^{1.11} g^{1.79}}{C_H^{3.4}} \ (\mathrm{MW}) . \tag{4.35}$$

The minor radius is

$$a \simeq \frac{4.1 C_H^{1.7}}{q_{\psi a}^{0.56} g^{0.90} (\bar{p}_{wn})^{0.5} (R/a)^{0.5}} \ \mathrm{m} . \tag{4.36}$$

By contrast the field (B) does depend on (R/a), and the factor $(R/a)^{0.66}(1-a^2/R^2)^{0.72}/(1.17-0.65a/R)^{0.35}$ varies from 1.53 to 2.77 as R/a varies from 2.5 to 5.0. However, the field ratio increases with increasing R/a, offsetting this effect. For the ARIES-1-like case, the

minimum field on the toroidal coil occurs at $R/a=4.5$, though it varies little in the range $R/a=3.5-5.0$. Other factors, notably the positioning and size of the inner poloidal coils, then set the aspect ratio.

(5) Low-aspect-ratio reactor. The approximate parameters of the low-aspect-ratio tokamak, described by Peng and Hicks (1990), may be derived by using the parameters $\bar{a}_w/a=1.1$, $\bar{p}_{wn}=10$ MW m^{-2}, $\kappa=2.7$, $q_{\psi a}=5$, $R/a=1.22$, $f_\alpha=1.0$, $n_{\rm DT}/ne=0.73$, $A_i=2.5$, $\bar{n}_{20}=4.4$, and $C_H=4.0$ in Eqs. (4.32) and (4.33). The multiplier on the beta limit formula, where beta is normalized to the vacuum field, must be set at $g\simeq 20$, assuming the benefit of the total field is above the vacuum level by a factor of about 2.9. Such reactors are very interesting from the point of view of higher power density and lower cost/kWe than conventional tokamaks. They pay the price of relatively high recirculating power and require the central column of the copper toroidal coils to be replaced regularly.

(6) Low-impurity reactor. The allowable fusion power is strongly dependent on the depletion of the D-T fuel, $(n_{\rm DT}/n_e)^{1.62}$ and the radiated power, which is accounted for in f_α. Only if confinement is very good, i.e., C_H large, can significant impurity levels be accommodated. A concern is that under conditions of better confinement it is often observed that impurities accumulate [for example, with counter neutral injection (Stacy *et al.*, 1985)], and edge-localized modes may be necessary to avoid accumulation in the H mode (Post *et al.* 1991). The ability to remove helium effectively is clearly very important.

K. Conclusions

(a) Parameters achieved independently in tokamaks are close to reactor levels; see Table I.

(b) Interesting tokamak reactors appear to be achievable provided present levels of confinement and beta can be sustained without impurity accumulation, with low divertor replacement rates, and without disruptions. However, the present physics base leads to a ~1-GW(e) reactor with a relatively high magnetic field on the toroidal coils ~16 T or more.

(c) With the present physics base, if higher-field coils turn out to be impractical, according to our present understanding of economic factors (mass power density), the economic reactor will be driven to a much larger unit size than ~1 GW(e).

(d) If beta levels can be improved, for example, in the second stable region, lower fields will be permitted at the ~1 GW(e) size.

(e) If better confinement can be achieved, either smaller reactors or reactors with a lower conducted heat flux will be possible.

V. STELLARATOR REACTORS

A. Introduction

A number of reactor studies have been made of a variety of stellarator configurations: Badger *et al.*, 1982; Uo *et al.*, 1983; Miller *et al.*, 1983; Volkov *et al.*, 1984, 1987; Lacatski *et al.*, 1985; Harmeyer *et al.*, 1986; Hubener and Maurer, 1987; Kazawa *et al.*, 1987; Painter and Lyon, 1991; Wobig *et al.*, 1991, 1993. Parameters of some of the recent studies are listed in Table XIII. The studies tend to be less detailed, and to include more *ad hoc* assumptions, than recent tokamak studies, reflecting the much smaller data base available for projecting reactor performance. However, there is an emerging data

TABLE XIII. Representative stellarator reactors.

	Reactor		
	HSR	H-1	ATR-2
Reference	Wobig *et al.*, 1991	Kazawa *et al.*, 1987	Lyon, 1989
Configuration	Helias	$m=15$, $l=2$ Heliotron	$m=9$, $l=2$ Torsatron
Major radius R (m)	20.0	16.0	10.5
Aspect ratio $R/\bar{a}$	12.5	8.0	4.66
Field $B(T)$	5.0	5.0	5.0
Maximum field at coil B_m (T)	10.5	10.0	13.5
Edge (center) transform ι	~0.9	~0.6 (1.5)	0.24 (0.97)
Confinement model	LGS	N.C.+Alcator	N.C.+const. anom.
Average beta $\langle\beta\rangle$ (%)	5	7.3	6.3
$\bar{p}_{wn}$ (MW m^{-2})	1.6	3.1	2.7
Divertor	Open semi-helical	Helical	Helical
Fusion power [MW(t)]	2800	5400	4000
Electric power [MW(e) net]		2000	1900

base supporting empirical scalings similar to those developed for tokamaks (Sudo *et al.*, 1990; Lackner and Gottardi, 1990). And major facilities are in construction (LHD) or proposed (WVII-X), which should be powerful enough to identify more clearly the best route to a viable stellarator reactor.

B. Stellarator characteristics

Reviews of stellarator research include those of Miyamoto (1978), Shohet (1981a, 1981b), Carreras, Grieger, *et al.* (1988), and Lyon (1990). The parameters of some representative stellarators are shown in Table XIV. Stellarators typically achieve parameters comparable to those of a tokamak of similar scale and power density. In today's devices, $\langle n_{20}\rangle \lesssim 3$, $T_{e0} \lesssim 3$ keV, $T_{i0} \leq 2$ keV, $\langle\beta\rangle \lesssim 2\%$, $\tau_E \lesssim 0.03$ s, $B \lesssim 2.5$ T.

A stellarator, in effect, is produced by a loosely wound toroidal solenoid. The open character of the helical windings leads to an average poloidal field and a helical ripple superimposed upon the background toroidal field (B_0) of the solenoid (Miyamoto, 1978; Shohet, 1981a, 1981b). A simple picture of the effect of the helical components can be seen in the case of a linear stellarator, in which the scalar potential ϕ_B and the magnetic field $\mathbf{B}=\nabla\phi_B$ are given in cylindrical coordinates by

$$\begin{aligned}
\phi_B &= B_0 z + \frac{1}{\alpha}\sum_l b_l I_l(l\alpha r)\sin l(\theta-\alpha z)\ , \\
B_r &= \sum_l l b_l I_l'(l\alpha r)\sin l(\theta-\alpha z)\ , \\
B_\theta &= \sum_l \left[\frac{1}{\alpha r}\right] b_l I_l(l\alpha r)\cos l(\theta-\alpha z)\ , \\
B_z &= B_0 - \sum_l l b_l I_l(l\alpha r)\cos l(\theta-\alpha z)\ ,
\end{aligned} \tag{5.1}$$

where l is the number of poles in the magnetic field, i.e., in a poloidal plane the number of separatrices formed at the plasma edge by a field component acting on its own. The helical pitch parameter is denoted by α, and b_l gives the magnitude of the lth component of the field. I_l is the modified Bessel function of the lth order. The magnetic flux ψ is represented by

$$\psi = B_0\frac{\alpha r^2}{2} - r\sum_l b_l I_l'(l\alpha r)\cos l(\theta-\alpha z)\ . \tag{5.2}$$

Representative magnetic surfaces are shown in Fig. 46, for $l=1$, 2, and 3 configurations. Note that, while the last closed flux surface is often referred to as a separatrix, it does not have the same degree of definition as in an axisymmetric system because toroidal effects tend to create a region of ergodic field lines.

TABLE XIV. Representative stellarator experiments.

Operating experiment	ATF	CHS	Heliotron-E	H-1	WVII-AS	Uragan 2M
Configuration	$l=2$, $m=12$ torsatron	$l=2$, $m=8$ heliotron	$l=2$, $m=19$ heliotron	$l=2$, $m=3$ heliac	$l=1,2,3$, $m=5$ mod. stell.	$l=2$, $m=4$ torsatron
Major radius R (m)	2.1	1.0	2.2	1.0	2.0	1.7
Aspect ratio $R/\bar{a}$	7.8	5.0	11.0	4.5	10.0	7.8
Field $B(T)$	2.0	1.5	2.0	1.0	2.5	2.4
Center (edge) transform ι [a]	0.35 (0.97)	0.33 (1.2)	0.5 (2.5)	≤ 1.3	~ 0.4	0.57 (0.75)

Present best parameters (not simultaneous)	Future experiment	LHD	TJ-II	WVII-X
$\langle n_{20}\rangle \sim 3$	Configuration	$l=2$ $m=10$ heliotron	$l=2$ $m=4$ heliac	$l=1,2,3$ $m=5$ helias
$T_{i0} \sim 2$ keV				
$\langle\beta\rangle \sim 2$				
$\tau_E \sim 0.03$ s				
	Major radius R (m) R (m)	3.9	1.5	5.5
	Aspect ratio $R/\bar{a}$ $R/\bar{a}$	6.0	6.8	10.4
	Field $B(T)$	3.0 (4.0)	1.0	3.0
	Center (edge) transform ι [a]	0.35 (0.98)	$\lesssim 2.5$	~ 0.84
	Operation	1998	1994	Proposed
	Reference	Motojima *et al.*, 1991	Alejadre *et al.*, 1990	Grieger *et al.*, 1992

[a]Nominal values are shown; ι profile and level can be varied.

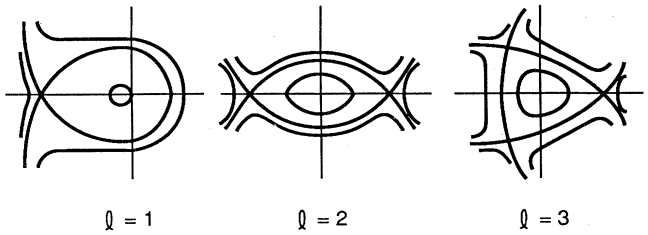

FIG. 46. Representative magnetic flux surfaces for $l=1$, 2, and 3 stellarators.

The poloidally averaged toroidal transform $\iota \equiv i/2\pi = 1/q$ is given in this approximation by

$$\iota \equiv 0.5 \left[\frac{b_l}{B_0}\right]^2 \frac{Rl^3}{3}\frac{d}{dx}\left[\frac{I_l I_l'}{x}\right]_{x=la r} . \tag{5.3}$$

In general, ι is in the opposite direction to that of a tokamak, varying from being lowest on axis (highest q) and rising towards the plasma boundary (lowest q), to being nearly constant.

Stellarators cover a wider range of configuration parameter space than do tokamaks, as illustrated in Fig. 47, which plots global shear ($\Delta\iota/\iota$) versus central transform $\iota(0)$ ($\iota \equiv 1/q$) for a variety of present-day experiments. Within this space, widely varying combinations of magnetic shear, magnetic well, and nonplanar axes are employed in the search for the optimum configuration.

The principal factors that guide stellarator design are the following:

(i) Neoclassical effects in the $1/\nu$ regime of transport, electric-field effects, energetic-particle confinement (the loss cone), and impurity transport, as discussed in Sec. III.B.

(ii) Equilibrium and stability limits, including second stable operation; Pfirsch-Schlüter and bootstrap currents; and the robustness of flux surfaces.

(iii) Practical aspects such as anomalous transport, impurity and particle control, helium ash accumulation, and coil design, e.g., the use of modular coils.

Good progress has been made in the development of theory and computer models and in their connection to experiment, and significant achievements in experimental plasmas have made it possible to focus this diversity of opportunity on two basis types of stellarator. In each approach, a tradeoff is made in the simultaneous optimization of beta, neoclassical transport (anomalous transport), and divertor and coil design.

(1) Stellarators with a spatially varying (helical) axis and a dominant $l=1$ component of the magnetic field form one class. They are characterized by a helical axis, low shear, and a magnetic well that is moderately deep but broad in minor radius. The "helias" device, which exemplifies this configuration (Nuhrenberg and Zille,

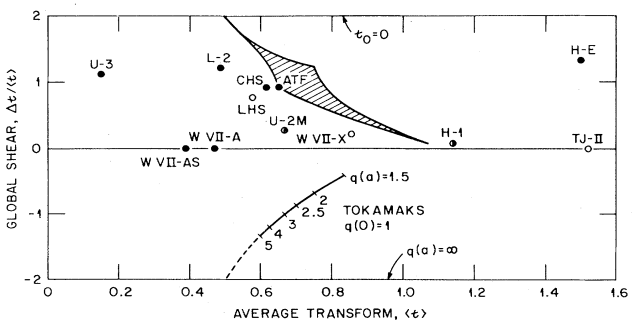

FIG. 47. Shear vs central rotational transform, showing the operating region for a number of existing and proposed stellarators and for tokamaks with $q(0)=1$.

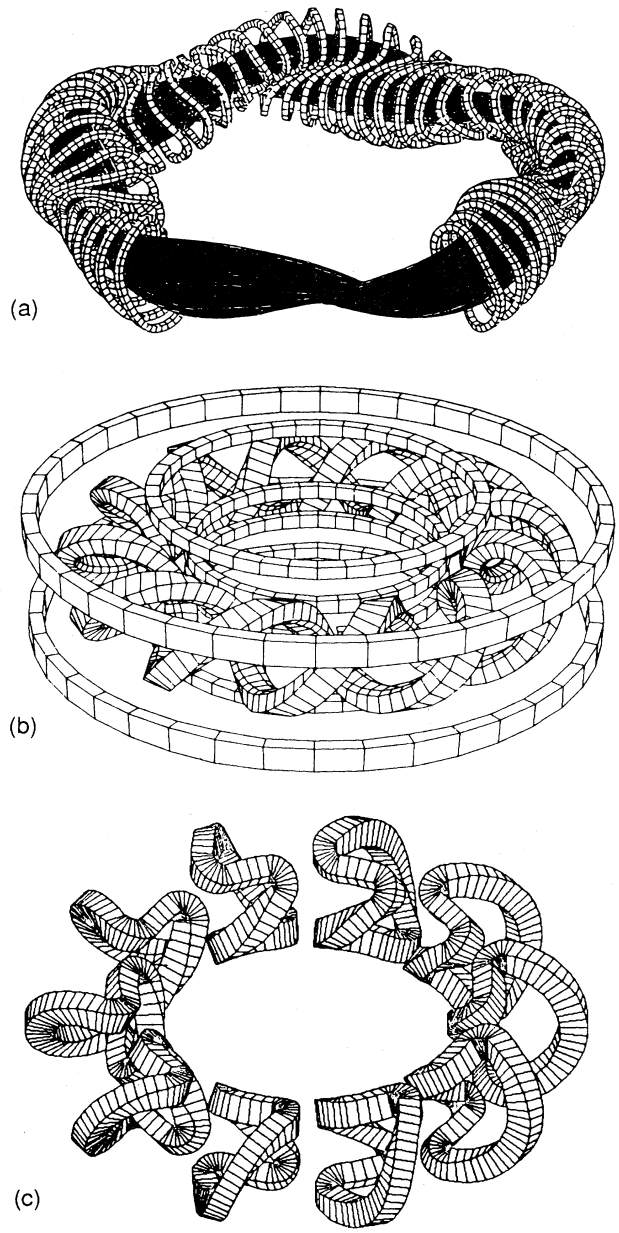

FIG. 48. Stellarator configurations: (a) helias, (b) torsatron/heliotron, (c) modular torsatron.

1986 and 1988), is designed to minimize Pfirsch-Schlüter currents so that the magnetic geometry varies little as the pressure is raised. The fields are configured to emphasize helical symmetry and suppress effects due to toroidicity. Stellarators with four, five, and six periods were studied. A five-period configuration was found to have the optimum combination of reduced low-collisionality transport, shown in Fig. 51 below, good confinement of alphas, maximum beta ($\langle\beta\rangle \simeq 5\%$), and optimized reactor size. A modular coil set, generated by a computer code, produces the configuration shown in Fig. 48(a). An alternative approach, the "heliac," originated by Furth *et al.* (1966), has modular coils, a higher beta capability, but less transport optimization.

(2) The $l=2$ heliotron/torsatron (Uo, 1961; Gourdon *et al.*, 1969) is the second class of device studied extensively as a reactor. It is characterized by moderate and/or high shear and moderate well, and has the virtue that the stable beta is inversely proportional to the aspect ratio. In addition, such devices at moderate aspect ratio may enter the second stable region (Carreras *et al.*, 1983). Maintaining flux surfaces at low aspect ratio, which are robust under the action of increasing pressure, is accomplished by careful tailoring of the helical coils, coupled with detailed control of currents in poloidal field windings (Carreras *et al.*, 1984). Relatively low-aspect-ratio torsatrons have been designed with $R/a \sim 3$. The main limit on lowering the aspect ratio is set by neoclassical transport. The peak in the transport coefficient in the $1/\nu$ regime is reduced by electric-field effects (see Fig. 51 below). However, the loss cone for energetic particles (alphas) is not affected, and a tradeoff must be made between this factor and the other benefits of the system. An example configuration is shown in Fig. 48(b). The device may also be modularized, though this configuration requires relatively sharp bends in the modular coils; see Fig. 48(c).

While stellarator reactor designs with continuous coils have been studied, the preferred option is to use modular coils. In principle, any stellarator magnetic configuration may be constructed from a set of nonplanar toroidal coils, as in the case of the helias. The goal of the program is to find configurations that satisfy the need for a divertor and have good access for maintenance while minimizing the complexity of the coil set. On the experimental front, modular stellarators have been operated successfully, showing a performance as good as any continuous-coil stellarator, notably, IMS (Doerner *et al.*, 1986) and WVII-AS (Jaenicke *et al.* 1993).

The field ratio for most stellarators is in the range $f_B \sim 0.5$ for $R/a > 7$. Sharp bends in modularized coils may reduce f_B.

Since stellarator fields are produced by external coils, the device is inherently steady state, and a plasma will be maintained as long as auxiliary heating (or alpha heating) is applied. In modern stellarators, startup is accomplished using electron cyclotron heating at the first or second harmonics. The plasma is sustained with a combination of electron cyclotron heating, ion cyclotron heating, and neutral beams. In a reactor, alpha power will sustain the plasma. See Sec. V.H for an example.

C. Stellarator transport

Neoclassical transport in toroidal devices is introduced in Sec. III.C. In a stellarator, the magnitude of the field along a field line is modulated by both the toroidal variation and the helical variation (see Fig. 49). This magnetic geometry leads to three classes of particles (Gibson and Taylor, 1967; Miyamoto, 1978; Kovrizhnykh, 1984). As in a tokamak, there are toroidally circulating particles and particles trapped in the magnetic mirrors of the high-field region on the inside of the torus. The third class are particles trapped in the helical field and reflected from its local mirror regions. A helically trapped particle that is also trapped toroidally has an orbit described as a "super banana" (see Fig. 50). An excellent review, comparing tokamak and stellarator transport, has been given by Wagner and Stroh (1993).

Helically trapped particles have drift surfaces that are not closely related to the magnetic surfaces, and they may escape. The characteristics of the transport depend upon the relative magnitude of the toroidal

$$\epsilon_\phi = \left[\frac{B_{\max} - B_{\min}}{B_{\max} + B_{\min}} \right]_t \tag{5.4}$$

and helical ϵ_h ripple. Super banana orbits exist when $\epsilon_h > \epsilon_\phi$, which generally occurs in large-aspect-ratio stellarators. The major new feature of the transport, for $\epsilon_h \gtrsim \epsilon_\phi$, compared to an axisymmetric system, is a substantially *increasing* particle transport as collisionality *decreases,* starting near the plateau-banana transition. For this region Galeev and Sagdeev (1968) derived the diffusion coefficient

$$D_h = \epsilon_h^{3/2} \epsilon_\phi^{1/2} \frac{\omega_0}{\nu_{ei}} \frac{T}{eB} , \tag{5.5}$$

where

$$\omega_0 \equiv \left[\frac{-T}{qB_0 r^2} \right] .$$

A schematic diagram showing the form of the diffusion

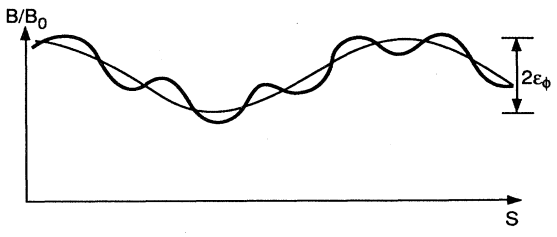

FIG. 49. Variation of the magnetic of the field along a field line in a toroidal stellarator, showing toroidal (ϵ_ϕ) and helical ripple.

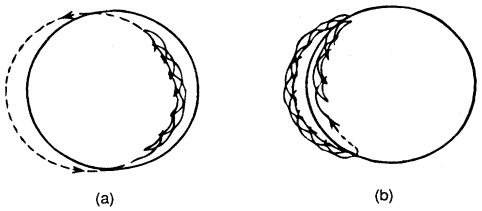

FIG. 50. Trajectories of (a) untrapped bananas and (b) trapped banana (superbanana).

coefficient as a function of collision frequency is shown in Fig. 51. The large level of transport at low collisionalities would make it very difficult to design an economic reactor were it not for the ability to tailor the magnetic geometry (Mynick, Chu, and Boozer, 1982; Nuhrenberg and Zille, 1986, 1988;). These analyses of Mynick *et al.* and of Nuhrenberg and Zille led to the development of the "helias" concept, in which the tailoring of the magnetic field not only improves neoclassical confinement but also optimizes the equilibrium, minimizing the plasma-driven currents and maximizing beta, in a way that is of great interest to reactor design (Nuhrenberg and Zille, 1986, 1988; Grieger *et al.*, 1992; Beidler *et al.*, 1992). Alternatively, the electric fields may reduce transport for, in contrast to a tokamak, stellarator transport does not lead inherently to the same fluxes for ions and electrons. Consequently large radial electric fields may be set up to equalize flows. A simplified formula for the ion thermal diffusivity derived by Shaing (1984) is given in Eq. (3.23).

As in the case of the tokamak, the bulk of the transport in anomalous, though in higher-T_e, lower-n cases neoclassical transport can dominate, as seen in stellarators such as ATF, Heliotron-E, and WVII-AS.

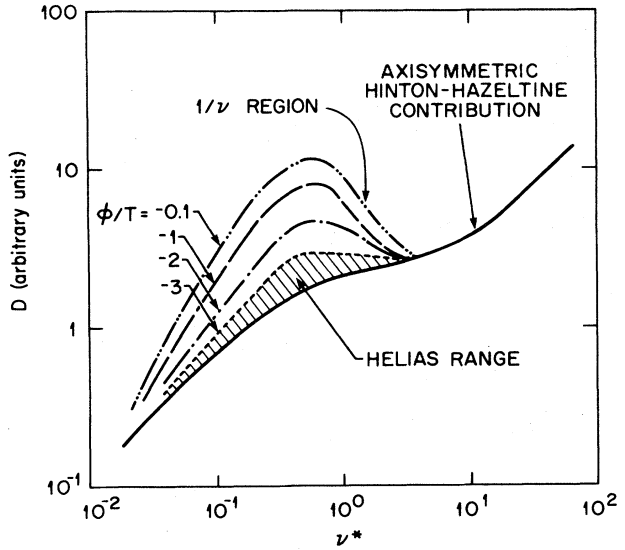

FIG. 51. Typical behavior of the diffusion coefficient D for a stellarator as the collisionality ν^* is varied. The effects of radial potential (ϕ) and magnetic field tailoring (helias) are illustrated.

Some progress has been made in characterizing edge transport in a comparative study with the TEXT tokamak (Wootton, 1991). However, for the plasma core, transport mechanisms are not known, and empirical formulas must be used in combination with neoclassical transport. The radial electric field, produced by the otherwise nonambipolar transport, must be included to ensure an accurate assessment of neoclassical losses (Mynick and Hitchon, 1983).

In general, there are two modes of operation of the reactor, depending on whether ion or electron transport dominates. They vary in the sign of electric field required to restrain the flow of the dominant species. The electric field may be determined self-consistently using the transport equations and a procedure for selecting the correct root (Hastings *et al.*, 1985). The two roots are shown in Fig. 52 for a reference heliotron/torsatron reactor.

In the $1/\nu$ regime, ion losses predominate and a nega-

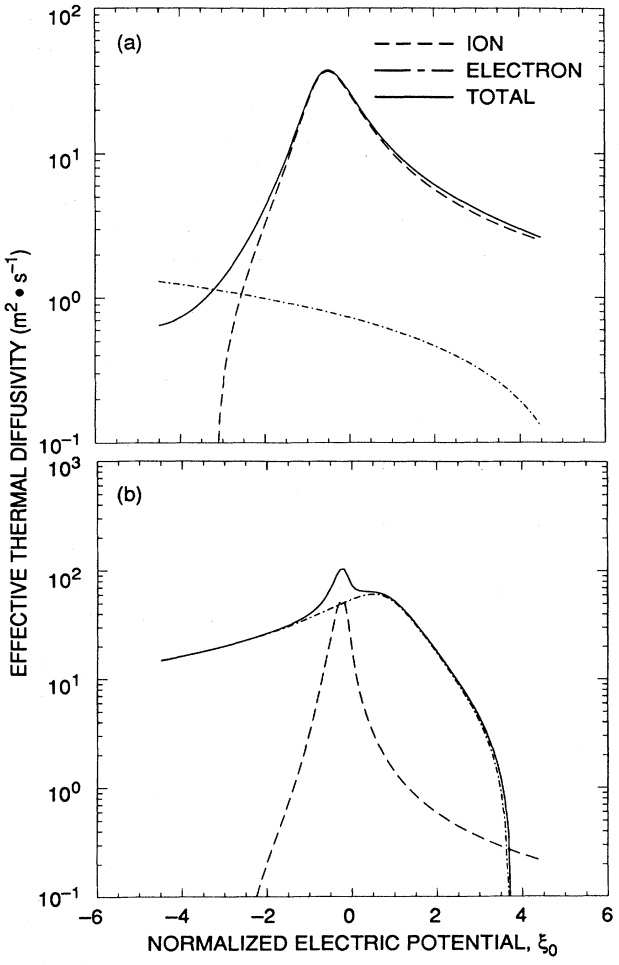

FIG. 52. Effective thermal diffusivity vs normalized electric potential for an $R/a=5$ heliotron-torsatron reactor: (a) at moderate collisionality ($\langle T\rangle=10$ keV, $\langle n\rangle=2\times10^{20}$ m^{-3}); and (b) at low collisionality ($\langle T\rangle=30$ keV, $\langle n\rangle=7.5\times10^{19}$ m^{-3}) (Painter and Lyon, 1991).

tive electric field is formed—the ion root. In a reactor this root tends to occur at high density ($>10^{20}$ m^{-3}) and low temperature (~ 10 keV).

In the collisionless detrapping regime, electron losses dominate, producing a positive electric field—the electron root. In a reactor, this root tends to occur at low density ($\lesssim 10^{20}$ m^{-3}) and high temperature ($\gtrsim 20$ keV). Because different parts of the plasma may be in different regimes, the electric field may vary in sign across a radius.

The experimental data from modern stellarators fits empirical scalings similar to those found in tokamaks [Eq. (4.21)].

The so-called large helical device (LHD) scaling (Sudo *et al.*, 1990) is

$$\tau_E^{\rm LHD}=0.17C_E\bar{n}_{20}^{0.69}B^{0.84}a_p^2R^{0.75}/p^{0.58}\ ({\rm s})\ , \qquad (5.6)$$

where $\bar{n}_{20}$ is the line-averaged density (10^{20} m^{-3}), B (T) is the axial field, a_p (m) is the average minor radius of the plasma, R (m) is the major radius, and P (MW) is the heat deposited in the plasma. The data show better-than-average performance; a factor C_E is included to allow for enhanced modes of confinement being established on a more regular basis, as in the tokamak H, VH, and supershot modes. There are encouraging data from WIII-AS (Jaenicke *et al.*, 1993) showing signs of improved performance and H-mode-like characteristics.

The formula has some interesting similarities to that expected from trapped-particle drift-wave turbulence and ripple-induced neoclassical transport (Painter and Lyon, 1991). In terms of dimensional scaling [see Eq. (3.47)], $\tau_E^{\rm LHD}\propto B^{-0.61}$ rather than the correct $B^{-1.0}$. Therefore modifications may be expected as more data are produced.

The Lackner-Gottardi (1990) plateau scaling, developed for tokamaks, is a good fit to WVII-A and WVII-AS data. It has the virtue of being dimensionally correct:

$$\tau_E^{\rm LGS}=0.17C_{\rm LG}\langle n_{20}\rangle^{0.6}\ell^{0.4} \times B^{0.8}a_p^2R\left[\frac{A_i}{1.5}\right]^{0.5}\Big/P^{0.6}\ ({\rm s})\ . \qquad (5.7)$$

The evidence for a positive A_i dependence is very limited, and in calculations below the term $(A_i/1.5)$ is set equal to unity.

The two scalings above are gyroreduced Bohm in form, as discussed at the end of Sec. III.C. A formula that fits ATF data is

$$\tau^{grB_m}\simeq\{0.35(\bar{n}_{20})^{0.6}R^{0.8}a_p^2R^{0.6}(A_i)^{-0.2}/P^{0.6}\} \times\{\nu_*^{-0.174}\langle\beta\rangle^{0.314}\}\ . \qquad (5.8)$$

The improvements in confinement with decreasing collisionality and increasing $\langle\beta\rangle$ are seen in experiments in which one is modulated and the other held constant (Murakami *et al.*, 1993).

As in the case of the tokamak, impurity accumulation may be a problem. Theoretically this may occur with the negative electric field of the ion root, while impurities may be expelled with the electron root (Shaing, 1983). There is some experimental evidence for this behavior in Heliotron-E (Obiki *et al.*, 1989). More work is required to find the optimum transport conditions that avoid impurity accumulation.

In the case of the torsatron-heliotron it is possible to modulate the poloidal field so as to form a central separatrix periodically, and temporarily enhance transport to eject helium ash and impurities (Lyon *et al.*, 1986).

D. MHD and density limits

The general MHD behavior of toroidal systems is introduced in Sec. III.C. The dominant mode for a stellarator is an interchange instability. Ballooning instabilities, which occur locally in the outer regions of poor magnetic curvature, are the primary limit on stability in the helias, with resistive effects coming into play at lower beta in the colder plasma edge. In the torsatron-heliotron, ballooning modes also play an important role and the interchange modes are unstable in the edge region owing to the lack of a magnetic well. The plasma equilibrium beta is limited by the shift of the plasma axis caused by Pfirsch-Schlüter currents, which increase with increasing plasma pressure. Optimized designs, which minimize Pfirsch-Schlüter currents, maximize the equilibrium limit, and minimize MHD activity, have predicted beta limits in the range of ~ 4–$5\,\%$ (Boozer, 1983; Carreras *et al.* 1983; Nuhrenberg and Zille, 1986, 1988).

The Pfirsch-Schlüter effect does not yield a net current:

$$j_\phi^{\rm PS}\simeq\frac{2}{\iota}\frac{\cos\theta}{B}\frac{dp}{dr}\ . \qquad (5.9)$$

On the other hand, the bootstrap current does. Shaing *et al.* (1989) give the formula

$$j_{\rm BS}=-3\left[\frac{f_t}{f_c}\right]G_b\frac{\nabla p}{B_\theta}\ , \qquad (5.10)$$

where f_t and f_c are the fractions of trapped and recirculating particles and G_b is a magnetic geometry factor (for a tokamak $G_b=1$). Measurements of these currents, showing agreement with theory, were made by Treffert *et al.* (1984).

Care must be taken to ensure that the bootstrap current does not become large enough to degrade the magnetic configuration. By careful adjustment of the magnetic geometry the current can be made zero or reverse sign (Murakami *et al.*, 1990).

The resistive interchange modes can lead to increased transport, as has been observed in ATF (Harris *et al.*, 1993).

The density limit in stellarators is related to having enough heating power to overcome radiation and conduction losses. At quite modest fields, $\lesssim 2$ T, densities of greater than 10^{20} m^{-3} are obtained. If inadequate power is applied, the energy content decays when the density is

raised—a "soft disruption" (Isler *et al.*, 1991). An empirical formula for the limit has been developed by Sudo *et al.* (1990),

$$\bar{n}_{m20} \simeq 0.25[P(\mathrm{MW})B(\mathrm{T})/a^2R]^{0.5} . \quad (5.11)$$

Beta self-stabilization of Mercier modes is possible in stellarators with shear (Carreras *et al.*, 1983; Shafranov, 1983). The condition for stability against interchange modes may be written as

$$\underset{\text{shear stabilization}}{\frac{1}{4}\hat{s}^2} + \underset{\text{pressure gradient driving}}{\frac{\rho}{B^2\iota^2}\frac{dp_0}{d\rho}}\left[\underset{\text{vacuum field curvature}}{RB^2V_0''} - \underset{\text{axis effect on } V''}{\frac{d(\rho^3\iota')}{d\rho}\frac{\Delta_p}{\iota\rho^3}}\right] \geq 0 . \quad (5.12)$$

Self-stabilization occurs when the axis shift is sufficient to overcome the effects of vacuum field curvature and suppress the pressure gradient driving term. This effect may allow access to the so-called second stable region, as illustrated in calculations for fixed profiles for ATF, shown in Fig. 53. The suppression of interchange modes as beta is raised has been observed in ATF, for a case with field errors and extremely peaked pressure profiles (Harris *et al.*, 1989, 1990). However, stability to ballooning modes can limit access (Cooper *et al.*, 1989), and further optimization is required, including the effects on stability of plasma flow.

E. Alpha-particle effects

The general effects of energetic alphas are discussed in Sec. II.F. The primary differences from the tokamak are the lack of the kink instability and the addition of a potentially severe loss cone owing to the nonaxisymmetric field. The potentially severe losses of alphas are a strong driver in stellarator reactor design, and careful optimization of the magnetic configuration must be used to reduce both thermal losses and alpha-particles losses (Nuhrenberg and Zille, 1988; Grieger *et al.*, 1989; Painter and Lyon, 1989, 1991). In the helias reactor, it is possible to reduce alpha losses to a very low level (Lotz *et al.*, 1992). The reduction in losses occurs because, as beta is raised, the increase in poloidal magnetic drift improves the confinement of trapped alpha particles; see Fig. 54. For the torsatron-heliotron the losses are more severe. However, the presence of a loss cone may be an advantage if the majority of the contained energetic alphas are lost when they start to scatter into the loss regions, thereby reducing helium accumulation problems. On the downside, protection must be provided for the wall in regions bombarded by the energetic alphas to prevent unacceptable damage An example of the effect of alpha losses, both direct and scattered, is shown for a reference torsatron-heliotron reactor in Fig. 55. The alpha-driven instabilities discussed for the tokamak in Sec. IV.G may also be important for stellarators—toroidal Alfvén modes for $v_\alpha \geq v_A$, and modified ballooning mode stability.

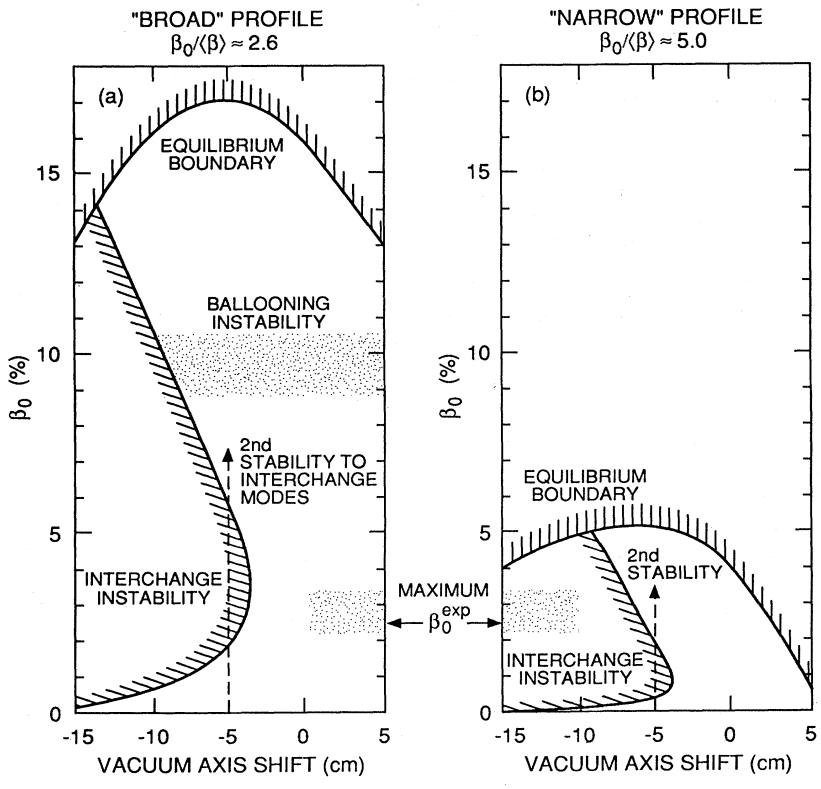

FIG. 53. Second stability region in the standard ATF configuration (a) at high beta for the broad pressure profile assumed in the original design study and (b) at the lower beta for the peaked pressure profiles obtained in the 1988 experiments. Beta self-stabilization (stability increasing with increasing beta for Mercier modes) occurs for $\beta(0) \sim 4\%$ in (a) and for $\beta(0) \sim 1\%$ in (b) (Lyon, 1990). Ballooning mode predictions for optimized pressure profiles in the standard configuration limit the attainable beta (Cooper *et al.*, 1989). The maximum experimental beta achieved for both cases, with moderate heating power, is indicated.

F. Power and particle control

Generic issues for power and particle handling are discussed in Sec. II.G. As in the case of tokamaks, the divertor is the preferred solution for the stellarator. For a continuous-coil system, such as the heliotron and/or torsatron, the plasma flux is naturally diverted between the continuous helical coils (Uo *et al.*, 1983; Iiyoshi *et al.*, 1990; see Fig. 56). The separatrix is not as clearly defined as in a tokamak, owing to field ergodization at the boundary. Nevertheless, diverted flux is observed clearly in experiments (Anderson and Bartlitt, 1989; Obiki *et al.*, 1990; Matsuura *et al.*, 1992). The situation for a modular stellarator is more complex, but here, too, techniques for forming a helical divertor and for diverting flux bundles have been formulated (Strumberger, 1992; Grieger *et al.*, 1992).

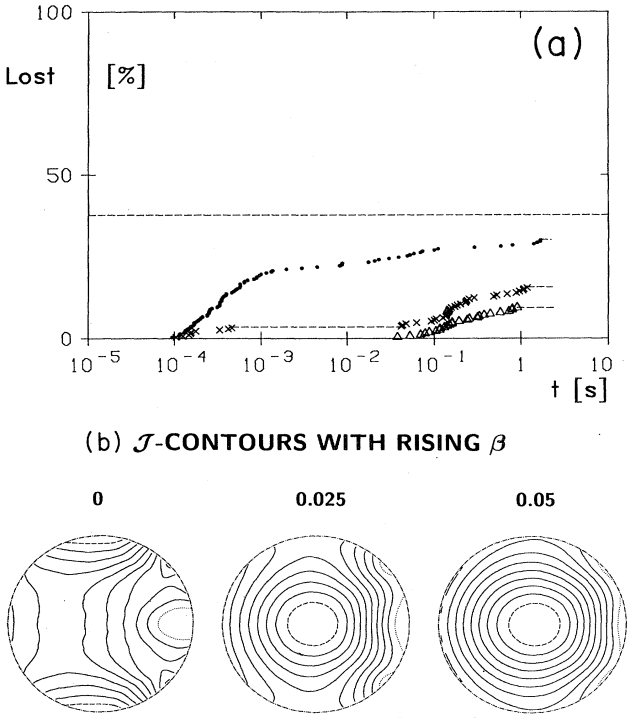

FIG. 54. Characteristics of α-particle losses and magnetic geometry in a Helias configuration, as a function of beta. (a) Collisionless α-particle losses in Helias 50B one of the configurations obtained while optimizing helias configurations for W7-X and characterized by a special structure of B with $\langle\beta\rangle=0$ (○), 0.024 (×), and 0.049 (△); α particles started at aspect ratio 40 and the loss is shown as a function of the collisionless time of flight. Each symbol indicates the loss of one particle. The number of reflected particles is 100 in all cases. Altogether there are 265 particles, i.e., 165 passing particles, (Lotz *et al.*, 1992). (b) Constant-J contours in Helias 50B with $\beta=0$, 0.024, and 0.049. Shown is a $\sqrt{s}$, θ plane with s the flux label and θ the poloidal magnetic coordinate. Dashed lines indicate region close to maxima, dotted lines those close to minima. The reflection value of B is a constant and defines the reflected particles considered as moderately deeply trapped (Lotz *et al.*, 1992).

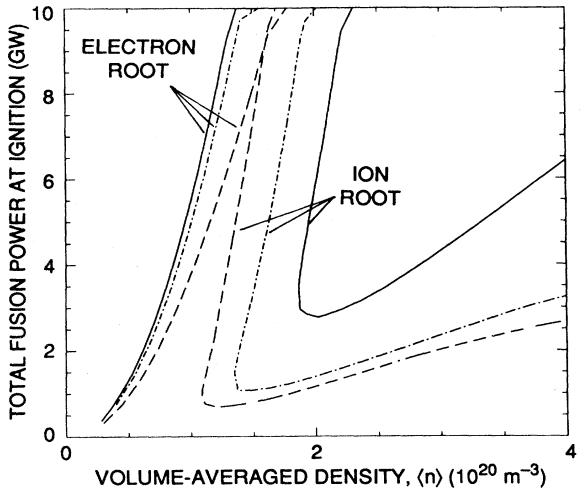

FIG. 55. Effect of alpha-particle losses on the ignition contour for a reference torsatron reactor operating in the electron or ion root mode: dashed curves, without alpha-particle losses; solid curves, all trapped alpha particles lost; chain-dashed curves, only scattered alpha-particle losses (Painter and Lyon, 1991).

Stellarator control is in a much earlier stage of development than that for tokamaks, and tests in existing and proposed facilities are crucial to establishing viable control systems.

Fueling requirements are similar to those in tokamaks, and pellet injection has been used on ATF, Heliotron-E, and WVII-A.

G. Computer modeling

Codes are available similar to those used for tokamaks e.g., a revised version of the WHIST code (Houlberg, 1982; Lacatski *et al.*, 1985), which incorporates a self-consistent calculation of the electric field, and HTRANS (Yamazuki and Amano, 1990). An example set of plasma operating contours (POPCONs) is shown in Fig. 57.

H. Stellarator reactor options

The parameters of some representative reactor designs are given in Table XIII. The options may be understood by using reference values for χ_E with the Lackner-Gottardi scaling, Eqs. (5.7), (2.27), and (2.42), and various values of beta (2.5 to 10%) in Eqs. (2.45) and (2.46), with a fixed value for $B_{\max}$ and $f_B \simeq 0.5$, for $R/a_p \gtrsim 5$:

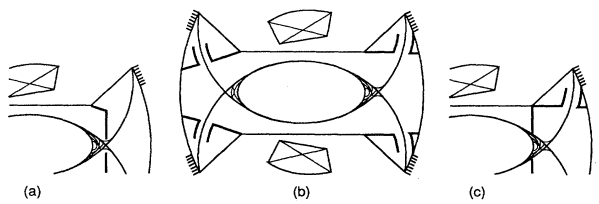

FIG. 56. Examples of baffle plate designs for the Large Helical Device divertor (Iiyoshi *et al.*, 1990).

TABLE XV. Values of $B(T)$ for typical stellarators.

$\langle\beta\rangle\%\backslash C_{LG}$	1	1.5	2.0
2.5	8.5	9.3	9.9
5.0	5.6	6.2	6.6
7.5	4.4	4.9	5.2

TABLE XVI. Values of P_F (GW) for typical stellarators, $\langle\beta\rangle=5\%$.

$R/a_p\backslash C_{LG}$	1	1.5	2.0
5.0	6.6	3.2	1.9
7.5	7.4	3.5	2.1
10.0	8.0	3.8	2.3
12.5	8.5	4.1	2.4

$$P_F=\frac{734(a_w/a)^{0.818}(R/a_p)^{0.273}(\bar{p}_{wn})^{0.818}\langle\beta\rangle^{0.727}}{C_{LG}^{1.82}(\bar{n}_{20})^{1.09}\ell^{0.727}f_\alpha^{0.727}\left[\frac{n_{DT}}{n_e}\right]^{1.27}}\ (\mathrm{MW}) \tag{5.13}$$

and

$$B=\frac{7.72(R/a_p)^{0.91}(a_w/a)^{0.263}(\bar{p}_{wn})^{0.263}(\bar{n}_{20})^{0.136}\ell^{0.091}f_\alpha^{0.091}C_{LG}^{0.228}}{\langle\beta\rangle^{0.591}\left[\frac{n_{DT}}{n_e}\right]^{0.341}}\ (\mathrm{T})\ . \tag{5.14}$$

For more peaked pressure profiles, the performance would be better; e.g., if there were a 20% higher P_F for a given beta, the multipliers in Eqs. (5.13) and (5.14) would be, respectively, 661 and 7.46.

Since $\bar{n}_{20}$ and $\langle\beta\rangle$ may be specified independently, it is necessary to confirm for a particular set of values that the average temperature $\bar{T}\gtrsim 7.5$ keV to justify the use of the formula for D-T fusion power.

(1) Note first that for the Lackner-Gottardi scaling the field (B) depends weakly on most parameters except $\langle\beta\rangle$. For example, if $a_w/a=1.1$, $\ell=0.7$, $\bar{p}_{wn}=2.5$ MW m^{-2}, $R/a_p=7.5$, $\bar{n}_{20}=7.5$, $\bar{n}_{20}=2.5$, $f_\alpha=0.8$, $n_{DT}/n_e=0.73$, and $\langle\beta\rangle$ and C_{LG} are varied, B has the values shown in Table XV. $A_i/1.5$ has been set at unity in Eq. (5.7).

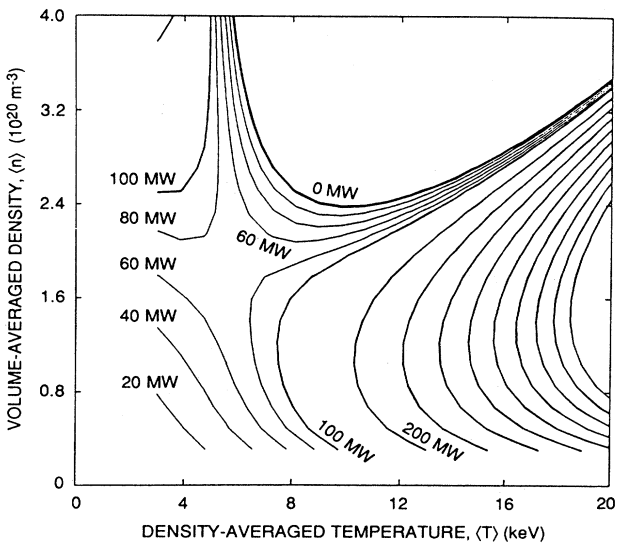

FIG. 57. Plasma operating contour (POPCON) plot for a torsatron obtained with the global LHD confinement model and $C_E=1.5$ (Painter and Lyon, 1991).

Since $f_B\simeq 0.5$, if $\langle\beta\rangle\simeq 5\%$, $B_{max}\simeq 13$ T. These parameters and those in Table XVI encompass the parameters of the torsatron-heliotrons shown in Table XIII.

(2) The fusion power P_F depends strongly on the enhancement factor C_{LG}. For $\langle\beta\rangle\simeq 5\%$ and the parameters above, enhancement (~ 1.5 to 2.0 times) is needed to bring the power down to a respectable level ($\lesssim 4$ GW) as shown in Table XVI. The formula in Eqs. (5.13) and (5.14) may be used to calculate helias reactor parameters. For $R/a_p=12.5$, $\ell=0.9$, $\bar{p}_{wn}=1.6$ MW/m^2, $n_{DT}/n_e=0.80$, $f_\alpha=0.9$, $a_w/a=1.1$, $\langle\beta\rangle=5\%$, and including the atomic mass term $(A_i/1.5)^{0.5}$ in the Lackner-Gottardi scaling with $A_i=2.5$ leads to a reactor of major radius $R=19$ m and fusion power $P_F=1830$ MW.

(3) Care must be taken to ensure that $\bar{\chi}_e^{LG}>\bar{\chi}_{iNc}$, Eq. (3.23). For the example above with $R/a_p=7.5$, $C_E=2$, $\langle\beta\rangle=5\%$, the stellarator parameters are $R=11.0$ m, $a_p=1.46$ m, $\bar{T}_k\simeq 11.6$ keV, $\tau_E\simeq 1.63$ s, and $\bar{\chi}_E^{LG}\simeq 0.50$ m^2 s^{-1}. To ensure $\bar{\chi}_E^{LG}>\bar{\chi}_{iNc}$ requires $f_E=\phi/T\gtrsim 2$.

(4) The density and temperature dependences of Large Helical Device scaling factor the ion root, i.e., high density and moderate temperature. To obtain reasonable values of P_F typically requires $C_{LG}\simeq 1.5$ to 2. Note that the ion root should be more satisfactory for alleviating divertor problems, but may be limited by impurity accumulation problems.

(5) The auxiliary power required to raise the plasma temperature to ignition may be calculated using Eq. (2.75). [The simple formula (2.77) may not be used because the temperature dependences of Lackner-Gottardi losses and alpha heating are similar.] To obtain a reference value of power, the temperature $\langle T_k\rangle=3.5$ is used for the example above, $R/a_p=7.5$, $C_{LG}=2$, $\langle\beta\rangle=5\%$, $Z_{eff}=1.8$ and $n_{DT}/n_e=0.8$,

$$P_a\simeq 27+54-41=40\ \mathrm{MW}\ .$$

Additional power is required to raise the temperature in a reasonable length of time, say +20 MW, giving a total $P_a = 60$ MW.

(6) In stellarators, alpha power loss varies from negligible (helias) to ~40% in some torsatron-heliotron designs. Configurations with a high loss remove essentially all of the alphas before they thermalize. Therefore there should be less dilution of the D-T fuel fraction owing to accumulation of helium (assumed to lead to a 10–20% dilution in ITER). Assuming the high-loss cases have negligible dilution, the reactor size might have to be increased by 2% to 10% for 40% losses, when compared to a 5% loss case, depending on design.

I. Conclusions

(1) Stellarator reactors at the 1-GW*e* level, are viable from an ignition point of view provided.

(a) An enhancement factor of $C_{LG} \simeq (1.5-2)$ can be obtained for Lackner-Gottardi scaling and $A_i/1.5 = 1$.

(b) There is a radial potential factor $f_E \gtrsim 2$ for torsatron-heliotron reactors.

(c) $\langle \beta \rangle \gtrsim 5\%$ for $B_{max} \lesssim 13$ T.

(2) For the Lackner-Gottardi scaling the ion root is favored (higher density and moderate temperature), which is good for divertor operation. Further research is required to determine the optimum conditions which will be free of impurity accumulation.

(3) The development of a stellarator reactor is on a longer time scale than that for tokamaks because TFTR-scale devices have not yet been operated. Successful operation of large devices such as the large Helical Device and WVII-X would give confidence in the underlying physics and permit consideration of a D-T-burning stellarator. The combined output of such a stellarator and ITER would be required to proceed to a demonstration stellarator reactor.

VI. REVERSED-FIELD-PINCH REACTORS

A. Introduction

The first type of magnetic fusion reactor to be patented was a pinch device (Thomson and Blackman, 1952). It was a simple toroidal pinch with a traveling-wave approach proposed to drive the toroidal current. Such devices were found to suffer from severe instabilities. The stability was improved by the addition of a weak toroidal magnetic field. However, the plasma remained turbulent and confinement was poor. Development of an interesting concept came from the discovery of a quiescent mode in the ZETA pinch experiment (Robinson and King, 1969). Subsequently, Taylor (1974, 1976), showed that the mode was a result of the magnetic field and plasma configuration's relaxing to a maximum energy state in which the toroidal magnetic field reversed sign as a function of the minor radius. This work accompanied a growth of interest in the reversed-field pinch (RFP). Excellent reviews of the subject have been written by Baker and Quinn (1981), Bodin *et al.* (1986), Taylor (1986), Baker (1988), Miyamoto (1988), Ortolani (1988, 1989), and Bodin (1990). An isometric sketch of the CRFPR reactor is shown in Fig. 58.

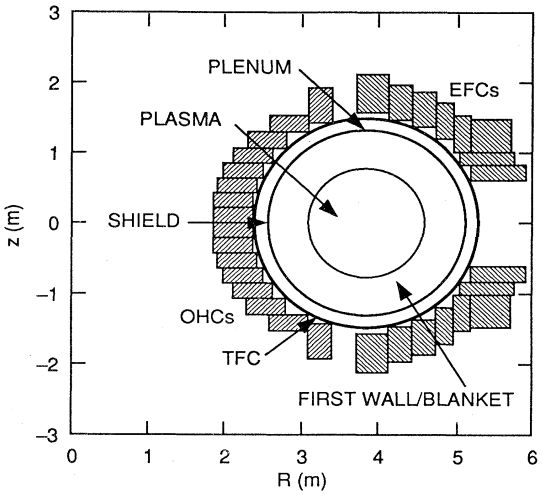

FIG. 58. Isometric sketch of CRFPR fusion power core. The reactor torus, defined as the plasma chamber, first wall, limiter, blanket, shield/structure, and toroid field coils, is installed and replaced as a single 400-tonne unit, drained of Li-Pb coolant (Hagenson and Krakowski, 1981).

B. RFP characteristics

The RFP is an axisymmetric magnetic-field configuration in which $B_\theta \gg B_\phi$ outside the plasma and $B_\theta \simeq B_\phi$ inside the plasma. The poloidal field (B_θ) is generated by a toroidal plasma current. The toroidal field (B_ϕ) is produced mainly by currents flowing in the plasma and partly by external coils. The reversed toroidal field shown in Fig. 59 is generated by a relaxation process, and it is sustained by the continued efforts of the configuration to remain in the minimum energy state—the dynamo effect.

1. Plasma startup

The RFP plasma is created in a thin-walled metal torus using an inductively driven plasma current. Normally, a thick-walled metal liner surrounds the torus and provides short-term stability. In early experiments, the pulse length was relatively short ($\lesssim$ ms), and the plasma characteristics depended strongly on the initial hydrogen filling pressure. In modern experiments the pulse length has been extended to tens of ms and the plasma density has been controlled using wall-conditioning techniques, gas puffing, and pellet injection (Wurden *et al.*, 1987). In some experiments the thin metal wall has been protected

TABLE XVII. Parameters of representative RFPs.

Experiment	ZT-40	MST[a]	HBTX	PBE-IR(M15)	RFX[b]
Major radius R (m)	1.14	1.50	0.8	0.72	2.0
Major radius a (m)	0.20	0.52	0.26	0.135	0.50
Peak current I (MA)	0.45	0.6(1.0)	0.50	0.2	2.0
Pulse length τ_{pulse} (ms)	$\lesssim 40$	<80	$\lesssim 14$	$\lesssim 0.8$	250
Average density n ($\times 10^{20}$ m^{-3})	0.1–1.0	0.1	0.1–1.0	0.1–1.0	
Axial electron temperature T_{e0} (keV)	500	350	450	600	
Axial ion temperature T_{i0} (keV)	500	300	450	600	
Poloidal beta β_θ	0.1–0.2	<0.17	0.1–0.2	~ 0.1	
Energy confinement time τ_E (ms)	$\lesssim 0.8$	1.5	$\lesssim 0.4$	~ 0.1	

[a]Initial operation.
[b]Beginning operation.

by graphite tiles. The parameters of some modern experiments are shown in Table XVII.

A weak B_ϕ field is applied prior to initiation of the plasma current. It is common practice, but not essential, to assist the field reversal by, for example, control of the toroidal field. This action can minimize the use of the poloidal flux converted to toroidal field by the dynamo action and maximize the poloidal flux inductively converted to toroidal plasma current. Because the reversal is sustained naturally by the dynamo effect (see below), and the plasma current provides the heating, the pulse length is determined by volt-second consumption, unless a noninductive current drive is used. It is observed that the volt-seconds used in startup increase with decreasing rate of rise of plasma current (Bodin *et al.*, 1986; Phillips *et al.*, 1988).

The resistivity (η) exceeds the Spitzer value, Eq. (4.5), by more ($\gtrsim 2$ times) than the correction due to impurities. There is evidence (Bodin, 1990) that the excess resistance may depend on edge effects connected to field errors and the equilibrium position of the plasma. For example, the plasma resistance increased when a carbon tile was inserted into the plasma, in proportion to the amount of flux intercepted. Some theoretical models invoke helicity dissipation in the plasma edge (Jarboe and Alper, 1987; Ho *et al.*, 1989; Ho and Prager, 1991) and momentum transport by energetic electrons (Moses *et al.*, 1988), to explain the phenomenon. Situations in which there is strong ion heating, and even $T_i/T_e > 1$, appear to be a consequence of the anomalous resistivity (see Fig. 60). The power density may be written as

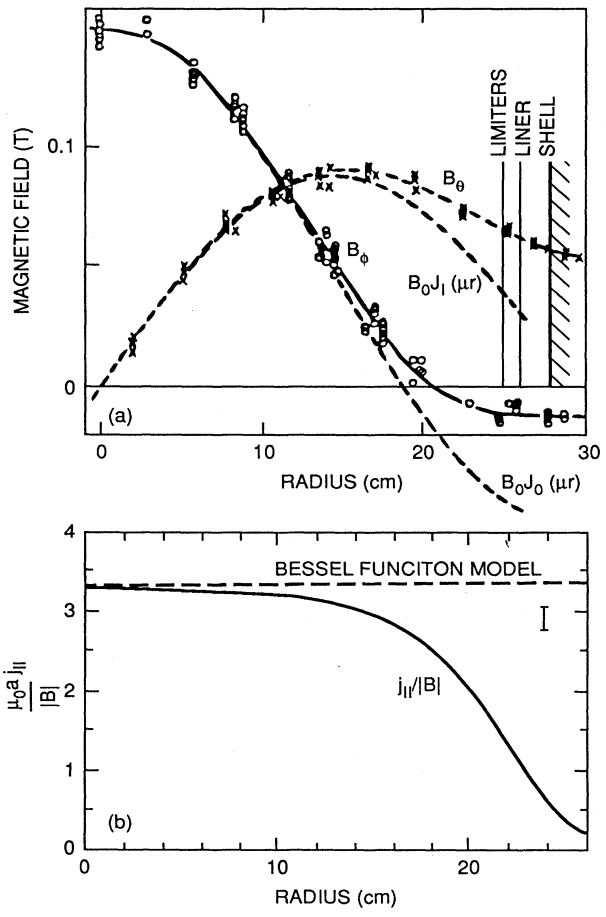

FIG. 59. Comparison of theoretical and experimental magnetic-field profiles for an RFP. (a) Experimental RFP magnetic-field profiles and profiles from the Bessel-function model; (b) corresponding μ profiles.

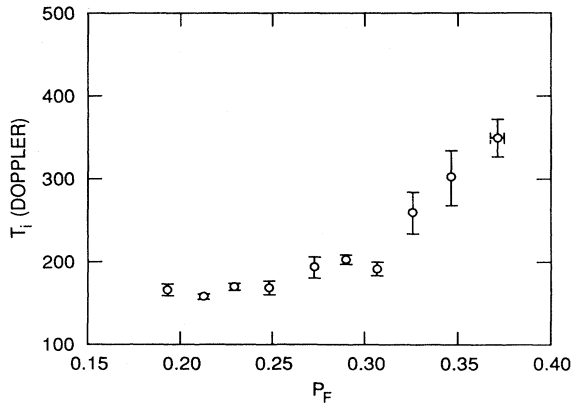

FIG. 60. Ion temperature T vs fluctuating power absorption P_F in ZT-40 (Schoenberg *et al.*, 1989).

$$\langle \mathbf{E} \rangle \cdot \langle \mathbf{i} \rangle = \langle \eta j^2 \rangle + \langle \tilde{u} + \tilde{B} \rangle \cdot \langle \mathbf{i} \rangle \ , \qquad (6.1)$$

Resistive Dynamo ,

where the first term heats the electrons and the second heats the ions. The latter effect should ease the attainment of ignition. Alternative explanations of the phenomenon center on viscous damping of tearing fluctuations and nonviscous damping of small-scale waves (Mattor *et al.*, 1992).

2. Relaxed states

The presence of turbulence and a small resistivity allow magnetic-field lines in a plasma to reconnect and self-organize into a state of minimum magnetic energy, when subject to certain constraints (Taylor, 1986). The force-free fields, current everywhere parallel to the magnetic field, with $\beta=0$, are described by

$$\nabla \times \mathbf{B} = \mu \mathbf{B} \ , \qquad (6.2)$$

where a uniform μ represents the lowest magnetic energy in a closed system with constant total magnetic helicity (Woltjer, 1958). In particular, in a toroidal pinch surrounded by an ideal conducting shell, the toroidal flux is conserved and a minimum energy state can be found where the only other constraint for a resistive plasma is that of total magnetic helicity invariance. An example of helicity-conserving reconnection is shown in Fig. 61.

The total magnetic helicity is given by

$$K_0 = \int_{V_0} \mathbf{A} \cdot \mathbf{B} dV \ , \qquad (6.3)$$

where the vector potential is given by $\mathbf{B} = \nabla \times \mathbf{A}$.

The solution of the equations for uniform μ in a large-aspect-ratio torus of circular cross section is referred to as the Bessel-function model. For low beta,

$$B_\theta = B_{\theta 0} J_1(\mu r), \quad B_\phi = B_{\phi 0} J_0(\mu r), \quad B_r = 0 \ . \qquad (6.4)$$

For finite β_θ,

$$\left[\frac{B_{\phi 0}}{B_{\theta 0}} \right]^2 = 1 - \beta_\theta \ .$$

The parameter (μ) and the radius of the flux-conserving boundary are related by

$$\mu a = 2\theta \ , \qquad (6.5)$$

where the pinch parameter is given by

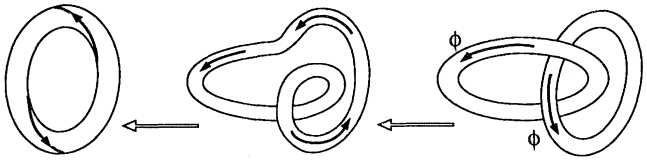

FIG. 61. Example of helicity-conserving reconnection between two flux tubes (Ortolani, 1988).

$$\theta = \frac{B_\theta(a)}{\langle B_\phi \rangle} \propto \frac{\mu_0}{2} \frac{aI}{\phi} \ . \qquad (6.6)$$

Here ϕ is the toroidal flux. Field reversal occurs when $\theta > 1.2$. It is customary to describe RFP operation in terms of θ and F, the field-reversal parameter,

$$F = \frac{B_\phi(a)}{\langle B_\phi \rangle} \ . \qquad (6.7)$$

A consequence of the theory is that if the current is sustained at a high enough level there will be continuous reversed-field generation (dynamo effect). This is observed experimentally; see Fig. 62 (Caramana and Baker, 1984). The nonlinear MHD calculations of Caramana *et al.* (1983) and Caramana and Schnack (1986) have been very successful in explaining the detailed dynamics of the dynamo and fluctuations (Watt and Nebel, 1983). The experimental field profiles do not have μ=constant near the plasma edge $\{\mu \simeq \mu_0[1-(r/a)^\alpha]\}$, owing to finite beta and resistivity effects. Nevertheless, the theory predicts the experimental equilibria well.

3. Equilibrium

In a large-aspect-ratio RFP the radial pressure balance is

$$\frac{d}{dt} \left[p + \frac{B_\theta^2 + B_\phi^2}{2\mu_0} \right] + \frac{B_\theta^2}{\mu_0 r} = 0 \ . \qquad (6.8)$$

With zero pressure at the plasma boundary (a) this reduces to

$$\beta_\theta = 1 + \frac{[B_\phi^2(a)]^2 - \langle B_\phi^2 \rangle}{(B_\theta(a))^2}$$

$$= 1 + \frac{1}{\theta^2} \left[F^2 - \frac{\langle B_\phi^2 \rangle}{\langle B\phi \rangle^2} \right] \simeq \left[1 + \left[q \frac{R}{a} \right]^2 \right] \ . \qquad (6.9)$$

More accurate calculations yield $\beta_\theta \simeq 2\beta$ (Bodin *et al.*, 1986), where β is the beta, normalized to the total field. The poloidal beta is typically in the range 0.1–0.2, which is lower than the limits predicted by resistive MHD theory. The tendency of the plasma to expand in major

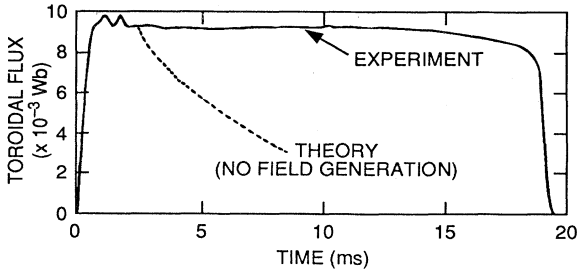

FIG. 62. Time variation of toroidal flux: measurement and calculation with no reversed-field generation (no dynamo) for ZT-40M, illustrating the dynamo effect (Caramana and Baker, 1984).

radius may be counteracted by image currents in a conducting shell or by an applied vertical field (B_v). The radial displacement in steady state, typically a few percent of the minor radius, is

$$\delta=\frac{a_c^2}{2R}\left[\left[\beta_\theta+\frac{(l_i-1)}{2}\right]\left[1-\frac{a^2}{a_c^2}\right]+\ln\left[\frac{a_c}{a}\right]\right] \quad (6.10)$$

where a_c is the radius of the conducting shell (Shafranov, 1966). Field errors, owing to the use of an imperfect conducting shell—poloidal gaps, ports—and coil-induced ripple are observed to degrade the equilibrium configuration and plasma performance. This is an important consideration in reactor design (Bodin *et al.*, 1986).

C. Transport

Neoclassical transport in an RFP is even lower than in a tokamak (see Sec. III.C), owing to improved orbits (Boozer, 1983). As in the case of the tokamak, however, the observed transport exceeds neoclassical levels, presumably due to the resistive-mode turbulence which produces the field reversal.

A principal issue for the RFP is at what scale (current, size) the resistive-mode activity, necessary to sustain the configuration, will be weak enough to allow reactor-grade temperatures to be reached. Two theoretical models have been used to characterize the anomalous losses, both based on the effects of resistive fluid turbulence.

Connor and Taylor (1984) use the invariance properties of the reduced resistive MHD equations to develop a scaling for transport, which indicates that beta should be approximately constant, as observed in some experiments (Phillips *et al.*, 1984). They derive a quantitative estimate for resistive g-mode losses,

$$\tau_E^{\mathrm{CT}}\sim\frac{a^2}{6\eta}\left[\frac{m_e}{m_i}\right]^{1/2}\frac{1}{\beta^2}$$
$$\propto\frac{I^3}{A_i^{0.42}an^{1.5}}\quad\text{for Ohmic heating .} \quad (6.11)$$

Because Ohmic power is much less than alpha power in an ignited reactor, it is necessary to rewrite this scaling formula in terms of total power delivered to the plasma. For heating in general the form $\tau_E^{\mathrm{CT}}\propto I^{2.67}/(A_i^{0.333}na^{0.667}P^{0.333})$ may be obtained. An analysis of experimental data by DiMarco (1988) and an analysis by Ortolani and Rostagni (1983) for operation near the density limit support this result. A plot of the best energy confinement times—typically higher beta is achieved at higher density—versus the scaling parameter $I^3/(an^{1.5})$ is shown in Fig. 63. Support for the thesis that beta confinement adjusts to keep beta constant comes from experiments in which krypton was added to the plasma (Pickrell *et al.*, 1984). As the fraction of radiated power in ZT-40M increased, beta remained roughly constant and the Ohmic power increased only slightly, showing an increase in τ_E (decrease in conduction).

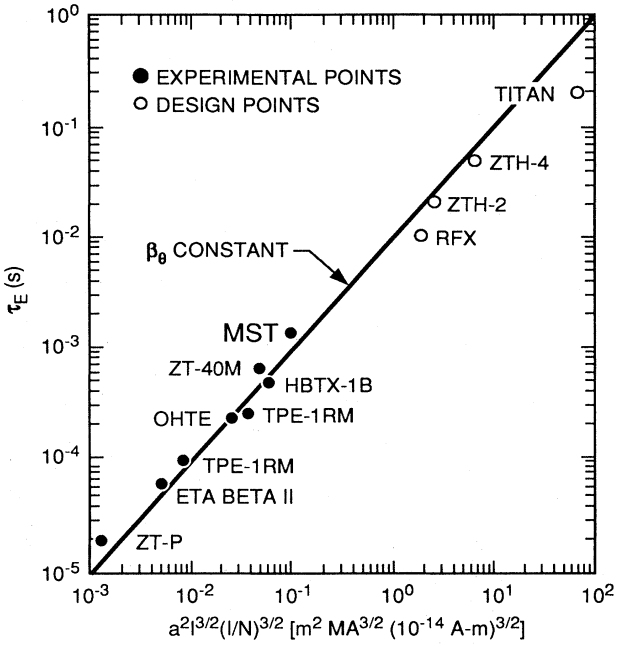

FIG. 63. Confinement time for RFP experiments Plotted vs the constant β_θ, Connor-Taylor scaling (DiMarco, 1988) (and updates).

However, there are experimental data showing β_θ decreasing with increasing current (Wurden *et al.*, 1985; Alper *et al.*, 1987). This effect may be the result of changes in plasma profiles, T_e/T_i, or radiation levels. This result is also consistent with a resistive interchange turbulence model (Carreras and Diamond, 1989), in which the restriction to equal scaling for electrostatic and magnetic fluctuations, used by Connor and Taylor, is removed. In the Carreras-Diamond model,

$$\tau_E^{\mathrm{CD}}\propto\frac{I^2}{A_I^{0.25}a^{0.25}n}\quad\text{for Ohmic heating .} \quad (6.12)$$

For heating in general this has the form $\tau_E^{\mathrm{CD}}\propto I^{1.82}R^{0.91}/(A_i^{0.182}n^{0.455}P^{0.455})$. When benchmarked against present experiments (DiMarco, 1988), the Connor-Taylor version becomes

$$\tau_E^{\mathrm{CT}}\simeq\left[\frac{2.9\times10^{-3}}{A_i^{0.42}Z_{\mathrm{eff}}^{0.167}}\right][I(\mathrm{MA})]^3/[n(\times10^{20}\ \mathrm{m}^{-3})]^{1.5}[a(\mathrm{m})]\ (\mathrm{s})\ . \quad (6.13)$$

The Carreras-Diamond model benchmarked against the same data becomes

$$\tau_E^{\rm CD} \simeq \left[\frac{2.8\times10^{-3}}{A_i^{0.25}Z_{\rm eff}^{0.25}}\right][I({\rm MA})]^2 \Big/ [n(\times10^{20}\ {\rm m}^{-3})][a({\rm m})^{0.25}]\ ({\rm s})\ . \tag{6.14}$$

For example, the TITAN reactor has $I=17.8$ MA, $n=9\times10^{20}$ m^{-3}, $a=0.6$ m, $A_i=2.6$, $Z_{\rm eff}=2$, and requires $\tau_E=0.22$ s. In the Connor-Taylor model, $\tau_E^{\rm CT}\simeq0.61$ s, while in the Carreras-Diamond model, $\tau_E^{\rm CD}\simeq0.072$ s. For confinement formulas written in terms of total power, i.e., not Ohmic power alone [see Eqs. (6.19) and (6.20)], the equivalent confinement times, using the full conduction power, are 0.31 and 0.06 s, respectively. If a large amount of power were radiated, and a lower conduction power were appropriate for use in the formulas, the confinement times would improve. The consequences of using the two formulas are discussed in Sec. IV.H.

Electrostatic fluctuations can account for particle transport in the edge but not heat transport (Ji *et al.*, 1991; Rempel *et al.* 1991; Tsui *et al.*, 1991). Energetic electrons from the plasma core traveling along the field lines remove 35–40 % of the input power in ZT-40 (Weber *et al.*, 1991). These losses are consistent with the Rechester-Rosenbluth 1978 model of stochastic magnetic-field transport (Schoenberg and Moses, 1991). It is important to realize that resistive MHD activity in present-day experiments may be masking other sources of turbulence that might emerge as important in the reactor regime. The ion temperature-gradient mode has been invoked as a candidate mechanism in the edge region (Schnack *et al.*, 1985), thought it was not observed in ZT-40M (Schoenberg *et al.*, 1989).

There is a density limit for RFP's similar to that observed in tokamaks (Ortolani and Rostagni, 1983),

$$\frac{na^2}{I} \lesssim 10^{14}\ {\rm A}^{-1}{\rm m}^{-1}\ . \tag{6.15}$$

However, in contrast to tokamaks, no major or density-limiting disruptions have been seen, even with high radiation fractions (0.95) and large pellet fueling (Wurden *et al.*, 1987).

The Connor-Taylor confinement model may be used to show that Ohmic heating to ignition may be possible in an RFP reactor. Substituting from Eq. (6.13), with $\chi_E\simeq a^2/6\tau_E$ in Eq. (2.75), yields

$$\frac{dW}{dt} = \underbrace{-\frac{1.21\times10^{-2}a^3RT_k}{n_{20}^{0.5}}\left[\frac{n_{20}}{I_m}\right]^3}_{\text{conduction losses}} \underbrace{-0.11Ra^2Z_{\rm eff}n_{20}^2T_k^{0.5}}_{\text{bremsstrahlung}} + \underbrace{\frac{0.08\gamma_RZ_{\rm eff}Rn_{20}^2}{a^2T_k^{1.5}}\left[\frac{I_m}{n_{20}}\right]^2}_{\text{Ohmic heating}} + \underbrace{1.9\times10^{-2}Ra^2n_{20}^2\left[\frac{n_{\rm DT}}{n_e}\right]^2T_k^{2.5}}_{\text{Alpha heating}}\ ({\rm MW})\ . \tag{6.16}$$

For the TITAN reactor, $R=3.9$ m, $a=0.6$ m, and I_m, n_{20}, and T_k are raised together during startup to the final values $I_m=17.8$ MA, $n_{20}=9\times10^{20}$ m^{-3}, $T_k=10$ keV. Setting $\gamma_R=1.5$, $Z_{\rm eff}=2$, and $n_{\rm DT}/n_e=0.83$, assuming no helium ash buildup during startup, and assuming a linear rise of current and density, $I_m/n_{20}=1.98$ MA/(10^{20} m^{-3}), we find that the power balance becomes

$$\frac{dW}{dt} = -19.4\frac{T_k}{n_{20}^{0.5}} - 0.31n_{20}^2T_k^{0.5} + \frac{10.2n_{20}^2}{T_k^{1.5}} + 0.018n_{20}^2T_k^{2.5}\ ({\rm MW})\ . \tag{6.17}$$

Balancing conduction losses against Ohmic heating, we find that $P_\Omega > P_{\rm cond}$, provided $n_{20}/T_k > 1.3$. At about $T_k\sim4.5$ keV, alpha heating dominates over the losses, and the plasma ignites. A plot of the required current as a function of T and N for the TITAN model is shown in Fig. 64.

At the TITAN operating point the alpha heating exceeds the losses, for both confinement scalings. This would permit the reactor parameters to be relaxed or impurities to be added, as in the TITAN case, to radiate power and relieve the divertor problems. The test done in ZT-40M in which krypton was added supports this hypothesis (Pickrell *et al.*, 1984; also see Werley, 1991). Such behavior implies an underlying confinement that may be better than the scalings indicate.

D. MHD limits

Owing to finite resistivity, the magnetic-field diffusion alters the configuration. Resistive instabilities act to restore the configuration to the Taylor minimum energy state. The increased plasma resistivity at the plasma

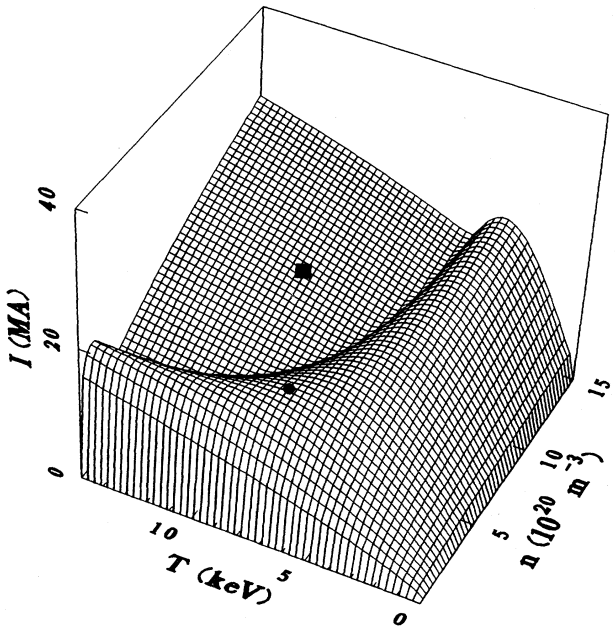

FIG. 64. The required power for power balance as a function of TITAN plasma density and temperature. The steady-state TITAN plasma is denoted by a filled square and the saddle point by a filled circle. The TITAN startup path to ignition and burn is located above this point and passes close to the saddle point (Najmabadi *et al.*, 1990).

edge leads to increased activity in that region to counteract the field diffusion.

1. Infinitely conducting shell

Configurations with tailored shear and pressure profiles have been found which are completely stable to ideal modes for the reversed state (Robinson, 1971; Goedblod and Sakanaka, 1974; Freidberg, 1982), provided $\beta_\theta \lesssim 0.5$ and $(a_c/a)^2\langle 3|B_\phi(0)|B_\phi(a_w)|$ and the total toroidal flux $\phi > 0$.

Stable configurations have also been found for resistive tearing modes for $\beta \simeq 0.2$ (Robinson, 1978; Schnack *et al.*, 1985). These modes have large toroidal mode numbers, $n \lesssim 20$, and $m=0$ and 1; such modes are observed. In experiments, RPF configurations with $\beta_\theta \sim 0.1$ are calculated to be stable or close to stability for resistive tearing modes (Bodin, 1990). However, the configurations are unstable to the local resistive interchange (or resistive g mode) (Hender and Robinson, 1983).

2. Resistive shell

The use of a resistive shell is an attractive option because it allows the use of plasma control with an applied B_V and also minimizes field errors from gaps and ports. Unfortunately, it is predicted to destabilize both ideal and resistive current-driven modes ($m=0$ and 1; Ho *et al.*, 1989, Ito and Prager, 1991). Tearing modes may be stabilized by plasma rotation (Bodin, 1990). In experiments on HBTX and OHTE, the current-driven modes were observed to grow when $\tau_{\text{pulse}} > \tau_{\text{wall}}$ (Alper *et al.*, 1989). The growth rate was proportional to τ_{wall} (Alper *et al.*, 1987). More information is required to determine whether a reactor could use a resistive wall and whether external feedback stabilization of the plasma would be possible. A comprehensive study of feedback control of such instabilities with a resistive wall has been made by Zita *et al.* (1992). In the TITAN study it was assumed that the first wall, liquid lithium coolant, and blanket materials would act as a conducting wall.

E. Current drive

For the condition proposed for an RFP reactor, e.g., TITAN, $n_{20}=9$, $T \sim 10$ keV, and $\beta_\theta \sim 0.2$, the bootstrap current is expected to be small; see Eq. (4.8). The noninductive current-drive techniques which use neutral beams and RF, discussed in Sec. IV.C, will be too inefficient at such high densities. A possible solution, to extend pulse lengths beyond a few 100 s, is to use magnetic helicity injection, either directly, as has been used in Spheromaks (Barnes, 1986) or by the oscillating-field current-drive (OFCD) approach (Bevir and Grey, 1982; Schoenberg *et al.*, 1984). In the latter approach, oscillating, out-of-phase fields are applied through the poloidal and toroidal circuits. The rate of helicity injection is given by $2\phi V_\phi$, where $d\phi/dt = -V_\theta$.

If $V_\phi = V_\phi \cos\omega t$ and $V_\theta = V_{\theta 0} \sin(wt+\theta)$, and it is assumed that the plasma will continually adjust to its relaxed state, the system acts as if it has a steady loop voltage V_s,

$$V_s = \frac{1}{2} f[\mu(r)] \frac{\delta\phi}{\phi} \left[\frac{V_{\phi 0} \sin\theta}{V_{\phi 0}} \right] V_{\phi 0} , \tag{6.18}$$

where $f \lesssim 1$ is a constant dependent on field distribution; $d\phi/\phi$ and $\sin\theta$ are the fractional oscillations in ϕ and V_ϕ. The relaxation occurs on an MHD time scale, which is much shorter than the oscillating-field period. Calculations for the TITAN reactor have been made using a 1D MHD model for oscillating-field current drive (Najmabadi *et al.*, 1990).

The requirement that $\langle \delta K/dt \rangle = 0$ results in $(\delta\phi/\phi_0)(\delta V_\phi/V_{\phi 0}) \simeq 2$. Toroidal flux oscillations, $\delta\phi/\phi \lesssim 0.05$, are required to avoid the loss of toroidal field reversal; therefore the ac toroidal voltage needed to sustain the current may be ~ 40 times greater than that required inductively. Similarly, there is a lower bound at which δI_ϕ becomes too large (I_ϕ becomes too small, so that reversal is lost), leaving a narrow window for $\delta\phi/\phi$. Modeling of the currents, including the conducting wall, showed that the wall must contain insulating breaks to avoid large power dissipation, but not so great as to impair wall stabilization. The operating window shrinks with decreas-

ing frequency and, for TITAN, ~25 Hz is required. The calculations for TITAN have $\delta\phi/\phi=0.0365$, leading to a variation in θ from 1.5 to 1.6 and F from -0.03 to 0.17, and a calculated dissipated power of 49 MW (for TITAN II) to 57 MW (for TITAN 1) to drive 17.8 MA.

Experiments on ZT-40 (Wurden, Schoenberg, *et al.*, 1987; Schoenberg *et al.*, 1988), showed the expected features of Eq. (6.18), notably an increase or decrease or loss of current for the appropriate phasing, but only at lower input powers. At higher drive power, current increases were masked by plasma-wall interactions, which increased the plasma resistance. A ramping of about 5% of the current was obtained at low power.

F. Power and particle handling

Generic issues for power and particle handling are discussed in Sec. II.G. To date, RFP's have operated with short pulse length, in limiter-defined plasmas. Poloidal pumped limiters and toroidal magnetic limiters have been considered for RFP reactors (Bathke and Krakowski, 1985; Najmabadi *et al.*, 1990; see Fig. 65). In TITAN a large percentage of the core power (~70%) is radiated using xenon impurities, on the assumption that there is excess confinement. The reduced power flux to the divertor, coupled with the high operating density of RFP, $\gg 10^{20}$ m^{-3}, leads to a low divertor plasma temperature. The plasma density is sustained by pellet fueling at the moderate velocities, $\lesssim 2$ km s^{-1}, required to fuel past the reversal radius.

G. Computer modeling

A number of computer codes have been applied to modeling RFP plasmas and reactors. Among the tools used have been 3D MHD stability codes (Aydemir *et al.*, 1985; Kusano and Sato, 1990; Schnack *et al.*, 1985), a 2D equilibrium code (Jardin *et al.*, 1986), a 1D core-plasma transport code (Nebel, 1980), and divertor, edge-plasma codes such as ODESSA (Prinja *et al.*, 1987) and DEGAS (Heifetz *et al.*, 1982; Werley, 1987, Braams, 1987). Detailed 3D field-line tracing codes and 3D MHD codes were used to assess the impact of field ripple on magnetic island formation. A systems code (Copenhaver *et al.*, 1985) marrying various physics, engineering, and costing elements was developed for the TITAN reactor studies.

H. RFP reactors

Studies of RFP reactors have been made by Hancox *et al.* (1981), Krakowski *et al.* (1986), and Najmabadi *et al.* (1990). The recent work has emphasized the value of the RFP's moderate beta (~10%) and high field ratio $f_B \sim 1-1.3$, which come with this current-dominated configuration and which permit a relatively higher-power-density reactor core than tokamaks and stellarators, e.g., p_{wn} up to 20 MW m^{-2}, rather than $\lesssim 6$ MW m^{-2}. To offset the power handling problems, it is assumed in the TITAN study, based on experimental evidence (Pickrell *et al.*, 1984), that confinement will be sufficiently good to permit added xenon impurities to radiate ~70% of the core power, with a substantial added fraction of the remaining power's being radiated at the plasma edge. Parameters of three reactors are shown in Table XVIII.

Two models of transport have been developed to describe RFP transport. They have been benchmarked against experimental data for Ohmic heating by DiMarco (1988). Quantitative formulas, taking into account impurity levels and atomic mass, are given in Eqs. (6.13) and (6.14). For a reactor, Ohmic heating is small compared to alpha heating, and it is necessary to rewrite the formula in terms of the total power P_m (MW):

$$\tau_E^{\mathrm{CT}} \simeq \frac{6.1\times10^{-3} C_{\mathrm{CT}} I_m^{2.67} R^{0.333}}{A_i^{0.333} a^{0.667} n_{20} P_m^{0.333}} \ (\mathrm{s}) \tag{6.19}$$

$$\tau_E^{\mathrm{CD}} \simeq \frac{9.5\times10^{-3} C_{\mathrm{CD}} I_m^{1.82} R^{0.455}}{A_i^{0.182} n_{20}^{3.455} P_m^{0.455}} \ (\mathrm{s}) \ . \tag{6.20}$$

I_m (MA) and C_{CT} and C_{CD} are multipliers to allow for degradation or enhancement. These formulas may be combined with Eqs. (2.45) and (2.46) to obtain a value for the fusion power and poloidal field needed for a self-sustained plasma. In deriving these formulas we set $\kappa=1$, $\tau_E \simeq a^2/6\chi_E$, and $P_m=0.2 f_\alpha P_F$, and we use Eq. (2.42) for $\bar{p}_{wn}$ to obtain

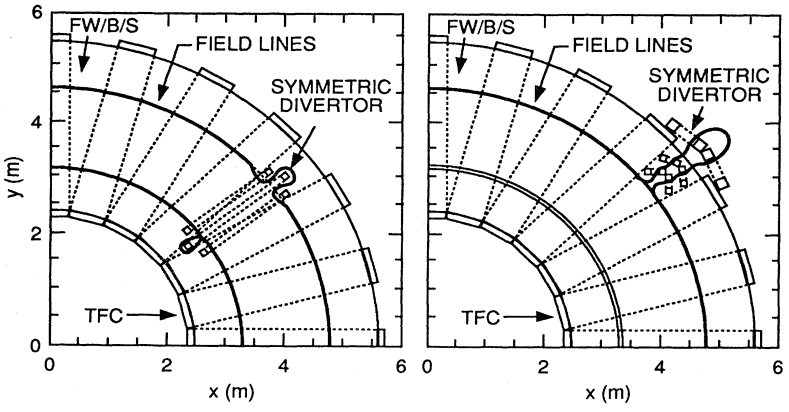

FIG. 65. Field-line tracing in the compact reversed-field pinch reactor equations plane for poloidally symmetric and bundle divertors (Hagenson and Krakowski, 1981).

TABLE XVIII. RFP reaction design.

Reactor	CRFPR (5)	CRFPR (20)	TITAN-1
p_{wn} (MW m^{-2})	5	20	18
P_F (MW)	2900	2740	2300
R (m)	7.6	3.8	3.9
a (m)	1.42	0.71	0.60
a_w (m)	1.52	0.75	0.66
$\bar{n}$ ($\times 10^{20}$ m^{-3})	2.3	6.3	9.0
T (keV)	10.0	10.0	10.0
β_θ	0.23[a]	0.23[a]	0.23[a]
τ_E (s)	0.70	0.23	0.22
$B_{\theta m}$ (T)	3.0	5.2	5.9
$B_{\max}$ (T) coil	2.6	4.5	5.7
I (MA)	21.6	18.4	17.8
P_{aux} (MW)	(−)	(73)	57
P_{net} [MW(e)]	1000	1000	970

[a]Includes 0.03 for alpha-particle pressure $\langle\beta\rangle \approx 0.12$.

$$P_F^{\text{CT}} = \frac{5.0\times 10^3 A_i^{1.333} n_{20}^{4.2} (R/a)(n_{\text{DT}}/n_e)^{1.34}\beta_\theta^{5.33}}{C_{CT}^{4.0} f_\alpha^{2.66} (a_w/a)^{2.33} (\bar{p}_{wn})^{2.33}} \text{ (MW)}, \tag{6.21}$$

$$P_F^{\text{CD}} = \frac{3.6\times 10^6 A_i^{0.884} n_{20}^{2.21} (R/a)\beta_\theta^{4.42}}{C_{\text{CD}}^{4.86} f_\alpha^{2.65} (n_{\text{DT}}/n_e)^{0.442} (a_w/a)^{1.43} (\bar{p}_{wn})^{1.43}} \text{ (MW)}, \tag{6.22}$$

$$B_\theta = \frac{1.53(R/a)^{0.125}(a_w/a)^{0.375}(\bar{p}_{wn})^{0.475}}{P_F^{0.125}(n_{\text{DT}}/n_e)^{0.5}\beta_\theta^{0.5}} \text{ (T)}. \tag{6.23}$$

(1) The Connor-Taylor scaling leads to a TITAN-like reactor. For example, with $A_i=2.5$, $n_{20}=9$, $R/a=6.33$, $n_{\text{DT}}/n_e=0.73$, $\beta_\theta=0.21$, $C_{\text{CT}}=1$, $f_\alpha=0.3$, $a_w/a=1.15$, and $\bar{p}_{wn}=19$ MW m^{-2}, we obtain $P_F^{\text{CT}}\simeq 2370$ MW, $B_\theta\simeq 5.8$ T, $I_m\simeq 17.7$ MA, $a=0.61$ m, $\langle T_k\rangle\simeq 10$ keV. Note that these parameters have sufficient excess confinement to permit a large amount of power to be radiated ($f_\alpha=0.3$), alleviating the divertor problem.

(2) By contrast, the Carreras-Diamond scaling leads to a large reactor with no margin to increase radiation levels above the normal ~20%. For example, $A_i=2.5$, $n_{20}=3.5$, $R/a=6.33$, $n_{\text{DT}}/n_e=0.83$, $\beta_\theta=0.15$, $C_{\text{CD}}=1$, $f_\alpha=0.8$, $a_w/a=1.15$, and $\bar{p}_{wn}=18$ MW m^{-2} leads to $P_F^{\text{CD}}\simeq 4790$ MW, $B_\theta\simeq 5.9$ T, $I_m\simeq 25.5$ MA, $a=0.86$ m, $\langle T_k\rangle\simeq 19$ keV. Decreasing f_α from 0.8→0.6 doubles P_F.

(3) To recover a similar TITAN-like reactor to that with Connor-Taylor scaling requires $C_{\text{CD}}=4.2$.

I. Conclusions

(1) The RFP has the potential to make an attractive reactor; however, the experimental data base is weak compared to that of the tokamak. As in the case of other configurations, uncertainty remains in transport scaling, and data from RFX and subsequent large experiments will be necessary to confirm the viability of the reversed-field pinch as a reactor. Of particular importance to the RFP is the relationship, under reactor conditions, between the maintenance of the configuration (dynamo effect) by turbulence and the level of transport due to this turbulence.

(2) With optimistic Connor-Taylor transport scaling, there is sufficient margin of confinement to permit a large amount of the fusion power to be radiated by added impurities, thereby easing the divertor problem. Under these circumstances it is beneficial to operate at high density. However, the "conventional" radio frequency and beam current-drive schemes are then too inefficient to be used. Because of the low poloidal beta, the bootstrap currents in an RFP are small compared to a tokamak. Helicity injection in one form or another offers an interesting opportunity to provide steady-state operation. Present results from experiments (F-θ pumping) are equivocal, and further tests are essential.

(3) With the more pessimistic Carreras-Diamond model the transport margin implied by the Connor-Taylor model is absent. As a consequence it is not possible to operate at high power density except with either very high fusion power (>10 000 MW) or an enhancement factor $C_{\text{CT}}\sim 4$. If transport adjusts to maintain beta, and is effectively lower than power is radiated, then this might provide an enhancement factor and permit substantial radiated power.

(4) Experiments and theory suggest that external feedback control and a conducting shell may be required near the plasma to stabilize MHD activity. Providing a shell

involves a tradeoff between stabilization and permitting time-varying fields to be applied to the plasma. Gaps required for oscillating-field current drive should not interfere with the stabilization.

VII. FIELD-REVERSED CONFIGURATIONS

A. Introduction

The compact torus area of research includes field-reversed configurations (FRC) and field-reversed mirrors ($B_\theta \gg B_\phi$ and $S>1$), spheromaks ($B_\theta \sim B_\phi$ and $S>1$), and the Astron ($B_\theta \gg B_\phi$ and $S<1$), where S is the ratio of the toroidal plasma radius to the external ion gyroradius (ρ_{ie}). Recent reviews of the area have been made by Tuszewski (1988) for FRC, Jarboe (1989) for spheromaks, and Wright (1990) for both configurations. FRC reactor studies include those of Willenburg *et al.* (1979), Willenberg (1980), Robson (1980), Krakowski *et al.* (1981), Hagenson and Krakowski (1981), Alikhanov *et al.* (1983), Hirano (1984), Vlases *et al.* (1986), Burtsev *et al.* (1987), Kernbichler *et al.* (1991), and Momota *et al.* (1992). The FRC represents a different class of toroidal device than the tokamak, stellarator, and RFP, since it has no coil down the center of the toroidal plasma. It must be emphasized that, while it is an intruging candidate for a fusion reactor, its experimental data base is far smaller than that of the other three configurations.

B. FRC characteristics

The FRC is a highly elongated torus of aspect ratio about one, formed without a toroidal field by a toroidal current sheet and an external axial field; see Fig. 66. The configuration may be formed in a linear "theta-pinch" device by creating a plasma in an insulating cylinder containing an initial axial magnetic field B_{z0}. The preionization is usually done with an oscillating discharge using the theta coil. It is sometimes supplemented by an axial discharge between electrodes or by other techniques to enhance the uniformity of the initial plasma. A main capacitor bank is then applied to the coil, and the toroidal current induced in the plasma leads to a reversal of the initial field and the formation of an elongated toroidal plasma. This plasma may be contained in the discharge chamber by mirror fields.

The configuration is particularly interesting because of its very high beta, 50–90 %, and small aspect ratio with no toroidal coil. The cylindrical geometry permits the use of a simple blanket, shield, and coil arrangement in a reactor. The very high beta allows the use of low-field coils and may result in reactor systems of relatively small unit size compared to other configurations, provided the transport scales favorably. The bulk of reactor studies have been on pulsed systems; however, steady-state systems are now being studied more seriously.

In pulsed systems the FRC plasmas may be translated through the blanket area using a weak gradient in the solenoidal magnetic field. This approach allows the use of efficient adiabatic compression and a separation of the high-technology formation phase from the burn and quench phases.

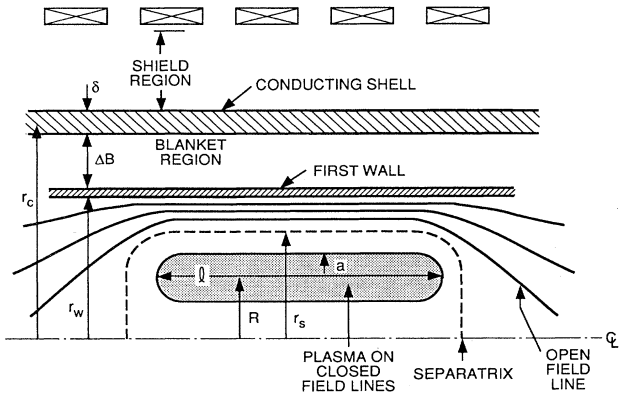

FIG. 66. FRC reactor geometry showing the radius of a conducting shell (r_c), first wall (r_w), separatrix (r_s), and plasmoid length (l). The conducting shell thickness (δ) is located outside a breeding blanket of thickness (Δb) (Hagenson and Krakowski, 1981).

In the steady-state system the plasma might be formed and then expanded into a reaction chamber, where it would be heated and the current sustained by neutral-beam or rf power (Kernbichler *et al.*, 1991; Momota *et al.*, 1992) and, in some cases, by current driven by the charged fusion products (Berk *et al.*, 1988). The magnetic structure includes a natural divertor. A schematic diagram of the pulsed reactor CTOR is shown in Fig. 67.

C. Equilibrium

The radial pressure balance may be written as

$$p_m = p + \frac{B_z^2}{2\mu_0} = \frac{B_e^2}{2\mu_0} , \tag{7.1}$$

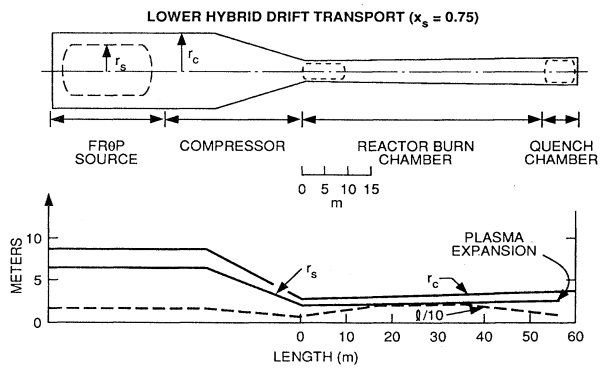

FIG. 67. Reactor dimensions showing plasmoid trajectory in the CTOR reactor, using lower-hybrid drift transport (Hagenson and Krakowski, 1981).

where B_e is the external equilibrium field.

If p is a function only of the poloidal flux variable, it is possible to show that $r_s=\sqrt{2}R$ where R is the radius of the field null, and r_s is the separatrix major radius. From the axial equilibrium (Barnes *et al.*, 1979),

$$\langle\beta\rangle=1-\frac{x_s^2}{2}\ , \tag{7.2}$$

where

$$\langle\beta\rangle=\left[\frac{2}{r_s^2}\right]\int_0^{r_s}\left[\frac{p}{p_m}\right]r\,dr$$

is the volume average of beta ($\beta=p/p_m$) within the separatrix, $x_s=r_s/r_c$, and r_c is the radius of the conductor which conserves the flux. Representative plasma and field profiles are shown in Fig. 68. It may also be shown that, for the range of possible poloidal profiles, the poloidal flux is bounded by the values $(x_s/\sqrt{2})^2\le\phi/(\pi R^2B_e)\le x_s/\sqrt{2}$ (Tuszewski *et al.*, 1982). In turn, the fluxes

$$\phi=\pi r_c^2B_e\left[\frac{x_s}{\sqrt{2}}\right]^{3+\epsilon} \tag{7.3}$$

where ϵ ranges from 0 to 1. The ratio of plasma scale length to ion gyroradius is defined as

$$s=\int_R^{r_s}\left[\frac{r}{r_s}\right]\frac{dr}{\rho_i}\ . \tag{7.4}$$

For a radially uniform ion temperature,

$$s=\frac{\phi}{2\pi r_s\rho_{ie}B_e}\ , \tag{7.5}$$

ρ_{ie} is the ion gyroradius in the external magnetic field. The parameter $S=R/\rho_{ie}$ is sometimes used, and $Sx_s^2/4\sqrt{2}\le s\le Sx_s/4$. Experimentally, equilibria have $l_s/2r_s\sim3-10$ (see Fig. 66). To match the experimental equilibria in code calculations it is necessary to invoke steep pressure gradients at the separatrix (Shumaker, 1984).

D. Startup

The FRC was discovered by accident in early theta-pinch research, when a bias field was applied in the reverse direction to the main magnetic field, and spontaneous formation of closed poloidal fields was observed. Subsequently, it was demonstrated that similar configurations could be formed using rotating magnetic fields (Hugrass *et al.*, 1980), with a coaxial geometry (Pietrzyk *et al.*, 1987), and in the field-reversed mirror (FRM) approach, by using neutral-beam injection into a magnetic mirror (Pearlstein *et al.*, 1979). The formation of a plasma in a theta pinch is illustrated in Fig. 69.

There are two main issues for startup of an FRC reactor. First, plasma tearing activity as a process for forming the plasma should be a avoided, as it can lead to asymmetries. Second, in present-day systems a fast formation scheme is generally used which, in a reactor, would require large voltages on the formation coil and large amounts of pulsed power. The former issue has been handled using additional coils, which form separatrices at the end of the plasma (Hoffman *et al.*, 1986). A number of potential solutions have been proposed to handle the latter issue: a coaxial slow source, which produces an annular FRC plasma between concentric coils carrying current (Barnes *et al.*, 1987); a rotating magnetic-field system, which drives a toroidal current, ROTOMAK (Blevin and Thonemann, 1962); the EXTRAP, which produces a toroidal current in an optupole field (Lehnert, 1977); and a field-reversed mirror (Simonen *et al.*, 1979).

In the present fast formation schemes the ions and, to

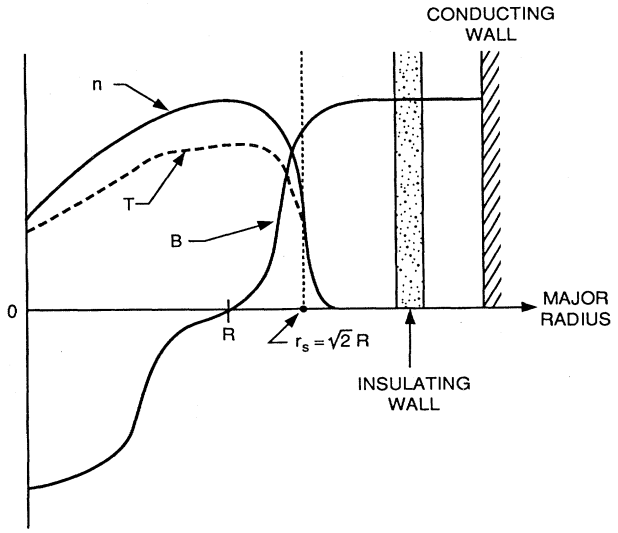

FIG. 68. Representative plasma field profiles for an FRC.

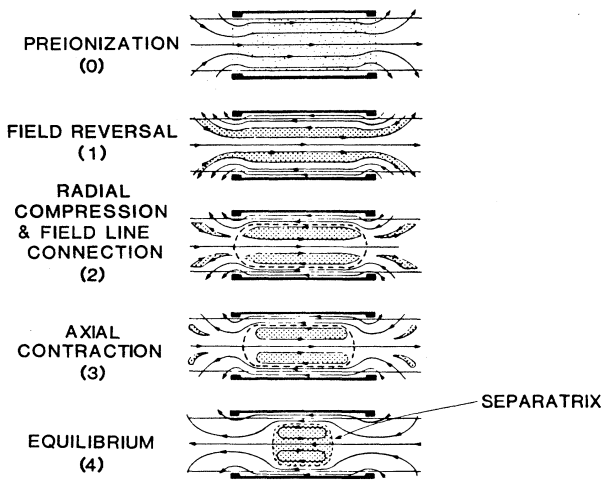

FIG. 69. Stages of formation of an FRC plasma in a theta pinch (Hoffman *et al.*, 1986).

a lesser extent, the electrons are shock heated and resistive heating occurs during a slow radial compression. Heating also occurs due to resistive magnetic-field annihilation. Temperatures in present-day experiments range from $T_i \sim 1.5$ keV, $T_e \sim 0.5$ keV at $n \sim 8\times10^{20}$ m^{-3}, $x_s \simeq 0.3$ to $T_i \sim T_e \simeq 0.15$ keV at $n \sim 2\times10^{21}$ m^{-3}, and $x_s \simeq 0.45$. In reactor-relevant formation schemes, shock heating will be less, though anomalous resistive heating may still lead to $T_i \gtrsim T_e$. Auxiliary heating will be required to raise the plasma to reactor conditions. The parameters of representative experiments are given in Table XIX.

Recently, studies have been made of D-^{3}He reactors, RUBY (Kernbichler *et al.*, 1991), and ARTEMIS (Momota *et al.*, 1992). While D-^{3}He reactors are outside the scope of this paper, it is worthwhile to indicate some of the interesting features of this concept. A principal issue for steady-state operation is sustaining the plasma current, $I \simeq l_s B/\mu_0$. For the previous example, $I \simeq 26$ MA. Fortunately, it appears that the orbits of energetic protons produced in D-^{3}He fusion lead naturally to a current supporting the initial plasma current, owing to losses associated with the large gyro-orbits (Berk *et al.*, 1988). If this effect works, then only a modest amount of noninductive current drive is required. For the alpha particles ($Z_b=2$) in D-T fusion, the effect would be smaller [see Eq. (4.11)]. An issue is whether the electron viscosity is sufficient to prevent shielding by a return plasma current. An analysis by Baldwin and Rensink (1978) suggests that, in a closed magnetic field-line system, the development of large potentials can lead to significant cancellation of the ion current by drifting electrons. For D-^{3}He fusion the neutron power is very low, in the case of the RUBY reactor 6% of the fusion power of 1.4 GW. For a steady-state D-T system with $x_s=0.57$, $l_s/r_s=6$, $a_w/a_s=1.13$, $n_{DT}/n_e=0.83$, $f_\alpha=1.0$, $\bar{p}_{wn}=6$ MW m^{-3}. $\bar{P}_F \simeq 3.7\times10^4/C_{Hm}^{0.727}$ MW. A large value of C_{Hm} ($\gtrsim 10$), or the equivalent confinement from the real transport, is required to make a conventional-size reactor. The reactors use direct conversion of the charged-particle power leaving the plasmoid. It will be important to verify the electrical efficiency assumed in the studies.

E. Adiabatic compression

Adiabatic compression has been proposed for pulsed reactors to heat to reactor conditions ($T \gtrsim 8$ keV), and it might be useful as part of the formation process in a steady-state reactor. Assuming $nT \sim B_e^2$, particle conservation (nV=constant), and the adiabatic law ($nT \sim V^{-5/3}$), yields $T \sim B_e^{4/5}$ and $n \sim B_e^{6/5}$. If flux is conserved, from Eq. (7.3), the length of the plasmoid varies as $l_s \sim r_c^{2/5} x_s^{2(4+3\epsilon)/5}$, which shows that the results of compression are affected by the profile factor ϵ ranging from 0 to 1. The adiabatic scalings may be written in terms of the changes in the x_s (where $\langle\beta\rangle = 1-x_s^2/2$) and the flux conserved radius r_c (Spencer *et al.*, 1983),

$$\begin{aligned} l_s &\sim x_s^{2(4+3\epsilon)/5}, \quad \langle\beta\rangle^{-(3+2\epsilon)/5} r_c^{2/5}, \\ T &\sim x_s^{-4(3+\epsilon)/5}, \quad \langle\beta\rangle^{2(1-\epsilon)/5} r_c^{-8/5}, \\ n_m &\sim x_s^{-6(3+\epsilon)/5}, \quad \langle\beta\rangle^{-2(1-\epsilon)/5} r_c^{-12/5}, \\ B_e &\sim x_s^{-(3+\epsilon)} r_c^{-2}. \end{aligned} \tag{7.6}$$

For present FRC data $\epsilon \sim 0.1-0.3$.

There are two methods of compression, flux compression, in which $x_s = r_s/r_c$ is changed, and wall compression, in which r_c is reduced either by moving the wall, as with a linear implosion, or by moving the FRC into smaller and smaller coils. The combination of translation and flux compression can have comparable efficiency to wall compression, as has been demonstrated experimentally (Rej *et al.*, 1992).

F. Transport

In FRC energy and particle transport are comparable in experiments ($\tau_E \sim 0.5\tau_p$), and transport is about an order of magnitude higher than the classical level. In the high-beta plasmas of the FRC both high-frequency instabilities, notably the lower-hybrid drift (LHD) mode (Davidson and Krall, 1977; Tuszewski and Linford, 1982) and the low-frequency high-beta electromagnetic drift wave (Krall, 1987), are predicted to be important contri-

TABLE XIX. Representative modern FRC experiments (Tuszewski, 1988).

Device	Coil length l_c (m)	Coil radius r_c (m)	Field B_m (T)	Configuration lifetime τ_l (μs)
TOR	1.5	0.15	1.0	100
NUCTE	2.0	0.08	1.0	60
OCT	0.6	0.11	1.0	130
CSS	1.0	0.225	0.3	60
FRXC/LSM	2.0	0.35	0.6	450
LSX	4.5	0.45	0.8	500

butors to transport. The LHD mode, which is driven primarily by the density gradient, is a flutelike mode with a predicted growth rate comparable to the hybrid gyrofrequency and a wavelength comparable to the electron gyroradius. The nonlinear evolution of the mode is not well understood. Experimental transport shows some of the features of LHD scaling, and in present experiments loss rates are consistent with predictions. However, the predicted negative temperature dependence T^{-2} is greater than the experimental observation of T^0–T^{-1}. Therefore, a modified LHD loss (MLHD) has been proposed for reactor design, which has a factor to allow for more favorable scaling (Hoffman and Milroy, 1983),

$$\tau_p^{\mathrm{MLHD}} = \frac{C_{\mathrm{HM}} 0.47\times 10^{-9} A_i^{3/2}\langle\beta\rangle x_s^6 S^4 (1+C/S)^3}{(1+T_e/T_i)B_e} \ (\mathrm{s}) , \tag{7.7}$$

$$\tau_E \simeq 0.5\tau_p ,$$

where

$$S = \frac{r_s e^{1/2} B_i}{(2m_i T_i)^{1/2}}$$

and

$$C = 9\left[1+\frac{T_e}{T_i}\right]^{1/2}\left[\frac{B_e(T) l_s(m)}{A_i T_i(\mathrm{keV})}\right]^{1/4}\frac{3}{2x_s^2} .$$

Various empirical transport formulas have been proposed (see Tuszewski, 1988), in the form $\tau_p \sim l_s^a x_s^b r_c^c n^d T^e$, $a=0$–0.75, $b=2$–3, $c=1.25$–2, $(b+c=1.4$–$3.6)$, $d=0.5$–0.9, and $T=-0.5$ to 0.5. The simplest parameter that scales like the measured particle confinement times is R^2/ρ_{ie} (Hamasaki and Krall, 1979).

With the aid of the power-balance equation (2.22), the formula for τ_E^{MLHD} may be rewritten as

$$\tau_E^{\mathrm{MLHD}} \alpha\ L^{3.3} B n^{0.67}/P^{0.67} \ (\langle\beta\rangle = \text{constant})$$

or

$$\tau_E^{\mathrm{MLHD}} \alpha\ L^{3.5} B^{0.5} n/P^{0.5} \ (\langle\beta\rangle = \text{variable}) ,$$

which are similar to tokamak and stellarator empirical scalings.

The amount of poloidal flux trapped during plasma formation is important, because the FRC lifetime depends mainly on the rate of decay of this flux (ϕ), assuming no additional drive mechanisms for the plasma current. Optimum trapping requires that the reversal time $\tau_r \sim 2B_0/\dot{B}$ be on the order of several radial Alfvén times, $\tau_A \sim r_c/v_A$, but not so fast that tearing instabilities cause flux loss. The trapping efficiency is impaired by impurities, and techniques are used to isolate the plasma from the walls during the formation phase. Initial flux retention factors in the range 0.3–0.6 are obtained experimentally.

In the equilibrium phase, loss of flux is expected to occur owing to resistive annihilation at the field null. Experimentally, the loss rate exceeds that expected from Spitzer resistivity by a factor of 3–10 (Slough *et al.*, 1984; Siemon *et al.*, 1986). The anomalous loss has not been explained. In present-day experiments $\tau_\phi \sim \tau_p$ (Hoffmann and Slough, 1986).

G. MHD limits

General features of MHD stability are discussed in Sec. III.C. The FRC might be expected to suffer from a variety of modes. However, various features promote stability (Tuszewski 1988): the compressive energy of the high-beta plasma is stabilizing in the absence of toroidal field; the region outside the separatrix has good curvature in the low-field regions; there is a nearby conducting boundary; there is strong elongation; toroidal rotation and Hall effects act to stabilize tearing and tilt modes: kinetic effects are important at low $s \sim 1$–2. The expected modes are listed in Table XX. Of particular importance are the $n=2$, $m=1$ global ideal mode in the presence of rotation and the $n \geq 1$, $m=1$ internal tilt mode.

TABLE XX. FRC stability: MHD theory vs experiment: Tuszewski, 1988 and Tuszewski *et al.*, 1991.

	n (toroidal)	m (poloidal)	Mode	Name	Experimental observation
1. Local ideal modes	∞	0		Interchange	yes
	∞	1–2	Axial or radial	Ballooning	maybe
2. Global ideal modes					
a. No rotation	0	1	Axial	Roman candle	no
	1	1	Radial	Sideways shift	no
	≥1	1	Axial	Tilt	yes
b. Rotation	1	1	Radial	Wobble	yes[a]
	2	1	Radial	$n=2$	yes[b]
	≥2	1	Radial	$n>2$	no
3. Resistive modes	0	2	Radial and axial	Tearing	no[c]

[a]Saturates at finite amplitude.
[b]Stabilized by multipole fields.
[c]Disappeared in modern experiments.

1. Rotational instability

These modes have been observed, notably the $n=2$ mode. The origin of the rotation is not fully understood, though it is expected that the Hall effect and particle losses may be important. Fortunately, the mode may be stabilized using multipole fields (Ohi *et al.*, 1983). Experiments work and are in fair agreement with theory (Harned, 1984; Ishimura, 1986). Helical multipoles have also proved effective. For a reactor, analysis is required to understand the possible impact of the additional field ripple on transport and alpha-particle confinement.

2. Tilt instability

This mode was predicted to occur in CT's by Rosenbluth and Bussac (1979). A computation of the time variation of the fields during the instability is shown in Fig. 70. It has not been observed in present-day experiments on LSX with $s \lesssim 8$ (Hoffman, 1992). However, evidence for the mode and its correlation with degraded confinement has been found in one experiment, FRX-C/LSM (Tuszewski *et al.*, 1991; Rej *et al.*, 1991). Candidate mechanisms to suppress the mode include rotation, Hall effects, and kinetic effects. Experiments at larger s will help to resolve the questions.

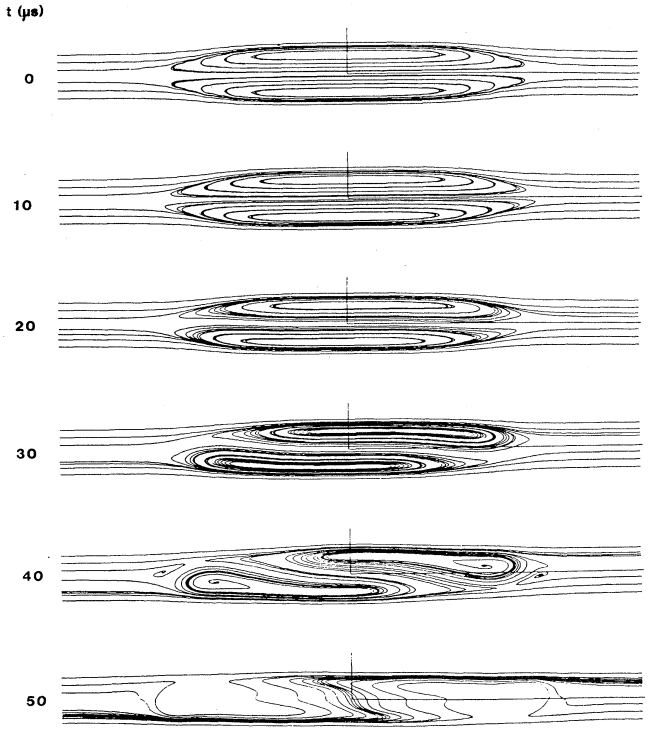

FIG. 70. Time sequence of magnetic-field lines from 3D MHD simulation, illustrating the internal tilt mode (Milroy *et al.*, 1987).

H. Alpha effects

The general effects of energetic alphas are discussed in Sec. II.F. There has been no study of such effects for FRC to the level of that for tokamaks. The symmetric FRC configuration and high currents (multi-mega-amps) should have, inherently, good containment. However, multipole fields used to stabilize rotational modes might adversely affect confinement. In the pulsed FRC reactors considered, only fractional burn is achieved $\lesssim 0.2$, so helium ash buildup would be limited even if all the ash were confined. In steady-state systems the same issue exists as for other toroidal devices, demonstrating that helium ash diffuses out at a rate not too different from the fuel.

I. Power and particle control

Generic issues for power and particle handling are discussed in Sec. II.G. For the pulsed FRC, with its natural divertor, clean startup, and isolation from both walls and chamber ends, wall-generated impurities should not be a problem. In a steady-state concept continuous fueling will be important. It will be necessary to develop a more detailed divertor system, notably to isolate the plasma source, and experimental demonstrations will be needed. Clearly, current-drive systems will be required.

J. FRC reactor options

Various types of compact torus reactor have been studied. They are reviewed by Hagenson and Krakowski (1981). More recently, pulsed FRC reactors have been studied by Vlases *et al.*, (1986), and steady-state reactors by Kernbichler *et al.* (1991) and Momota *et al.* (1992). Parameters of some designs are given in Table XXI.

For simplicity, in indicating the parameters required for a plasmoid that is self sustained by alpha heating, the FRC plasma may be treated as a cylinder of length l_s and radius r_s, with flat plasma profiles. In reality, with strong central alpha heating the temperature profiles may be more peaked than in present-day experiments, leading to higher fusion power for a given beta. The energy confinement time of the plasma for $T_e = T_i = T$ is

$$\tau_E = \frac{1.5\pi r_s^2 l_s e \sum \langle nT \rangle}{P_\alpha} \text{ (s)} . \tag{7.8}$$

The alpha power is

$$P_\alpha = 0.5\times 10^{-42} \left[\frac{n_{\rm DT}}{n_e} \right] \langle n_i^2 T_i^2 \rangle r_s^2 l_s \text{ (W)} . \tag{7.9}$$

Allowing for impurities and helium ash, we set $\langle n_i T_i \rangle \simeq 0.42 \sum \langle nT \rangle$. For flat profiles $\langle n_i^2 T_i^2 \rangle = \langle n_i T_i \rangle^2$. The neutron flux to the wall (a_w) is

$$\hat{p}_{wn} = \frac{0.8 \hat{P}_F}{2\pi (l_s/r_s)(a_w/r_s) r_s^2} \text{ (MW m}^{-2}) . \tag{7.10}$$

TABLE XXI. Representative FRC reactor options.

Name	CTOR	FIREBIRD B	RUBY	ARTEMIS
Reference	(Hagenson and Krakowski 1981)	(Vlases *et al.*, 1986)	(Kernbichler *et al.*, 1991)	(Momota *et al.*, 1992)
r_s (m)[a]	2.25	0.80	1.25	1.12
a_w (m)[a]	2.55	0.90		2.0
r_c (m)[a]	3.0	1.40		2.0
l_s	8.5	4.80	17.0	17.0
Burn chamber length (m)	53	67		
Plasma burn time (s)	1.9	0.07	SS	SS
Density $\langle n_{21} \rangle$ ($\times 10^{21}$ m^{-3})	2.1	4.26	5.2	0.66
Temperature $\langle T_k \rangle$ (keV)	10	10	100	87.5
Transport model	LHD	MLHD	$\lesssim 10$ classical	~ 200 classical
$\bar{P}_F$ (MW average)	2600	1917	1400	1610
$\bar{p}_{wn}$ (MW m^{-2} average)[b]	2.0	4.0	NBI+fusion product 1 MeV drive	
Net P_e MW(e)		752	~ 1000	1052
Applied field (T)	2.0	4.3		6.7
Trapped field (T)	4.4	6.4	4.9	3.7
Repetition rate (s^{-1})	0.033	0.2		
Translation velocity (m/s)	25	95		
Reactor type	Pulsed D-T	Pulsed D-T	Steady-state D-^{3}He	Steady-state D-^{3}He

[a]Initial parameters during burn for pulsed systems.
[b]For pulsed system. Current-drive scheme for steady-state systems. ($\bar{p}_{wn} \sim 0.3$ MW m^{-2}).

Combining these equations to eliminate the explicit dependence on r_s yields

$$\tau_E = \frac{1.21(\hat{P}_F)^{0.25}(n_e/n_{\rm DT})}{f_\alpha(\hat{p}_{wn})^{0.75}(a_w/r_s)^{0.75}(l_s/r_s)^{0.25}} \ (\rm s) \ . \qquad (7.11)$$

Here $\hat{P}_F$ (MW) and $\hat{p}_{wn}$ are the instantaneous values for a pulsed reactor and f_α is the fraction of alpha power available for plasma heating. In a steady-state reactor with current drive, f_α allows for the additional power. Combining Eqs. (2.37) and (7.7)–(7.11) leads to formulas for $\hat{P}_F$ and B_i.

$$\hat{P}_F = \frac{128(\hat{p}_{wn})^{0.091}(a_w/r_s)^{0.091}(l_s/r_s)(n_e/n_{\rm DT})^{0.364}\langle\beta\rangle^{0.364}}{f_\alpha^{0.727}C_{\rm HM}^{0.727}(1+C/S)^{2.18}x_s^{4.36}} \ (\rm MW) \ , \qquad (7.12)$$

$$B_i^2 = \frac{313(\hat{p}_{wn})^{0.75}(a_w/r_s)^{0.75}(l_s/r_s)^{0.25}(n_e/n_{\rm DT})}{\langle\beta\rangle\hat{P}_F^{0.25}} \ (\rm T^2) \ , \qquad (7.13)$$

where $\langle\beta\rangle$ is in % and, for the D-T reactor, the temperature has been set at 10 keV (see Table XIX).

1. Pulsed reactor

The geometry of a pulsed reactor is illustrated in Fig. 65. The plasmoid, created by a slow process to minimize coil voltages (Farengo and Brooks, 1992), may be heated to ignition by adiabatic compression. The plasmoid may then be translated by active coils or by a modest flaring of the flux conserver, with an angle $\lesssim 0.5$ degrees. The flaring minimizes the drag force (Hagenson and Krakowski, 1981). The plasmoid velocity V_p is set so that in the time l_s/V_p the flux leakage is less than the external flux between the separatrix and the wall. The design of the conducting shell must carefully balance between minimizing dissipation of the changing magnetic field and confining the flux. A thin graphite shell inside the first wall has been proposed to provide stabilization (Vlases *et al.*, 1986).

In order to obtain a sufficient energy gain, it is cus-

tomary to let the plasma burn for $\tau_B \sim 10\tau_E$. Since $\tau_p \sim 2\tau_E$, it will be necessary to fuel the plasmoid as it translates. It is tacitly assumed that under reactor conditions the flux dissipation time will be much longer, so that current drives will not be required.

The total energy produced will be $E_F \simeq \hat{P}_F \tau_B$. If the time between plasmoids is $\tau_{\rm rep}$, the average power is

$$\bar{P}_F = \hat{P}_F \frac{\tau_B}{\tau_{\rm rep}} \ ({\rm MW}) \ . \tag{7.14}$$

The average wall loading, where L is the burn chamber length, is

$$\bar{p}_{wn} = \frac{\bar{P}_F}{L \pi a_w^2} = \frac{l_s}{L} \frac{\tau_B}{\tau_{\rm rep}} \hat{p}_{wn} \ ({\rm MW\,m^{-2}}) \ . \tag{7.15}$$

Typical values are $\tau_B \simeq 1$ s, $\tau_{\rm rep} \simeq 10$ s, $l_s \simeq 5$ m, and $L \simeq 50$ m, so we see that $\hat{P}_F \sim 10\bar{P}_F$ and $\hat{p}_{wn} \sim 100\bar{p}_{wn}$.

In Sec. II, it was pointed out that a typical value required for neutron wall loading for an attractive reactor was about 4 MW m^{-2} on average. This indicates that an attractive pulsed FRC reactor may have to handle peak loads as high as a few hundred MW m^{-2}.

The substitution of representative values for $x_s = 0.75$ and 0.57 $\langle\beta\rangle = 72\%$ and 84%, respectively, and $l_s/r_s = 6$, $T = 10$ keV, $a_w/r_s = 1.13$ in Eqs. (7.12)–(7.15) yields parameters similar to those of early studies, namely, those of Hagenson and Krakowski (1981) and Vlases *et al.*, 1986, respectively, in which forms of LHD scaling were used. An enhancement factor of $C_{\rm HM} \sim 10$ is needed (Vlases *et al.*, 1986) to produce a reasonable scale and field reactor. For the parameters above, with $x_s = 0.57$, $C_{\rm HM} = 10$, $n_{\rm DT}/n_e = 0.9$, $f_\alpha = 1.0$ $\tau_B = 10\tau_E$, $\tau_{\rm rep} = 5$ s, and $L = 70$ m, we obtain $\hat{P}_F = 10\,000$ MW $\bar{P}_F = 2000$ MW, $\hat{p}_{wn} = 300$ MW m^{-2}, $\bar{p}_{wn} = 4.0$ MW m^{-2}, $r_s = 0.80$ m, $B_i = 6.8$ T, and $n = 4.3 \times 10^{21}$ m^{-3}.

The number of alpha particles produced during the burn is $N_\alpha = 3.7 \times 10^{21}$ m^{-3}, which is about 9% of the total number of electrons in the plasmoid. Consequently, even if all helium ash were retained, there would still be a high percentage of D-T fuel.

2. Conclusions

Principle issues for an FRC reactor include the requirement for slow formation of the initial plasma and the still unsettled questions of confinement scaling, flux confinement, and the tilt instability. Substantially more experimental work in LSX and large-scale experiments will be needed to verify the reactor potential of this interesting configuration.

The ARTEMIS reactor is neutral-beam driven. Neutral beams are also proposed for flux buildup from a present-sized FRC. The beam ions may also provide stability against tilt and/or shift modes. Beams of the required energy will need a substantial development program.

For a pulsed reactor, key issues are the design of the conducting shell, the high instantaneous neutron flux required for a useful average neutron flux ($\sim$4 MW m^{-2}), and cyclic fatigue of the wall, shield, and blanket.

For a steady-state system current-driven power is a major concern. The problem may be alleviated by a natural current drive due to the orbits of the charged fusion products. The efficient conversion of charged-particle energy to electricity needs to be demonstrated.

ACKNOWLEDGMENTS

Now that the paper is completed, I am reminded of the story of the man who was observed banging his head against a wall. When asked why he did it he replied, "Because it feels so nice when I stop." Now that I am feeling well again I can express my appreciation to Richard Hazeltine (University of Texas) for encouraging me to undertake this review. I am grateful to Darcus Johnson for her patience and skill in typing and retyping the manuscript, as various changes were made. I am also very appreciative of the advice and contributions of a number of colleagues, including: Jurgen Nührenberg and Horst Wobig (Institut für Plasma Physik, Garching); Charles Bathke, Robert Krakowski, Ron Miller, Kurt Schoenberg, Richard Siemon, and Kenneth Werley (Los Alamos National Laboratory), Dieter Sigmar (MIT); Kimitaka Itoh (National Institute for Fusion Science, Nagoya); Don Batchelor, Benjamin Carreras, James Lyon, Donald Spong, and Nermin Uckan (Oak Ridge National Laboratory); Douglass Post (Princeton Plasma Physics Laboratory); Kenro Miyamoto (Seikei University); Alan Hoffman (University of Washington); and Stewart Prager (University of Wisconsin). I also thank the many people who provided valuable figures and tables. Research on this paper was sponsored by the Office of Fusion Energy, U.S. Department of Energy, under Contract No. DE-AC05-84OR21400 with Martin Marietta Energy Systems, Inc.

REFERENCES

Alejadre, C., J. J. A. Gozalo, J. B. Perez, F. Magaña, J. R. C. Diaz, J. G. Perez, A. Lopez-Fraguas, L. García, V. I. Krivenski, R. Martín, *et al.*, 1990, Fusion Technol. **17**, 131.

Alikaev, V. V., and V. V. Parail, 1991, Plasma Phys. Controll. Fusion **33**, 1639.

Alikhanov, S. G., V. P. Bakhtin, A. G. Es'kov, R. Kh. Kurtmullaev, V. N. Semenov, E. F. Strizhov, N. P. Kozlov, V. I. Khvesyuk, and A. V. Yaminskij, 1983, in *Plasma Physics and Controlled Nuclear Fusion Research: Proceedings of the 9th International Conference, Baltimore, 1982* (IAEA, Vienna), Vol. 3, p. 319.

Alper, B., V. Antoni, M. K. Bevir, H. A. B. Bodin, C. A. Bunting, P. G. Carolan, J. Cunnane, D. E. Evans, A. R. Field, S. J. Gee, *et al.*, 1987, in *Plasma Physics and Controlled Nuclear Fusion Research: Proceedings of the 11th International Conference, Baltimore, 1986* (IAEA, Vienna), Vol, 2. p. 399.

Alper, B., M. K. Bevir, H. A. B. Bodin, C. A. Bunting, P. G. Carolan, J. Cunnane, R. F. Ellis, D. E. Evans, A. R. Field, C. G. Gimblett, *et al.*, 1989, in *Plasma Physics and Controlled Nuclear Fusion Research: Proceedings of the 12th International Conference, Nice, 1988* (IAEA, Vienna), Vol, 2. p. 431.

An, Z. G., P. H. Diamond, R. D. Hazeltine, J. N. LeBoeuf, M. N. Rosenbluth, and B. A. Carreras, L. Garcia, T. C. Hender, H. R. Hicks, H. R. Strauss, *et al.*, 1985, in *Plasma Physics and Controlled Nuclear Fusion Research: Proceedings of the 10th International Conference, London, 1984* (IAEA, Vienna), Vol. 2, p. 231.

Anderson, J. L., and J. R. Bartlitt, 1989, Fusion Technol. **15**, 1327.

Artsimovich, L.A., 1972, Nucl. Fusion **2**, 215.

Asdex Team, 1989, Nucl. Fusion **29**, 1959.

Axon, K. B., G. A. Baxter, J. Burt, W. H. M. Clark, G. M. McCracken, S. J. Field, R. D. Gill, D. H. J. Goodall, M. Hobby, J. Hugill, *et al.*, 1979, in *Plasma Physics and Controlled Nuclear Fusion Research: Proceedings of the 7th International Conference, Innsbruck, 1978* (IAEA, Vienna), Vol. 1, p. 51.

Aydemir, A. Y., C. C. Barnes, E. J. Caramana, A. A. Mirin, R. A. Nebel, D. D. Schnack, and A. G. Sgro, 1985, Phys. Fluids **28**, 898.

Aydemir, A. Y., J. C. Wiley, and O. W. Ross, 1989, Phys. Fluids B **1**, 774.

Badger, B., *et al.*, 1979, "NUWMAK: A Tokamak Reactor Design Study," Nuclear Engineering Department, University of Wisconsin, Madison Report UWFDM-330.

Badger, B., *et al.*, 1982, "UWTOR-M: A Conceptual Modular Stellarator Power Reactor," University of Wisconsin, Madison Report UWFDM-550.

Baker, C. C., M. A. Abdou, R. M. Arons, A. E. Bolon, D. A. DeFreece, C. A. Trachsel, N. G. Bond, D. W. Graumann, J. S. Alcorn, J. Kokoszenski, K. Barry, *et al.*, 1980, "STARFIRE-A Commercial Tokamak Fusion Power Plant Study," Argonne National Laboratory, Report ANL/FPP-80-1.

Baker, D. A., and W. Quinn, 1981, *The Reversed-Field Pinch, Fusion,* Vol. 1, Part A, Chapter 7, edited by Edward Teller (Academic, New York).

Baker, D. A., 1988, "A Review of the Experimental and Theoretical Status of the Reversed-Field Pinch," *Fusion Energy and Plasma Physics,* edited by P. H. Sakanaka (World Scientific, U.S. Office, Teaneck, N.J.), p. 730.

Baldwin, D. E., and M. E. Rensink, 1978, Comments Plasma Phys. Control. Fusion **4**, 55.

Barnes, D. C., W. T. Armstrong, E. J. Caramana, D. S. Harned, S. Okada, C. E. Seyler, D. E. Shumaker, H. Tuczek, G. Vlases, R. D. Brooks, *et al.*, 1987, in *Plasma Physics and Controlled Nuclear Fusion Research: Proceedings of the 11th International Conference, Kyoto, 1986* (IAEA, Vienna), Vol. 2, p. 673.

Barnes, C. W., J. C. Fernandez, I. Henins, H. W. Hoida, T. R. Jarboe, S. O. Knox, A. J. Marklin, and K. F. McKenna, 1986, Phys. Fluids **29**, 3415.

Barnes, D. C., C. E. Segler, and D. V. Anderson, 1979, in *Compact Toruses and Energetic Particle Injection,* Proceedings U.S.-Japan Joint Symposium (Princeton Plasma Physics Laboratory, Princeton, NJ), p. 110.

Batchelor, D. B., E. F. Jaeger, and M. D. Carter, 1990, "Fast Wave Current Drive for ITER Using the ORION Code," ITER Conceptual Design Activity, Garching, Report ITER-IL-HD-7-0-2.

Bateman, G., 1978, *MHD Instabilities* (MIT, Cambridge, MA).

Bathke, C. G., and R. A. Krakowski, 1985, Fusion Technol. **8**, 1616.

Beidler, C., G. Grieger, E. Harmeyer, N. Karulin, J. Kisslinger, W. Lotz, J. Nührenberg, F. Rau, and H. Wobig, 1992, in *Plasma Physics and Controlled Nuclear Fusion Research Proceeding of the 14th International Conference, Würzburg, 1992* (IAEA, Vienna), paper EN 56/G-1-2.

Beiser, A., and B. Raab, 1962, Phys. Fluids **177**, 1962.

Bell, M. G., *et al.*, 1989, in *Plasma Physics and Controlled Nuclear Fusion Research: Proceedings of the 12th International Conference, Baltimore, 1988* (IAEA, Vienna), Vol. 1, p. 27.

Berk, H. L., H. Momota, and T. Tajima, 1988, Phys. Fluids **30**, 3024.

Berk, H. L., B. N. Breizman, and H. Ye, 1992, Phys. Lett. A **162**, 475.

Bernard, L. C., F. J. Helton, R. W. Moore, and T. N. Todd, 1983, Nucl. Fusion **23**, 1475.

Bernstein, I., E. A. Frieman, M. D. Kruskal, and R. M. Kulsrud, 1958, Proc. R. Soc. London Ser. A **244**, 17.

Bespoludennov, S. G., L. M. Degtyarev, and S. Yu. Medvedev, 1986, Sov. J. Plasma Phys. **12**, 44.

Betti, R., and J. P. Freidberg, 1992, Phys. Fluids B **4**, 1465.

Bevir, M. K., and J. W. Gray, 1980, in *Reversed Field Pinch Theory: Proceedings of Workshop 1980, Session III* (Los Alamos Scientific Laboratory, Los Alamos, NM), paper A-3.

Bickerton, R. J., 1977, "Survey of Tokamak Experiments" (Culham Laboratory, Abingdon, England), Report CLM-R176.

Bickerton, R. J., 1989, Comments Plasma Phys. Control. Fusion **13**, 29.

Bickerton, R. J., J. W. Connor, and J. B. Taylor, 1971, Nature (London) Phys. Sci. **229**, 110.

Bickerton, R. J., and H. London, 1958, Proc. Phys. Soc. London **72**, 116.

Biglari, H., and L. Chen, 1991, Phys. Rev. Lett. **67**, 3681.

Biglari, H., P. H. Diamond, and P. W. Terry, 1990, Phys. Fluids B **2**, 1.

Biglari, H., P. H. Diamond, Y.-B. Kim, B. A. Carreras, V. E. Lynch, F. L. Hinton, G. M. Staebler, R. E. Waltz, C. P. Ritz, H. Lin, T. L. Rhodes, A. J. Wootton, P. W. Terry, L. Garcia, *et al.*, 1991, in *Plasma Physics and Controlled Nuclear Fusion Research: Proceedings of the 13th International Conference, Washington, 1990* (IAEA, Vienna), Vol. 2, p. 191.

Biglari, H., F. Zonca, and L. Chen, 1992, Phys. Fluids B **4**, 2385.

Bishop, C. M., 1991, "A Review of Alpha Particle Physics in Tokamaks," Culham Laboratory, Abingdon, England, Report AES Fusion 81.

Blevin, H. A., and P. C. Thonemann, 1962, in *Plasma Physics and Controlled Nuclear Fusion Research: Proceeding of the 1st International Conference, Salzburg, 1961* (IAEA, Vienna), Nuclear Fusion Supplement, Part 1, p. 55.

Bloom, E. E., 1990, Nucl. Fusion **30**, 1879.

Bodin, H. A., 1990, Nucl. Fusion **30**, 1717.

Bodin, H. A., R. A. Krakowski, and S. Ortolani, 1986, Fusion Technol. **10**, 307.

Boivin, R. L., S. Kirkpatrick, D. Manos, and S. Zweben, 1990, Rev. Sci. Instrum. **61**, 3208.

Bol, K., J. L. Cecchi, C. C. Daughney, F. DeMarco, R. A. Ellis, Jr., H. P. Eubank, H. P. Furth, H. Hsuan, E. Mazzucato, and R. R. Smith, 1990, 1975, in *Plasma Physics and Controlled Nuclear Fusion Research: Proceedings of the 5th International Conference, Tokyo, 1974* (IAEA, Vienna), Vol. 1, p. 83.

Book, D. L., 1990 "NRL Plasma Formulas" (Naval Research Laboratory, Washington, DC), Report NRL Publication

177–4405.
Boozer, A. H., 1983, Phys. Fluids **26**, 496.
Boozer, A. H., T. K. Chu, R. L. Dewar, H. P. Furth, J. A. Goree, J. L. Johnson, R. M. Kulsrud, D. A. Monticello, G. Kuo-Petravic, G. V. Sheffield, S. Yoshikawa, and O. Betancourt, 1983, in *Plasma Physics and Controlled Nuclear Fusion Research: Proceedings of the 9th International Conference, Baltimore, 1992* (IAEA, Vienna), Vol. III, p. 129.
Bornatici, M., R. Cano, O. DeBarbieri, F. Engelmann, 1983, Nucl. Fusion **23**, 1153.
Borrass, K., 1989, "Disruptive Tokamak Density Limit as Scrape-Off Layer/Divertor Phenomenon," Commission of the European Communities NET Report 95, EUR-FU/80/89-95.
Bosch, H.-S., and G. M. Hale, 1992, Nucl. Fusion **32**, 611.
Braams, B. J., 1987, "A Multi-Fluid Code for Simulation of the Edge Plasma in Tokamaks," Commission of the European Communities, NET Report 68, EUR-FU-XII-80/87/68, January.
Braginskii, S. I., 1965, in *Reviews of Plasma Physics,* Vol. 1, edited by M. A. Leontovich (Consultants Bureau, New York), p. 205.
Brambilla, M., 1976, Nucl. Fusion **16**, 47.
Bridgeman, P. W., 1937, *Dimensional Analysis* (Yale University, New Haven, Connecticut).
Brooks, J. N., 1990, Fusion Technol. **18**, 239.
Buckingham, E., 1914, Phys. Rev. Lett. **4**, 345.
Burrell, K. H., and the L to H Transition Physics Task Group, 1991, Bull. Am. Phys. Soc. **36**, 2474.
Burtsev, V. A., V. M. Kozhevin, and A. N. Makhanokov, 1987, in *Fusion Reactor Design and Technology: Proceedings of the 4th IAEA Technical Committee Meeting and Workshop, Yalta, 1986* (IAEA, Vienna), Vol. 1, p. 413.
Cairns, R. A., 1991, *Radio Frequency Heating of Plasmas* (Adam Hilger, Bristol).
Callen, J. D., 1990, Phys. Fluids B **2**, 2869.
Callen, J. D., 1991, "Transport Processes in Magnetically Confined Plasmas," University of Wisconsin, Madison, Report UW-CPTC 91-18, December.
Callen, J. D., B. A. Carreras, and R. A. Stambaugh, 1992, Phys. Today **45**, 34.
Callen, J. D., *et al.*, 1979, in *Plasma Physics and Controlled Nuclear Fusion Research: Proceedings of the 7th International Conference, Innsbruck, 1978* (IAEA, Vienna), Vol. 1, p. 415.
Campbell, D. J., D. F. H. Start, J. A. Wesson, D. V. Bartlett, V. P. Bhatnagar, M. Bures, J. G. Cordey, G. A. Cottrell, P. A. Dupperex, A. W. Edwards, *et al.*, 1988, Phys. Rev. Lett. **60**, 2148.
Caramana, E. J., and D. A. Baker, 1984, Nucl. Fusion **24**, 423.
Caramana, E. J., R. A. Nebel, and D. D. Schnack, 1983, Phys. Fluids **26**, 1305.
Caramana, E. J., and D. D. Schnack, 1986, Phys. Fluids **29**, 3023.
Carlson, A. W., 1987, Phys. Fluids **30**, 1497.
Carreras, B. A., 1992, "Transport Mechanism Acting in Toroidal Devices: A Transitions View," Oak Ridge National Laboratory Report ORNL/TM-12209.
Carreras, B. A., and P. H. Diamond, 1989, Phys. Fluids B **1**, 1011.
Carreras, B. A., L. Garcia, and V. E. Lynch, 1991, Phys. Fluids B **3**, 1438.
Carreras, B. A., H. R. Hicks, J. A. Holmes, V. E. Lynch, L. Garcia, J. H. Harris, T. C. Hender, and B. F. Masden, 1983, Phys. Fluids **26**, 3569.
Carreras, B. A., H. R. Hicks, J. A. Holmes, V. E. Lynch and G. H. Neilson, 1984, Nucl. Fusion **24**, 1347.
Carreras, B. A., G. Grieger, J. H. Harris, J. L. Johnson, J. F. Lyon, O. Motojima, 1988, Nucl. Fusion **28**, 1613.
Carreras, B. A., H. R. Hicks, J. A. Holmes, and B. V. Waddell, 1980, Phys. Fluids **23**, 1811.
Challis, C. D., J. G. Cordey, H. Hamnen, P. M. Stubberfield, J. P. Christiansen, E. Lazzaro, D. G. Muir, D. Stork, and E. Thompson, 1989, Nucl. Fusion **29**, 563.
Chang, C. S., and F. L. Hinton, 1982, Phys. Fluids **25**, 1493.
Chang, C. S., and F. L. Hinton, 1986, Phys. Fluids **29**, 3314.
Chen, L., R. B. White, and M. N. Rosenbluth, 1984, Phys. Rev. Lett. **52**, 1122.
Cheng, C. Z., 1990, Phys. Fluids B **2**, 1427.
Cheng, C. Z., L. Chen, and M. S. Chance, 1984, Ann. Phys. (N.Y.) **161**, 21.
Christiansen, J. P., J. G. Cordey, K. Thomsen, A. Tanga, and JET Team, J. C. DeBoo, D. P. Schissel, T. S. Taylor, and DIII-D Research Team, O. J. W. F. Kardaun, F. Wagner, F. Ryter, and ASDEX Team, S. M. Kaye, and PDX and PDX-M Teams, Y. Miura, N. Suzuki, and the JET-2M Group, 1992, Nucl. Fusion **32**, 291.
Christiansen, J. P., B. Balet, D. Boucher, C. D. Challis, J. G. Cordey, C. Gormezano, C. Gowers, G. Kramer, D. G. Muir, S. V. Neredatchin, *et al.*, 1992, Plasma Phys. Control. Fusion **34**, 1881.
Cohen, R. H., 1987, Phys. Fluids **30**, 2442; **31**, 421(E).
Cohen, S. A., K. A. Werley, D. E. Post, B. J. Braams, J. L. Perkins, and D. Pearlstein, 1990, J. Nucl. Mater. **176&77**, 909.
Cohn, D. R., R. R. Parker, and D. L. Jassby, 1976, Nucl. Fusion **16**, 31.
Cohn, D. R., J. E. C. Williams, L. Bromberg, K. Kreischer, D. B. Montgomery, and R. R. Parker, 1978, in "Fusion Reactor Design Concepts " (IAEA Vienna), p. 113.
Colchin, R. J., S. C. Aceto, A. C. England, R. C. Isler, M. Murakami, D. A. Rasmussen, T. Uckan, J. B. Wilgen, and J. J. Zielinski, 1992, Nucl. Fusion **7**, 1225.
Colestock, P. L., 1984, IEEE Transactions on Plasma Science, Vol. PS-12, 64.
Combs, S., 1993, Rev. Sci. Instrum. **64**, 1679.
Conn, R. W., 1981, in *Fusion,* edited by E. Teller (Academic, New York), Vol. 1, Part B, p. 193.
Conn, R. W., and R. Gross, 1985, Chairmen, "Report on High Power Density Fusion Systems," United States Department of Energy, Magnetic Fusion Advisory Committee, Panel X.
Connor, J. W., and J. B. Taylor, 1977, Nucl. Fusion **17**, 1047.
Connor, J. W., and J. B. Taylor, 1984, Phys. Fluids **27**, 2676.
Cooke, P. I. H., R. Hancox, and W. Spears, 1989, "Parameters of a Reference Tokamak Reactor" (Culham Laboratory, Abingdon, England), Report CLM-R298.
Cooper, W. A., S. P. Hirshman, and D. K. Lee, 1989, Nucl. Fusion **29**, 617.
Copenhaver, C., R. A. Krakowski, N. M. Schnurr, R. L. Miller, C. G. Bathke, R. L. Hagenson, C. R. Mynard, A. D. Chaffee, C. Cappiello, and J. W. Davidson, 1985, "Compact Reversed-Field Pinch Reactors (CRFPR): Fusion Power-Core Integration Study," Los Alamos National Laboratory, Report LA-10500-MS (August, 1985).
Coppi, B., 1977, Comments Plasma Phys. Controll. Fusion **3**, 47.
Coppi, B., A. Ferreira, J. W.-K. Mark, and J. J. Ramos, 1979, Nucl. Fusion **19**, 715.
Coppi, B., S. Migliuolo, F. Pegoraro, and F. Porcelli, 1990, Phys. Fluids B **2**, 927.
Cordey, J. G., 1977, in *Theory of Magnetically Confined Plasma:*

Proceedings of the Course, Varenna, Italy (Pergamon, Oxford, England), p. 323.
Cordey, J. G., R. J. Goldston, and D. R. Mikkelsen, 1981, Nucl. Fusion **21**, 581.
Cordey, J. G., R. J. Goldston, and R. R. Parker, 1992, Phys. Today **45**, 22.
Cordey, J. G., E. M. Jones, D. F. H. Start, A. R. Curtis, and I. P. Jones, 1979, Nucl. Fusion **19**, 249.
Core, W. F., 1974, private communications, JET Team, Culham, England.
Davidson, R. C., and N. A. Krall, 1977, Nucl. Fusion **17**, 1313.
DeBoo, J., R. Waltz, and T. Osborne, 1991, in *Proceedings of the 18th European Conference on Controlled Fusion and Plasma Physics, Berlin* (European Physical Society), Vol. 1, p. 173.
DeGrassie, J. S., T. E. Evans, G. L. Jackson, N. Ohyabu, S. C. McCool, K. W. Gentle, W. L. Rowan, A. J. Wootton, F. Karger, and G. Haas, 1989, in *Plasma Physics and Controlled Nuclear Fusion Research: Proceedings of the 12th International Conference, Nice, 1988* (IAEA, Vienna), Vol. 1, p. 341.
Diamond, P. H., Y.-M. Liang, B. A. Carreras, and K. Siddikman, 1991, Bull. Am. Phys. Soc. **36**, 2348.
Diamond, P. H., and Y. B. Kim, 1991, Phys. Fluids B **3**, 1626.
DiMarco, J. N., 1988, "Update of RFP Scaling Data," Los Alamos Scientific Laboratory Report LA-UR-Rev-88-3375.
Doerner, R.-P., D. T. Anderson, F. S. B. Anderson, P. H. Probert, J. L. Shohet, J.N. Talmadge, 1986, Phys. Fluids **29**, 3807.
Ecker, G. H., 1972, *Theory of Fully Ionized Plasma* (Academic, New York/London).
Efthimion, P. C., C. W. Barnes, M. G. Bell, H. Biglari, N. Bretz, P. H. Diamond, G. Hammett, W. Heidbrink, R. Hulse, D. Johnson, *et al.*, 1991, Phys. Fluids B **3**, 2315.
Ehst, D. A., and C. F. F. Karney, 1990, "Neoclassical Effects on RF Current Drive," Argonne National Laboratory Report ANL/FPP/TM-247.
Emmert, G. A., R. M. Wieland, A. T. Mense, and J. N. Davidson, 1980, Phys. Fluids **23**, 803.
Engelmann, F., 1987, Phys. Scr. T **16**, 16.
Farengo, R., and R. D. Brooks, 1992, Nucl. Fusion **32**, 67.
Fisch, N. J., 1980, Phys. Rev. Lett. **41**, 873.
Fisch, N. J., 1987, Rev. Mod. Phys. **59**, 175.
Fisch, N. J., and A. H. Boozer, 1980, Phys. Rev. Lett. **45**, 720.
Freeman, R. L., and E. M. Jones, 1974, "Atomic Collision Processes in Plasma Physics Experiments," Culham Laboratory, Abingdon, England, Report CLM-R-137.
Freidberg, J. P., 1982, Rev. Mod. Phys. **54**, 801.
Freidberg, J. P., 1987, *Ideal Magneto-Hydrodynamics* (Plenum, New York).
Fu, G. Y., and J. Van Dam, 1989, Phys. Fluids B **1**, 1949.
Fujisawa, N., 1990a, "Bootstrap Current and Neutral Beam Current Drive," International Thermonuclear Experimental Reactor Report ITER-IL-PH-6-9-J-1.
Fujisawa, N., 1990b, "Comments on Bootstrap Currents in ITER and Improved Operation Scenario," International Thermonuclear Experimental Reactor Report ITER-IL-PH-6-0-J-10.
Furth, H. P., 1975, Nucl. Fusion **15**, 487.
Furth, H. P., R. J. Goldston, S. J. Zweben, D. J. Sigmar, 1990, Nucl. Fusion **30**, 1799.
Furth, H., P. J. Killeen, G. Coppi, and M. N. Rosenbluth, 1966, in *Plasma Physics and Controlled Nuclear Fusion Research: Proceedings of the 2nd International Conference, Culham, 1965* (IAEA, Vienna), Vol. I, p. 103.
Furth, H., P. J. Killeen, and M. N. Rosenbluth, 1963, Phys. Fluids **6**, 459.
Furth, H. P., P. H. Rutherford, and H. Selberg, 1973, Phys. Fluids **16**, 1054.
Fussmann, G., W. Engelhardt, W. Feneberg, J. Gernhardt, E. Glock, F. Karger, S. Sesnic, and H. P. Zehrfeld, 1979, in *Plasma Physics and Controlled Nuclear Fusion Research: Proceedings of the 7th International Conference, Innsbruck, 1978* (IAEA, Vienna), Vol. 1, p. 401.
Galeev, A. A., 1971, Sov. Phys. JETP **32**, 752.
Galeev, A. A., and R. Z. Sagdeev, 1968, Sov. Phys. JETP **26**, 233.
Gang, F. Y., D. J. Sigmar, and J.-N. LeBoeuf, 1992, Phys. Lett. A **161**, 517.
Gauster, W. B., 1990, Nucl. Fusion **30**, 1897.
Gibson, A., 1978, J. Nucl. Mater. **76&77**, 92.
Gibson, A., and J. B. Taylor, 1967, Phys. Fluids **10**, 2653.
Gilgenbach, R. M., M. E. Read, K. E. Hackett, R. Lucey, B. Hui, V. L. Granatstein, K. R. Chu, A. C. England, C. M. Loring, O. C. Eldridge, *et al.*, 1980, Phys. Rev. Lett. **44**, 647.
Glasstone, S., and R. H. Lovberg, 1960, *Controlled Thermonuclear Reactions* (Van Nostrand, New York).
Goedbloed, J. P., and P. H. Sakonaka, 1974, Phys. Fluids **17**, 908.
Goldston, R. J., 1984, Plasma Phys. Control. Fusion **26**, 87.
Goldston, R. J., R. E. Waltz, G. Bateman, D. P. Stotler, C. E. Stringer, and J. Kinsey, 1992, Fusion Technol. **21**, 1077.
Gorelenkov, N. N., and S. E. Sharapov, 1992, Phys. Scr. **45**, 163.
Gouge, M. J., J. T. Hogan, S. L. Milora, and C. E. Thomas, 1988, "Compact Toroid Refueling of Reactors," Oak Ridge National Laboratory Report ORNL/TM-10720.
Gourdon, C., D. Marty, E. K. Maschke, and J. P. Dumont, 1969, in *Plasma Physics and Controlled Nuclear Fusion Research: Proceedings of the 3rd International Conference, Novosibirsk, 1968* (IAEA, Vienna), Vol. I, p. 847.
Grad, H., 1967, Phys. Fluids **10**, 137.
Greenwald, M., *et al.*, 1984, Phys. Rev. Lett. **53**, 352.
Greenwald, M., J. L. Terry, S. M. Wolfe, S. Ejima, M. G. Bell, S. M. Kaye, and G. H. Neilson, 1988, Nucl. Fusion **28**, 2199.
Grieger, G., C. Beidler, E. Harmeyer, J. Junker, J. Kisslinger, W. Lotz, P. Merkel, A. Montvai, J. Nührenberg, F. Rau, A. Schlüter, H. Wobig, and R. Zille, 1989, in *Plasma Physics and Controlled Nuclear Fusion Research: Proceedings of the 12th International Conference, Nice, 1988* (IAEA, Vienna), Vol. 2, p. 369.
Grieger, G., C. Beidler, E. Harmeyer, W. Lotz, J. Kisslinger, P. Merkel, J. Nührenberg, F. Rau, E. Strumberger, and H. Wobig, 1992, Fusion Technol. **21**, 1767.
Grimm, R. C., R. L. Deward, and J. Manickam, 1983, J. Comput. Phys. **49**, 94.
Groebner, R. A., K. H. Burrell, and R. P. Seraydarian, 1990, Phys. Rev. Lett. **64**, 3015.
Hagenson, R. L., *et al.*, 1979, "The Reversed-Fluid Pinch Reactor (RFPR) Concept," Los Alamos Scientific Laboratory Report LA-9747-MS.
Hagenson, R. L., and R. A. Krakowski, 1981, "A Compact Toroid Fusion Reactor Based on the Reversed Field θ-Pinch," Los Alamos Scientific Laboratory Report LA-8758-MS.
Hamasaki, S., and N. A. Krall, 1979, in *Plasma Science, Proceedings of IEEE International Conference, Montreal, 1979* (IEEE, New York), p. 143.
Hancox, R., R. A. Krakowski, and W. R. Spears, 1981, Nucl. Eng. Es. **63**, 251.
Haney, S. W., L. J. Perkins, J. Mandrekas, and W. M. Stacey, Jr., 1990, Fusion Technol. **18**, 606.

Harbor, P. J., 1981, *Introduction to Plasma Physics for Fusion Reactors, Ispra, Italy, Oct 1979–Jan 1980* (Harwood Academic, Chur, Switzerland).
Harmeyer, E., J. Kisslinger, F. Rau, and H. Wobig, 1986, in *Fusion Reactor Design and Technology: Proceedings of the 4th IAEA Technical Committee Meeting, Yalta, 1986* (IAEA, Vienna), Vol. 1, p. 361.
Harned, D. S., 1984, Phys. Fluids **27**, 554.
Harris, J. H., M. Murakami, B. A. Carreras, J. D. Bell, G. L. Bell, T. S. Bigelow, L. A. Charlton, N. Dominguez, J. L. Dunlap, J. C. Glowienka, *et al.*, 1989, Phys. Rev. Lett. **63**, 1249.
Harris, J. H., E. Anabitarte, G. L. Bell, J. D. Bell, T. S. Bigelow, B. A. Carreras, L. R. Baylor, T. S. Bigelow, R. J. Colchin, R. A. Dory, *et al.*, 1990, Phys. Fluids B **2**, 1353.
Harris, J. H., J. B. Wilgren, G. R. Hanson, J. D. Bell, M. Murakami, S. C. Aceto, L. A. Charlton, R. J. Colchin, E. C. Crume, N. Dominguez, *et al.*, 1990, 1993, *Plasma Physics and Controlled Nuclear Fusion Research, Proceedings of the 14th International Conference* (IAEA, Vienna), Vol. 2, p. 413.
Harrison, M. F. A., and E. S. Hotston, 1990, J. Nucl. Mater. **176&177**, 256.
Hastings, D. E., W. A. Houlberg, and K. C. Shaing, 1985, Nucl. Fusion **25**, 445.
Hawryluk, J., 1987, in *Plasma Physics and Controlled Nuclear Fusion Research: Proceedings of the 11th International Conference, Kyoto, 1986* (IAEA, Vienna), Vol. 1, p. 51.
Heidbrink, W. W., and E. J. Strait, 1992, Nucl. Fusion **31**, 1635.
Heidbrink, W. W., E. J. Strait, D. Doyle, G. Sager and R. J. Snider, 1991, Nucl. Fusion **31**, 1635.
Heifetz, D., D. Post, M. Petravic, J. Weisheit, and G. Bateman, 1982, J. Comput. Phys. **46**, 309.
Heifetz, D., J. Schmidt, M. Ulrickson, and D. Post, 1983, J. Vac. Sci. Technol. A **1**, 911.
Hender, T. C., 1993, in *Plasma Physics and Controlled Nuclear Fusion Research: Proceedings of the 14th International Conference, Würzburg, 1992* (IAEA, Vienna), paper G-2-5.
Hender, T. C., and D. C. Robinson, 1983, in *Plasma Physics and Controlled Nuclear Fusion Research: Proceeding of the 9th International Conference, Baltimore, 1982* (IAEA, Vienna), Vol. 3, p. 417.
Hershkowitz, N., S. Miyoshi, and D. D. Ryutov, 1990, Nucl. Fusion **30**, 1761.
Hinton, F. L., and R. D. Hazeltine, 1976, Rev. Mod. Phys. **48**, 239.
Hirano, K., 1984, Nucl. Fusion **24**, 1159.
Hirshman, S. P., 1980, Phys. Fluids **23**, 1238.
Hirshman, S. P., and D. J. Sigmar, 1981, Nucl. Fusion **21**, 1079.
Hively, L. M., and D. J.Sigmar, 1989, "Biblography of Fusion Product Physics in Tokamaks," Oak Ridge National Laboratory Report ORNL/TM-11177.
Ho, Y. H., and S. C. Prager, 1991, Phys. Fluids B **3**, 3099.
Ho, Y. H., S. C. Prager, and D. D. Schnack, 1989, Phys. Rev. Lett. **62**, 1504.
Hoffman, A. L., 1992, "Proposed Research Program on Field Reversed Configurations Using the LSX Facility," University of Washington, Seattle, WA, Presentation to the Office of Fusion Energy, Germantown, MA.
Hoffman, A. L., L. N. Carey, E. A. Crawford, D. G. Harding, T. E. DeHart, K. F. McDonald, J. I. McNeil, R. D. Milroy, J. T. Slough, R. Maqueda, and G. A. Wurden, 1993, Fusion Technol. **23**, 2.
Hoffman, A. L., R. D. Milroy, 1983, Phys. Fluids **26**, 3170.
Hoffman, A. L., R. D. Milroy, J. T. Slough, and L. C. Steinhauer, 1986, Fusion Technol. **9**, 48.
Hoffman, A. L., and J. T. Slough, 1986, Nucl. Fusion **26**, 1693.
Hogan, J. T., and D. L. Hillis, 1991, "Helium Transport and Exhaust in Tokamaks," Oak Ridge National Laboratory Report ORNL/TM-11935 and ITER/US/91/PH-13-02.
Holdren, J. P., D. H. Berwald, R. J. Budnitz, J. G. Crocker, J. G. Delene, R. D. Endicott, M. S. Kazimi, R. A. Krakowski, B. G. Logan, and K. R. Schultz, 1988, Fusion Technol. **13**, 7.
Holdren, J. P., D. H. Berwald, R. J. Budnitz, J. G. Crocker, J. G. Delene, R. D. Endicott, M. S. Kazimi, R. A. Krakowski, B. G. Logan, and K. R. Schultz, 1989 "Report of Senior Committee on Environmental Safety and Economic Aspects of Magnetic Fusion Energy," Lawrence Livermore National Laboratory Report UCRL 53766.
Holdren, J. P., 1991, Annual Review of Energy and the Environment Vol. **17**, p. 235.
Houlberg, W. A., 1982, Nucl. Fusion **22**, 935.
Houlberg, W. A., D. W. Ross, G. Bakeman, S. C. Cowley, P. C. Efthimion, W. W. Pfeiffer, G. D. Porter, D. E. Shrimaker, L. E. Sugiyama, and J. C. Wiley, 1990, Phys. Fluids B **2**, 2913.
Howe, H. C., 1981, "Physics Considerations for the FED Limiter," Oak Ridge National Laboratory Report ORNL/TM-7803.
Howe, H. C., 1990, "Physics Models in the Toroidal Transport Code PROCTR," Oak Ridge National Laboratory Report ORNL/TM-11521.
Hsu, C. T., and D. J. Sigmar, 1992, Phys. Fluids B **4**, 1492.
Hübener, J., and W. Maurer, 1987, in *Fusion Reactor Design and Technology: Proceedings of the 4th IAEA Technical Committee Meeting and Workshop, Yalta, 1986* (IAEA, Vienna), Vol. 1, p. 333.
Hugrass, W. N., I. R. Jones, K. F. McKenna, M. G. R. Phillips, R. G. Storer, and H. Tuczek, 1980, Phys. Rev. Lett. **44**, 1676.
Hwang, D. Q., and J. R. Wilson, 1981, Proc. IEEE **69**, 1030.
Ida, K., S. Hidekuma, Y. Miura, T. Fujita, M. Mori, K. Hoshino, N. Suzuki, T. Yamauchi, and JFT-2M Group, 1990, Phys. Rev. Lett. **65**, 1364.
Iiyoshi, A., M. Fujiwara, O. Motojima, N. Ohyabu, and K. Yamazaki, 1990, Fusion Technol. **17**, 169.
Ishimura, T., 1986, Phys. Fluids **27**, 2139.
Isler, R. C., E. C. Crume, L. D. Horton, M. Murakami, L. R. Baylor, G. L. Bell, T. S. Bigelow, A. C. England, J. C. Glowienka, T. C. Jernigan, *et al.*, 1991, Nucl. Fusion **31**, 245.
ITER Conceptual Design Team, 1991, ITER Conceptual Design report, IAEA Vienna ITER Documentation Series, No. 18.
Itoh, K., H. Sanuki, S.-I. Itoh, and K. Tani, 1991, Nucl. Fusion **31**, 1405.
Itoh, S-I., and K. Itoh, 1988, Phy. Rev. Lett. **60**, 2276.
Itoh, S-I., and K. Itoh, 1989, Nucl. Fusion **29**, 1031.
Itoh, S-I., and K. Itoh, 1990, J. Phys. Soc. Jpn. **59**, 3815.
Itoh, S-I., N. Ueda, and K. Itoh, 1990, Plasma Phys. Control. Fusion **32**, 415.
Itoh, S., N. Hiraki, V. Nakamura, K. Nakamura, A. Nagao, S. Moriyama, T. Fujita, E. Jotaki, and S. Kawasaki, 1991, in *Plasma Physics and Controlled Nuclear Fusion Research: Proceedings of the 13th International Conference, Washington, 1990* (IAEA, Vienna), Vol. 1, p. 733.
Itoh, S-I., and K. Itoh, 1991, in *Plasma Physics and Controlled Nuclear Fusion Research: Proceedings of the 13th International Conference, Washington, 1990* (IAEA, Vienna), Vol. 2, p. 321.
Jackson, G. L., J. Winter, T. S. Taylor, K. H. Burrell, J. C. DeBoo, C. M. Greenfield, R. J. Groebner, T. Hodapp, K. Holtrop, E. A. Lazarus, *et al.*, 1991, Phys. Rev. Lett. **67**, 3098.
Jacobsen, A. R., and R. W. Moses, 1984, Phys. Rev. A **29**, 3335.

Jaenicke, R., A. Weller, H. J. Hartfuss, A. Lazaros, S. Sattler, H. Zoom, and the W7-AS Team, 1993, in *Plasma Physics and Controlled Nuclear Fusion Research: Proceedings of the 14th International Conference, Würzburg, 1992* (IAEA, Vienna), paper C-2-1.

Janev, R. K., 1991, Ed., "Atomic and Plasma-Material Interaction Data for Fusion," Nucl. Fusion Supplement, Vol. 1.

Jarboe, T. R., 1989, Fusion Technol. **15**, 7.

Jarboe, T. R., and B. Alper, 1987, Phys. Fluids **30**, 1177.

Jarboe, T. R., I. Henins, H. W. Hoida, R. K. Linford, J. Marshal, D. A. Platts, and A. R. Sherwood, 1980, Phys. Rev. Lett. **45**, 1264.

Jardin, S. C., N. Pomphrey, and J. DeLucia, 1986, J. Comput. Phys. **66**, 481.

Jassby, D. L., 1976, Nucl. Fusion, **16**, 15.

Jensen, R. V., D. E. Post, W. H. Grassberger, G. B. Tartar, and W. A. Lokke, 1977, Nucl. Fusion **17**, 1187.

JET Team, 1992, Nucl. Fusion **32**, 187.

Ji, H., H. Toyama, K. Miyamoto, S. Shinohara, and A. Fujisawa, 1991, Phys. Rev. Lett. **67**, 62.

Johnson, C. E., G. W. Hollenberg, N. Roux, and H. Watanabe, 1989, in *Proceedings of the 1st International Symposium on Fusion Nuclear Technology, Tokyo, 1988, Fusion Engineering and Design* (North-Holland, Amsterdam), Pt. A, p. 145.

Jones, L. P. D. F., L. Galbiati, M. Gredel, and W. Neddermeyer, 1991, in *Proceedings of the 16th Symposium on Fusion Technology, London, U.K., September 1990* (North-Holland, Amsterdam), Vol. 2, p. 1378.

Kadomtsev, B. B., 1965, *Plasma Turbulence* (Academic, London).

Kadomtsev, B. B., 1975, Sov. J. Plasma Phys. **1**, 295.

Kadomtsev, B. B., and O. P. Pogutse, 1970, in *Review of Plasma Physics,* edited by M. A. Leontovich (Consultants Bureau, New York), Vol. 5, p. 249.

Kadomtsev, B. B., and O. P. Pagutse, 1971, Nucl. Fusion **11**, 67.

Kadomtsev, B. B., F. S. Troyon, and M. L. Watkins, 1990, Nucl. Fusion **30**, 1675.

Kardaun, O., 1993, in *Plasma Physics and Controlled Nuclear Fusion Research: Proceedings of the 14th International Conference, Würzburg, 1992* (IAEA, Vienna), paper F-1-3.

Karger, F., and K. Lackner, 1977, Phys. Lett. A **61**, 385.

Kaye, S. M., and R. J. Goldston, 1985, Nucl. Fusion **25**, 65.

Kazawa, Y., Y. Itou, S. Suzuki, T. Okazaki, O. Motojima, and K. Uo, 1987, in *Proceedings International Stellarator/Heliotron Workshop (IAEA Tech. Comm. Mtg. Kyoto, 1986),* Report PPLK-5 (Plasma Physica Laboratory, Kyoto University), Vol. 2, p. 540.

Keilhacker, M., and the Jet Team, 1991, Plasma Phys. Control. Fusion **33**, 1453.

Kieras, C., and J. Tataronis, 1982, J. Plasma Phys. **28**, 395.

Kelley, G. G., 1973, "Toroidal Band Limiter and Pump for a Tokamak," patent submission, Oak Ridge National Laboratory.

Kernbichler, W., H. Heindler, H. Momota, Y. Tomita, A. Ishida, S. Ohi, M. Ohnishi, K. Sato, G. H. Miley, H. L. Berk, W. Dove, *et al.*, 1991 in *Plasma Physics and Controlled Nuclear Fusion Research: Proceedings of the 13th International Conference, Washington, 1990* (IAEA, Vienna), Vol. 3, p. 555.

Kikuchi, M., M. Azumi, S. Tsuji, K. Tani and H. Kubo, 1990, Nucl. Fusion **30**, 343.

Killeen, J., 1992, "Magnetic Fusion Computing: A Personal Retrospective View," Varenna-Lausanne International Workshop, Varenna, Italy, Lawrence Livermore National Laboratory preprint UCRL-JC-111405.

Kolesnichenko, Ya. I., 1980, Nucl. Fusion **20**, 727.

Komarek, P., C. C. Baker, G. O. Filatov, S. Shimamoto, 1990, Nucl. Fusion **30**, 1817.

Kovrizhnykh, L. M., 1984, Nucl. Fusion **24**, 851.

Krakowski, R. A., 1991, Fusion Technol. **20**, 121.

Krakowski, R. A., R. L. Hagenson, N. M. Schnurr, C. Copenhaver, C. G. Bathke, R. L. Miller, and M. J. Embrechts, 1986, Nucl. Eng. Design Fusion **4**, 75.

Krakowski, R. A., R. L. Miller, C. G. Bathke, R. L. Hagenson, A. S. Tai, C. E. Wagner, R. W. Bussard, R. A. Shanny, J. S. Herring, L. M. Lidsky, *et al.*, 1981 in *Plasma Physics and Controlled Nuclear Fusion Research: Proceedings of the 13th International Conference, Brussels, 1980* (IAEA, Vienna), Vol. 2, p. 607.

Krall, N. A., 1987, Phys. Fluids **30**, 878.

Kulcinski, G. L., G. A. Emmert, J. P. Blanchard, L. A. El-Guebaly, H. Y. Khater, J. F. Santarius, M. E. Sawan, I. N. Sviatoslavsky, L. J. Wittenberg, and R. J. Witt, 1989, Fusion Technol. **15**, 1233.

Kusano, K., and T. Sato, 1990, Nucl. Fusion **30**, 2075.

Lacatski, J. T., W. A. Houlberg, and N. A. Uckan, 1985, "Plasma Engineering Analysis of a Small Torsatron Reactor," Oak Ridge National Laboratory Report ORNL/TM-9533.

Lackner, K. H., and N. A. O. Gottardi, 1990, Nucl. Fusion **30**, 767.

Langley, R. A., J. Bohdansky, W. Eckstein, P. Mioduszewski, J. Roth, R. Taglauer, E. W. Thomas, H. Verbeek, and K. L. Wilson, 1984, Data Compendium for Plasma Surface Interactions," Special Issue, Nuclear Fusion.

LeBoeuf, J.-N., D. K. Lee, B. A. Carreras, N. Dominguez, J. H. Harris, C. L. Hedrick, C. Hidalgo, J. A. Holmes, J. Ruiter, P. H. Diamond, A. S. Ware, Ch. P. Ritz, A. J. Wootton, W. L. Rowan, and R. V. Bravenec, 1991, Phys. Fluids B **3**, 2291.

Li, Y. M., S. M. Mahajan, and D. W. Ross, 1987, Phys. Fluids **30**, 1466.

Lehnert, B., 1977, Phys. Scr. **16**, 147.

Liewer, P. C., 1985, Nucl. Fusion **25**, 543.

Lisak, M., and N. Wilhelmson, 1987, Eds., "Symposium on the Role of Alpha Particles in Magnetically Confined Fusion Plasmas," Phys. Scr. T **16**,

Lloyd, B., G. L. Jackson, T. S. Taylor, E. A. Lazarus, T. C. Luce, and R. Prater, 1991, Nucl. Fusion **31**, 2031.

Logan, B. G., 1988, J. Fusion Eng. **4**, 242.

Logan, B. G., C. D. Henning, G. A. Carlson, W. L. Barr, G. W. Hamilton, R. W. Moir, B. M. Boghosian, B. M. Johnson, W. S. Neef, R. S. DeVoto, *et al.*, 1983, "Mirror Advanced Reactor Study," Lawrence Livermore National Laboratory Report UCRL-53333.

Lohr, J., R. W. Harvey, R. A. James, T. C. Luce, C. C. Petty, V. V. Alikaev, A. A. Bagdasarov, A. A. Borshchegovsky, Yu. V. Esipchuk, *et al.*, 1991, in *Radio Frequency Power in Plasmas,* AIP Conference Proceedings No. 244, edited by Donald B. Batchelor (AIP, New York), p. 255.

Lotz, W., P. Merkel, J. Nührenberg, and E. Strumberger, 1992, Plasma Phys. Control. Fusion **34**, 1037.

Luce, T. C., R. A. James, A. N. Fyakhretdinov, B. De Gentile, G. Giruzzi, Yu. Gorelov, J. De Haas, R. W. Harvey, S. Janz, J. M. Lohr, *et al.*, 1991, in *Plasma Physics and Controlled Nuclear Fusion Research: Proceedings of the 13th International Conference, Washington, 1990* (IAEA, Vienna), Vol. 1, p. 631.

Lyon, J. F., 1989, Fusion Technol. **15**, 1401.

Lyon, J. F., 1990, Fusion Technol. **17**, 19.

Lyon, J. F., B. A. Carreras, K. K. Chipley, M. J. Cole, J. H. Harris, T. C. Jernigan, R. L. Johnson, V. E. Lynch, B. E. Nel-

son, J. A. Rome, J. Sheffield, and P. B. Thompson, 1986, Fusion Technol. **10**, 179.
Lyon, J. F., G. Grieger, R. Rau, A. Iiyoshi, A. P. Navarro, L. M. Kovrizhnykh, O. S. Pavlichenko, and S. M. Hamberger, 1990, Nucl. Fusion **30**, 1695.
Matsuura, H., T. Mizuuchi, and T. Obiki, 1992, Nucl. Fusion **32**, 405.
Mattor, N., P. Terry, and S. C. Prager, 1992, Comments Plasma Phys. Control. Fusion **15**, 65.
McCracken, G. M., and P. E. Stott, 1979, Nucl. Fusion **19**, 889.
McNamara, B., 1981, Proc. IEEE **69**, 1043.
McNally, J. Rand, Jr., 1982, Nucl. Tech. Fusion **2**, 9.
Meade, D., 1974, Nucl. Fusion **14**, 289.
Menon, M. M., 1981, Proc. IEEE **69**, 885.
Mercier, C., 1960, Nucl. Fusion **1**, 47.
Mercier, C., 1979, in *Plasma Physics and Controlled Nuclear Fusion Research: Proceedings of the 7th International Conference, Innsbruck, 1978* (IAEA, Vienna), Vol. 1, p. 701.
Mikhailovskii, A. B., 1974, *Theory of Plasma Instabilities,* Vols. 1 and 2 (Consultants Bureau, New York).
Mikhailovski, A. B., 1975, Sov. Phys. JETP **41**, 890.
Mikkelsen, D. R., and C. E. Singer, 1983, Nucl. Fusion Tech. **4**, 237.
Miller, R. L., 1985, Fusion Technol. **8**, 1581.
Miller, R. L., C. G. Bathke, R. A. Krakowski, F. M. Heck, L. Green, J. S. Karbowski, J.H. Murphy, R. B. Tupper, R. A. DeLuca, A. Moazed, and R. A. Terry, 1983, "The Modular Stellator Reactor: A Fusion Power Plant," Los Alamos National Laboratory Report LA-9737-MS.
Miller, R. L., R. A. Krakowski, and C. G. Bathke, 1982, "Parametric Systems Analysis of the Modular Stellarator Reactor," Los Alamos National Laboratory Report, LA-9344-MS.
Milora, S. L., 1981, J. Fusion Energy **1**, 15.
Milora, S. L., 1989, J. Vac. Sci. Technol. A **7**, 925.
Milroy, R. D., D. C. Barnes, D. D. Schnack, and R. Bishop, 1987, in *Physics and Technology of Compact Toroids, Proceedings of the 8th Symposium, University of Maryland* (University of Maryland, College Park), p. 155.
Miyamoto, K., 1978, Nucl. Fusion **18**, 243.
Miyamoto, K., 1988, in *Physics of Mirrors, Reversed Field Pinches and Compact Tori: Proceedings of the Course and Workshop (EUR-11335-EN), Varenna, Italy* (Editrice Compositori, Bologna, Italy), p. 79.
Momota, H., A. Ishida, Y. Kohzaki, G. H. Miley, S. Ohi, M. Ohnishi, K. Sato, L. C. Steinhauer, Y. Tomita, and M. Tuszewski, 1992, Fusion Technol. **21**, 2307.
Monier-Garbet, P., C. DeMichelis, P. Ghendrih, C. Grisolia, A. Grosman, M. Mattioli, L. Poutchy, and J. C. Vallet, 1993, in *Plasma Physics and Controlled Nuclear Fusion Research: Proceedings of the 14th International Conference, Würzburg, 1992* (IAEA, Vienna), Vol. 1, p. 317.
Moreau, D., D. Becoulet, and Y. Peysson, 1991, Eds. "Fast Wave Current Drive in Reactors Scale Tokamaks," Arles, France (Ministère de la Recherche et de la Technologie, Delegation à l'Information Scientifique et Technique, Paris, France).
Moses, R. W., K. F. Schoenberg, and D. A. Baker, 1988, Phys. Fluids **31**, 3152.
Motojima, O., M. Fujiwara, and LHD Design Group, 1991, in *Recent Status of Large Helical Device Project, VIII Stellarator Workshop, Kharkov, U.S.S.R.* (IAEA, Vienna), p. 481.
Murakani, M., T. S. Bigelow, J. B. Wilgen, R. A. Dory, B. A. Carreras, S. C. Aceto, D. B. Batchelor, L. R. Baylor, G. L. Bell, J. D. Ball, *et al.*, 1993, in *Plasma Physics and Controlled Nuclear Fusion Research: Proceedings of the 14th International Conference, Würzburg, 1992* (IAEA, Vienna), Vol. 2, p. 391.
Murakami, M., K. H. Burrell, T. C. Jernigan, T. Amano, S. C. Bates, C. E. Bush, R. E. Clausing, R. J. Colchin, E. C. Crume, Jr., J. C. DeBoo, *et al.*, 1979, in *Plasma Physics and Controlled Nuclear Fusion Research: Proceedings of the 7th International Conference, Innsbruck, 1978* (IAEA, Vienna), Vol. 1, p. 269.
Murakami, M., J. D. Callen, and L. A. Berry, 1976, Nucl. Fusion **16**, 347.
Murakami, M., *et al.*, 1990, Phys. Rev. Lett. **66**, 707.
Mynick, H. E., 1992, "Transport of Energetic Ions by low-*n* Magnetic Perturbations," Princeton Plasma Physics Laboratory Report PPPL-2856.
Mynick, H. E., T. K. Chu, and A. H. Boozer, 1982, Phys. Rev. Lett. **48**, 322.
Mynick, H. E., and W. G. N. Hitchon, 1983, Nucl. Fusion **23**, 1053.
Nagami, N., and the JT-60 Team, 1991, in *Plasma Physics and Controlled Nuclear Fusion Research: Proceedings of the 13th International Conference, Washington, 1990* (IAEA, Vienna), Vol. 1, p. 53.
Najmabadi, F., R. W. Conn, N. Ghoniem, J. P. Blanchard, Y.-Y. Chu, P. I. H. Cooke, K. R. Schultz, R. A. Krakowski, S. Steiner, D.-K. Sze, P. J. Gierszewski, *et al.*, 1990, "The TITAN Reversed-Field-Pinch Fusion Reactor Study," University of California, Los Angeles Report UCLA-PPG-1200.
Najmabadi, F., R. W. Conn, and the ARIES Team, 1991, Fusion Technol. **19**, 783.
Navratil, G., R. A. Gross, M. E. Mauel, S. A. Sabbagh, M. G. Bell, R. Bell, N. Bretz, and J. Kesner, E. S. Marmar, J. L. Terry, P. A. Politzer, L. L. Lao, G. D. Porter, *et al.*, 1991, in *Plasma Physics and Controlled Nuclear Fusion Research: Proceedings of the 13th International Conference, Washington, 1990* (IAEA, Vienna), Vol. 1, p. 209.
Nebel, R. A., 1980, "Quasi-Steady Operation of Reversed Field Pinches," Ph.D. Thesis (University of Illinois, Nuclear Engineering Program).
Nishitani, T., K. Tobita, K. Tani, A. A. E. Van Blokland, T. Fujita, Y. Kusama, M. Matsuoka, S. Miura, Y. Neyatani, H. Takeuchi, M. Yamagiwa, and the JT-60 Team, 1993, in *Plasma Physics and Controlled Nuclear Fusion Research: Proceedings of the 14th International Conference, Würzburg, 1992* (IAEA, Vienna), paper A-6-2.
Nuclear Fusion Review, 1990, Nucl. Fusion **30**, 9.
Nuhrenberg, J., and R. Zille, 1986, Phys. Lett. A **114**, 129.
Nuhrenberg, J., and R. Zille, 1988, Phys. Lett. A **129**, 113.
Nygren, R. E. J. Bohdansky, A. Pospieszczyk, R. Lehmer, Y. Ra, R. W. Conn, R. Doerner, W. L. Leung, and L. Schmitz, 1981, Proc. IEEE **69**, 1056.
Nygren, R. E., J. Bohdansky, A. Pospieszczyk, R. Lehmer, Y. Ra, R. W. Conn, R. Doerner, W. K. Leung, and L. Schmitz, 1990, J. Nucl. Mater. **176&177**, 445.
Obiki, T., T. T. Mizuuchi, H. Zushi, K. Kondo, F. Sano, S. Sudo, N. Noda, M. Sato, T. Mutoh, S. Morimoto, *et al.*, 1989, in *Plasma Physics and Controlled Nuclear Fusion Research: Proceedings of the 12th International Conference, Nice, 1988* (IAEA, Vienna), Vol. 2, p. 337.
Obiki, T., M. Wakatani, M. Sato, S. Sudo, F. Sano, T. Mutoh, K. Itoh, K. Kondo, M. Nakasuga, K. Hanatani, *et al.*, 1990, Fusion Technol. **17**, 101.
Odajima, K., and Y. Shimomura, 1988, "Energy Confinement Scaling Based on Offset Linear Characteristic," Japan Atomic Energy Research Establishment Report JAERI-M-88-068.
Ohi, S. T., Minato, Y. Kawakami, M. Tanjyo, S. Okada, Y. Ito,

M. Kako, S. Goto, T. Ishimura, and H. Ito, 1983, Phys. Rev. Lett. **51**, 1042.
Ohkawa, T., 1970, Nucl. Fusion **10**, 185.
Ohyabu, N., D. R. Baker, N. H. Brooks, J. C. DeBoo, and M. Ali Mahdav, 1982, General Atomics Report GA-A16484.
Oren, L., and R. J. Taylor, 1977, Nucl. Fusion **17**, 1143.
Ortolani, S., 1988, in *Fusion Energy and Plasma Physics,* edited by P. H. Sakanaka (World Scientific, U.S. Office, Teaneck, NJ), p. 620.
Ortolani, S., 1989, Plasma Phys. Control. Fusion **31**, 1665.
Ortolani, S., and G. Rostagni, 1983, Nucl. Instrum. Methods **35**, 207.
Owens, T. L., 1986, IEEE Trans. Plasma Sci. **6**, 935.
Painter, S. L., and J. F. Lyon, 1989, Fusion Technol. **16**, 157.
Painter, S. L., and J. F. Lyon, 1991, Nucl. Fusion **31**, 2271.
Parail, V. V., and V. V. Alikaev, 1984, in *Heating in Toroidal Plasmas: Proceedings of the 4th International Symposium (Rome, 1984), International School of Plasma Physics, Varenna, Italy,* edited by H. Knoepfel and E. Sindoni (Monotypia Franchi, Citta di Castello, Italy), Vol. II, 753.
Park, W., S. Parker, H. Biglari, M. Chance, L. Chen, C. Z. Cheng, T. S. Hahm, W. W. Lee, R. Kulsrud, D. Monticello, L. Sugiyama, and R. White, 1992, Phys. Fluids B **4**, 2033.
Parker, R. R., G. Bateman, P. L. Colestock, H. P. Furth, R. J. Goldston, W. A. Houlberg, D. Ignat, S. Jardin J. L. Johnson, S. Kaye, *et al.*, 1989, in *Plasma Physics and Controlled Nuclear Fusion Research: Proceedings of the 12th International Conference, Nice, 1988* (IAEA, Vienna), Vol. 3, p. 341.
Parker, R. R., M. Greenwald, S. C. Luckhardt, E. A. Marmar, M. Porkolab, and S. M. Wolfe, 1985, Nucl. Fusion **25**, 1127.
Parks, P. B., R. J. Turnbull, and C. A. Foster, 1977, Nucl. Fusion **17**, 539.
Pearlstein, L. D., D. V. Anderson, D. E. Baldwin, J. A. Byers, B. I. Cohen, R. H. Cohen, W. C. Condit, T. K. Fowler, R. F. Freis, *et al.*, 1979, in *Plasma Physics and Controlled Nuclear Fusion Research: Proceedings of the 7th International Conference, Innsbruck, 1978* (IAEA, Vienna), Vol. 2, p. 457.
Pease, R. S., 1987, Plasma Phys. Control. Fusion **29**, 1177.
Peng, Y-K. M., and J. B. Hicks, 1990, in *Engineering Feasibility of Tight Aspect Ratio Tokamak (Spherical Torus) Reactors, 16th Symposium on Fusion Technology,* London (AEA Fusion, Culham Laboratory, AEA FUS 64).
Perkins, F. W., 1984, in *Heating in Toroidal Plasmas: Proceedings of the 4th International Symposium (Rome 1984), International School of Plasma Physics, Varenna, Italy,* Vol. II, p. 977.
Perkins, L. J., S. K. Ho, and J. H. Hammer, 1987, "Deep Penetration Fueling of Reactor-Grade Plasmas with Accelerated Compact Toroids," Lawrence Livermore National Laboratory Report UCRL-96894.
Petravic, M., D. Heifetz, and D. Post, 1985, *Plasma Physics and Controlled Nuclear Fusion Research: Proceedings of the 13th International Conference, Washington, 1984* (IAEA, Vienna), Vol. 2, p. 103.
Pfeiffer, W. W., R. H. Davidson, R. L. Miller and R. E. Waltz, 1980, "ONETWO: A Computer Code for Modeling Plasma Transport in Tokamaks," General Atomic Co. Report GA-A16178.
Pfeiffer, W. W., F. B. Marcus, C. J. Armentrout, G. L. Jahns, T. W. Petrie, and R. E. Stockdale, 1985, Nucl. Fusion **25**, 655.
Pfeiffer, W. W., and R. E. Waltz, 1979, Nucl. Fusion **19**, 51.
Phillips, C. K., J. Hosea, E. Marmar, M. W. Phillips, J. Snipes, J. Stevens, J. Terry, J. R. Wilson, M. Bell, M. Bitter, *et al.*, 1992, "ICRH Stabilization of Sawteeth on TFTR," Princeton Plasma Physics Laboratory Report PPPL-2820.
Phillips, J. A., D. A. Baker, R. F. Gribble, and C. Munson, 1988, Nucl. Fusion **28**, 1241.
Phillips, J. A., C. Munson, and G. Wurden, 1984, Bull. Am. Phys. Soc. **29**, 1403.
Pickrell, M. M., J. A. Phillips, C. J. Buchenauer, T. Cayton, J. N. Downing, A. Haberstich, J. C. Ingraham, E. M. Little, C. P. Munson, K. P. Schoenberg, P. G. Weber, and G. A. Wurden, 1984, Bull. Am. Phys. Soc. **29**, 1403.
Pickrell, M. M., J. A. Phillips, C. P. Munson, P. G. Weber, G. Miller, K. F. Schoenberg, and J. C. Ingraham, 1989, in *Controlled Fusion and Plasma Physics, Proceedings of the 16th, European Conference, Venice, 1989* (European Physical Society, Managing editor, G. Thomas, Geneva, Switzerland), Vol. 13B, Part II, p. 749.
Piet, S. J., 1986, Fusion Technol. **10**, 7.
Pietrzyk, Z. A., G. V. Vlases, R. D. Brooks, K. D. Hahn, and R. Raman, 1987, Nucl. Fusion **27**, 1478.
Podesta, G., and F. Engelmann, 1973, in *Toroidal Plasma Confinement, Proceedings 3rd* International Symposium, Garching, 1973 (*Max-Planck Institut für Plasmaphysik, Garching*), Paper C.9.
Pogutse, O. P., N. V. Chudin, and E. J. Yurchenko, 1980, Sov. J. Plasma Phys. **6**, 341.
Pogutse, O. P., and E. I. Yurchenko, 1979, Sov. J. Plasma Phys. **5**, 441.
Post, D. E., and R. Behrisch, 1986, *Physics of Plasma Wall Interactions,* NATO ASI Series B, Vol. 131 (Plenum, New York).
Post, D. E., D. B. Heifetz, and M. Petravic, 1982, J. Nucl. Mater. **111&112**, 383.
Post, D. E., and N. A. Uckan, 1992, Fusion Technol. **21**, 1427.
Post, D. E., K. Borrass, J. D. Callen, S. A. Cohen, J. G. Cordey, F. Engelmann, N. Fujisawa, M. F. A. Harrison, J. T. Hogan, H. J. Hopman, *et al.*, 1991, "ITER Physics," ITER Documentation Series No. 21 (IAEA, Vienna).
Post, R. F., 1987, Nucl. Fusion **27**, 1579.
Post, R. F., 1988, *Physics of Mirrors, Reversed Field Pinches and Compact Tori, Proceedings of the Course and Workshop (EUR-11335-EN), Varenna Italy, September 1987* (Editrice Compositori, Bologna, Italy), p. 51.
Post, R. F., and F. L. Ribe, 1974, Science **186**, 397.
Pourrahimi, S., C. L. H. Thieme, and S. Foner, 1987, IEEE Trans. Magn. **MAG-23**, 661.
Prinja, A. K., R. F. Schafer, Jr., R. W. Conn, and H. C. Howe, 1987, J. Nucl. Mater. **145-147**, 868.
Proceedings of the IEEE, 1981, Special Issue on Magnetic Fusion Development.
Ramos, J. J., 1991, Phys. Fluids B **3**, 2247.
Ramos, J. J., 1992, in "TPX MHD Physics, Meeting, Princeton, NJ, November, 1972," Princeton Plasma Physics Laboratory Report No. 93-921103-PPPL/S. Jardin-01.
Rawls, J., R. A. Dory, J. L. Dunlap, R. J. Goldston, G. E. Guest, J. T. Hogan, D. L. Jassby, M. Murakami, R. R. Parker, P. H. Rutherford, J. Schmidt, and D. Steiner, 1979, "Status of Tokamak Research," U.S. Department of Energy Report DOE/ER-0034.
Rebut, P-H., 1993, in *Proceedings of the 15th Symposium on Fusion Engineering, Hyannis, Massachusetts, Oct. 11–15, 1993* (IEEE, Piscataway, NJ), p. 1.
Rebut, P-H., M. Brusati, M. Hugon, and P. Lallia, 1987, in *Plasma Physics and Controlled Nuclear Fusion Research: Proceedings of the 11th International Conference, Kyoto, 1986* (IAEA, Vienna), Vol. 2, p. 187.
Rebut, P-H., P. P. Lallia, and M. L. Watkins, 1989, in *Plasma Physics and Controlled Nuclear Fusion Research, Nice, 1988*

(IAEA Vienna) Vol. 2, p. 191.
Rebut, P-H., M. L. Watkins, D. J. Gambier, and D. Boucher, 1990, in JET Joint Undertaking, Abingdon, England, 1990, preprint of Invited Review Paper at 32nd Meeting of Division of Plasma Physics, APS, Cincinnati, Ohio, JET-P(90) 75.
Rebut, P-H., M. l. Watkins, D. J. Gambier, and D. Boucher, 1991, Phys. Fluids B **3**, 2209.
Rechester, A. B., and M. B. Rosenbluth, 1978, Phys. Rev. Lett. **40**, 38.
Reidel, K., 1990, Nucl. Fusion **30**, 755.
Rej, D. J., M. Tuszewski, D. C. Barnes, A. D. Bailey, G. A. Barnes, M. H. Baron, R. E. Chrien, J. W. Cobb, A. Ishida, R. E. Siemon, *et al.*, 1991, in *Plasma Physics and Controlled Nuclear Fusion Research: Proceedings of the 13th International Conference, Washington, 1990* (IAEA, Vienna), Vol. 2, p. 647.
Rej, D. J., D. P. Taggart, M. H. Baron, R. E. Chrien, R. J. Gribble, M. Tuszewski, W. J. Waganaar, and B. L. Wright, 1992, "High-Power Magnetic Compression Heating of Field-Reversed Configurations," Los Alamos National Laboratory Report LA-UR-92-0177, and Phys. Fluids B **4**, 1909.
Rempel, T. D., C. W. Spragins, S. C. Prager, S. Assadi, D. J. Den Hartog, and S. Hokin, 1991, Phys. Rev. Lett. **67**, 1438.
Rewoldt, G., 1988, Phys. Fluids **31**, 3727.
Ribe, F. L., 1975, Rev. Mod. Phys. **47**, 7.
Robinson, D. C., and R. E. King, 1969, in *Plasma Physics and Controlled Nuclear Fusion Research: Proceedings of the 3rd International Conference, Novosibirsk, 1968* (IAEA, Vienna), Vol. 1, p. 263.
Robinson, D. C., 1971, Plasma Phys. **13**, 439.
Robinson, D. C., 1978, Plasma Phys. **18**, 939.
Robinson, D. C., 1980, Bull. Am. Phys. Soc. **25**, 685.
Robson, A. E., 1980, in *Megagauss Physics and Technology,* edited by P. J. Turchi (Plenum, New York), p. 425.
Romanelli, F., 1989, Plasma Phys. Control. Fusion **31**, 1535.
Rose, D. J., 1969, Nucl. Fusion **9**, 183.
Rose, D. J., and M. Clark, Jr., 1961, *Plasmas and Controlled Fusion* (MIT Press and Wiley, New York).
Rosenbluth, M. N., H. L. Berk, J. W. Van Dam, and D. M. Lindberg, 1992, Phys. Rev. Lett. **68**, 596.
Rosenbluth, M. N., and M. N. Bussac, 1979, Nucl. Fusion **19**, 489.
Rosenbluth, M. N., and P. H. Rutherford, 1975, Phys. Rev. Lett. **34**, 1428.
Rosenbluth, M. N., and P. H. Rutherford, 1981, in *Fusion,* edited by E. Teller (Academic, New York), Vol. 1, Part A, p. 32.
Rosenbluth, M. N., R. Z. Sagdeev, J. B. Taylor, and G. M. Zaslavski, 1966, Nucl. Fusion **6**, 297.
Ross, D. W., 1987, "Thermal and Particle Transport in Tokamaks—Theoretical Models for Ignition Studies," University of Texas Report DOE/ET-53193-7.
Ross, D. W., 1990, "Standard Forms for Transport Equations and Fluxes, Part II," University of Texas Report DOE/ER-53266-30, FRCR No. 357.
Ryter, F., 1993, in 20th European Physical Society Conference on Controlled Fusion and Plasma Physics, Lisboa, Portugal (unpublished), Vol. 17C, Part 1, paper I-15.
Samain, A., A. Grossman, and W. Feneberg, 1984, J. Nucl. Mater. **128-129**, 395.
Samm, U., 1993, in *Plasma Physics and Controlled Nuclear Fusion Research: Proceedings of the 14th International Conference, Würzburg, 1992* (IAEA, Vienna), paper A-5-3.
Schivell, J. F., 1977, "Method of Plasma Impurity Control Without Magnetic Divertor," Princeton Plasma Physics Laboratory Report PPPL-1342.
Schmidt, G., 1979, *Physics of High Temperature Plasmas, 2nd Edition* (Academic, New York).
Schmidt, J. A., K. I. Thomassen, R. J. Goldston, G. H. Neilson, W. M. Nevins, and J. C. Sinnis *et al.*, 1993, J. Fusion Energy, **12**, 221.
Schnack, D. D., E. J. Caramana, and R. A. Nebel, 1985, Phys. Fluids **28**, 321.
Schoenberg, K. F., C. J. Buchenauer, R. S. Massey, J. G. Melton, R. W. Moses, Jr., R. A. Nebel, and J. A. Phillips, 1984, Phys. Fluids **27**, 548.
Schoenberg, K. F., J. C. Ingraham, C. P. Munson, P. G. Weber, D. A. Baker, R. F. Gribble, R. B. Howell, G. Miller, W. A. Reass, A. E. Schofield, S. Shinohara, and G. A. Wurden, 1988, Phys. Fluids **31**, 2285.
Schoenberg, K. F., J. C. Ingraham, R. W. Moses, Jr., P. G. Weber, L. C. Burkhardt, A. F. Almagri, S. Assadi, J. A. Beckstead, G. Chartas, D. J. Den Hartog, *et al.*, 1989, in *Plasma Physics and Controlled Nuclear Fusion Research: Proceedings of the 12th International Conference, Nice, 1988* (IAEA, Vienna), Vol. 2, p. 419.
Schoenberg, K. F., and R. W. Moses, Jr., 1991, Phys. Fluids B **3**, 1467.
Scott, S. D., C. W. Barnes, D. R. Mikklesen, F. W. Perkins, M. G. Bell, R. E. Bell, C. E. Bush, D. Ernst, E. D. Fredrickson, B. Grek, *et al.* 1993, in *Plasma Physics and Controlled Nuclear Fusion Research: Proceedings of the 14th International Conference, Würzburg, 1992* (IAEA,Vienna), paper 56/G-3-3.
Scott, S. D., J. F. Lyon, J. K. Munro, D. J. Sigmar, S. C. Bates, J. D. Bell, C. E. Bush, A. Carnevall, J. L. Dunlap, P. H. Edmonds, *et al.*, 1985, Nucl. Fusion **25**, 359.
Seki, Y., M. Kikuchi, S. Nishio, A. Oikawa, T. Ando, Y. Ohara, M. Seki, T. Takizuka, K. Tani, T. Ozeki, *et al.*, 1991, "Concept Study of the Steady State Tokamak Reactor (SSTR)," Japan Atomic Energy Research Institute Report JAERI-M 91-081.
Shafranov, V. D., 1966, in *Reviews of Plasma Physics 2* (Consultants Bureau, New York), p. 103.
Shafranov, V. D., 1983, Phys. Fluids **26**, 357.
Shafranov, V. D., and E. I. Yurchenko, 1968, Nucl. Fusion **8**, 329.
Shaing, K. C., 1983, Phys. Fluids **26**, 3164.
Shaing, K. C., 1984, Phys. Fluids **27**, 1567.
Shaing, K. C., 1991, Comments Plasma Phys. Control. Fusion **14**, 41.
Shaing, K. C., B. A. Carreras, N. Dominguez, V. E. Lynch, and J. S. Tolliver, 1989, Phys. Fluids B **1**, 1663.
Shaing, K. C., and E. C. Crume, Jr., 1989, Phys. Rev. Lett. **63**, 2369.
Shaing, K. C., E. C. Crume, Jr., and W. A. Houlberg, 1990, Phys. Fluids B **2**, 1492.
Shaing, K. C., W. A. Houlberg, and E. C. Crume, Jr., 1988, Comments Plasma Phys. Control. Fusion **12**, 69.
Sheffield, J., 1981, Proc. IEEE **69**, 885.
Sheffield, J., 1985, Nucl. Fusion **25**, 1733.
Sheffield, J., 1986, in *Tokamak Start-up,* edited by H. Knoepfel (Plenum, New York), p. 7.
Sheffield, J., 1990, in *17th EPS Conference on Controlled Fusion and Plasma Physics, Amsterdam* (European Physical Society, Managing editor, G. Thomas, Geneva, Switzerland), p. 102.
Sheffield, J., R. A. Dory, S. M. Cohn, J. G. Delene, L. Parsly, D. E. T. F. Ashby, and W. T. Reiersen, 1986, Fusion Technol. **9**, 199.
Sheffield, J., and A. Gibson, 1975, Nucl. Fusion **15**, 677.
Shimada, M., M. Nagami, K. Ioki, S. Izumi, M. Maeno, H.

Yokomizo, K. Shinya, H. Yoshida, A. Kitsunezaki, N. H. Brooks, C. L. Hsieh, and J. S. deGrassie, 1981, Phys. Rev. Lett. **47**, 796.

Shohet, J. L., 1981(a), in *Fusion,* edited by E. Teller (Academic, New York), Vol. 1, Part A, p. 243.

Shohet, J. L., (guest editor), 1981(b), IEEE Trans. Plasma Sci. **PS-9**, 4.

Shumaker, D. E., 1984, J. Comput. Phys. **53**, 456.

Siemon, R. E., W. T. Armstrong, R. E. Chrien, P. L. Klingner, R. K. Linford, K. F. McKenna, N. T. Gladd, D. S. Harned, D. Schumaker, C. E. Seyler, *et al.*, 1985, *Plasma Physics and Controlled Nuclear Fusion Research: Proceedings of the 10th International Conference, London, 1984* (IAEA, Vienna), Vol. 2, p. 511.

Siemon, R. E., W. T. Armstrong, D. C. Barnes, R. R. Bartsch, R. E. Chrien, J. C. Cochrane, W. N. Hugrass, R. W. Kewish, Jr., P. L. Klinger, H. R. Lewis, R. K. Linford, *et al.*, 1986 Fusion Technol. **9**, 13.

Sigmar, D. J., 1989, Phys. Scr. T **16**, 6.

Sigmar, D. J., D. B. Batchelor, G. Bateman, M. G. Bell, B. J. Braams, J. N. Brooks, C. Z. Cheng, D. R. Cohn, R. J. Goldston, J. Haines, *et al.*, 1991, in *Plasma Physics and Controlled Nuclear Fusion Research: Proceedings of the 13th International Conference, London, 1990* (IAEA, Vienna), Vol. 3, p. 455.

Sigmar, D. J., C. T. Hsu, R. White, and C. Z. Cheng, 1992, Phys. Fluids B **4**, 1506.

Simonen, T. C., J. F. Clauser, F. H. Coensgen, D. L. Correll, W. F. Cummins, R. P. Drake, J. H. Foote, A. H. Futch, R. K. Goodman, D. P. Grubb, *et al.*, 1979, in *Plasma Physics and Controlled Nuclear Fusion Research: Proceedings of the 7th International Conference, Innsbruck, 1978* (IAEA, Vienna), Vol. 2, p. 389.

Singer, C. E., D. E. Post, D. R. Mikkelsen, M. H. Redi, A. McKenney, A. Silverman, F. G. P. Seidl, P. H. Rutherford, R. J. Hawryluk, W. D. Langer, *et al.*, 1986, "BALDUR: A One-Dimensional Plasma Transport Code," Princeton Plasma Physics Laboratory Report PPPL-2073.

Slough, J. T., A. L. Hoffman, R. D. Milroy, D. G. Harding, and L. C. Steinhauer, 1984, Nucl. Fusion **24**, 1537.

Spears, W. R., and J. A. Wesson, 1980, Nucl. Fusion **20**, 1525.

Spencer, R. L., M. Tuszewski, and R. K. Linford, 1983, Phys. Fluids **26** 1564.

Spitzer, L., Jr., 1962, *Physics of Fully Ionized Gases* (Interscience, New York).

Spong, D. A., B. A. Carreras, and C. L. Hedrick, 1992, Phys. Fluids **4**, 3316.

Spong, D., J. A. Holmes, J-N. Leboeuf, P. J. Christenson, 1990, Fusion Technol. **14**, 496.

Spong, D., D. J. Sigmar, W. A. Cooper, D. E. Hastings, and K. T. Tsang, 1985, Phys. Fluids **28**, 2494.

Spong, D. A., D. J. Sigmar, K. T. Tsang, J. J. Ramos, D. E. Hastings, and W. A. Cooper, 1987, Phys. Scr. **T16**, 18.

Stacey, W. M., Jr., 1981, *Fusion Plasma Analysis* (Wiley, New York).

Stacey, W. M., Jr., 1984, *Fusion: An Introduction to the Physics and Technology of Magnetic Confinement Systems* (Wiley, New York).

Stacey, W. M., Jr., A. W. Bailey, D. J. Sigmar, and K. C. Shaing, 1985, Nucl. Fusion **25**, 463.

Stix, T. H., 1972, Plasma Phys. **14**, 367.

Stix, T. H., 1992, *Waves in Plasma* (AIP, New York).

Stodiek, W., R. Goldston, N. Sauthoff, V. Arunasalam, C. Barnes, M. Bitter, D. Boyd, N. Bretz, R. Chrien, S. Cohen, *et al.*, 1981, in *Plasma Physics and Controlled Nuclear Fusion Research: Proceedings of the 8th International Conference, Brussels, 1980* (IAEA, Vienna), Vol. 1, p. 9.

Strumberger, E., 1992, Nucl. Fusion **32**, 737.

Strumberger, E., F. Rau, and J. Kisslinger, 1991, in *Proceedings of the 4th Workshop on Wendelstein 7-X,* Schloss Ringberg, October 1991, edited by J. Junker (Max Planck Institut für Plasma Physik, Garching, Report IPP 313), p. 145.

Sudo, S., Y. Takeiri, H. Zushi, F. Sano, K. Itoh, K. Kondo, and A. Iiyoshi, 1990, Nucl. Fusion **30**, 11.

Sviatoslavsky, I., S. W. Van Seiver, G. L. Kulcinski, D. T. Anderson, A. W. Bailey, J. D. Callen, J. A. Derr, G. A. Emmert, L. El-Guebaly, A. Khalil, *et al.*, 1981, IEEE Transaction on Plasma Science, **PS-9**, 163.

Swain, D. W., M. Murakami, S. C. Bates, C. E. Bush, J. L. Dunlap, P. H. Edmonds, D. Hutchinson, P. W. King, E. A. Lazarus, J. F. Lyon, *et al.*, 1981, Nucl. Fusion **21**, 1409.

Sykes, A., M. F. Turner, and S. Patel, 1983, in *Proceedings of the 11th European Physical Society Meeting on Controlled Fusion and Plasma Physics, Aachen* (European Physical Society, Managing editor, G. Martin, Geneva, Switzerland), II, 363.

Tait, G., J. Bell, M. G. Bell, M. Bitter, W. R. Blanchard, F. Boody, D. Boyd, N. Bretz, C. Bush, J. L. Cecchi, S. Cohen, *et al.*, 1985, in *Plasma Physics and Controlled Nuclear Fusion Research: Proceedings of the 10th International Conference, London, 1984* (IAEA, Vienna), Vol. 1, p. 141.

Tang, W. M., 1978, Nucl. Fusion **18**, 1089.

Tani, K., T. Takizuka, M. Azumi, M. Yamagiwa, Y. Kishimoto, K. Hamamatsu, and J. J. Foit, 1989, *Plasma Physics and Controlled Nuclear Fusion Research: Proceedings of the 12th International Conference, Nice, 1988* (IAEA, Vienna), Vol. 2, p. 121.

Taylor, J. B., 1974, Nucl. Fusion (IAEA Vienna) Special Supplement 403.

Taylor, J. B., 1976, in *Pulsed High Beta Plasma, Proceedings of the Third Topical Conference, Abingdon, 1975,* edited by D. E. Evans (Pergamon, Oxford/New York), p. 59.

Taylor, J. B., 1986, Rev. Mod. Phys. **58**, 741.

Taylor, R. J., *et al.*, 1989, Phys. Rev. Lett. **63**, 2365.

Tendler, M. B., and O. Ågren, 1982, Phys. Fluids **25**, 1037.

TFR Equipe, 1980, Nucl. Fusion **20**, 1227.

TFTR Team, 1993, private communication, December.

Thomas, P. R., and the JET Team, 1990, J. Nucl. Mater. **176&177**, 3.

Thomas, P. R., and the JET Team, 1991, *Plasma Physics and Controlled Nuclear Fusion Research: Proceedings of the 13th International Conference, Washington, 1990* (IAEA, Vienna), Vol. 1, p. 375.

Thomassen, K. I., R. J. Goldston, and G. H. Neilson, 1993, J. Fusion Energy **12**, 215.

Thomson, Sir George P., and M. Blackman, 1952, United Kingdom, Patent Application 1034/52 and U.S. Patent Application 1953.

Todd, A. M. M., J. Manickam, M. Okabayashi, M. S. Chance, R. C. Grimm, J. M. Greene, and J. L. Johnson, 1979, Nucl. Fusion **19**, 763.

Treffert, J. D., J. L. Shohet, and H. L. Berk, 1984, Phys. Rev. Lett. **53**, 2409.

Troyon, F., R. Gruber, H. Saurenmann, S. Semenzato, and S. Succi, 1984, Plasma Phys. Control. Fusion **26**, 209.

Trubnikov, B. A., 1979, in *Reviews of Plasma Physics,* edited by M. A. Leontovich (Consultants Bureau, New York), **7**, 345.

Tsui, H. Y. W., 1988, Nucl. Fusion **28**, 1543.

Tsui, H. Y. W., C. P. Ritz, G. Miller, J. C. Ingraham, C. P. Munson, K. F. Schoenberg, and P. G. Weber, 1991, Nucl. Fusion **31**, 2371.

Tsytovich, V. N., 1970, *Nonlinear Effects in Plasma* (Plenum, New York).

Tubbing, B. J. D., B. Balet, D. V. Bartlett, C. D. Challis, S. Corti, R. D. Gill, C. Gormezano, C. W. Gowers, M. Von Hellermann, M. Hugon, *et al.*, 1991, Nucl. Fusion **31**, 839.

Tuszewski, M., 1988, Nucl. Fusion **28**, 2033.

Tuszewski, M., and R. K. Linford, 1982, Phys. Fluids **25**, 765.

Tuszewski, M., W. T. Armstrong, R. R. Bartsch, R. E. Chrien, J. C. Cochrane, Jr., R. W. Kewish, Jr., P. Klingner, R. K. Linford, K. F. McKenna, D. J. Rej, E. G. Sherwood, and R. E. Siemon, 1982, Phys. Fluids **25**, 1696.

Tuszewski, M., D. P. Taggart, R. E. Chrien, D. J. Rej, R. E. Siemon, and B. L. Wright, 1991, Phys. Fluids B **3**, 2856.

Uckan, N. A., 1985, "Non-inductive Current Drive in Tokamaks," Oak Ridge National Laboratory Report ORNL/TM-9296.

Uckan, N. A., J. S. Tolliver, W. A. Houlberg, and S. E. Attenberger, 1988, Fusion Technol. **13**, 411.

Uckan, N. A., and the ITER Physics Group, 1990, "ITER Physics Design Guidelines," ITER Documentation Series No. 10 (IAEA, Vienna), International Thermonuclear Experimental Reactor Report ITER-TN-PH-0-5.

Ueda, K., K. Itoh, and S.-I. Itoh, 1989, Nucl. Fusion **29**, 173.

Uo, K., 1961, J. Phys. Soc. Jpn. **16**, 1380.

Uo, K., A. Iiyoshi, T. Obiki, O. Motojima, S. Morimoto, A. Sasaki, K. Kondo, M. Sato, T. Mutoh, H. Zushi, *et al.*, 1983, in *Plasma Physics and Controlled Nuclear Fusion Research: Proceedings of the 9th International Conference, Baltimore, 1982* (IAEA, Vienna), Vol. 2, p. 209.

Vershkov, V. A., and S. V. Mirnov, 1974, Nucl. Fusion **2**, 383.

Vlases, G. S., D. S. Rowe, and the FIREBIRD Design Team, 1986, Fusion Technol. **9**, 116.

Volkov, E. D., V. A. Rudakov, and V. A. Suprunenko, 1984, Vopr. At. Nauki, Tech., Ser. Termoyadernyi Sintez **15**, 36.

Volkov, E. D., A. V. Georglevskij, Yu. K. Kuznetsov, Yu. A. Litvinenko, O. S. Pavlichenko, V. A. Rudakov, and Yu. F. Sergeev, 1987, in *Fusion Reactor Design and Technology: Proceedings of the 4th IAEA Technical Committee Meeting and Workshop, Yalta, 1986* (IAEA, Vienna), Vol. 1, p. 393.

Wagner, C. E., 1981, Phys. Rev. Lett. **46**, 854.

Wagner, F., G. Becker, K. Behringer, D. Campbell, A. Eberhagen, W. Engelhardt, G. Fussman, O. Gehre, J. Gernhardt, G. V. Gierke, *et al.*, 1982, Phys. Rev. Lett. **49** 1408.

Wagner, F., and U. Stroh, 1993, Plasma Phys. Control. Fusion **35**, 1321.

Waltz, R., J. DeBoo, and M. Rosenbluth, 1990, Phys. Rev. Lett. **65**, 2390.

Watkins, M. L., T. E. Stringer, A. Gibson, W. G. F. Core, I. L. Robertson, J. G. Cordey, and J. J. Field, 1981, in *Plasma Physics and Controlled Nuclear Fusion Research: Proceedings of the 8th International Conference, Brussels, 1980* (IAEA, Vienna), Vol. 1, p. 639.

Watt, R. G., and R. A. Nebel, 1983, Phys. Fluids **26**, 1168.

Weber, P. G., *et al.*, 1991, in *Plasma Physics and Controlled Nuclear Fusion Research: Proceedings of the 13th International Conference, Washington, 1990* (IAEA, Vienna), Vol. 2, p. 509.

Werley, K. A., 1987, in *Proceedings of the 12th Symposium on Fusion Engineering, Monterey, California* (IEEE, Piscataway, NJ), p. 1414.

Werley, K. A., 1991, Nucl. Fusion **31**, 567.

Werley, K. A., 1992, "Burning *D-T* Plasmas in the Reversed Field Pinch (RFP)," Los Alamos National Laboratory Report LA-12259-MS.

Werley, K. A., C. G. Bathke, R. A. Krakowski, R. L. Miller, and J. N. DiMarco, 1991, Fusion Technol. **19**, 1266.

Wesson, J. A., 1978, Nucl. Fusion **18**, 87.

Weynants, R., and R. J. Taylor, 1990, Nucl. Fusion **30**, 945.

White, R. B., F. Romanelli, and M. N. Bussac, 1990, Phys. Fluids **32**, 745.

Willenberg, H. J., A. L. Hoffman, L. C. Steinhauer, and P. H. Rose, 1979, in *Compact Torus and Energetic Particle Injection: Proceedings U.S.-Japan Joint Symposium, Princeton, New Jersey, 1979* (Princeton Plasma Physics Laboratory, Princeton University), p. 233.

Willenberg, H. J., L. C. Steinhauer, A. L. Hoffman, T. L. Churchill, and P. H. Rose, 1980, in *TRACT Fusion Reactor Studies: Proceedings of the 4th ANS Topical Meeting on the Technology of Controlled Nuclear Fusion, King of Prussia, Pennsylvania,* edited by F. H. Tenney and C. C. Hopkins (NTIS, Springfield, VA), p. 894.

Wobig, H., C. Beidler, E. Harmeyer, J. Kisslinger, L. Ott, F. Rau, and V. Welge, 1991, in *Proceedings of the 4th Workshop on Wendelstein 7-X Schloss Ringberg, Bavaria, October 1991,* edited by J. Junker (Max-Planck Institut für Plasma Physik, Report IPP 2/313), pp. 189 and 228.

Woltjer, L., 1958, Proc. Natl. Acad. Sci., USA **44**, 489.

Wong, K. L., R. J. Fonck, S. F. Paul, D. R. Roberts, E. D. Fredrickson, R. Nazikian, H. K. Park, M. Bell, N. L. Bretz, R. Budny, *et al.*, 1991, Phys. Rev. Lett. **66**, 1874.

Wootton, A. J., 1991, "Turbulence and Transport," Varenna Lecture, University of Texas Report, DOE ER-53267-89, FRCR No. 393, August 1991.

Wootton, A. J., B. A. Carreras, H. Matsumoto, K. McGuire, W. A. Peebles, C. P. Ritz, P. W. Terry, and S. J. Zweben, 1990, Phys. Fluids B **2**, 2879.

Wright, B. L., 1990, Nucl. Fusion **30**, 1739.

Wurden, G. A., K. F. Schoenberg, M. M. Pickrell, D. A. Baker, C. J. Buchenauer, L. C. Burkhardt, T. E. Cayton, R. E. Chrien, J. N. Downing, R. F. Ellis, *et al.*, 1987, in *Physics of Mirrors, Reversed Field Pinches and Compact Tori: Proceedings Course and Workshop, Varenna, 1987* (Editrice Compositori, Bologna), Vol. 1, p. 159.

Wurden, G. A., P. G. Weber, R. G. Watt, C. P. Munson, T. E. Cayton, K. Buchl, and E. J. Nilles, 1987a, in *Physics of Mirrors, Reversed Field Pinches and Compact Tori: Proceedings Course and Workshop, Varenna, 1987* (Editrice Compositori, Bologna), Vol. 1, p. 411.

Wurden, G. A., P. G. Weber, R. G. Watt, C. P. Munson, J. C. Ingraham, R. B. Howell, T. E. Cayton, K. Buchl, and E. J. Nilles, 1987b, Nucl. Fusion **27**, 857.

Wurden, G. A., D. M. Weldon, P. G. Weber, R. G. Watt, A. E. Schofield, M. M. Pickrell, J. A. Phillips, C. P. Munson, G. Miller, J. C. Ingraham, R. B. Howell, and C. J. Buchenauer, 1985, Bull. Am. Phys. Soc. **30**, 1402.

Yamazaki, K., and T. Amano, 1990, "Plasma Transport Simulation Modeling for Helical Confinement Systems," National Institute for Fusion Studies, Nagoya, Japan, Report, NIF S104.

Yoshikawa, S., and H. Yamato, 1966, Phys. Fluids **9**, 1814.

Yushmanov, P. N., T. Takizuka, K. S. Riedel, O. J. W. F. Kardaun, J. G. Cordey, S. M. Kaye, and D. E. Post, 1990, Nucl. Fusion **30**, 1999.

Zakharov, L. E., September 1989, "$m=2$ Tearing Mode Stabilization With Local Current Drive in ITER," talk presented at

ITER Specialists Meeting on Disruptions, Garching, Germany.
Zarnstorff, M. C., M. G. Bell, M. Bitter, R. J. Goldston, B. Grek, R. J. Hawryluk, K. Hill, D. Johnson, D. McCune, H. Park, A. Ramsey, G. Taylor, and R. Wieland, 1988, Phys. Rev. **60**, 1306.
Zita, E. J., S. C. Prager, Y. L. Ho, and D. D. Schnack, 1992, Nucl. Fusion **32**, 1941.
Zweben, S. J., R. Boivin, D. S. Darrow, E. D. Fredrickson, H. E. Mynick, R. B. White, H. Biglari, N. L. Bretz, R. V. Budny, C. E. Bash, C. S. Chang, *et al.*, 1993, in *Plasma Physics and Controlled Nuclear Fusion Research: Proceedings of the 14th International Conference, Würzburg, 1992* (IAEA, Vienna), paper 56/A-6-3.
Zweben, S. J., H. P. Furth, R. J. Goldston, and D. J. Sigmar, 1990, Nucl. Fusion **30**, 1799.